State of Oregon
Oregon Department of Geology and Mineral Industries
Brad Avy, State Geologist

**GEOLOGIC MAP 127**

# GEOLOGIC MAP OF THE DUFUR AREA, WASCO COUNTY, OREGON

by Jason D. McClaughry[1], Heather H. Herinckx[2], Clark A. Niewendorp[3], Carlie J.M. Azzopardi[4], and Joshua A. Hackett[5]

2021

[1] Oregon Department of Geology and Mineral Industries, Baker City Field Office, Baker County Courthouse, 1995 3rd Street, Suite 130, Baker City, OR 97814
[2.] GeoDesign Inc., 9450 SW Commerce Circle, Suite 300, Wilsonville, OR 97070; previously with Oregon Department of Geology and Mineral Industries
[3] Oregon Department of Geology and Mineral Industries, 800 NE Oregon Street, Suite 965 Portland, OR 97232; retired
[4] Oregon Department of Geology and Mineral Industries, 800 NE Oregon Street, Suite 965 Portland, OR 97232
[5] Oregon Water Resources Department, 725 Summer Street NE, Suite A, Salem, OR 97301

## NOTICE



## WHAT'S IN THIS REPORT?

This publication provides an updated and spatially accurate geologic framework for the Dufur area as part of a multi-year study of the geology of the larger Middle Columbia Basin. Geologic data in the publication provide significant new details about the volcanic and structural geologic history of the area and the geologic conditions controlling the distribution of water resources, aggregate and other mineral resources, and geologic hazards.

Cover photograph: View southeast to the city of Dufur and the Fifteenmile Creek drainage. (45.458202, -121.139477 WGS84 geographic coordinates). Photo credit: Jason McClaughry, 2018.


Expires: 12/1/2021

Oregon Department of Geology and Mineral Industries Geologic Map Series GMS-127
Published in conformance with ORS 516.030.

For additional information:
Administrative Offices
800 NE Oregon Street, Suite 965
Portland, OR 97232
Telephone (971) 673-1555
Fax (971) 673-1562
https://www.oregon.gov/dogami

# TABLE OF CONTENTS

## LIST OF FIGURES

# LIST OF TABLES

## GEODATABASES

WRF2021_GeMS_v10.7.gdb
DWPS2021_GeMS_v10.7.gdb
DESBSR2021_GeMS_v10.7.gdb

*See the appendix for geodatabase description. See the digital publication folder for files. Geodatabases are Esri® version 10.7 format. Metadata is embedded in the geodatabases and shapefiles and is also provided as separate .xml format files.*

## SHAPEFILES AND SPREADSHEETS

**Shapefiles**
Orientation Points: WRF2021_OrientationPoints.shp
Geochemistry: WRF2021_GeochemPoints.shp
Geochronology: WRF2021_GeochronPoints.shp
Magnetics: WRF2021_MagneticPoints.shp
Wells: WRF2021_WellPoints.shp
Reference map: WRF2021_RefMap.shp
Cross Section Lines: WRF2021_XSectionLines.shp

**Spreadsheets (Microsoft® Excel®)**
**WRF2021_DATA.xlsx** master file contains sheets:
Orientation Points: WRF2021_OrientationPoints
Geochemistry: WRF2021_GeochemPoints
Geochronology: WRF2021_GeochronPoints
Magnetics: WRF2021_MagneticPoints
Wells: WRF2021_WellPoints

**Shapefiles**
Orientation Points: DWPS2021_OrientationPoints.shp
Geochemistry: DWPS2021_GeochemPoints.shp
Alteration Geochemistry: DWPS2021_AltChemistry.shp
Geochronology: DWPS2021_GeochronPoints.shp
Magnetics: DWPS 2021_MagneticPoints.shp
Wells: DWPS2021_WellPoints.shp
Reference map: DWPS2021_RefMap.shp
Cross Section Lines: DWPS2021_XSectionLines.shp

**Spreadsheets (Microsoft® Excel®)**
**DWPS2021_DATA.xlsx** master file contains sheets:
Orientation Points: DWPS2021_OrientationPoints
Geochemistry: DWPS2021_GeochemPoints
Alteration Geochemistry: DWPS2021_AltChemistry
Geochronology: DWPS2021_GeochronPoints
Magnetics: DWPS2021_MagneticPoints
Wells: DWPS2021_WellPoints

**Shapefiles**
Orientation Points: DESBSR2021_OrientationPoints.shp
Geochemistry: DESBSR2021_GeochemPoints.shp
Alteration Geochemistry: DESBSR2021_AltChemistry.shp
Magnetics: DESBSR2021_MagneticPoints.shp
Wells: DESBSR2021_WellPoints.shp
Reference map: DESBSR2021_RefMap.shp
Cross Section Line: DESBSR2021_XSectionLines.shp

**Spreadsheets (Microsoft® Excel®)**
**DESBSR2021_DATA.xlsx** master file contains sheets:
Orientation Points: DESBSR2021_OrientationPoints
Geochemistry: DESBSR2021_GeochemPoints
Alteration Geochemistry: DESBSR2021_AltChemistry
Magnetics: DESBSR2021_MagneticPoints
Wells: DESBSR2021_WellPoints

## MAP PLATES

Plate 1. Geologic map of the Wolf Run and northern part of the Friend 7.5’ quadrangles, Wasco County, Oregon

Plate 2. Geologic map of the Dufur West and northern part of the Postage Stamp Butte 7.5’ quadrangles, Wasco County, Oregon

Plate 3. Geologic map of the Dufur East and parts of the Sherars Bridge and Summit Ridge 7.5’ quadrangles, Wasco County, Oregon

# 1.0 INTRODUCTION

The Dufur area of Wasco County, Oregon encompasses an area of ~567 km$^2$ (219.1 mi$^2$) in the Middle Columbia Basin, lying across the eastern slopes of the northern Oregon Cascade Range, ~46 km (28.5 mi) east of Mount Hood volcano (**Figure 1-1**; Plates 1, 2, and 3). The oldest rocks cropping out in the Dufur area are part of the Columbia River Basalt Group (CRBG), the smallest and youngest flood basalt province in the world (Reidel and others, 2013). Younger upper Miocene to lower Pleistocene volcanic rocks unconformably overlie the CRBG in the Dufur area, recording part of the volcano-tectonic development of the northern Oregon Cascade Range over the past 9 m.y. (McClaughry and others, 2020a).

The geology of the Dufur area was mapped by the Oregon Department of Geology and Mineral Industries (DOGAMI) between 2014 and 2020, in collaboration with geoscientists from the Oregon Water Resources Department. Mapping covers the Wolf Run, Dufur West, and Dufur East 7.5′ quadrangles, as well as parts of the Friend, Postage Stamp Butte, Sherars Bridge, and Summit Ridge 7.5′ quadrangles lying within the watershed boundary of the Middle Columbia Basin. The primary objective of this investigation is to provide an updated and spatially accurate geologic framework for the Dufur area as part of a multi-year study of the geology of the larger Middle Columbia Basin (**Figure 1-1**, **Figure 1-2**). Additional key objectives of this project are to: 1) determine the geologic history of volcanic rocks in this part of the northern Oregon Cascade Range; 2) provide significant new details about the structure and fault history of the Yakima Fold Belt and eastern slopes of the northern Oregon Cascade Range; 3) characterize the stratigraphic framework and geologic conditions controlling the distribution of water resources; 4) determine the distribution of potential aggregate sources and other mineral resources; and 5) describe the nature of geologic hazards. New detailed geologic data presented here also provides a basis for future geologic, geohydrologic, and geohazard studies in the Middle Columbia Basin (**Figure 1-1**).

The core products of this study are this report, accompanying geologic maps and cross sections (Plates 1, 2, and 3), Esri ArcGIS™ geodatabases, and Microsoft Excel® spreadsheets tabulating point data for geochemistry, geochronology, magnetic polarity, orientation points, and well data. The geodatabases present new geologic mapping in a digital format consistent with the USGS National Cooperative Geologic Mapping Program Geologic Map Schema (GeMS) (U.S. Geological Survey National Cooperative Geologic Mapping Program, 2020). They contain spatial information, including geologic polygons, contacts, structures, geochemistry, geochronology, magnetic observation, orientation points, and well data, as well as data about each geologic unit such as age, lithology, mineralogy, and structure. Digitization at scales of 1:8,000 or better was accomplished using a combination of high-resolution lidar topography and imagery. Surficial and bedrock geologic units in the geodatabase are depicted on Plates 1, 2, and 3 at a scale of 1:24,000. The three plates include: 1) a detailed geologic map showing the relationship of both bedrock and surficial units; and 2) a simplified derivative bedrock geologic map used to more readily show the distribution of contrasting bedrock lithologies and critical structural relationships in the map area. Both the geodatabases and geologic maps are supported by this report describing the geology in detail.

Detailed geologic mapping in this part of the Middle Columbia Basin is a high priority of the Oregon Geologic Map Advisory Committee (OGMAC), supported in part by grants from the STATEMAP component of the U.S. Geological Survey (USGS) National Cooperative Geologic Mapping Program under cooperative agreement numbers G15AC00180 and G20AC00202, and by the Oregon Water Resources Department (OWRD) through Interagency Agreements DOGAMI/OWRD IAA #12102013/OWRD 13 057 (2014) and DOGAMI IAA# DASPS-2542-16/OWRD IAA 16 047 (2016). Additional funds were provided by the State of Oregon through the Oregon Department of Geology and Mineral Industries.

**Figure 1-1. Location of the Dufur study area in the Middle Columbia Basin of north-central Oregon. The study area is shown by a black outline. The solid orange line corresponds to the watershed boundary of the Middle Columbia Basin. The Columbia River, flowing from east to west, in the upper part of the figure, separates Oregon on the south from Washington State on the north. The Deschutes River marks the boundary between Wasco County on the west and Sherman County on the east. The city of Dufur is located near the north-central part of the study area.**

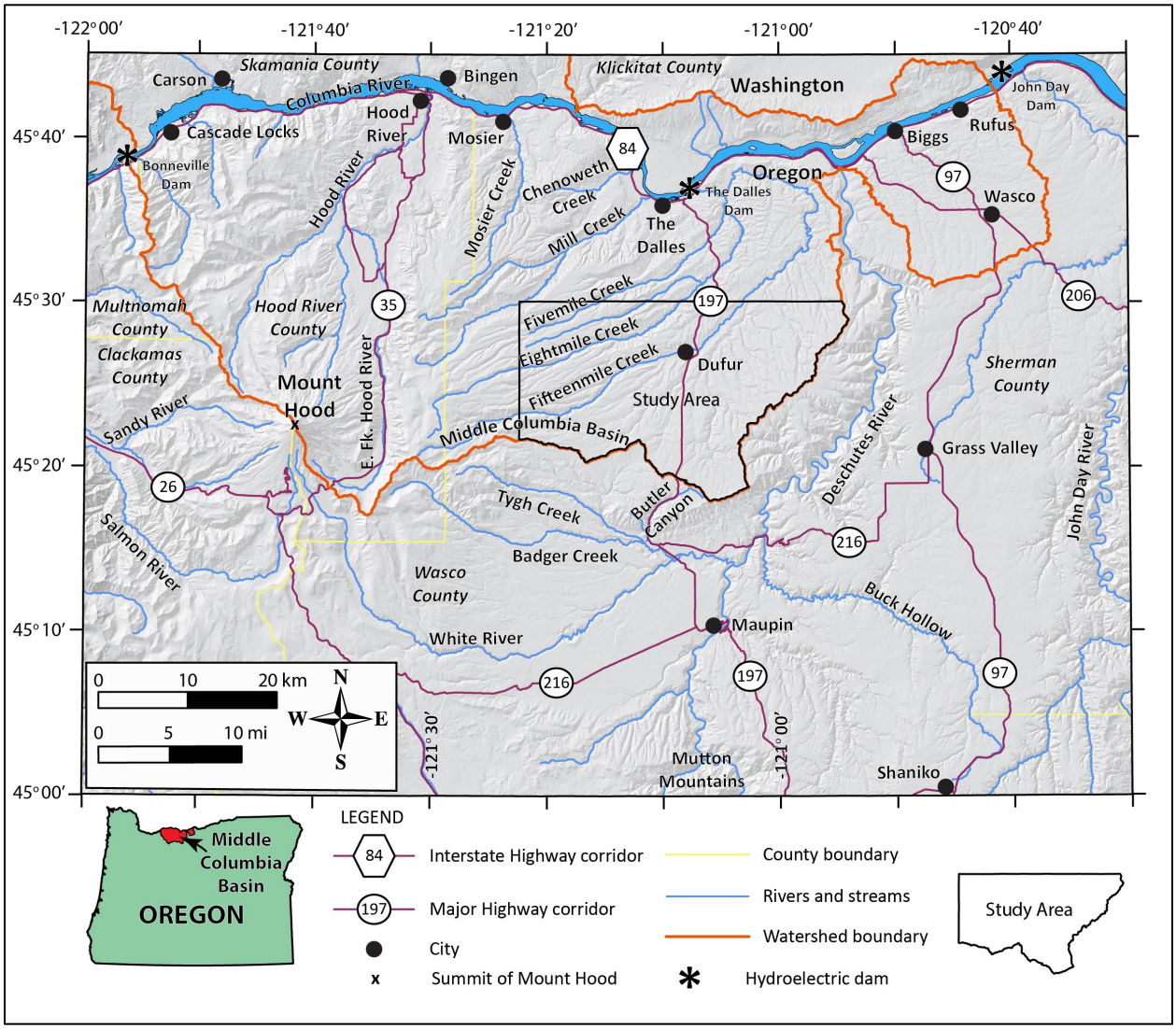

**Figure 1-2. Status map of geologic mapping completed, in progress, and planned in the Middle Columbia Basin. The yellow-shaded area encompasses geologic mapping in the Dufur area completed for this report. Orange-shaded quadrangles include areas that have been mapped by DOGAMI with funding from OWRD and STATEMAP between 2011 and 2020. Blue-shaded quadrangles include areas where geologic mapping is currently being conducted by the USGS (FEDMAP). Purple-shaded quadrangles include targets of future geologic mapping by DOGAMI. Label abbreviations are as follows: B—Bingen; BD—Bonneville Dam; C—Carson; CL—Cascade Locks; D—Dufur; GV—Grass Valley; HR—Hood River; JDD—John Day Dam; R—Rufus; TD—The Dalles; TDD—The Dalles Dam; W—Wasco.**

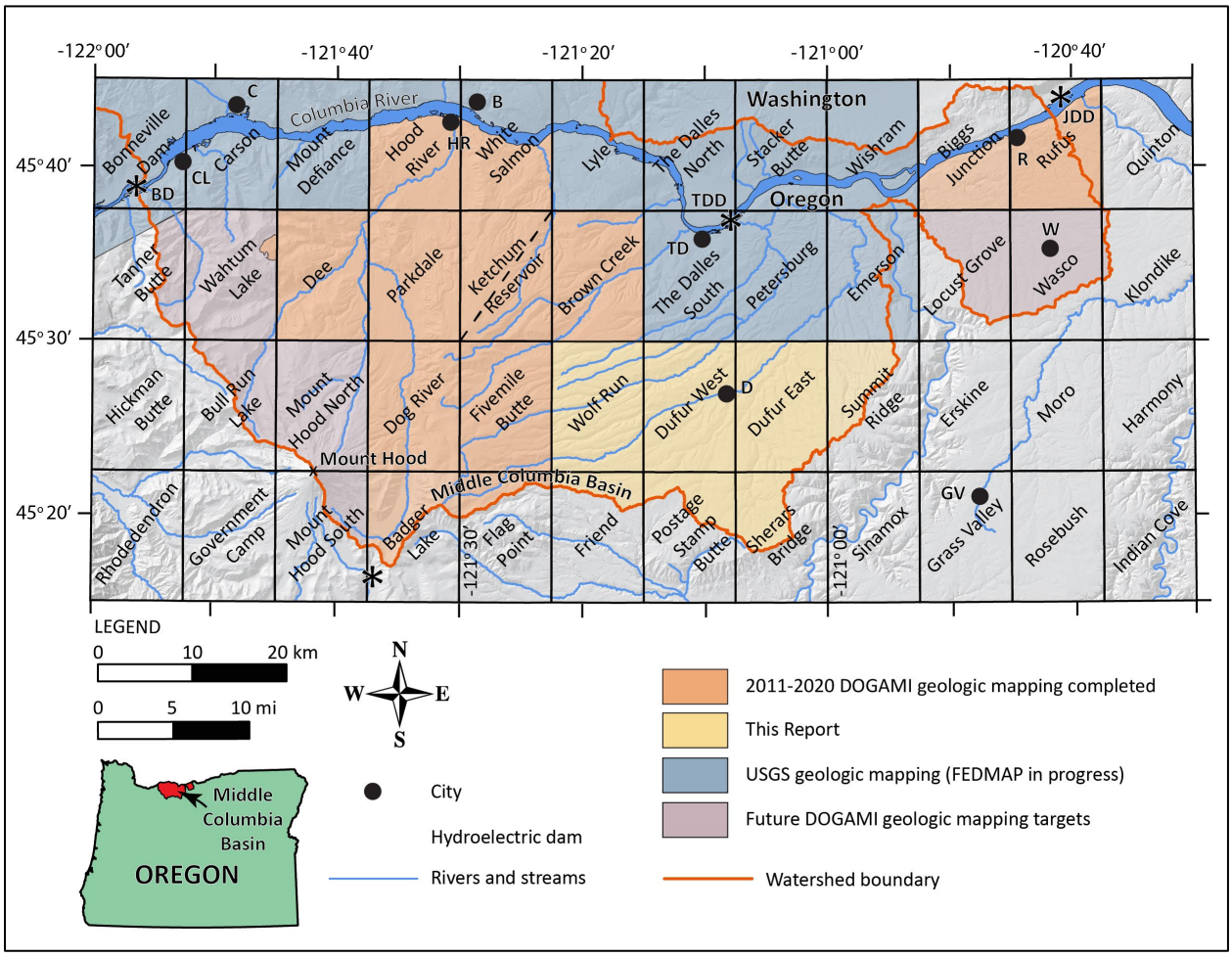


## 2.0 GEOGRAPHY

The Dufur area encompasses an area of ~567 km² (219.1 mi²) in the southeast part of the Middle Columbia Basin in north-central Oregon (**Figure 1-1**, **Figure 1-2**). The Middle Columbia Basin extends from the city of Wasco and John Day Dam on the east to Mount Hood and Bonneville Dam on the west and to Butler Canyon on the south. The northern part of the basin is bound by the Columbia River Gorge. Major tributaries to the Columbia River include Hood River, Mosier Creek, Mill Creek, Fivemile Creek, Eightmile Creek, Fifteenmile Creek, and Deschutes River (**Figure 1-1**, **Figure 1-2**). This part of north-central Oregon is typically rugged, transitioning from the steep mountainous terrain of the Cascade Range on the west to more subdued broad plateaus and ridges incised by deep canyons on the east. Topographic relief in the Middle Columbia Basin is substantial ranging from 3,428 m (11,244 ft) at the summit of Mount Hood along

the crest of the Cascade Range to 23 m (75 ft) at the Columbia River at Bonneville Dam (**Figure 1-1**). In the Dufur area, elevations range from 1,116 m (3,660 ft) southwest of Friend to 305 m (1,002 ft) along Fifteenmile Creek as it exits the northeastern part of the map area. Climate varies across the Middle Columbia Basin due to its transitional location between the wet marine airflow-dominated Cascade Range and the semi-arid continental climate of eastern Oregon. The upland and western parts of the basin have a relatively wet climate, averaging ~77 cm (30.5 in) of precipitation annually (NOAA, 2020). The rain shadow of the Cascade Range reduces annual precipitation eastward sharply to <40 cm (15.8 in) across the semi-arid eastern part of the Middle Columbia Basin (NOAA, 2020; **Figure 1-1**).

Most of the Dufur area is privately held range and agricultural land. The far western edge of the Wolf Run and Friend 7.5′ quadrangles (Plate 3) includes public national forest land managed by the US Forest Service (USFS). U.S. Highway 197 is the major transportation corridor in the Dufur area, bisecting the project area from south to north (**Figure 1-1**). Dufur Mill Road runs from the city of Dufur west to Oregon Highway 35, through the Mount Hood National Forest. A number of other local paved and graveled roads provide access to the remainder of the map area.

## 3.0 METHODOLOGY

The suite of CRBG and Cascade Range volcanic rocks mapped in the Dufur area is stratigraphically complex, reflecting the variable processes of deposition and reworking of volcanic and volcaniclastic units adjacent to a structurally active subaerial volcanic arc environment. Thus, reliable map correlations, even of similar appearing stratigraphic sequences, benefits greatly from the use of detailed digital lidar-based geologic mapping, combined with numerous direct field observations. Conventional lithologic criteria, in combination with geochemical analyses, corroborating isotopic ages, and measurements of natural remanent magnetization were used to assign rocks and deposits to geologic map units. Comparative visual analysis of unanalyzed rocks with analyzed rocks, in the context of stratigraphic position, allowed for wider correlation of map units.

Mapping presented in this report was collected digitally using a GPS-enabled Apple® iPad® 4, loaded with Esri™ Collector, following standard DOGAMI procedures outlined in Duda and others (2018, 2019). Detailed field mapping used 1-m lidar DEMs (8 pts/$m^2$), USGS digital raster graphics (DRGs) of traditional topographic maps, and digital Esri™ imagery as basemaps. Fieldwork conducted during this study consisted of data collection along main highways and roads, combined with numerous traverses across private lands mapping lithologic contacts and faults.

Geologic linework portrayed on the geologic map is based upon detailed observations at more than 1,000 field stations visited by the authors between 2014 and 2018. Supplementary lithologic information was obtained from comparison of more than 450 rock samples collected from field sites. Lithologic map correlations also rely on 420 new and 17 compiled X-ray fluorescence (XRF) whole rock geochemical analyses, 11 Inductive Coupled Mass Spectrometry (ICP-MS) and Inductive Coupled Atomic Emission Spectrometry (ICP-AES) geochemical analyses of rocks from hot-spring alteration zones, 6 X-ray diffraction (XRD) analyses of rocks from hot-spring alteration zones, 12 new $^{40}Ar/^{39}Ar$ and 2 compiled K-Ar isotopic ages, petrographic analysis of 43 thin-sections, 226 field measurements of natural remanent magnetization, and 580 field and remotely collected orientation measurements (Plates 1, 2, and 3; Appendix).

In this report, volcanic rocks with fine-grained (<1 mm [0.04 in]; Mackenzie and others, 1997; Le Maitre and others, 2004) average crystal or particle size in the groundmass are characterized in the following manner:

- A coarse groundmass if the average crystal or particle size is <1 mm (0.04 in) and can be determined using the naked eye (>~0.5 mm [0.02 in]).
- A medium groundmass if crystals of average size cannot be determined by eye but can be distinguished by using a hand lens (>~0.05 mm [0.002 in]).
- A fine groundmass if crystals or grains of average size can be determined only by using a microscope, or by hand lens recognition of sparkle or sheen in reflected light, indicating the presence of crystalline groundmass.
- A glassy groundmass if the groundmass has (fresh), or originally had (altered), groundmass with the characteristics of glass (e.g., conchoidal fracture; sharp, transparent edges; vitreous luster; etc.).
- Mixtures of crystalline and glassy groundmass are described as intersertal; ratios of glass to crystalline materials may be indicated by textural terms including holocrystalline, hypocrystalline, hyalophitic, hyalopilitic, and holohyaline.
- Microphenocrysts are defined as crystals larger than the overall groundmass and <1 mm across (0.04).

Grain size of clastic sedimentary rocks is described following the Wentworth (1922) scale. Hand samples of unconsolidated sediments and clastic sedimentary rocks were compared in the field and/or in the laboratory to graphical representations (comparator) of the Wentworth scale to determine average representative grain size in various parts of a respective sedimentary geologic unit.

Whole-rock XRF geochemical data are essential for separating difficult-to-distinguish lava flows and pyroclastic rocks into eruptive units in the volcanic-dominated terrain of the Dufur area. Many lava flows are too fine grained and glassy to be adequately characterized by mineralogical criteria alone and lithologically and mineralogically similar appearing units may have meaningfully different chemical signatures. Descriptive rock unit names for volcanic rocks are based in part on the online British Geological Survey classification schemes (Gillespie and Styles, 1999; Robertson, 1999; Hallsworth and Knox, 1999), and normalized major element analyses plotted on the total alkali ($Na_2O + K_2O$) versus silica ($SiO_2$) diagram (TAS) of Le Bas and others (1986), Le Bas and Streckeisen (1991), and Le Maitre and others (1989, 2004). Whole-rock geochemical samples were prepared and analyzed by XRF at the Washington State University GeoAnalytical Lab, Pullman, Washington, and at the Department of Geosciences, Franklin and Marshall College, Lancaster, Pennsylvania (Appendix). Analytical procedures for the Washington State University GeoAnalytical Lab are described by Johnson and others (1999) and are available online at https://environment.wsu.edu/facilities/geoanalytical-lab/technical-notes/. Analytical procedures for the Franklin and Marshall X-ray laboratory are described by Boyd and Mertzman (1987) and Mertzman (2000), and are available online at http://www.fandm.edu/earth-environment/laboratory-facilities/xrf-and-xrd-lab. Major element determinations are normalized to a 100-percent total on a volatile-free basis and recalculated with total iron expressed as FeO*. Further details of this process are described in the Appendix under the heading *Geochemistry*.

Individual CRBG units can be difficult to identify with certainty in the field, but can be distinguished on the basis of a multi-criteria mapping approach using stratigraphic position and thickness, geochemistry, magnetic polarity, paleomagnetic analysis of oriented core samples, and petrography following the work of Swanson and others (1979a,b), Reidel and others (1989), Beeson and others (1985, 1989), Wells and others (1989, 2009), and Hooper (2000) (**Figure 5-7**, **Figure 5-10**). The primary uncertainties in accurately mapping these flows arise from: 1) poor exposure and recognition of flow contacts; 2) intraflow chemical variation; and 3) the effect of weathering on chemical composition (Wells and others, 2009). Where lava flows are correlated chemically, we follow the work of Wells and others (2009) and use FeO*

<11 weight percent as an indicator of weathered samples (Appendix). In areas of isolated outcrops, or where additional analytical techniques could not be applied, a lithologic approach to mapping these units was used by comparing outcrop samples to hand sample standards obtained from detailed and stratigraphically continuous reference sections in Hood River and Butler Canyon.

The distribution of alteration zones in the Dufur area is defined on the basis of field mapping during the current study and unpublished mineral resource reports archived by DOGAMI. Eleven samples obtained from hot-spring alteration zones in the Dufur area were analyzed at ALS Chemex (ALS) in Reno, Nevada by ICP-MS and ICP-AES methods using their ME-MS41 analytical package. Six additional samples were analyzed by XRD at the Department of Geosciences, Franklin and Marshall College, Lancaster, Pennsylvania under the direction of S. A. Mertzman. Detailed analytical procedures for the Franklin and Marshall X-ray laboratory are described by Boyd and Mertzman (1987) and Mertzman (2000) and are available online at http://www.fandm.edu/earth-environment/laboratory-facilities/xrf-and-xrd-lab. Further details of this process are described in the Appendix under the heading *Alteration Geochemistry*.

Our mapping presents 12 new $^{40}Ar/^{39}Ar$ ages (Plates 1 and 2; Appendix). Samples for age determinations were prepared and analyzed by Dr. Dan Miggins at the College of Oceanic and Atmospheric Sciences, Oregon State University, Corvallis (OSU). The methodology for $^{40}Ar/^{39}Ar$ geochronology at OSU is summarized in Duncan and Keller (2004) and the OSU laboratory website http://geochronology.coas.oregonstate.edu/. Two additional K-Ar ages in the area come from studies by Anderson (1987) and Gray and others (1996) (Plate 1; Appendix). Numerical ages assigned to dated units are described using standard conventions in reporting age in millions of years ago (mega-annum, abbreviated Ma) for units >1 m.y. old. Further details of this process are described in the Appendix under the heading *Geochronology*.

The magnetic polarity of strongly magnetized lava flows was determined at numerous outcrops in the Dufur area using a handheld digital fluxgate magnetometer (Appendix). Magnetic polarity reversals, commonly preserved by volcanic rocks and readily measured in the field, provide for: 1) distinguishing between flow units with normal and reversed magnetic polarity; 2) a check on the permissible age of isotopically-dated samples, when compared to the paleomagnetic time scale (Cande and Kent, 1992); and 3) another means to constrain possible depositional ages for some undated strata. Further details of this process are described in the Appendix under the heading *Natural Remanent Magnetization*.

Orientation measurements of geological planes (e.g., inclined bedding) were obtained in the field area by traditional compass and clinometer methods and compiled from data published by previous workers. Additional bedding measurements were generated using a routine and model developed by DOGAMI in Esri ArcGIS™ Model Builder to calculate three-point solutions from lidar bare-earth DEMs (Duda and others, 2018, 2019). Further details of this process are described in the Appendix under the heading *Orientation Points*.

Subsurface geology shown in the geologic cross sections incorporates lithologic interpretations from water-well drill records available through the Oregon Water Resources Department (OWRD) GRID system (Plate 1; Appendix). An attempt was made to locate water wells and other drill holes that have well logs archived by OWRD. Approximate locations were estimated using a combination of sources, including internal OWRD databases of located wells, Google Earth™, tax lot maps, street addresses, and aerial photographs. The accuracy of the locations ranges widely, from errors up to 0.8 km (0.5 mi) for wells located only by Township/Range/Section (2.6 $km^2$ [1 $mi^2$]) and plotted at the section centroid to a few tens of meters for wells located by address or tax lot number on a city lot with bearing and distance from a corner. For each well, the number of the well log is indicated in the database. This number can be combined with the first four letters of the county name (e.g., WASC 50922), to retrieve an image of the

well log from the OWRD web site (http://apps.wrd.state.or.us/apps/gw/well_log/). Water wells in the map area are sparse; a database of 209 located water-well logs with interpreted subsurface geologic units is provided in the Appendix. Further details of this process are described in the Appendix ander the heading *Water Wells*.

Microsoft Excel® spreadsheets tabulating geochemical and geochronological analyses, magnetic polarity, orientation measurements, and well points are provided as part of this publication. The Appendix contains a more detailed summary of data collection methods and a list of the data fields for the spreadsheets mentioned above.

New mapping was compiled with published and unpublished data and converted into digital format using Esri ArcGIS™ ArcMAP™ GIS software. On-screen digitizing was performed through heads-up digitizing using georeferenced 1-m lidar DEMs, 1:24,000-scale USGS digital raster images (DRGs) of traditional topographic maps, hillshade derivative of USGS 10-m DEMs, and 2014 and 2018 National Agriculture Imagery Program digital orthophotos. Remote sensing of the locations of both contacts and faults is improved through the use of enhanced 1-m lidar DEMs, processed using the Sky-View Factor computation tool (Zakšek and others, 2011). The Sky-View Factor computation tool is part of the Relief Visualization Toolbox (RVT), open-source processing software produced by the Institute of Anthropological and Spatial Studies at the Research Centre of the Slovenian Academy of Sciences and Arts (ZRCSAZU), to help visualize raster elevation model datasets (http://iaps.zrc-sazu.si/en/rvt#v). Sky-View visualizes hillshade models using diffuse illumination, overcoming the common problem of direct illumination, which can obscure linear objects that lie parallel to the direction of the light source and saturation of shadow areas. Surficial units within the project area were delineated on the basis of geomorphology as interpreted from a combination of field observations, 1-m lidar DEMs, 2014 and 2018 National Agriculture Imagery Program orthophotos, USGS 7.5' topographic maps, and Natural Resources Conservation Service soils maps (Green, 1982). Digitization and the final digital Esri ArcGIS™ format geodatabase was completed at a minimum scale of 1:8,000, supported by 3D visualization of lidar topographic data in Quick Terrain Modeler™ (Duda and others, 2018, 2019). The geologic time scale used is the 2020 (v2020/01), version of the International Stratigraphic Commission on chronostratigraphic chart (https://stratigraphy.org/chart) revised from Gradstein and others (2004), Ogg and others (2008), and Cohen and others (2013). Colors given for hand-sample descriptions are from the Geological Society of America Rock-Color Chart Committee (1991).

Geographic map coordinates (decimal degree, datum = WGS84) are provided for outcrop photographs shown for report figures, allowing the interested reader to visit these sites in the field or to remotely visualize the area using Google Earth™. Coordinates can be entered into the "Fly to" box (e.g., 45.661323, -121.471230) in the search toolbar and Google Earth™ will automatically locate and focus on the specified site.

## 4.0 PREVIOUS WORK

The Dufur area was mapped in this study as part of a larger effort to construct an updated geologic framework for the Middle Columbia Basin (**Figure 1-1**, **Figure 1-2**). The index map shown in **Figure 4-1** graphically summarizes the sources of mapping reviewed for our geologic depiction and other sources consulted during the preparation of this report. **Table 4-1** shows a list of previous regional geologic investigations reviewed during the current geologic study of the Dufur area. Reports listed in **Table 4-1** are organized in chronological order; those shown in bold are geologic maps that lie within the Dufur study area. Earlier geologic maps and reports displaying the bedrock geology in the Dufur area include

those by Piper (1932), Waters (1968), Swanson and others (1981), Bela (1982), Sherrod and Scott (1995), and Sherrod and Smith (2000). A county soil survey produced for Wasco County (Green, 1982) by the Soil Conservation Survey and the Natural Resources Conservation Service was used locally to interpret the distribution of surficial units. This soil survey has been digitized and is available online through the Natural Resources Conservation Service at http://soildatamart.nrcs.usda.gov/.

**Figure 4-1. Sources of regional geologic mapping reviewed and consulted during the preparation of the Dufur area geologic maps and this report. See DataSourcePolys feature class in the geodatabase. Study area shown by a white outline.**

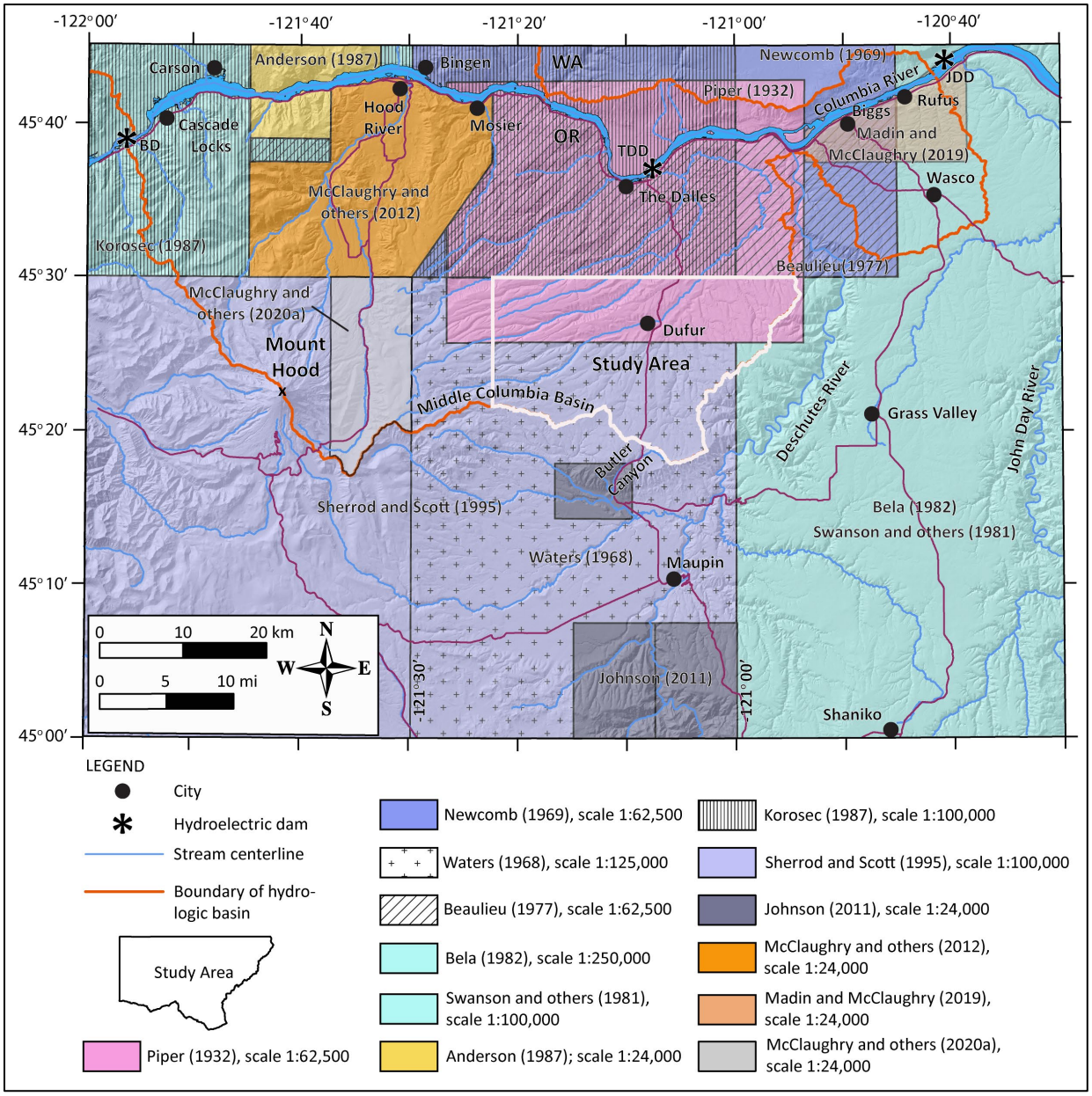

**Table 4-1. Partial chronological listing of maps and reports on which this study builds. Maps shown in boldface are totally or partially within the study area.**

| Author | Year | Subject | Scale |
|---|---|---|---|
| **Piper** | **1932** | **Geology and ground-water resources of The Dalles region** | **1:62,500** |
| **Waters** | **1968** | **Geologic map of the Dufur Quadrangle** | **1:62,500** |
| Newcomb | 1969 | Tectonic structure/groundwater Mosier area | 1:62,500 |
| Shannon and Wilson | 1973 | Boardman Nuclear Project | 1:250,000 |
| Beaulieu | 1977 | Geologic Hazards of Parts of Northern Wasco County | 1:62,500 |
| **Swanson and others** | **1981** | **Regional geologic map of the Columbia River Basalt Group** | **1:100,000** |
| Beeson and others | 1982 | Geologic map and geothermal potential Hood River area | |
| **Bela** | **1982** | **Geologic map Dalles 1- × 2-degree quadrangle** | **1:250,000** |
| **Green** | **1982** | **Soil Survey Wasco County** | **GIS** |
| Beeson and others | 1985 | Frenchman Springs Member Columbia River Basalt | |
| Korosec | 1987 | Geologic map Hood River 30 X 60-minute quadrangle | 1:100,000 |
| Anderson | 1987 | Geologic map Columbia River Gorge area | 1:24,000 |
| Lite and Grondin | 1988 | Groundwater/geology Mosier area | 1:24,000 |
| **Sherrod and Scott** | **1995** | **Geologic map Mount Hood 30 x 60-minute quadrangle** | **1:100,000** |
| Conrey and others | 1996 | Isotopic ages Hood River/Mount Hood area | |
| Gray and others | 1996 | Isotopic ages Hood River/Mount Hood area | |
| Conrey and others | 1997 | Petrology Cascade arc | |
| **Sherrod and Smith** | **2000** | **Geologic map of the Cascade Range in Oregon** | **1:500,000** |
| Tolan and others | 2002 | Evolution of the Columbia River | |
| Wells and others | 1989 | Columbia River Basalt, Columbia River Gorge | |
| Wells and others | 2009 | Columbia River Basalt, Columbia River Gorge | |
| Johnson | 2011 | Geologic map of Tygh Ridge and Dant areas | 1:24,000 |
| McClaughry and others | 2012 | Geologic map of the Hood River Valley | 1:36,000 |
| Burns and others | 2012 | Evaluation of basalt aquifers near Mosier | GIS |
| Martin and others | 2013 | Revisions to the stratigraphy of the Frenchman Springs Member | |
| Reidel and Tolan | 2013 | The Grande Ronde Basalt, Columbia River Basalt Group | |
| Lite | 2013 | Hydrogeology of the Mosier area | |
| McClaughry and others | 2020a | Geologic map of the Dog River/Badger Lake 7.5' quadrangles | 1:24,000 |

# 5.0 GEOLOGIC AND TECTONIC SETTING

The Dufur area lies along the eastern side of the Cascade Range in northern Oregon, ~ 46 km (28.5 mi) east of Mount Hood volcano (**Figure 1-1**; Plates 1, 2, and 3). The Cascade Range is a north-south-trending volcanic arc stretching for ~1,300 km (800 mi) between northern California and southern British Columbia (**Figure 5-1**). Volcanoes making up the range and their eroded remnants are the observable magmatic expression of oblique convergence since ~40 Ma along the Cascadia subduction zone, where the offshore Juan de Fuca tectonic plate is subducted beneath North America (**Figure 5-1**; Lux, 1982; Phillips and others, 1986; Verplanck and Duncan, 1987; Conrey and others, 2002; Sherrod, 2019). The Cascade Range in Oregon is traditionally separated into two subprovinces on the basis of this ~40 m.y. geologic history: the Western Cascades and High Cascades (**Figure 5-2**; Dicken, 1965). The Western Cascades subprovince is a deeply eroded terrane of Eocene to Pliocene volcanic and sedimentary rocks, while the High Cascades encompasses the Pliocene to Holocene little eroded, active volcanic arc, including major young volcanoes (e.g., Mount Hood).

**Figure 5-1. Tectonic setting of the northwest United States and southwest Canada showing regional plate boundaries, the Cascadia subduction zone, volcanoes of the Cascade Range, and the location of the study area in north-central Oregon. The deformation front (red line) is defined by bathymetry where the abyssal plain meets the continental slope and is inferred to represent the surface projection of the Cascadia megathrust. Modified from Nelson and others (2006).**

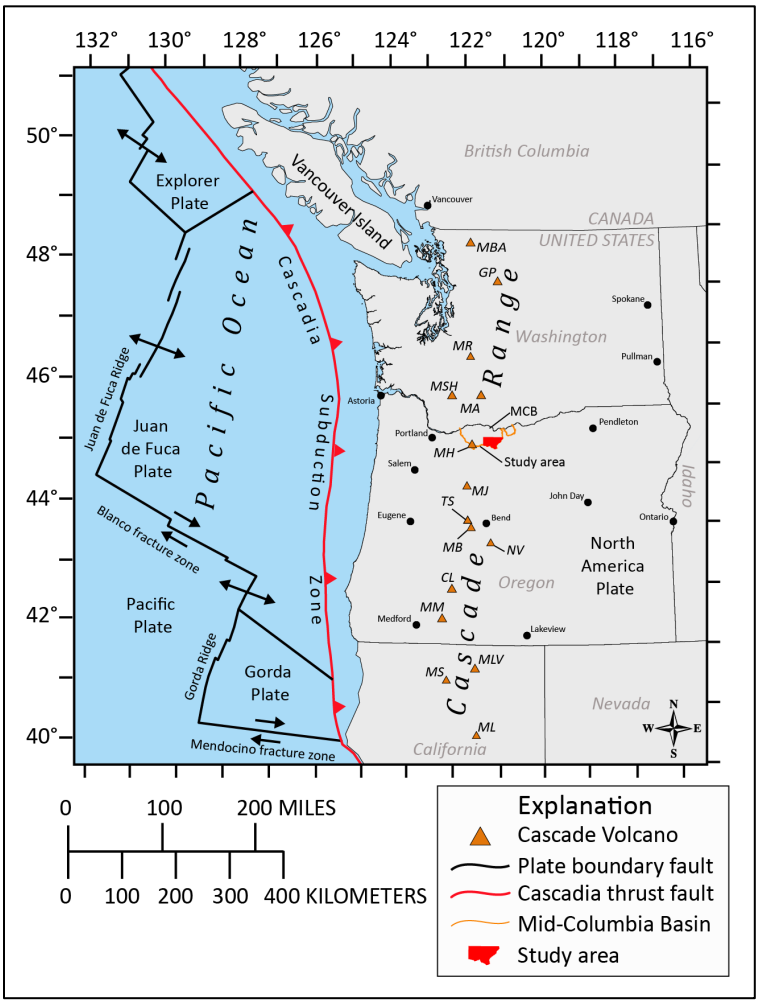

**Figure 5-2. Map of the Cascade Range in the Pacific Northwest showing geographic locations, approximate extent of the Western (tan) and High Cascades (purple), and the relationships of some major structural features of Oregon (*following page*). Note that the names Western Cascades and High Cascades are not used in Washington or south of Mount Shasta in California. The study area is shown by a red polygon in north-central Oregon. Numerals 1,2, and 3 refer to the three segments of the High Cascades graben from south to north: 1) Green Ridge segment, 2) middle segment, and 3) Hood River graben. Labels: BV – Boring Volcanic Field; HRF – Hood River fault zone; HCF – Horse Creek fault zone; GCF – Gales Creek fault; GRF – Green Ridge fault zone; PB – Portland Basin; PHF – Portland Hills fault; MCB – Middle Columbia Basin (orange outline); MHFZ – Mount Hood fault zone; SV – Simcoe Mountains; TB – Tualatin Basin. Labeled physiographic provinces are outlined by gray lines. Oregon physiographic provinces after Dicken (1965). Washington physiographic provinces are from Washington Department of Natural Resources (https://www.dnr.wa.gov/programs-and-services/geology/explore-popular-geology/geologic-provinces-washington).**

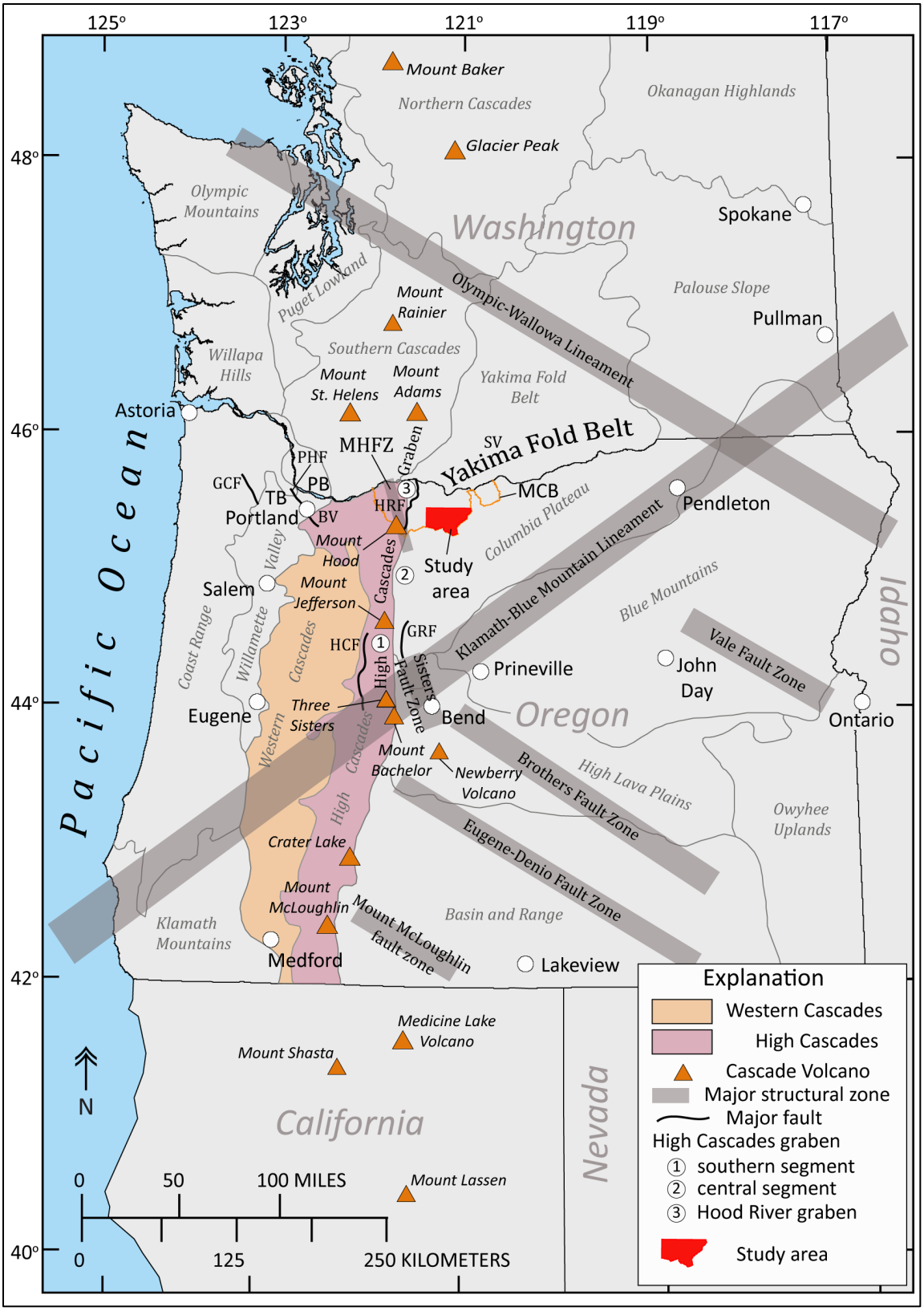
125°
123°
121°
119°
117°
48°
46°
44°
42°
40°
Mount Baker
Northern Cascades
Okanagan Highlands
Glacier Peak
Olympic Mountains
Washington
Spokane
Puget Lowland
Olympic-Wallowa Lineament
Palouse Slope
Mount Rainier
Pullman
Willapa Hills
Southern Cascades
Mount St. Helens
Mount Adams
Yakima Fold Belt
Astoria
Yakima Fold Belt
MHFZ
Graben
SV
PHF
GCF
TB
PB
MCB
Pendleton
Portland
BV
HRF
Columbia Plateau
Mount Hood
Study area
Valley
Cascades
Salem
Mount Jefferson
Klamath-Blue Mountain Lineament
Blue Mountains
Idaho
Pacific Ocean
Coast Range
Willamette
Cascades
HCF
GRF
High
Sisters
Fault Zone
Prineville
John Day
Vale Fault Zone
Eugene
Three Sisters
Western
Cascades
Bend
Oregon
Ontario
Mount Bachelor
Newberry Volcano
Brothers Fault Zone
High Lava Plains
High
Cascades
Owyhee Uplands
Crater Lake
Eugene-Denio Fault Zone
Mount McLoughlin
Basin and Range
Klamath Mountains
Medford
Mount McLoughlin fault zone
Lakeview
Medicine Lake Volcano
Mount Shasta
N
California
Nevada
Mount Lassen
0
50
100 MILES
0
125
250 KILOMETERS
Explanation
Western Cascades
High Cascades
Cascade Volcano
Major structural zone
Major fault
High Cascades graben
① southern segment
② central segment
③ Hood River graben
Study area

## 5.1 Yakima Fold Belt

The axis of the High Cascades in north-central Oregon is superimposed across the Yakima Fold Belt, a series of northeast-southwest-trending, asymmetric, locally overturned and faulted anticlinal ridges separated by broad synclinal valleys (**Figure 5-2**; Swanson and others, 1979a,b, 1981; Anderson, 1987; Watters, 1989; Reidel and Campbell, 1989; Tolan and Reidel, 1989; Anderson and others, 2013). The Yakima Fold Belt occurs over much of the western and west-central Columbia Plateau (Oregon) and Yakima Fold Belt (Washington State) physiographic provinces and continues westward through the Cascade Range (**Figure 5-2**; Tolan and others, 2009a). Structural deformation associated with the Yakima Fold Belt may occur as far west as the Oregon Coast Range, where Siletz River and younger rocks are broadly folded along northeast-trending fold axes (**Figure 5-2**; McClaughry and others, 2010).

Folds in the Yakima Fold Belt are generally east-west-trending across eastern Oregon and Washington, while across the Cascade Range, fold axes are more northeast in trend (Swanson and others, 1981; Bela, 1982; Reidel and others, 1989; Tolan and others, 2009a). East-west-directed folds in the Yakima Fold Belt east of the Cascade Range are inferred to have formed in response to a general north-south compressional regime (Reidel and others, 1989; Beeson and Tolan, 1990), while northeast-directed folds in the northern Oregon Cascade Range indicate a stress regime with the major compressive stress oriented northwest-southeast (Venkatakrishnan and others, 1980; Williams and others, 1982). Northeast-trending folds between the Dufur area and the Cascade Range are locally segmented by north-northwest-striking cross faults (N.20°W. to N.30°W.; **Figure 5-3**). Previous workers in the Columbia River Gorge and on the Columbia Plateau have referred to these faults as wrench faults (Anderson, 1987).

Deformation in the Yakima Fold Belt has persisted since at least the early to middle Miocene, with a majority of the present structural relief developing since ~10.5 Ma (Reidel and others, 1989; Tolan and others, 2009a). Structural warping in the western part of the Yakima Fold Belt during the middle Miocene is inferred to have increasingly restricted the distribution of the younger parts of the Grande Ronde, Wanapum, and Saddle Mountains Basalts to structural lows in the Columbia River Gorge and Willamette Valley (Vogt, 1981; Beeson and others, 1985; Anderson and Tolan, 1986). Successively younger lava flows, most notably lava flows in the Priest Rapids and Pomona Members, were partially or wholly confined to paleocanyons, possibly structurally controlled by the Yakima Fold Belt. The thickness and distribution of these CRBG units through the Columbia River Gorge locally show evidence of restricted distribution and thinning across anticlines, although these ancient channel remnants do not precisely correspond to present-day structural highs and lows (Anderson, 1987; Anderson and Vogt, 1987; Beeson and Tolan, 1990).

Folds continued to develop in post-CRBG time, as large accumulations of volcaniclastic and sedimentary detritus shed from the late Miocene Cascades (e.g., Dalles Formation) preferentially accumulated in basins along synclinal troughs. Thrust faults associated with the growth of anticlinal ridges in the Yakima Fold Belt regionally remained active following deposition of the ~9 to 5 Ma Dalles Formation. Regional thrust faults in the vicinity of Dufur area include the Tygh Ridge thrust fault (south of the map area), North Fork Mill Creek thrust fault (northwest of the map area; J.D. McClaughry unpublished geologic mapping, 2016), and Hellroaring Creek thrust fault (southwest of the map area; McClaughry and others, 2020a) (**Figure 5-3**). Compressional deformation in the Middle Columbia Basin has continued into the Pliocene and Pleistocene. Lava flows as young as 3.05 Ma, are broadly folded and are structurally dismembered by fold-associated, north-northwest-striking strike-slip or oblique-slip faults in the Hood River Valley (**Figure 5-3**; McClaughry and others, 2012). Similarly oriented normal or oblique slip faults in the Dog River-Mill Creek divide fault zone along East Fork Hood River show

significant lateral and vertical offset of geologic units as young as 1.87 Ma (McClaughry and others, 2020a). Other evidence for recent activity on north-northwest-striking faults in the wider Middle Columbia Basin is found where these structures are redirecting modern stream drainages (McClaughry and others, 2012). Spatial and crosscutting relationships between folds, thrust faults, and strike-slip faults indicate a mutual development of all three components during progressive deformational phases occurring in the Yakima Fold Belt from the early to middle Miocene to late Pliocene (Anderson, 1987).

**Figure 5-3. Physiographic map of the Dufur area and greater Mount Hood region, highlighting structural features. Red outline is the study area (*following page*). Mapped faults are shown as black lines. Fold axes are shown as magenta lines. Label abbreviations are as follows: BB – Badger Butte; BH – Booth Hill; BR – Bluegrass Ridge; BRFZ – Blue Ridge Fault Zone; CCT – Cat Creek thrust fault; CF – Chenoweth (Reverse) fault; CL – Clear Lake; DRMF – Dog River-Mill Creek divide fault zone; EF – East Fork Hood River; FM – Fifteenmile Creek; GCWF – Gate Creek-Wyeth fault; GP – Grasshopper Point; GPF – Gibson Prairie fault; HCT – Hellroaring Creek thrust fault; HRF – Hood River fault zone; HRV –Hood River Valley; MCFZ – Mays Canyon Creek fault; MM – Middle Mountain; MMF – Multorpor Mountain fault; MT – North Fork Mill Creek thrust fault; PL – Parkdale Lava; PFZ – Pine Creek fault zone; PCFZ – Pocket Creek fault zone; RPF – Rocky Prairie thrust fault; TLF – Twin Lakes fault; UHRV – Upper Hood River Valley; WCF – Whiskey Creek thrust fault. Question mark over dashed line identifies the location of an inferred concealed thrust fault underlying the Upper Hood River Valley.**

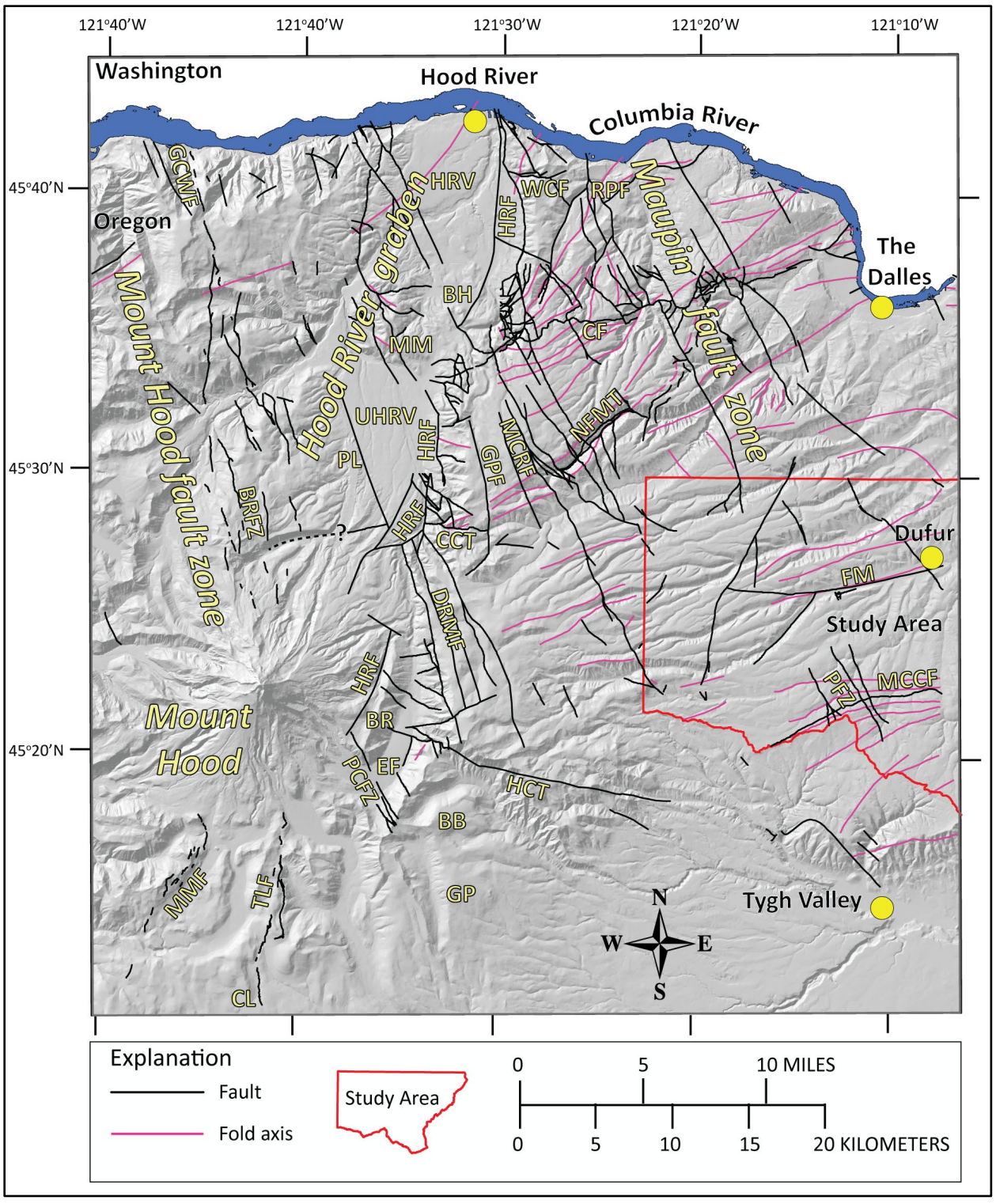
121°40'W
121°40'W
121°30'W
121°20'W
121°10'W
45°40'N
45°30'N
45°20'N
Washington
Oregon
Hood River
Columbia River
The Dalles
Dufur
Study Area
Tygh Valley
Mount Hood
Mount Hood fault zone
Hood River graben
Maupin fault zone
GCWF
HRV
WCF
RPF
HRF
BH
CF
MM
UHRV
PL
MCRF
NFMT
GPF
BRFZ
CCT
DRMF
FM
MCCF
PFZ
BR
EF
PCFZ
HCT
BB
GP
MMF
TLF
CL
N
W
E
S
Explanation
Fault
Fold axis
Study Area
0
5
10 MILES
0
5
10
15
20 KILOMETERS

## 5.2 High Cascades graben

Since ~3.7 Ma, compressional deformation in the north-central Oregon part of the Yakima Fold Belt has been accompanied by and overprinted by extension and intra-arc graben formation along the axis of the High Cascades (**Figure 5-1**, **Figure 5-2**; McClaughry and others, 2020a). From the Three Sisters (Oregon) north to Mount Adams (Washington State), the High Cascades occupy an ~30-km-wide (18.6 mi) structural graben formed by a northward propagating rift (**Figure 5-2**; Allen, 1966; Taylor, 1981; Williams and others, 1982; Smith and Taylor, 1983; Smith and others, 1987; Conrey and others, 2002; McClaughry and others, 2012, 2013, 2020a). The High Cascades graben is segmented into three northward younging parts, including a southern segment between the Three Sisters and Mount Jefferson, a central segment between Mount Jefferson and Mount Hood, and a northern segment between Mount Hood and Mount Adams known as the Hood River graben (the respective segments are numbered 1 through 3 in **Figure 5-2**; Conrey and others, 2002; Conrey and others, 2019). Older rocks, which along strike are foundered within the graben, crop out near the Cascade Range crest in the vicinity of Mount Jefferson and Mount Hood, thus precluding the presence of a significant through-going rift or graben as originally proposed by Allen (1966). All segments of the graben are defined by significant offset along eastern boundary normal faults and asymmetric uplift of the western graben margin (**Figure 5-2**). Paleo-drainages west of the graben are elevated 600 to 800 m (1,969 to 2,625 ft) above modern base levels, suggesting broad uplift of the Western Cascades concurrent with rifting (Conrey and others, 2002). Tilted fault blocks invariably dip eastward off the structural high.

The segmented and structurally discontinuous High Cascades graben is time-transgressive, propagating northward from Green Ridge in central Oregon to Mount Adams in Washington State at an overall rate of 4 cm/yr (1.6 in/yr) since 5.3 Ma (**Figure 5-2**; Smith and others, 1987; Sherrod and Smith, 2000; Conrey and others, 2002). Geothermal drill-core data suggest a total subsidence of 3 km (1.9 mi) in the southern segment and 1 km (0.6 mi) in the central segment (Conrey and others, 2002), while subsidence in the Hood River graben is <1.2 km (0.7 mi) (**Figure 5-2**; McClaughry and others, 2012, 2013, 2020a). Subsidence developed along each graben segment as volcanic eruptions declined, typically after ~2 m.y. of elevated eruption rates. Pre-graben eruptions are notable for the presence of Mid-Ocean Ridge Basalt-like low-potassium tholeiites, iron-rich intermediate lava flows, rhyolites, and ash-flow tuffs (Conrey and others, 2002; McClaughry and others, 2012; Conrey and others, 2019; McClaughry and others, 2020a). The High Cascades graben corresponds to the area with the greatest production of Quaternary volcanic material in the Cascade Range of California, Oregon, and Washington (Williams and others, 1982).

## 5.3 Hood River graben

The Hood River graben is the northernmost segment of the High Cascades intra-arc graben, forming the complex tectonic depressions of the Hood River and Upper Hood River valleys (**Figure 5-2**, **Figure 5-3**; McClaughry and others, 2012, 2013, 2020a). The graben occurs from an area just south of Mount Hood, north ~50 km (31 mi) at least to Underwood Mountain along the north side of the Columbia River in Washington State. It is defined by an ~20- to 25-km-wide (12.4 to 15.5 mi) zone of distributed north-south oriented normal faults and complex graben subsidence, bounded by north-northwest-striking right-lateral normal-oblique slip master faults, including the Mount Hood fault zone on the west and Maupin fault zone on the east (**Figure 5-3**; Plate 1). Middle Mountain, a partially fault-bounded structural block

composed of Columbia River Basalt divides the Hood River graben into two rhombohedral-shaped segments identified as the Hood River and Upper Hood River Valleys (**Figure 5-3**).

The timing of initial graben formation in the Hood River area was contemporaneous with a major pulse of mafic volcanism in the northern Oregon Cascade Range between 4.4 and 2.1 Ma (Conrey and others, 1996; Gray and others, 1996; McClaughry and others, 2012, 2013, 2020a). This pulse of mafic volcanism was distinctly younger than a similar episode that had culminated in the southern segment of the High Cascades graben of central Oregon by ~5 Ma (**Figure 5-2**). It contrasts with the preceding ten million years, when andesitic eruptions dominated the northern Oregon Cascade Range (~14 to 5 Ma; Wise, 1969; Priest and others, 1983; Keith and others, 1985; Conrey and others, 1996). Subsidence may be time transgressive at the scale of the Hood River graben, chiefly post ~3.7 Ma on the south end at Mount Hood versus <3.05 Ma on the north at Hood River (**Figure 5-3**; McClaughry and others, 2012, 2013, 2020a).

The Hood River graben appears to share similar structural characteristics and a tectonic setting consistent with formation as a complex, transtensional fault-bounded pull-apart basin across the north-central part of the High Cascades. Classic pull-apart basins, described elsewhere and in theoretical models, are characterized as rhombic- to spindle-shaped basins, formed between two or more bounding strike-slip faults and bounded on their ends by diagonal transfer faults (Burchfiel and Stewart, 1966; Crowell, 1974; Wu and others, 2009). Relative motion of crustal blocks in a pull-apart basin can be either parallel to bounding displacement zones (pure strike-slip) or occur along faults oblique (transtensional) to the bounding displacement zones (Wu and others, 2009). The spindle- to rhombic-shape, association with middle Miocene to recent Yakima Fold Belt deformation and geographic position between two master north-northwest-trending right-lateral normal-oblique slip fault zones (e.g., Mount Hood fault zone on the west and Maupin fault zone on the east), suggests the Hood River graben's probable origin as a pull-apart basin (**Figure 5-3**). The transtensional nature of the Hood River graben is suggested by both oblique slip on bounding master faults and an eastern margin bounded longitudinally by a transverse system of oblique-slip faults (Hood River fault zone) possibly linking with bounding master faults (**Figure 5-3**) (McClaughry and others, 2012, 2020a). This interpretation of the Hood River graben is consistent with characteristics described in the Tualatin basin of the northern Oregon Coast Range, which shares a similar tectonic setting along the western edge of the Cascades volcanic arc, ~80 km (50 mi) west of Mount Hood (**Figure 5-2**; McPhee and others, 2014). Bennett and others (2019) suggested that the Hood River graben may accommodate both intra-arc rifting as well as the northward translation of rotating crustal blocks in the upper plate of the Cascadia subduction zone (**Figure 5-1**).

### 5.3.1 Hood River graben, eastern boundary

The eastern boundary of the Hood River graben is defined by the prominent west-facing escarpment of the Hood River fault zone (**Figure 5-3**; McClaughry and others, 2012, 2013, 2020a). The Hood River fault zone is ~50 km (31 mi) long, stretching from an area just north of Underwood Mountain in Washington State south to Bluegrass Ridge along the east flank of Mount Hood (**Figure 5-3**). The fault zone may continue farther south from Mount Hood where it joins more southern strands of the eastern boundary fault of the more extensive High Cascades graben, but its presence or precise location in that area is not well constrained (Sherrod and Pickthorn, 1989).

The Hood River fault zone is a 1- to 3-km-wide (0.6 to 2.0 mi) zone of generally north-striking and west-dipping, en echelon, down-on-the-west normal faults that run obliquely and link to the north-northwest-striking right-lateral normal-oblique slip faults **Figure 5-3**; McClaughry and others, 2020a). North-south-striking fault strands occur as discontinuous right-stepping en echelon faults that

progressively shift the location of the Hood River fault zone to the east, moving north from Mount Hood to the Columbia River (e.g., East Fork Hood River at the mouth of Crystal Springs Creek; Booth Hill area) (**Figure 5-3**; McClaughry and others, 2012, 2020a). The Hood River fault zone has accommodated hundreds of meters of vertical offset along the eastern graben margin since Pliocene and latest Pleistocene time, with cumulative displacement apparently progressively decreasing to the north. The Hood River graben shallows to the north, with local subsidence of at least 1,220 m (4,000 ft) on the south, in contrast to ~130 m (426 ft) at Hood River (McClaughry and others, 2012, 2020a).

### 5.3.2 Hood River graben, western boundary

The western boundary of the Hood River graben is notably obscure, but appears to be defined by the ~55-km-long (35 mi), north-northwest-striking Mount Hood fault zone (Madin and others, 2017), extending from the Columbia River south through the summit of Mount Hood volcano to Clear Lake (**Figure 5-3**). Components of the Mount Hood fault zone from north to south include the Gate Creek-Wyeth fault (Madin and others, 2017; Bennett and others, 2019), Blue Ridge fault zone (Sherrod and Scott, 1995; McClaughry and others, 2012; Madin and Ma, 2012; Madin and others, 2017), and the Twin Lakes fault (Madin and others, 2017). The Pocket Creek fault zone striking northwest along the southern end of Bluegrass Ridge lies along the southern end of the Mount Hood fault zone (**Figure 5-3**). Bennett and others (2019) recognized a protracted history of right-lateral normal-oblique fault slip along the 10- to 20-km-long (6 to 12.5 mi), north-northwest-striking and east-northeast-dipping Gate Creek-Wyeth fault, with ~100 to 200 m (328 to 656 ft) cumulative down-on-the-east vertical offset, antithetic to offset along the Hood River fault zone bounding the east side of the Hood River graben. The Blue Ridge fault zone on the northern flank of Mount Hood is a 12-km-long (7.5 mi) and 4.5-km-wide (2.8 mi) zone of normal faults (**Figure 5-3**; McClaughry and others, 2012; Madin and Ma, 2012; Madin and others, 2017). All but one segment in the Blue Ridge fault zone has west-side-down displacement (Madin and others, 2017), while Mount Hood fault zone strands between Gate Creek and Blue Ridge have variable senses of vertical offset, both to the west and east. The Twin Lakes fault at the southern end of the Mount Hood fault zone, extends for more than 12 km (7.5 mi) from Clear Lake to Oregon Highway 35 and consists of two en-echelon, west-dipping normal fault segments (**Figure 5-3**).

Quaternary activity is indicated on several of these faults, including the west-dipping Blue Ridge and east-dipping Gate Creek faults, as they locally offset late Pleistocene and/or Holocene glacial moraines (Madin and others, 2017; Bennett and others, 2019). Isotopic ages ($^{14}C$) obtained from organic material within the Blue Ridge fault zone shows evidence for a single earthquake event which occurred between ~13,540 and 9,835 years B.P. (Madin and others, 2017).

## 5.4 Stratigraphic and structural synopsis

The following synopsis summarizes the distribution, composition, lithology, and age of map units and structural development of the Dufur area. The Dufur area is characterized by a broadly folded and generally shallow north-dipping (~1° to 3°) section of Neogene volcanic and sedimentary rocks and Quaternary surficial deposits that provide a partial record of the volcanic, depositional, and deformational history in north-central Oregon since the early Miocene (**Figure 5-4**). The synopsis is divided on the basis of the broad periods of time used in the Explanation of Map Units starting on page 40 and shown in **Figure 5-5** and on Plates 1, 2, and 3. From oldest to youngest, broad geologic units in the Dufur area include: (a) the ~16.2 to 15.9 Ma CRBG; (b) ~9 to 5 Ma Dalles Formation; (c) ~3.8 to 3 Ma Pliocene volcanics; (d) ~2.6 to 1.87 Ma products of regional volcanoes; and (e) Late Pleistocene and Holocene surficial deposits.

**Figure 5-4. Generalized geology of north-central Oregon. Geology is from OGDC-6, compiled by Smith and Roe (2015). Study area shown by black outline. Solid orange line corresponds to the watershed hydrologic boundary of the Middle Columbia Basin. Label abbreviations are as follows: BD—Bonneville Dam; JDD—John Day Dam; TDD—The Dalles Dam.**

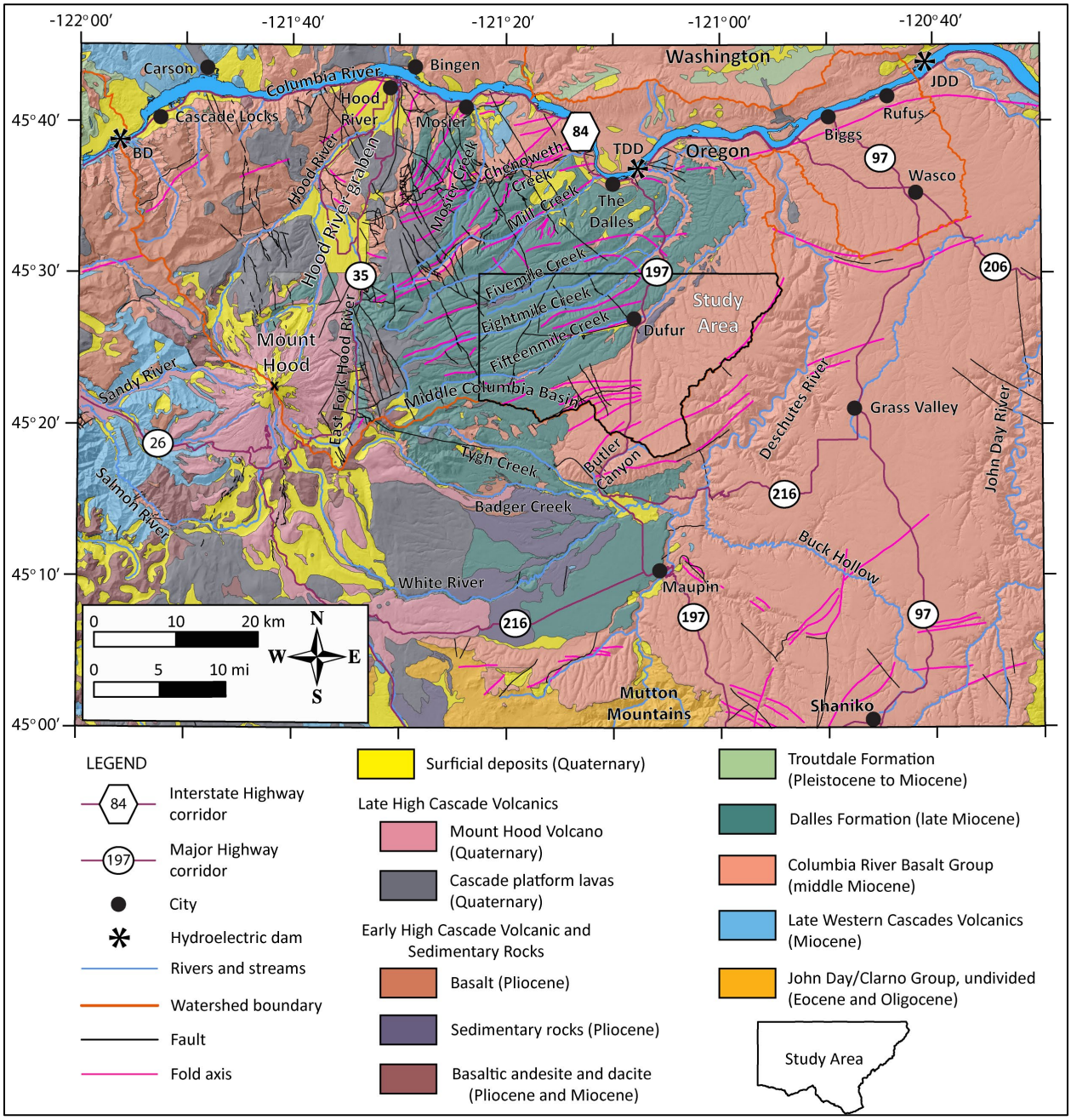

**Figure 5-5. Distribution of the broad geologic units mapped in the Dufur area. From oldest to youngest, broad geologic units in the Dufur area include: (a) CRBG; (b) Dalles Formation; (c) Pliocene to early Pleistocene volcanics; (d) Quaternary regional volcanoes; (e) surficial deposits.**

A. Columbia River Basalt Group
*~16.2 to 15.9 Ma*

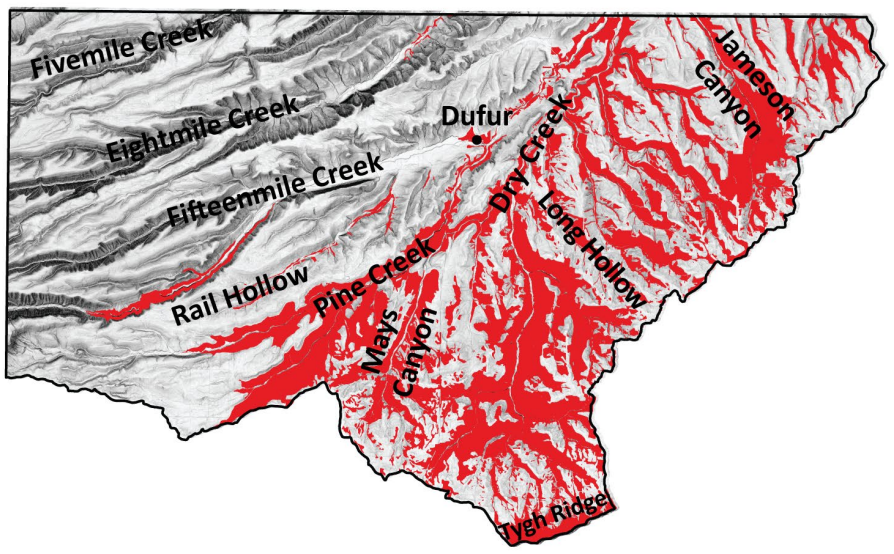


B. Dalles Formation
*~9 to 5 Ma*

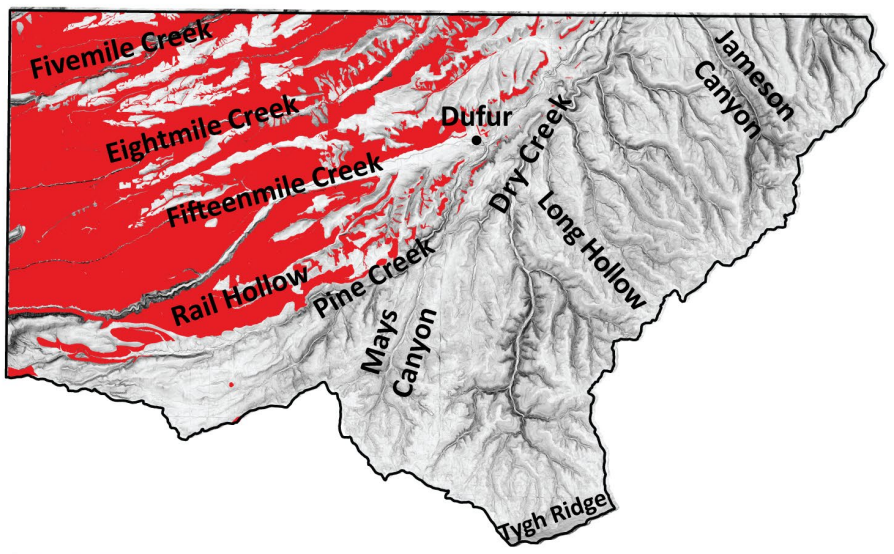


C. Pliocene to early Pleistocene volcanics *3.8 to 3 Ma*

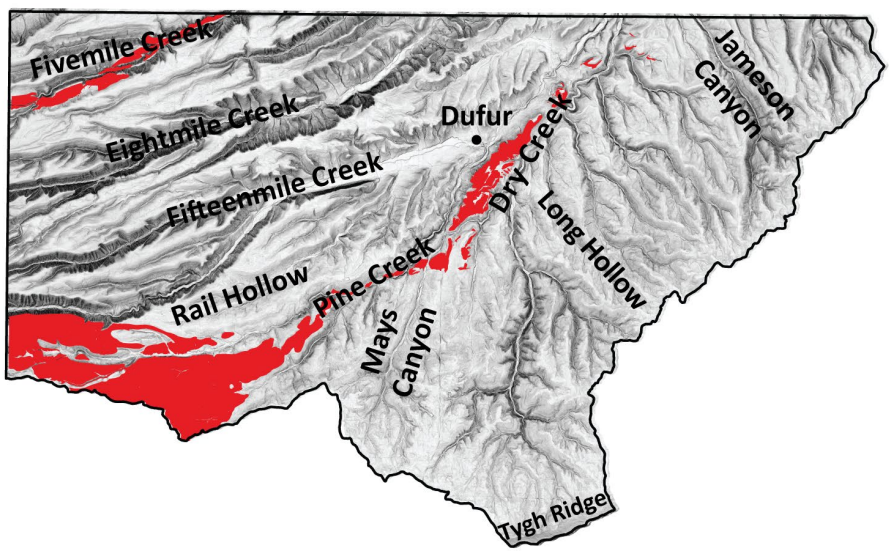


D. Quaternary regional volcanoes
*2.6 to 1.87 Ma*

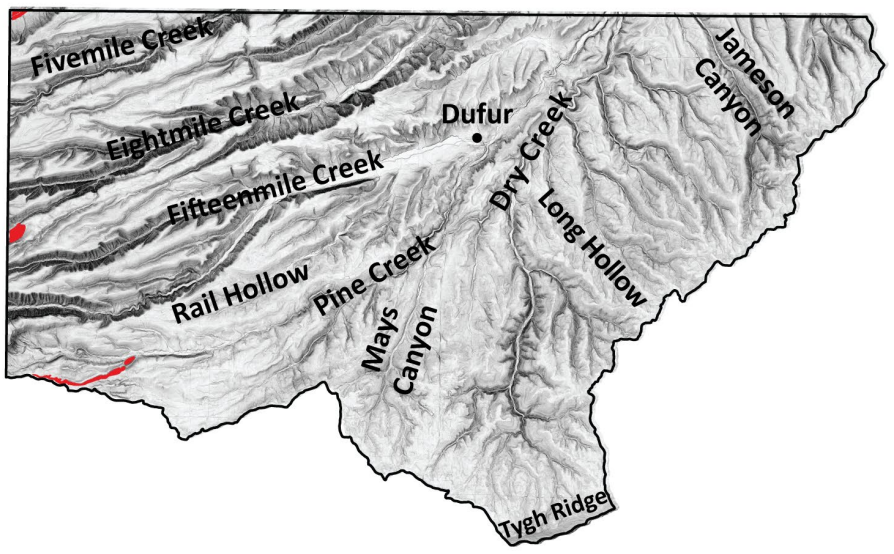


E. Surficial deposits
*Late Pleistocene and Holocene*

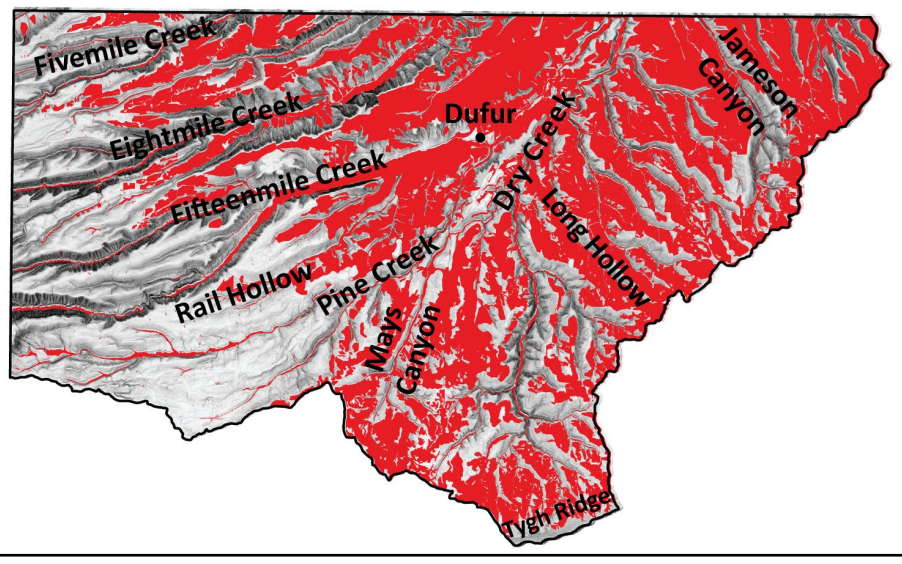

## 5.4.1 Lower to Middle Miocene volcanic rocks

### 5.4.1.1 Columbia River Basalt Group

#### 5.4.1.1.1 *Distribution, composition, and lithology*

The oldest exposed rocks in the Dufur area are part of the lower to middle Miocene CRBG, an extensive succession of tholeiitic basalt and basaltic andesite lava flows that cover more than 210,000 km$^2$ (130,488 mi$^2$) in parts of Washington, Oregon, and Idaho (**Figure 5-4**, **Figure 5-5**, **Figure 5-6**, **Figure 5-7**, **Figure 5-8**, **Figure 5-9**; **Figure 5-10**; Tolan and others, 1989; Reidel and others, 2013). Members of the CRBG exposed in the map area include the Priest Rapids Member (**Twpr**) and Frenchman Springs Member (**Twfs, Twfh, Twfg**) of the Wanapum Basalt and Sentinel Bluffs (**Tgsb**) and Winter Water (**Tgww**) members of the Grande Ronde Basalt (**Figure 5-7**, **Figure 5-10**; Plates 1, 2, and 3). A thick section of lava flows forming the N2 and R2 magnetostratigraphic units of the Grande Ronde Basalt (**Tgo**, **Tgac**, **Tgbc**, **Tggc**, **Tgu**) and Prineville Basalt (**Tpba, Tpbd**) are well exposed beneath the Winter Water Member (**Tgww**) just southeast of the map area in Butler Canyon (**Figure 5-4**, **Figure 5-7**). These older lava flows are presumed to be present in the subsurface in the Dufur area and are shown in the cross sections on Plates 1, 2, and 3. Generally thin (<2 m [6.6 ft]) and discontinuous horizons of fragmental sedimentary rock or paleosols are locally found separating individual lava flows. CRBG units commonly form distinctive bench and slope topography, resulting from differential erosion within and between flows. More easily erodible interflow zones are often marked by bands of trees, while more resistant flow interiors typically form continuous cliffs with grass-topped benches. Aggregate thickness of the CRBG in the map area is as much as 480 m (1,575 ft).

CRBG lava flows were erupted from north-northwest-striking linear fissure systems in the eastern part of the Columbia Plateau at ~16 Ma and flowed west through the Columbia Trans-Arc Lowland toward the low-relief topography of western Oregon (**Figure 5-6**; Tolan and Beeson, 1984; Beeson and others, 1985, 1989; Tolan and others, 1989; Wells and others, 1989, 2009; Kasbohm and Schoene, 2018). The Columbia Trans-Arc Lowland was a generally southwest-northeast-directed, ~60-km-wide (37 mi), topographic low laying across the ancestral Cascade Range during the early to middle Miocene (**Figure 5-6**; Beeson and others, 1989; Beeson and Tolan, 1990). The lowland was likely structural in origin and related to fold-deformation of Eocene to middle Miocene rocks underlying north-central Oregon; it was likely not related to the development of the early Cascades volcanic arc (Beeson and Tolan, 1990). The position of the lowland, however, may have influenced later development and growth of the volcanic arc in this area (Beeson and Tolan, 1990).

Geochemical analyses of CRBG lava flows across the Middle Columbia Basin are tholeiitic basalt and basaltic andesite ($SiO_2$ = 48.6 to 57.6 weight percent) with an enrichment in iron (FeO* = 10.23 to 16.86 weight percent; *n* = 588 analyses) (**Figure 5-8**, **Figure 5-9**). Older early Miocene Grande Ronde lava flows are siliceous basaltic andesite ($SiO_2$ = 52.99 to 57.6 weight percent; *n* = 70 analyses), with magnesium contents ranging between 3.10 and 5.22 weight percent MgO and titanium contents between 1.71 and 2.19 weight percent $TiO_2$. By contrast, younger lava flows making up the Wanapum Basalt, have basaltic compositions ($SiO_2$ = 48.6 to 52.88 weight percent; *n* = 500 analyses), with magnesium content ranging between 2.60 and 6.18 weight percent MgO and distinctly higher amounts of titanium (2.77 to 4.13 weight percent $TiO_2$), relative to Grande Ronde Basalt (**Figure 5-8**, **Figure 5-10**a). Lava flows in both the Wanapum and Grande Ronde Basalt can be distinguished on the basis of small but analytically significant variations in $TiO_2$, $P_2O_5$, MgO, CaO, Cr, Zr, and Ba (**Figure 5-10**). Mineralogy of the CRBG includes plagioclase and pyroxene; olivine is relatively sparse. Grande Ronde Basalt is generally aphyric and non-

distinctive, while the Wanapum Basalt contains widely scattered to locally abundant plagioclase phenocrysts up to 3 cm (1.2 in) across.

**Figure 5-6. Sketch map showing the outcrop distribution of the CRBG (orange fill). The extent of flows includes areas from which the lava flows have been eroded, in addition to areas where lava flows are concealed by younger units. Modified from Reidel and others (2013) and Ferns and McClaughry (2013). Label abbreviations are as follows: CJD – Chief Joseph Dike Swarm; PDG – Picture Gorge Dike Swarm; SD – Steens Dike Swarm; SM – Strawberry Mountain; ST – Steens Mountain.**

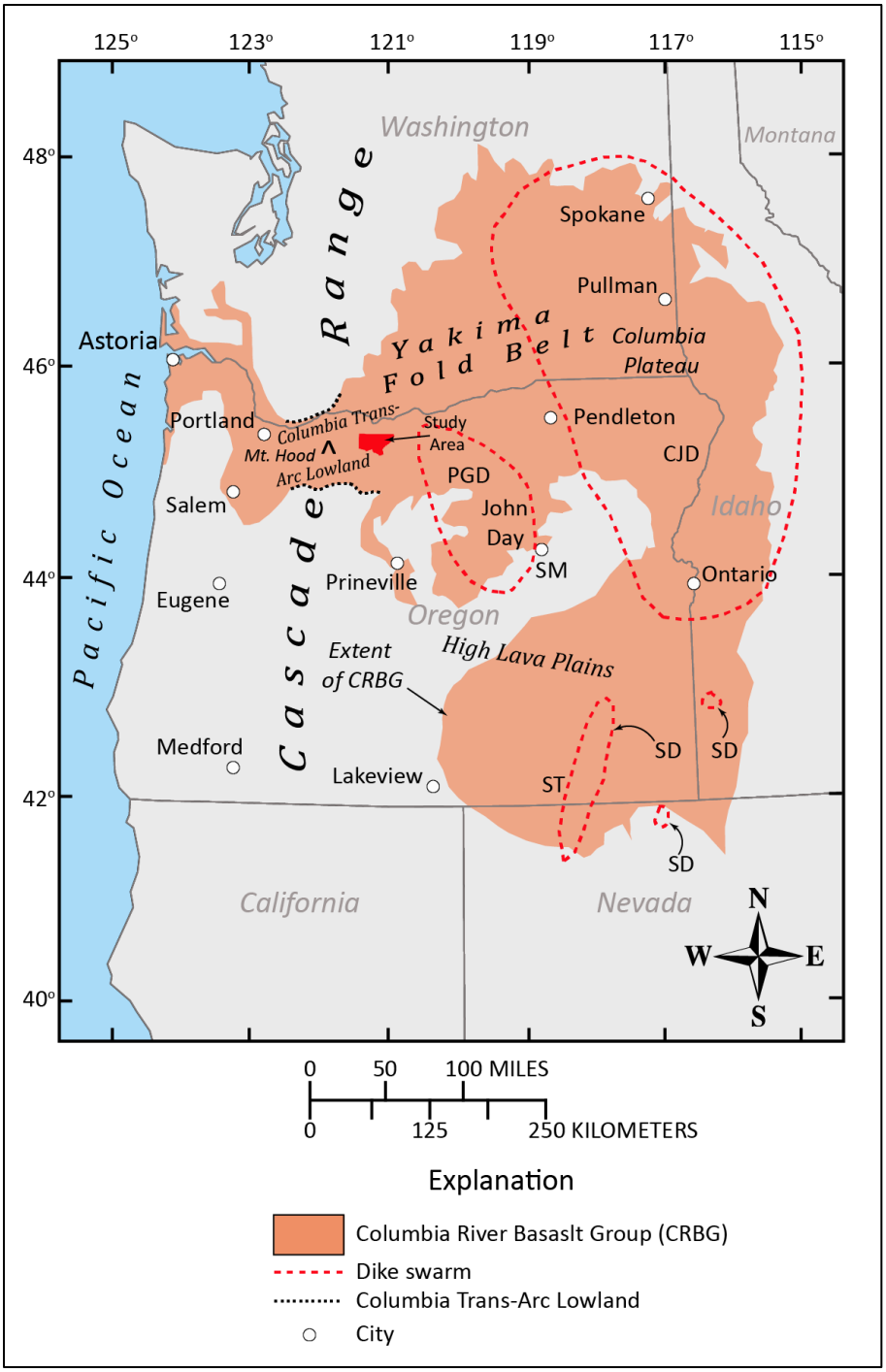

#### 5.4.1.1.2 *Age*

Isotopic dating of CRBG lava flows has struggled with accuracy and precision issues, complicating the development of an unambiguous chronology for the timing and duration of CRBG volcanism (Baksi, 2013; Barry and others, 2013). Isotopic dating of lava flows in the Grande Ronde Basalt by K-Ar and $^{40}Ar/^{39}Ar$ techniques suggests main-phase Grande Ronde eruptions occurred over a 0.4 m.y. interval, between ~16.0 and 15.6 Ma (**Figure 5-7**). The eruption of the younger Wanapum Basalt is considered to span a time period between ~15.6 and <15 Ma (Barry and others, 2010, 2013).

Work by Kasbohm and Schoene (2018) has established a more accurate and precise age model for the CRBG, improving understanding of the eruption timing of Wanapum and Grande Ronde lava flows that traversed the Columbia Trans-Arc Lowland (**Figure 5-6**). Kasbohm and Schoene (2018) examined silicic tuff interbeds between basalt lava flows in central and eastern parts of the Columbia Plateau, dating them by U-Pb geochronology on single zircon crystals (**Figure 5-6**). High precision U-Pb zircon dates of interbedded tuffs indicate slightly older ages for CRBG lava flow units across the Columbia Plateau, including those present in the Dufur area. The age of the Basalt of Rosalia (**Twpr**) in the Priest Rapids Member and the Frenchman Springs Member (**Twfs**, **Twfh**, **Twfg**) is now bracketed by U-Pb dates of 15.895 ± 0.019 Ma for ash between the Basalt of Rosalia and Basalt of Lolo and 16.066 ± 0.04 Ma for ash from the Vantage Horizon between the Basalt of Ginkgo (**Twfg**) and the Sentinel Bluffs Member (**Tgsb**) (**Figure 5-7**). Upper Grande Ronde lava flow units, including the Sentinel Bluffs (**Tgsb**), Winter Water (**Tgww**), Ortley (**Tgo**), and Grouse Creek (**Tggc**) members are bracketed by U-Pb dates of 16.066 ± 0.04 Ma for ash from the overlying Vantage Horizon and 16.254 ± 0.034 Ma for ash between the Wapshilla Ridge and Meyers Ridge Members of the underlying R2 magnetostratigraphic unit (**Figure 5-7**). U-Pb ages place an end to Grande Ronde volcanism at ~16 Ma, while >77 percent of Wanapum Basalt completed eruption prior to ~15.9 Ma.

**Figure 5-7. Chart showing stratigraphy and nomenclature for the CRBG (*following page*). Modified from Reidel and others (2002), with updated stratigraphy from Reidel and others (2013) and Reidel and Tolan (2013). Updated U/Pb ages from Kasbohm and Schoene (2018) shown in parentheses, for example (15.895). Updated $^{40}Ar/^{39}Ar$ ages from Mahood and Benson (2017) shown in square brackets, for example [16.54]. Selected $^{40}Ar/^{39}Ar$ ages for the Picture Gorge Basalt from Cahoon and others (2020) are shown in curly brackets, for example {16.06}. The age of the base of Steens Basalt from Moore and others (2018) is in vertical brackets, for example |16.97|. Geologic units exposed and interpreted in the subsurface in the Dufur area are shown in boldface.**

**Figure 5-7. (CRBG stratigraphy – *caption on previous page*)**

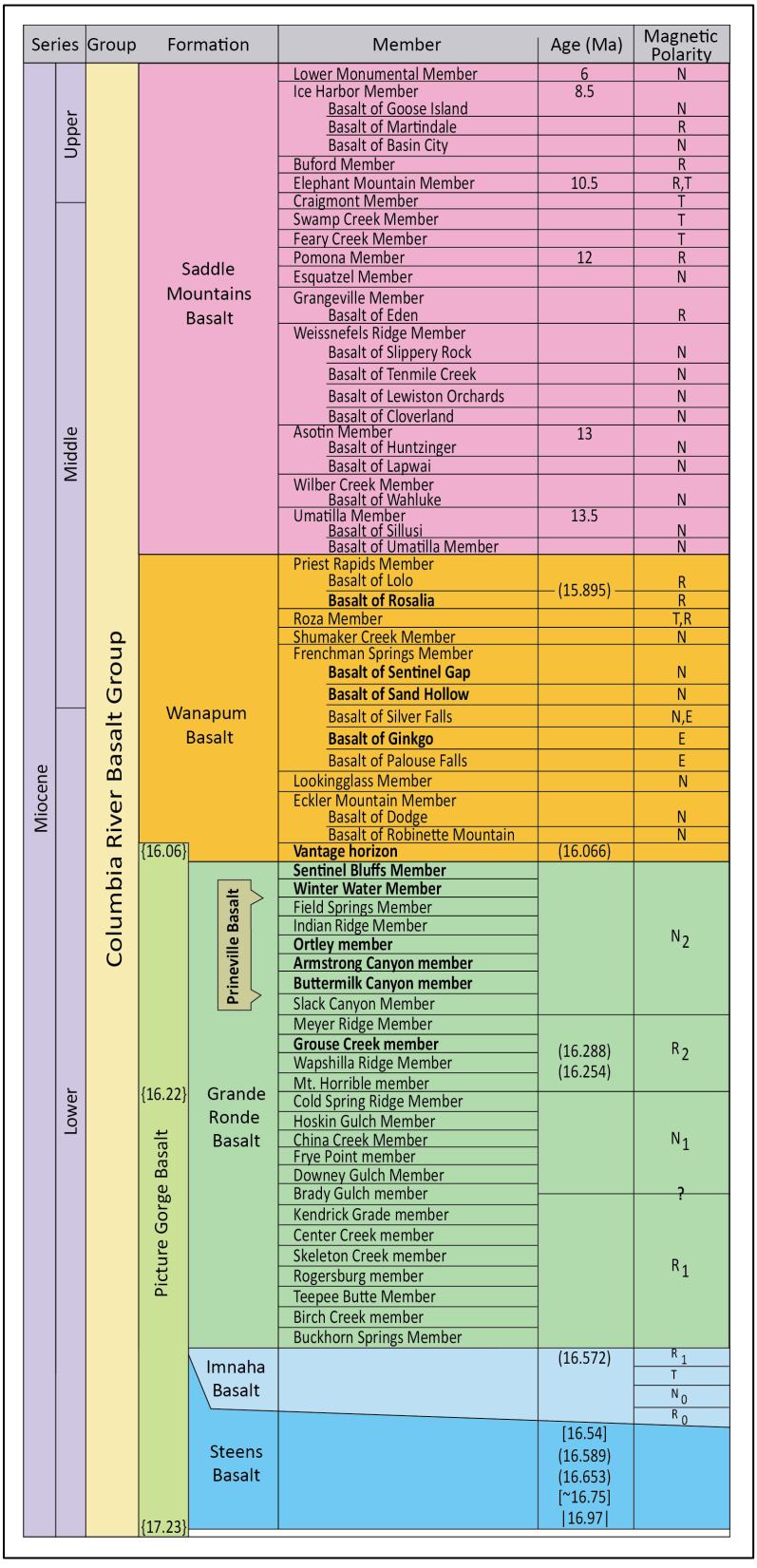

**Figure 5-8. Total alkalis ($Na_2O + K_2O$) vs. silica ($SiO_2$) (TAS) classification of the CRBG from whole-rock XRF analyses (normalized to 100 percent anhydrous). Fields and rock names are from Le Bas and others (1986) and Le Maitre and others (1989). Red-dashed line is the dividing line between alkaline, subalkaline/tholeiitic fields after Cox and others (1979). Data shown includes 588 CRBG analyses from the Middle Columbia Basin reported in this paper, McClaughry and others (2012), Madin and McClaughry (2019), and McClaughry and others (2020a). Additional data points are unpublished analyses in the Middle Columbia Basin collected by J.D. McClaughry (2014 to 2018). Note flows of the Saddle Mountains Basalt included in this diagram are not exposed in the Dufur area.**

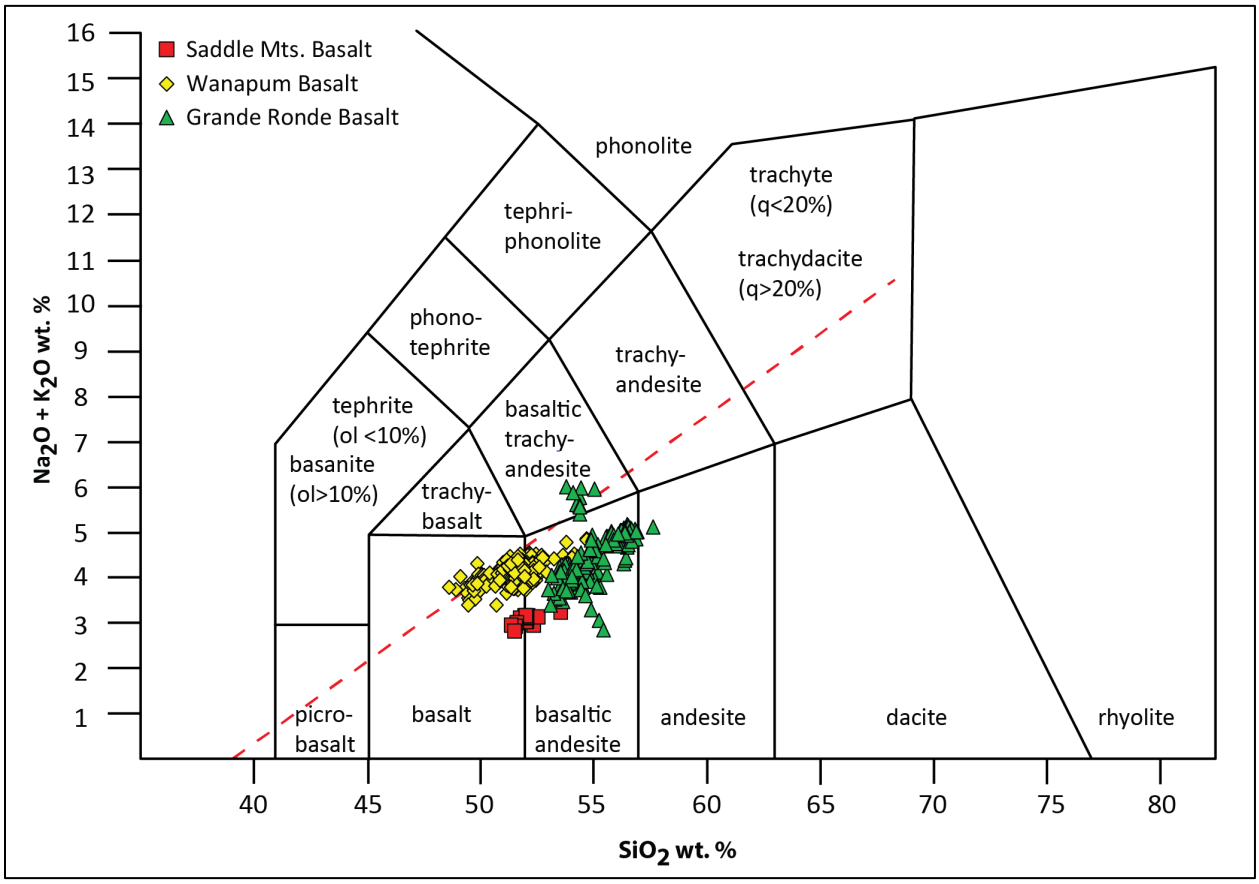

**Figure 5-9. Total iron/magnesium (FeO*/MgO) versus silica ($SiO_2$) diagram for CRBG lava flows wherein the FeO*/MgO ratio increases as $SiO_2$ increases. Tholeiitic and calc-alkaline dividing line is from Miyashiro (1974). Data include 588 CRBG analyses from the Middle Columbia Basin reported in this paper, McClaughry and others (2012), Madin and McClaughry (2019), and McClaughry and others (2020a). Additional data from J.D. McClaughry unpublished geologic mapping. Note flows of the Saddle Mountains Basalt are not exposed in the Dufur area.**

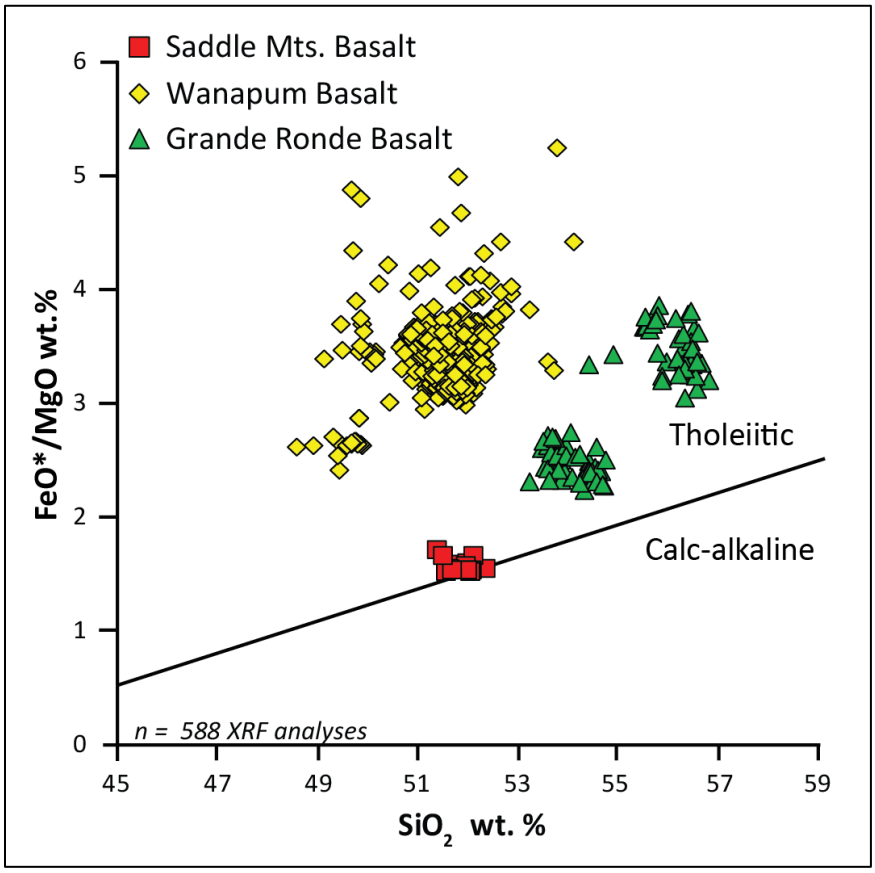

**Figure 5-10. Chemical variation diagrams for the CRBG.(a) Phosphorous ($P_2O_5$) versus titanium ($TiO_2$). The "titanium gap" is after Seims and others (1974). (b) Titanium ($TiO_2$) versus chromium (Cr). (c) Chromium (Cr) versus titanium/zirconium (Ti/Zr). (d) Phosphorous ($P_2O_5$) versus titanium/zirconium (Ti/Zr). Data includes 588 CRBG analyses from the Middle Columbia Basin reported in this paper, McClaughry and others (2012), Madin and McClaughry (2019), and McClaughry and others (2020a). Additional data from J.D. McClaughry unpublished geologic mapping. Note the Pomona, Lolo, Ortley, and Grouse Creek units are not exposed in the map area.**

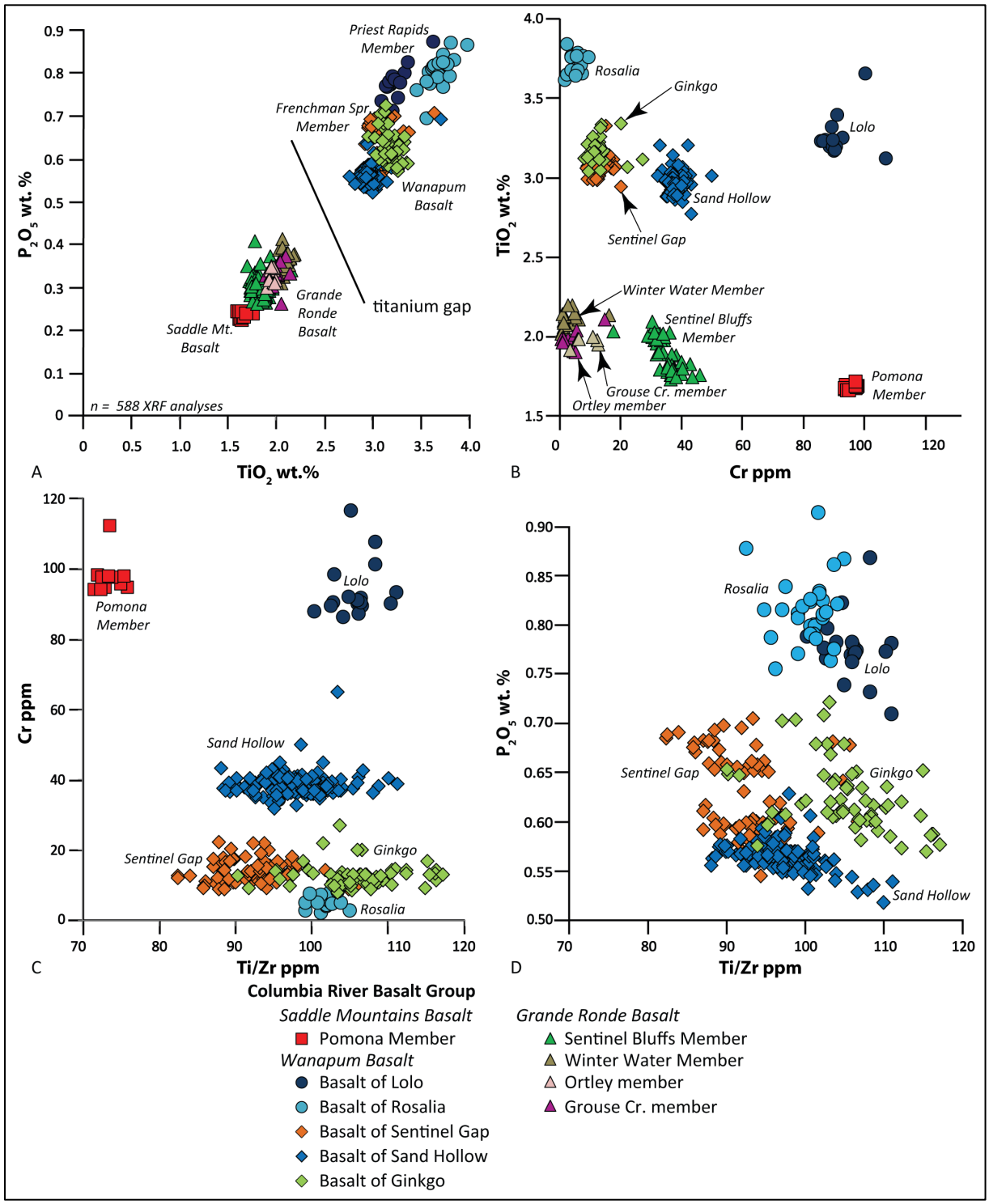

## 5.4.2 Lower Pliocene and upper Miocene volcanic and sedimentary rocks of the early High Cascades

### 5.4.2.1 Dalles Formation

#### 5.4.2.1.1 *Distribution, composition, and lithology*

Regional CRBG units in this part of north-central Oregon are unconformably overlain by volcanic and sedimentary rocks of the upper Miocene and lower Pliocene Dalles Formation (**Figure 5-5**). The Dalles Formation was emplaced across a broad constructional volcanic highland along East Fork Hood River and in areas underlying present day Mount Hood (McClaughry and others, 2020a). Correlative strata form a broad northeast-sloping arc-adjacent volcanic plain stretching ~40 km (25 mi) from East Fork Hood River, northeast to the Columbia River (**Figure 5-4**; McClaughry and others, 2020a). In the eastern escarpment of the Hood River graben, along East Fork Hood River, the Dalles Formation is characterized by interlayered vent-proximal lava flows and domes, hypabyssal intrusions, block-and-ash flow deposits, and ash-flow tuff (McClaughry and others, 2020a). Distal deposits mapped eastward to The Dalles and through the Dufur area, become increasingly rich in thick sections of block-and-ash-flow deposits, volcanogenic debris flow (lahar) deposits, hyperconcentrated flood-flow deposits, and ash-flow tuff, interbedded with horizons of fluvial conglomerate, sandstone, and siltstone (**Tmdl**, **Tmdg**, **Tmtw**, **Tmdt**, **Tmdd**, **Tmdtp**, **Tmdx**) (Plates 1, 2, and 3). Intracanyon lava flows (**Tmdj**, **Tmdv**, **Tmdw**) are nested into volcaniclastic rocks along several northeast-directed drainages (Plates 1 and 2). These lithologic associations indicate a transition from proximal volcanic dominated highlands along East Fork Hood River on the west to a more distal broad volcaniclastic apron on the east, characterized by east-northeast-directed stream drainages (**Figure 5-4**, **Figure 5-5**). The maximum thickness of the Dalles Formation in the map area is ≥343 m (1,000 ft) (Plates 1, 2, and 3). The formation thins and pinches out to the south and thickens northward toward The Dalles where it reaches a maximum thickness of ~457 m (1,500 ft) (**Figure 5-5**; Plates 1 and 2; Piper, 1932). The Dalles Formation is deeply incised in the eastern part of the Middle Columbia Basin, yielding a distinctive and rugged finger-mesa and canyon topography (**Figure 5-4**, **Figure 5-5**; Plates 1, 2, and 3).

Geochemical analyses of Dalles Formation volcanic units (primary deposits and clasts) in the Dufur area and analyses on lava flows and domes mapped further west (Wise, 1969; Gray and others, 1996; Westby, 2014; McClaughry and others, 2020a; J.D. McClaughry unpublished geologic mapping) show the formation is dominated by medium- to low-potassium calc-alkaline andesite and dacite, with $SiO_2$ ranging between 57.47 and 67.35 weight percent and $K_2O$ ranging between 0.42 and 2.22 weight percent (avg $K_2O$ = 1.27 weight percent at $SiO_2$ = 63.83 weight percent [avg]; *n* = 199 analyses) (**Figure 5-11**; **Figure 5-12a**). Intermediate composition rocks also contain characteristically low concentrations of yttrium (Y<32 ppm; avg Y = 15 ppm), high-field strength elements, such as barium (Ba <573 ppm; avg Ba = 308 ppm), niobium (Nb<19.1 ppm; avg Nb = 8.3 ppm) and zirconium (Zr<248 ppm; avg Zr = 148 ppm), and the light rare earth elements, such as lanthanum (La<39 ppm; avg La = 17 ppm) and cerium (Ce<61 ppm; avg Ce = 34 ppm) (**Figure 5-12**). The 7.91 Ma dacite of Wolf Run (**Tmdw**) is enigmatic in the Dalles Formation, having markedly higher potassium (avg = 2.87 weight percent $K_2O$ at 64.38 weight percent $SiO_2$ [avg]; *n* = 13 analyses), zirconium (avg Zr = 317 ppm), niobium (avg Nb = 15.9 ppm), lanthanum (avg La = 35 ppm), and cerium (avg Ce = 66 ppm). Mineralogy of Dalles rocks includes plagioclase, pyroxene (orthopyroxene ≥ clinopyroxene), and ± hornblende.

**Figure 5-11. Total alkalis ($Na_2O + K_2O$) vs. silica ($SiO_2$) (TAS) classification of Miocene and Pliocene volcanic rocks in the Dufur area from whole-rock XRF analyses (normalized to 100 percent anhydrous). Fields are from Le Bas and others (1986) and Le Maitre and others (1989). Red-dashed line is the dividing line between alkaline (above), subalkaline/tholeiitic (below) fields after Cox and others (1979). Data from this paper, Wise, (1969), Gray and others (1996), Westby (2014), and McClaughry and others (2020a). Additional data from unpublished analyses in the Middle Columbia Basin collected by J.D. McClaughry (2014 to 2018).**

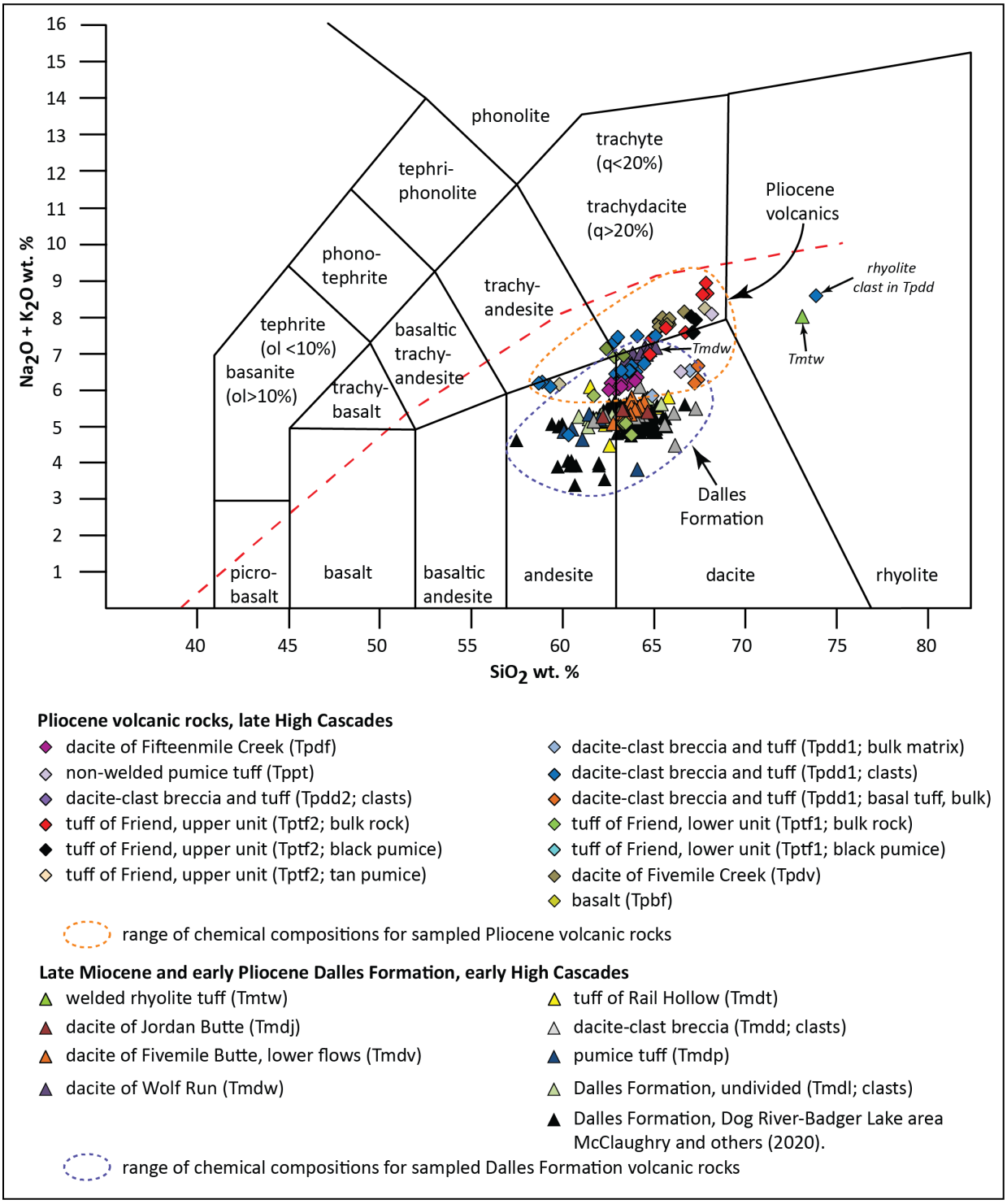


**Pliocene volcanic rocks, late High Cascades**

- dacite of Fifteenmile Creek (Tpdf)
- non-welded pumice tuff (Tppt)
- dacite-clast breccia and tuff (Tpdd2; clasts)
- tuff of Friend, upper unit (Tptf2; bulk rock)
- tuff of Friend, upper unit (Tptf2; black pumice)
- tuff of Friend, upper unit (Tptf2; tan pumice)
- dacite-clast breccia and tuff (Tpdd1; bulk matrix)
- dacite-clast breccia and tuff (Tpdd1; clasts)
- dacite-clast breccia and tuff (Tpdd1; basal tuff, bulk)
- tuff of Friend, lower unit (Tptf1; bulk rock)
- tuff of Friend, lower unit (Tptf1; black pumice)
- dacite of Fivemile Creek (Tpdv)
- basalt (Tpbf)

range of chemical compositions for sampled Pliocene volcanic rocks

**Late Miocene and early Pliocene Dalles Formation, early High Cascades**

- welded rhyolite tuff (Tmtw)
- dacite of Jordan Butte (Tmdj)
- dacite of Fivemile Butte, lower flows (Tmdv)
- dacite of Wolf Run (Tmdw)
- tuff of Rail Hollow (Tmdt)
- dacite-clast breccia (Tmdd; clasts)
- pumice tuff (Tmdp)
- Dalles Formation, undivided (Tmdl; clasts)
- Dalles Formation, Dog River-Badger Lake area McClaughry and others (2020).

range of chemical compositions for sampled Dalles Formation volcanic rocks

**Figure 5-12. Chemical variation diagrams for Miocene and Pliocene volcanic rocks in the Dufur area. (a) Potassium ($K_20$) versus silica ($SiO_2$). (b) Barium (Ba) versus silica ($SiO_2$). (c) Zirconium (Zr) versus Niobium (Nb). (d) Cerium (Ce) versus silica ($SiO_2$). Classification boundaries distinguishing low-, medium, and high-$K_2O$ rocks in A are from Peccerillo and Taylor (1976). Data from this paper.**

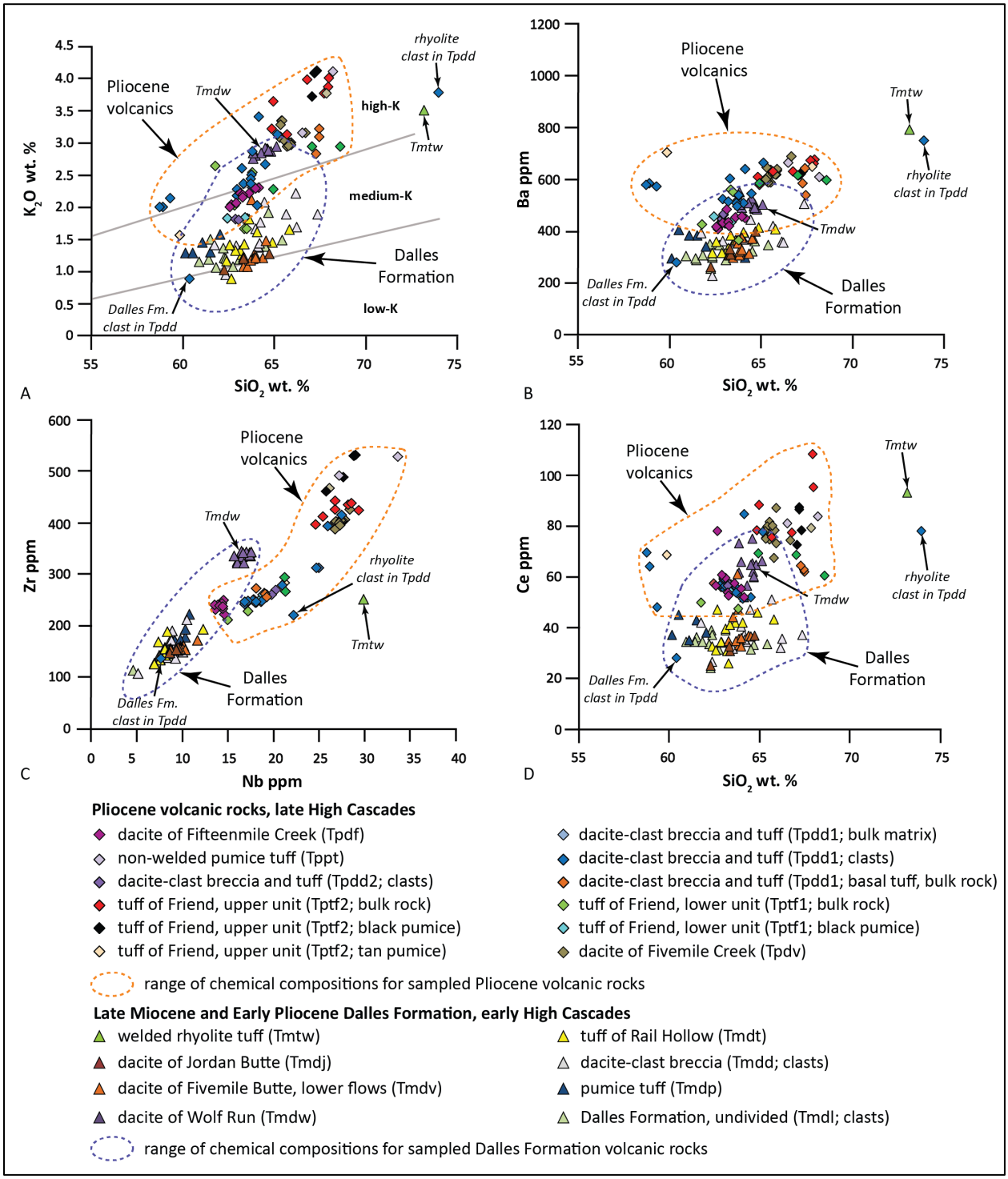

Upper Miocene and lower Pliocene rocks in the map area are equivalent to the Dalles Formation as defined by previous workers (Condon, 1874; Cope, 1880; Piper, 1932; Newcomb, 1966, 1969; Gannett, 1982; Korosec, 1987; Luttrell and others, 1991; Gray and others, 1996). Farooqui and others (1981a,b) suggested substituting the name Chenoweth in place of Dalles Formation in this area and the promotion of Dalles to group status. Their Dalles Group was considered to include all upper Miocene and lower Pliocene volcanogenic and epiclastic sedimentary rocks, pyroclastic rocks, and basaltic lava flows that unconformably overlie the lower to middle Miocene CRBG east of the Cascade Range in Oregon. Five mappable formations were assigned to the Dalles Group by Farooqui and others (1981a,b), including the Chenoweth (previously Dalles), Deschutes, Alkali Canyon, McKay, and Tygh Valley formations. Several workers in the northern Oregon Cascade Range have adopted usage of the Chenoweth Formation and Dalles Group (Farooqui and others, 1981a,b; Tolan and Beeson, 1984; Lite and Grondin, 1988; Burns and others, 2012). However, usage of the term Dalles Group is inappropriate as the terminology combines geographically separated, lithologically diverse, and genetically unrelated geologic formations (e.g., intra-Cascade arc and rift related Deschutes and Tygh Valley Formations versus the pre-rift Dalles Formation or epiclastic sedimentary rocks of the Alkali Canyon and McKay Creek Formations; Conrey and others, 1996; McClaughry and others, 2012; McClaughry and others, 2020a). We therefore retain the conventional name Dalles Formation as established by earlier workers (Condon, 1874).

#### 5.4.2.1.2 *Age*

Rocks of the upper Miocene and lower Pliocene Dalles Formation represent part of the early High Cascade episode in this part of the High Cascades of north-central Oregon (**Figure 5-4**). They were chiefly erupted between ~8.8 and 5 Ma as determined by a number of isotopic ages (**Table 5-1**; **Figure 5-13**; Plates 1 and 2). Several $^{40}Ar/^{39}Ar$ ages have been obtained on Dalles Formation rocks, both from proximal volcanic units in the East Fork Hood River area (McClaughry and others, 2020a) and from distal volcaniclastic apron deposits in the Dufur area (**Table 5-1**). $^{40}Ar/^{39}Ar$ ages determined on distal apron deposits in the Dufur area, include 8.75 ± 0.05 Ma obtained from a lahar clast (**Tmdd**) near the base of the formation at the intersection of Fifteenmile Creek and Rail Hollow (hornblende; sample 212 DFWJ 14), 8.07 ± 0.10 Ma on the tuff of Rail Hollow (**Tmdt**) in the upper reaches of Rail Hollow (hornblende; sample 29 DFWJ 14), and 7.91 ± 0.08 Ma on the dacite of Wolf Run (**Tmdw**) mapped along Eightmile Creek (plagioclase; sample 291 DFWJ 14) (**Table 5-1**; **Figure 5-13**; Plates 1 and 2). Welded tuff (**Tmtw**) cropping out near Friend has an $^{40}Ar/^{39}Ar$ age of ~ 5.3 Ma (plagioclase; sample 30 DFWJ 15) (Plate 1). The original data for sample 30 DFWJ 15 yielded no good plateau age, but adjustment of the age spectrum considering the inverse isochron $^{40}Ar/^{36}Ar$ intercept value yielded a revised plateau age of 5.27 ± 0.46 Ma (**Table 5-1**; **Figure 5-13**). Broadly similar $^{40}Ar/^{39}Ar$ ages in vent-proximal areas include 6.83 ± 0.01 Ma on a microdiorite dome forming part of Mill Creek Buttes and 5.37 ± 0.06 Ma on a hypabyssal intrusion mapped along East Fork Hood River (McClaughry and others, 2020a). A basalt lava flow interbedded in the Dalles Formation at Fulton Ridge, near the mouth of the Deschutes River, returned an $^{40}Ar/^{39}Ar$ age of 5.4 Ma (Cannon and O'Connor, 2019).

Previously published K-Ar ages on Dalles Formation rocks have returned similar, but typically less precise ages (**Figure 5-13**). Along East Fork Hood River, lava flows comprising the andesite and dacite of East Fork (McClaughry and others, 2020a) have returned K-Ar ages of 7.15 ± 0.8 Ma (Wise, 1969) and 8.18 ± 0.06 Ma (Keith and others, 1985). Other K-Ar ages include 7.74 ± 0.16 Ma obtained from a lahar clast in Fifteenmile Creek (**Table 5-1**; **Figure 5-13**; Plate 1; Gray and others, 1996), 7.71 ± 0.17 Ma from lava flows forming Fivemile Butte (west of study area, Gray and others, 1996), 7.5 ± 0.4 Ma from domes forming Mill Creek Buttes (Hull and Riccio, 1979; McClaughry and others, 2020a), 5.87 ± 0.6 Ma and 5.7 ±

0.6 Ma obtained from lahar clasts on Chenoweth Creek (northeast of study area; Farooqui and others, 1981a,b; Bunker and others, 1982), and 5.28 ± 0.5 Ma (Bunker and others, 1982) and 5.1 ± 0.5 Ma (Farooqui and others, 1981a,b) for lava flows at Jordan Butte (southwest of study area). Vertebrate and leaf fossil data reported by Buwalda (1929), Buwalda and Moore (1929, 1930), and Newcomb (1966) are also consistent with a late Miocene and early Pliocene age for the Dalles Formation.

**Table 5-1. Summary of isotopic ages in the Dufur area.**

| Map Unit | Age | Sample | Method | Material Analyzed | Source | UTM N (NAD 83) | UTM E (NAD 83) |
|---|---|---|---|---|---|---|---|
| QTbf | 2.57 ± 0.02 Ma | 159 DFWJ 15 | $^{40}Ar/^{39}Ar$ | groundmass | this study | 5026882 | 630131 |
| Tpdf | 3.02 ± 0.02 Ma | 146 DFWJ 15 | $^{40}Ar/^{39}Ar$ | groundmass | this study | 5026882 | 630131 |
| Tptf2 | 3.68 ± 0.02 | 154 DFWJ 15 | $^{40}Ar/^{39}Ar$ | plagioclase | this study | 5029062 | 643030 |
| Tpdv | 3.69 ± 0.01 | 173 DFWJ 15 | $^{40}Ar/^{39}Ar$ | groundmass | this study | 5037478 | 631448 |
| Tpdv | 3.7 ± 0.1 | JA85022 | K-Ar | whole Rock | Anderson (1987) | 5038928 | 634133 |
| Tpdd1 | 3.71 ± 0.02 | 265 DFWJ 14 | $^{40}Ar/^{39}Ar$ | plagioclase | this study | 5029062 | 643030 |
| Tpbf | 3.72 ± 0.02 | 172 DFWJ 15 | $^{40}Ar/^{39}Ar$ | groundmass | this study | 5037452 | 631478 |
| Tpdd1 | 3.83 ± 0.01 | 373 DFWJ 14 | $^{40}Ar/^{39}Ar$ | plagioclase | this study | 5029826 | 644838 |
| Tmtw | 5.13 ± 0.76 | 30 DFWJ 15* | $^{40}Ar/^{39}Ar$ | plagioclase | this study | 5024197 | 636779 |
| Tmtw | 5.27 ± 0.46 | 30 DFWJ 15* | $^{40}Ar/^{39}Ar$ | plagioclase | this study | 5024197 | 636779 |
| Tmdl | 7.74 ± 0.16 | S88-24 | K-Ar | plagioclase | Gray and others (1996) | 5033078 | 642673 |
| Tmdw | 7.91 ± 0.08 | 291 DFWJ 14 | $^{40}Ar/^{39}Ar$ | plagioclase | this study | 5035066 | 637284 |
| Tmdt | 8.07 ± 0.10 | 29 DFWJ 14 | $^{40}Ar/^{39}Ar$ | hornblende | this study | 5027344 | 638107 |
| Tmdd | 8.75 ± 0.05 | 212 DFWJ 14 | $^{40}Ar/^{39}Ar$ | hornblende | this study | 5033078 | 642673 |

$^{40}Ar/^{39}Ar$ ages determined at the College of Oceanic and Atmospheric Sciences, Oregon State University, Corvallis, Oregon. All ages reported as plateau ages, except for sample 30 DFWJ 15*which is reported as an inverse isochron age of 5.13 ± 0.76. The original data for sample 30 DFWJ 15* yielded no good plateau age, but adjustment of the age spectrum considering the inverse isochron $^{40}Ar/^{36}Ar$ intercept value yields a revised plateau age of 5.27 ± 0.46 Ma.

**Figure 5-13. Correlation of late Neogene volcanic units in the Dufur area with the paleomagnetic time scale of Cande and Kent (1992) (*following page*). Patterns show natural magnetization: dark fill – normal polarity; white fill – reversed-polarity. Units shown to the right of the time scale are samples with isotopic age-date determinations (bars showing age and standard deviation are patterned similar to time scale). Upper case abbreviations following unit names indicate natural remanent magnetization determined by using a portable fluxgate magnetometer (N – normal polarity; R – reversed-polarity; ND – indeterminate or no data).**

**Figure 5-13. (Paleomagnetic time scale – *caption on previous page*)**

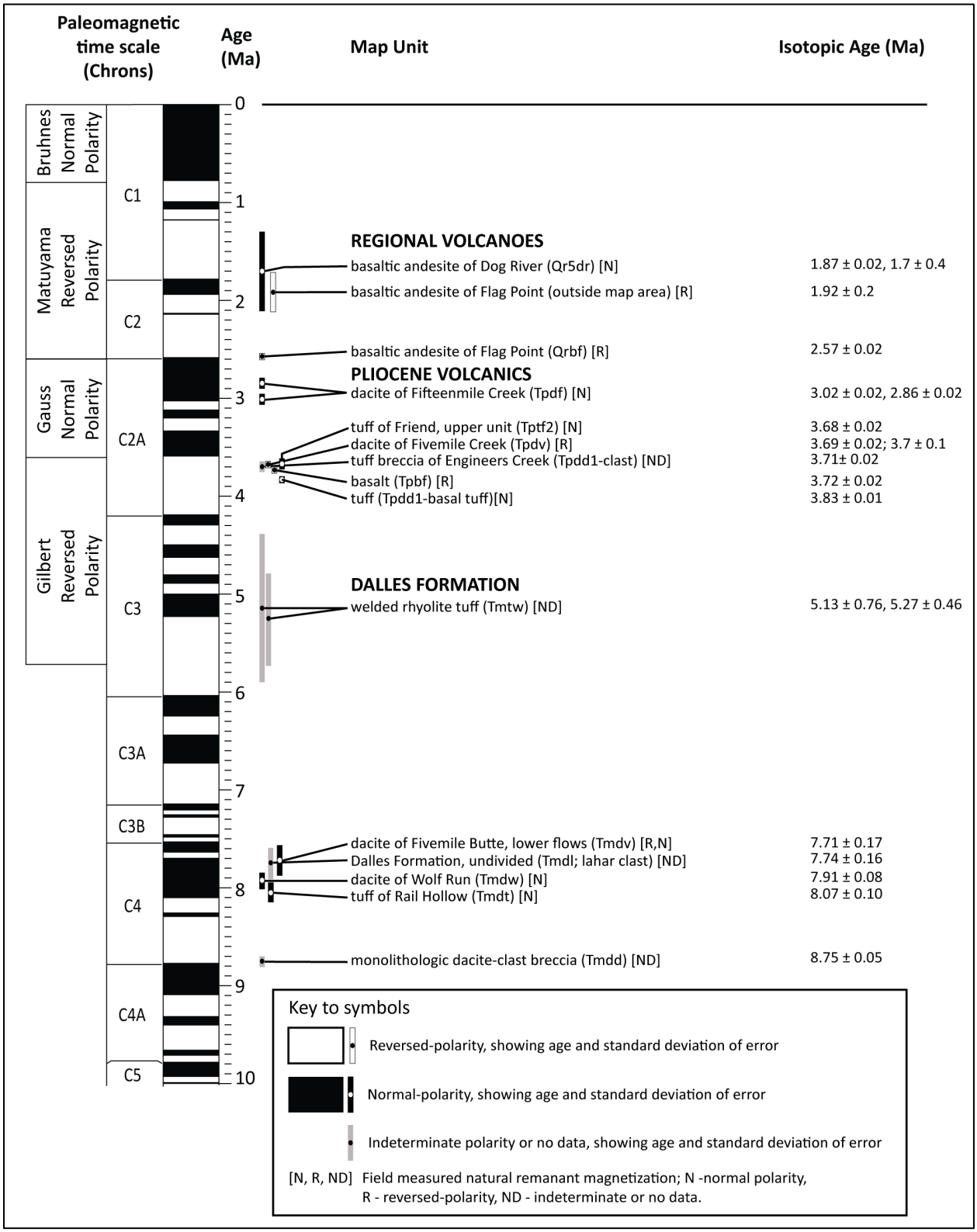

### 5.4.3 Pliocene volcanic and sedimentary rocks of the late High Cascades

#### 5.4.3.1 Pliocene volcanic and sedimentary rocks in the Dufur area

##### 5.4.3.1.1 *Distribution, composition, and lithology*

The Dalles Formation and CRBG are unconformably overlain in the Dufur area by less extensive Pliocene volcanic and volcaniclastic sedimentary rocks that partially fill paleochannels carved into older units (**Figure 5-5**). Pliocene units in the Dufur area include a basaltic lava flow (**Tpbf**), breccia (**Tpdd1**, **Tpdd2**), welded and non-welded ash-flow tuffs (**Tpdd1**, **Tppt**, **Tptf1**, **Tptf2**), and dacite lava flows (**Tpdv**, **Tpdf**) (Plates 1, 2, and 3). The trachydacite of Fivemile Creek (**Tpdv**) and breccia (**Tpdd1**) are locally overlain by sand and gravel of unit **QTpg** that may be of latest Pliocene or earliest Pleistocene age (Plates 1 and 2). Early Pliocene volcanics in the map area are inferred to have been erupted from source volcanic vents located to the west, closer to East Fork Hood River (**Figure 5-4**; McClaughry and others, 2020a). Thickness of Pliocene volcanic units in the map area ranges widely from thin gravel and tuff beds <2 m (6.6 ft) thick to lava flows as thick as as 70 m (230 ft).

Geochemical analyses of Pliocene volcanic units (primary deposits and clasts) in the map area indicate a succession characterized by medium-to high-potassium andesitic to dacitic and trachydacitic chemical compositions with $SiO_2$ ranging between 58.73 and 73.93 weight percent and $K_2O$ ranging between 1.56 and 4.14 weight percent (avg $K_2O$ = 2.49 weight percent at $SiO_2$ = 66.48 weight percent [avg]; *n* = 70 analyses) (**Figure 5-11; Figure 5-12a**). Relative to the older Dalles Formation, Pliocene rocks in the Dufur area contain higher amounts of large-ion lithophile elements such as potassium (avg $K_2O$ = 2.49 weight percent at $SiO_2$ = 66.48 weight percent [avg]) and barium (Ba<748 ppm; avg Ba = 505 ppm), high-field strength elements, such as niobium (Nb<33.7 ppm; avg Nb = 20.1 ppm) and zirconium (Zr<525 ppm; avg Zr = 296 ppm), and the light rare earth elements, such as lanthanum (La<64 ppm; avg La = 30 ppm), cerium (Ce<108 ppm; avg Ce = 59 ppm), and yttrium (Y<62 ppm; avg Y = 35 ppm) (*n* = 70) (**Figure 5-12**). The 3.72 Ma basalt mapped in Fivemile Creek contains 51.84 weight percent $SiO_2$ and 0.89 weight percent $K_2O$. Correlative Pliocene and lower Pleistocene volcanics in the East Fork Hood River area have similar compositions to the Dufur area, ranging from primitive olivine basalt ($SiO_2$ = 50.89 weight percent) to rhyolite ($SiO_2$ = 76.30 weight percent) (**Figure 5-4**; McClaughry and others, 2020a; McClaughry and others, 2020a). The full range of silica is present in the East Fork Hood River area with all units having an average low-silica dacite composition (avg $SiO_2$ = 63.08; avg $K_2O$ = 2.38 weight percent; *n* = 101 analyses). Mineralogy of silicic to intermediate composition Pliocene volcanics in the Dufur area is dominated by plagioclase and pyroxene (orthopyroxene ≥ clinopyroxene); olivine is a primary component of mafic rocks in the sequence.

Pliocene volcanics in the Dufur area are age equivalent to a similar suite of silicic volcanic rocks emplaced outside the map area at nearby Gordon Butte (8.6 km [5.4 mi] southeast of Lookout Mountain) and Graveyard Buttes (28 km [17.4 mi] southeast of Lookout Mountain) between 3.8 and 3.6 Ma (Westby, 2014). Westby (2014) considered early-phase silicic volcanism in the Gordon and Graveyard Buttes areas to share geochemical and mineralogical traits consistent with petrogenesis in an intra plate or extensional setting, while late phase silicic rocks appear to be more arc related. Intermediate to silicic volcanism between Gordon Butte and East Fork Hood River was also contemporaneous with a more widespread pulse of high-magnesium mafic volcanism in the northern Oregon Cascade Range dated between 4.4 Ma and 2.1 Ma (Conrey and others, 1996; McClaughry and others, 2012; McClaughry and others, 2020a). Extrusion of mafic lava flows during the late Pliocene was accompanied by Yakima Fold Belt deformation, inception of rifting along the axis of this part of the Cascade arc, and formation of the Hood River graben

after 3.7 Ma (**Figure 5-2**; McClaughry and others, 2012; McClaughry and others, 2013; McClaughry and others, 2020a). Foundering of the Cascade volcanic arc into a half graben during the early to late Pliocene was accompanied by regional uplift or upwarp of the Cascade Range and formation of the modern Columbia River Gorge after 3 Ma (Tolan and Beeson, 1984; Beeson and Tolan, 1990).

#### 5.4.3.1.2 *Age*

Pliocene volcanics in the Dufur area were chiefly emplaced between 3.83 and 3.02 Ma and represent part of the late High Cascade episode in this part of the High Cascades of north-central Oregon (**Table 5-1**; **Figure 5-13**; Plates 1 and 2). The oldest recognized Pliocene deposit in the Dufur area is a non-welded tuff outcropping at the base of canyon-filling breccia unit **Tpdd1** in Pine Creek and Mays Canyon (Plate 2). The unit **Tpdd1** basal tuff has an $^{40}Ar/^{39}Ar$ age of 3.83 ± 0.01 Ma (plagioclase; sample 373 DWFJ 14), while a single clast obtained from the breccia (**Tpdd1**) directly overlying the tuff has an $^{40}Ar/^{39}Ar$ age of 3.71 ± 0.02 Ma (plagioclase; sample 265 DFWJ 14) (**Table 5-1**; **Figure 5-13**; Plate 2). Near Friend, unit **Tpdd1** is interbedded with and overlain by two units forming the tuff of Friend (**Tptf1**, **Tptf2**; Plate 1). The upper unit of the tuff of Friend **(Tptf2**) has an $^{40}Ar/^{39}Ar$ plateau age of 3.68 ± 0.02 Ma (plagioclase; sample 154 DFWJ 15) for a sample obtained from an outcrop located in the upper part of Larch Creek, west of Friend (**Table 5-1**; **Figure 5-13**; Plate 1). Similar-aged rocks mapped along Fivemile Creek include a basaltic lava flow (**Tpbf**) and the trachydacite of Fivemile Creek (**Tpdv**) (Plate 1). The older basaltic lava flow (**Tpbf**) has an $^{40}Ar/^{39}Ar$ plateau age of 3.72 ± 0.01 Ma (groundmass; sample 172 DFWJ 15), while the younger trachydacite of Fivemile Creek (**Tpdv**) has an $^{40}Ar/^{39}Ar$ plateau age of 3.69 ± 0.02 Ma (groundmass, sample 173 DFWJ 15) and an indistinguishable K-Ar age of 3.7 ± 0.2 Ma (whole rock; sample JA85022; Anderson, 1987) (**Table 5-1**; **Figure 5-13**; Plate 1). The youngest dated Pliocene unit in the Dufur area is the dacite of Fifteenmile Creek (**Tpdf**). A sample of unit **Tpdf**, obtained from an outcrop between Fifteenmile and Larch Creeks in the southwestern part of the map area, has an $^{40}Ar/^{39}Ar$ plateau age of 3.02 ± 0.02 Ma (groundmass; sample 146 DFWJ 15) (**Table 5-1**; **Figure 5-13**; Plate 1). The 3.02 Ma age is similar to an older K-Ar age of 2.86 ± 0.06 Ma (sample RCS88-25) reported by Sherrod and Scott (1995) and Gray and others (1996) for a sample from the lava flow unit near Cold Point, ~7 km (4.3 mi) southwest of the map area.

Isotopic ages on Pliocene volcanics in the Dufur area correspond closely to $^{40}Ar/^{39}Ar$ results for stratigraphically and age equivalent sections mapped along East Fork Hood River (McClaughry and others, 2020a) and those found southwest of the map area at Graveyard and Gordon Buttes (Westby, 2014). The oldest part of the Pliocene section in the East Fork Hood River area is marked by the 4.19 ± 0.01 Ma basalt and basaltic andesite of Rimrock (sample 184 MCB-DRJ 17; McClaughry and others, 2020a). Several younger units overly the trachydacite of Fivemile Creek (**Tpdv**) between East Fork Hood River and Lookout Mountain, including the 3.77 ± 0.02 Ma porphyritic trachydacite of Culvert Creek (sample RC14-9/22 DRBLJ 19) and the 3.14 ± 0.2 Ma andesite and dacite of Senecal Spring (70-WISE) (Wise, 1969; McClaughry and others, 2020a). The uppermost part of the Pliocene and early Pleistocene volcanic section in the East Fork Hood River area is defined by the andesite of Tumble Creek, a hornblende-bearing andesite with a K-Ar age of 2.74 ± 0.3 Ma (sample 79SWC0010A) and high-titanium lava flows with ages of 2.43 ± 0.14 Ma (sample S91-H47), 2.5 ± 0.026 Ma (sample 940616-1), and 2.63 ± 0.01 Ma (sample 380 MCB-DRJ 17) (Keith and others, 1985; Conrey and others, 1996; Scott and Gardner, 2017; McClaughry and others, 2020a). Westby (2014) reported similar $^{40}Ar/^{39}Ar$ plateau ages of 3.86 ± 0.07 Ma for andesite (sample S12-6) and 3.67 ± 0.01 Ma (sample X3) and 3.65 ± 0.01 Ma (sample CC14) for rhyolite at Graveyard Butte and 3.64 ± 0.03 Ma for rhyolite (sample GB4-3) at Gordon Butte, southwest of the map area.

### 5.4.4 Quaternary and/or upper Pliocene volcanic and sedimentary rocks of the late High Cascades

#### 5.4.4.1 Products of Regional Quaternary volcanoes

##### 5.4.4.1.1 *Distribution, composition, and lithology*

Pliocene and older rocks are locally disconformably overlain in the Dufur area by a series of upper Pliocene and Quaternary olivine-phyric basalt, basaltic andesite, and andesite lava flows (**Qr5dr**, **Qrbp**, **Qrbe**, **Qrbf**) erupted from small volcanoes located along the eastern escarpment of the Hood River graben (**Figure 5-2**). Scott and Gardner (2017) and McClaughry and others (2020a) referred to these basaltic to andesitic lava flows and corresponding vents of Quaternary age surrounding Mount Hood as products of regional Quaternary volcanoes. In the Mount Hood region Quaternary volcanic rocks crop out over a 160-km-wide (99 mi) area between the forearc Boring Volcanic Field in the Portland Basin, through the Cascade Range, and eastward to the backarc Simcoe Mountains (Washington State) (**Figure 5-2**; Hildreth, 2007). More than 300 vents of Quaternary age lie within an ~ 50-km-wide (31 mi) region north and south of the Columbia River, including the large composite volcanoes of Mount St. Helens, Mount Adams, and Mount Hood (**Figure 5-2**).

Mafic to intermediate volcanism was predominant along the axis of the High Cascades arc during the Quaternary, with basalt, basaltic andesite, and andesite lava flows erupting from a north-south-striking belt of source volcanoes coincident with northwest-striking fault strands high on the broad eastern escarpment of the Hood River graben (McClaughry and others, 2020a). Several of these lava flows, with basaltic to andesitic compositions ($SiO_2$ = 48.89 to 57.56 weight percent; $K_2O$ = 0.69 to 1.38 weight percent; *n* = 49 analyses), flowed east into the Dufur area (**Qr5dr**, **Qrbp**, **Qrbe**, **Qrbf**) (**Figure 5-14**, **Figure 5-15**). Mineralogy of regional Quaternary lava flows includes plagioclase and olivine ± pyroxene.

Lava flows erupted high along the eastern escarpment of the Hood River graben in the East Fork Hood River area flowed east away from source vents down an east-sloping landscape, confined to north-northeast-directed drainages carved into older late Miocene and Pliocene rocks (**Figure 5-4**). These drainages were of similar location and orientation to those of Pliocene intracanyon lava flows, tuffs, and sediment-gravity flows (**Tpbf**, **Tpdv**, **Tptf1**, **Tpdd1**, **Tptf2**, **Tpdd2**, **Tppt**, **Tpdf**). The 2.57 Ma basaltic andesite of Flag Point (**Qrbf**) was erupted from an extant cinder cone-capped vent underlying the lookout at Flag Point (southwest of the map area, J.D. McClaughry unpublished geologic mapping, 2016). Lava flows (**Qrbf**) erupted from Flag Point flowed north into the upper parts of Cedar Creek and northeast into Jordan Creek and Owl Hollow; the distal snout of intracanyon lava flows reached ~14 km (8.7 mi) northeast to the upper part of Larch Creek in the map area. The 1.87 Ma basaltic andesite of Dog River (**Qr5dr**) erupted from a fault-controlled cinder cone-capped fissure at an altitude of 1,391 m (4,565 ft) along the Dog River-Mill Creek divide near Mill Creek Buttes (McClaughry and others, 2020a). The Dog River lava flow (**Qr5dr**) descended northeast into South Fork Mill Creek flowing at least 26 km (16 mi) downstream to Oak Flat near The Dalles. An additional lobe of the basaltic andesite of Dog River (**Qr5dr**) was also directed west and northwest into the structural low of the Hood River graben (McClaughry and others, 2020a). This western lobe extended at least 6 km (3.7 mi) from the vent area to now down-faulted exposures, outcropping at an elevation of 716 m (2,350 ft) in the canyon of the East Fork Hood River.

**Figure 5-14. Total alkalis ($Na_2O + K_2O$) vs. silica ($SiO_2$) (TAS) classification of late Pliocene and early Pleistocene lava flows in the Dufur area from whole-rock XRF analyses (normalized to 100 percent anhydrous). Fields are from Le Bas and others (1986) and Le Maitre and others (1989). Red-dashed line is the dividing line between alkaline (above), subalkaline/tholeiitic (below) fields after Cox and others (1979). Data shown includes 50 analyses from the Middle Columbia Basin reported in this paper, Wise (1969), and McClaughry and others (2020a). Additional data points are unpublished XRF analyses in the Middle Columbia Basin collected by J.D. McClaughry (2014 to 2018).**

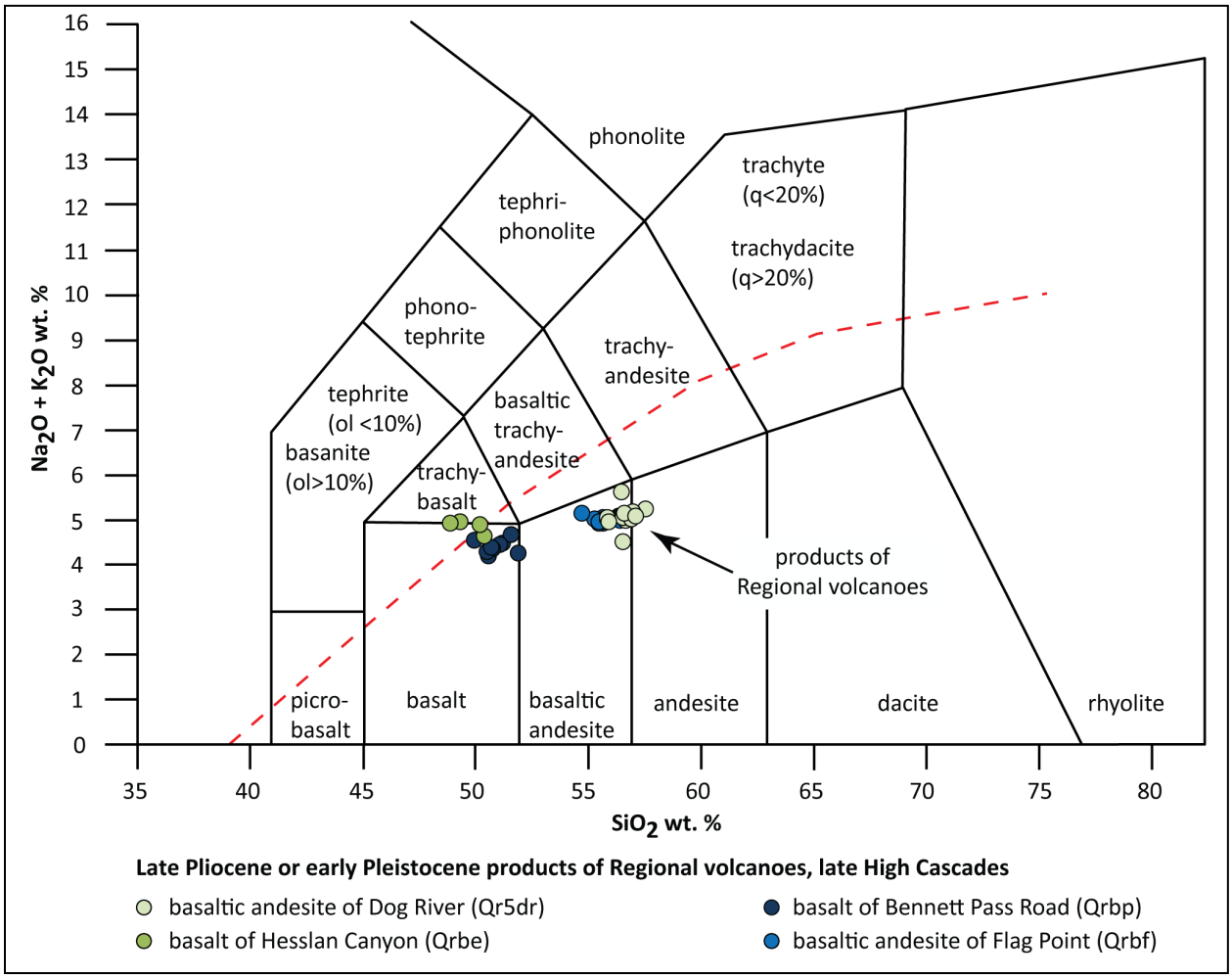

**Figure 5-15. Chemical variation diagrams for late Pliocene and early Pleistocene lava flows in the Dufur area. (a) Total iron/magnesium (FeO*/MgO) versus silica ($SiO_2$). (b) Titanium ($TiO_2$) versus silica ($SiO_2$). (c) Magnesium (MgO) versus silica ($SiO_2$). (d) Potassium ($K_20$) versus silica ($SiO_2$). Data shown includes 50 analyses from the Middle Columbia Basin reported in this paper, Wise (1969), and McClaughry and others (2020a). Additional data points are unpublished analyses in the Middle Columbia Basin collected by J.D. McClaughry (2014 to 2018).**

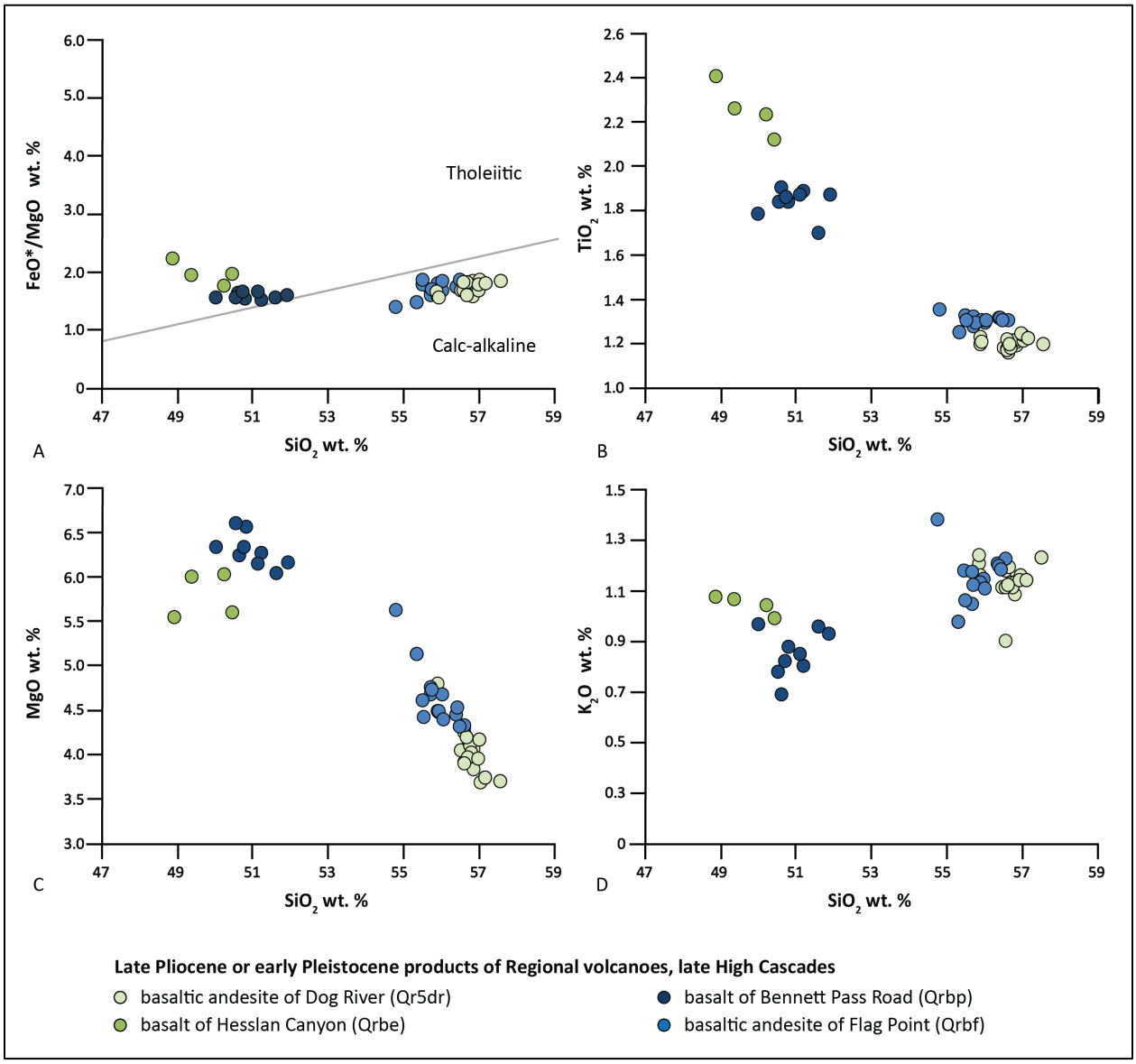

#### 5.4.4.1.2 *Age*

Lava flows capping the eastern escarpment of the Hood River graben are assigned a latest Pliocene or Quaternary age on the basis of intracanyon geomorphic setting, spatial and temporal association with still present cinder cones on the Hood River graben escarpment, and isotopic ages (**Table 5-1**; **Figure 5-13**; Plate 1). Isotopic ages include an $^{40}Ar/^{39}Ar$ age of 2.57 ± 0.02 Ma for the basaltic andesite of Flag Point (**Qrbf**) (groundmass; sample 157 DFWJ 15; **Table 5-1**; **Figure 5-13**; Plate 1) and a K-Ar age of 2.35 ± 0.03 Ma for the basalt of Bennett Pass Road (**Qrbp**) (whole rock; sample S92-H271a/WISE-104; Conrey and others, 1996; McClaughry and others, 2020a). The basaltic andesite of Dog River (**Qr5dr**) has an $^{40}Ar/^{39}Ar$ plateau age of 1.87 ± 0.02 Ma (groundmass; sample 178 DFWJ 15; McClaughry and others, 2020a); Anderson (1987) reported a similar, but less precise K-Ar age of 1.7 ± 0.4 Ma (whole-rock, sample JA85023) for the basaltic andesite of Dog River (**Qr5dr**) along South Fork Mill Creek (north of the map area). Emplacement of Quaternary lava flows predates erosion that carved the modern canyons in the Dufur area.

### 5.4.5 Upper Cenozoic surficial deposits

#### 5.4.5.1 Late Pleistocene and Holocene surficial deposits

#### 5.4.5.1.1 *Distribution, composition, and lithology*

Upper Pleistocene and Holocene surficial units have accumulated on steep slopes and in valley bottoms in the Dufur area, including stream alluvium (**Qa, Qao**), fan deposits (**Qaf**), landslide deposits (**Qls**), and colluvium (**Qc**) (Plates 1, 2, and 3). These units reflect late Pleistocene and younger landscape adjustments as major drainages have continued to incise into bedrock units. In the Dufur area streams and landforms are adjusting to late Quaternary variations in climate, young faulting (after 3 Ma), changes in base level at the Columbia River, and land-use changes. These geomorphic adjustments are further complicated by the presence of alternating hard and soft rock in the subsurface and nesting of Pliocene and Quaternary intracanyon lava flows within older bedrock units.

The landscape of rolling hills and deeply incised valleys in the Dufur area are capped by a variably thick and discontinuous blanket of Pleistocene loess (**Qlo**) that has accumulated as a result of episodic deposition of airborne silts by southwesterly winds during the Quaternary (McDonald and others, 2012). Over the last century loess deposits (**Qlo**) have been extensively modified by dry-land agriculture. Microrelief features, known as Mima mounds, are also a prevalent geomorphic feature in the Dufur area, preserved mantling the landscape in areas between tilled loess-dominated agricultural fields or areas considered unsuitable for agriculture.

#### 5.4.5.1.2 *Age*

Surficial deposits in the Dufur area largely range in age from the Late Pleistocene to the upper Holocene, but age constraints are few. Most surficial deposits postdate the emplacement of widespread loess (**Qlo**). Loess deposits in the eastern Middle Columbia Basin are assigned a Middle to Late Pleistocene age on the basis of stratigraphic position and may be as old as ~600 ka. Medley (2012) interpreted loess deposits and Missoula Flood deposits exposed along U.S. Highway 197 between Dufur and The Dalles to lie above a series of older paleosols that contain pumice correlated to the ~600 ka Dibekulewe tuff from Nevada (Cordero, 1997). Pluhar and others (2014) reported paleomagnetically reversed paleosols at the base of the U.S. Highway 197 section, so loess in this area may in some places be older than 0.78 Ma.

# 6.0 EXPLANATION OF MAP UNITS

The Explanation of Map Units describes the basis for subdividing rocks into stratigraphic units on the geologic maps shown on Plates 1, 2, and 3. A time-rock chart graphically displaying age ranges and relations for the 44 late Cenozoic bedrock and surficial map units is shown in **Figure 6-1** and on Plates 1, 2, and 3. Unit names follow formal stratigraphic names or local stratigraphic nomenclature when available; informal names are given on the basis of composition or sites of good exposure when formal rock names are lacking.

Formal stratigraphic names have been established only for the CRBG; those rocks are assigned to units following conventions established by Tolan and others (1989, 2009a) and Reidel and others (2013). The Dalles Formation is formally named, but separate strata within the formation are only informally named. Few Cascade Range units have been formally named, and none in the map area. Late Miocene to Holocene Cascade volcanic rocks in the Dufur area are subdivided here on the basis of conventions established by Peck and others (1964), Priest and others (1983), Priest (1990), and Conrey and others (1997) for rocks of the Cascade Range. Priest and others (1983) divided rocks of the Western Cascades into four time-stratigraphic units on the basis of apparent time-breaks that generally correspond to regional compositional changes. These time-stratigraphic intervals include: 1) an early Western Cascade episode at ~ 40 to 18 Ma; 2) a late Western Cascade episode at ~18 to 9 Ma; 3) an early High Cascade episode at ~9 to 4 Ma; and 4) a late High Cascade episode at ~4 Ma to present. Rocks of the late Miocene to early Pliocene Dalles Formation correspond to volcanism during an early High Cascades episode at ~9 to 4 Ma, while younger Pliocene to Holocene volcanic rocks are considered part of a ~4 Ma to present late High Cascades episode. CRBG lava flows are temporally correlative with the late Western Cascade episode, but are not included within this time-stratigraphic unit, as they were erupted from distant vents located in northeast Oregon and southeast Washington (**Figure 5-6**).

## 6.1 Overview of map units

***UPPER CENOZOIC SURFICIAL DEPOSITS***

**Qf** modern fill and construction material (upper Holocene)
**Qa** alluvium (Holocene and Upper Pleistocene)
**Qaf** fan deposits (Holocene and Upper Pleistocene)
**Qls** landslide deposits (Holocene and Upper Pleistocene)
**Qc** colluvium (Holocene and Upper Pleistocene)
**Qsvf** silty valley fill (Holocene and Upper Pleistocene)
**Qao** older alluvium (Holocene and Upper Pleistocene)
**Qlo** loess (Holocene and Pleistocene)

**Unconformity**

## *UPPER CENOZOIC VOLCANIC AND SEDIMENTARY ROCKS*

### *QUATERNARY AND/OR UPPER PLIOCENE VOLCANIC AND SEDIMENTARY ROCKS OF THE LATE HIGH CASCADES*

#### *PRODUCTS OF REGIONAL QUATERNARY VOLCANOES*

**Qr5dr** basaltic andesite of Dog River (lower Pleistocene) 1.87 ± 0.01 ($^{40}Ar/^{39}Ar$); 1.7 ± 0.4 Ma (K-Ar)

**Qrbe** basalt of Hesslan Canyon (lower Pleistocene)

**Qrbp** basalt of Bennett Pass Road (lower Pleistocene) 2.35 ± 0.03 Ma (K-Ar)

**Qrbf** basaltic andesite of Flag Point (lower Pleistocene or upper Pliocene) 2.57 ± 0.02 Ma ($^{40}Ar/^{39}Ar$)

**Disconformity**

### *LOWER PLEISTOCENE AND PLIOCENE VOLCANIC AND SEDIMENTARY ROCKS OF THE LATE HIGH CASCADES*

**QTpg** sedimentary deposits (lower Pleistocene and/or upper Pliocene)

**Tpdf** dacite of Fifteenmile Creek (upper Pliocene) 3.02 ± 0.02 Ma ($^{40}Ar/^{39}Ar$); 2.86 ± 0.06 Ma (K-Ar)

**Tppt** non-welded pumice tuff (lower Pliocene)

**Tpdd2** tuff breccia of Engineers Creek, upper unit (lower Pliocene)

**Tptf2** tuff of Friend, upper unit (lower Pliocene) 3.68 ± 0.02 Ma ($^{40}Ar/^{39}Ar$)

**Tpdd1** tuff breccia of Engineers Creek, lower unit (lower Pliocene) 3.71 ± 0.02 Ma (clast; $^{40}Ar/^{39}Ar$); 3.83 ± 0.02 Ma (basal tuff; $^{40}Ar/^{39}Ar$)

**Tptf1** tuff of Friend, lower unit (lower Pliocene)

**Tpdv** trachydacite of Fivemile Creek (lower Pliocene) 3.69 ± 0.01 ($^{40}Ar/^{39}Ar$); 3.7 ± 0.2 Ma (K-Ar)

**Tpbf** basalt (lower Pliocene) 3.72 ± 0.01 Ma ($^{40}Ar/^{39}Ar$)

**Disconformity**

### *LOWER PLIOCENE AND UPPER MIOCENE VOLCANIC AND SEDIMENTARY ROCKS OF THE EARLY HIGH CASCADES*

#### *DALLES FORMATION*

**Tmdl** Dalles Formation, undivided (lower Pliocene and upper Miocene)

**Tmdg** plateau-capping conglomerate (lower Pliocene and/or upper Miocene)

**Tmtw** welded rhyolite tuff (lower Pliocene or upper Miocene) 5.27 ± 0.46 Ma ($^{40}Ar/^{39}Ar$)

**Tmdj** dacite of Jordan Butte (lower Pliocene or upper Miocene) 5.28 ± 0.5 Ma (K-Ar)

**Tmdv** dacite of Fivemile Butte, lower flows (upper Miocene) 7.71 ± 0.17 Ma (K-Ar)

**Tmdw** dacite of Wolf Run (upper Miocene) 7.91 ± 0.08 Ma ($^{40}Ar/^{39}Ar$)

**Tmdt** tuff of Rail Hollow (upper Miocene) 8.07 ± 0.01 Ma ($^{40}Ar/^{39}Ar$)

**Tmdd** tuff breccia of Fifteenmile Creek (upper Miocene) 8.75 ± 0.05 Ma ($^{40}Ar/^{39}Ar$; clast)

**Tmdtp** pumice tuff (upper Miocene)

**Tmdx** heterolithologic andesite and dacite-clast breccia (upper Miocene)

**Angular unconformity to disconformity**

***MIDDLE TO LOWER MIOCENE VOLCANIC AND SEDIMENTARY ROCKS***

***COLUMBIA RIVER BASALT GROUP***

*Wanapum Basalt*

*Priest Rapids Member*

**Twpr** Basalt of Rosalia (middle Miocene)

*Frenchman Springs Member*

**Twfs** Basalt of Sentinel Gap (middle or lower Miocene)

**Twfh** Basalt of Sand Hollow (middle or lower Miocene)

**Twfg** Basalt of Ginkgo (middle or lower Miocene)

**Disconformity—Vantage Member of the Ellensburg Formation**

*Grande Ronde Basalt*

*Normal-polarity (N2) magnetostratigraphic unit subdivided into:*

**Tgsb** Sentinel Bluffs Member (lower Miocene)

**Tgww** Winter Water Member (lower Miocene)

**Tgo** Ortley member (lower Miocene) (cross section only)

**Tgac** Armstrong Canyon member (lower Miocene) (cross section only)

**Tgbc** Buttermilk Canyon member (lower Miocene) (cross section only)

*Reversed-polarity (R2) magnetostratigraphic unit subdivided into:*

**Tggc** Grouse Creek member (lower Miocene) (cross section only)

**Tgu** Grande Ronde Basalt, undivided (lower Miocene) (cross section only)

*Prineville Basalt*

**Tpba** Prineville Basalt, basaltic andesite (lower Miocene) (cross section only)

**Tpbd** Prineville Basalt, Bowman Dam chemical type (lower Miocene) (cross section only)

**Figure 6-1. Time rock chart showing the 44 geologic units portrayed on the geologic maps and in geologic cross sections in the Dufur area. Note that depth of exposure in the map area does not extend beneath the Winter Water Member (Tgww).**

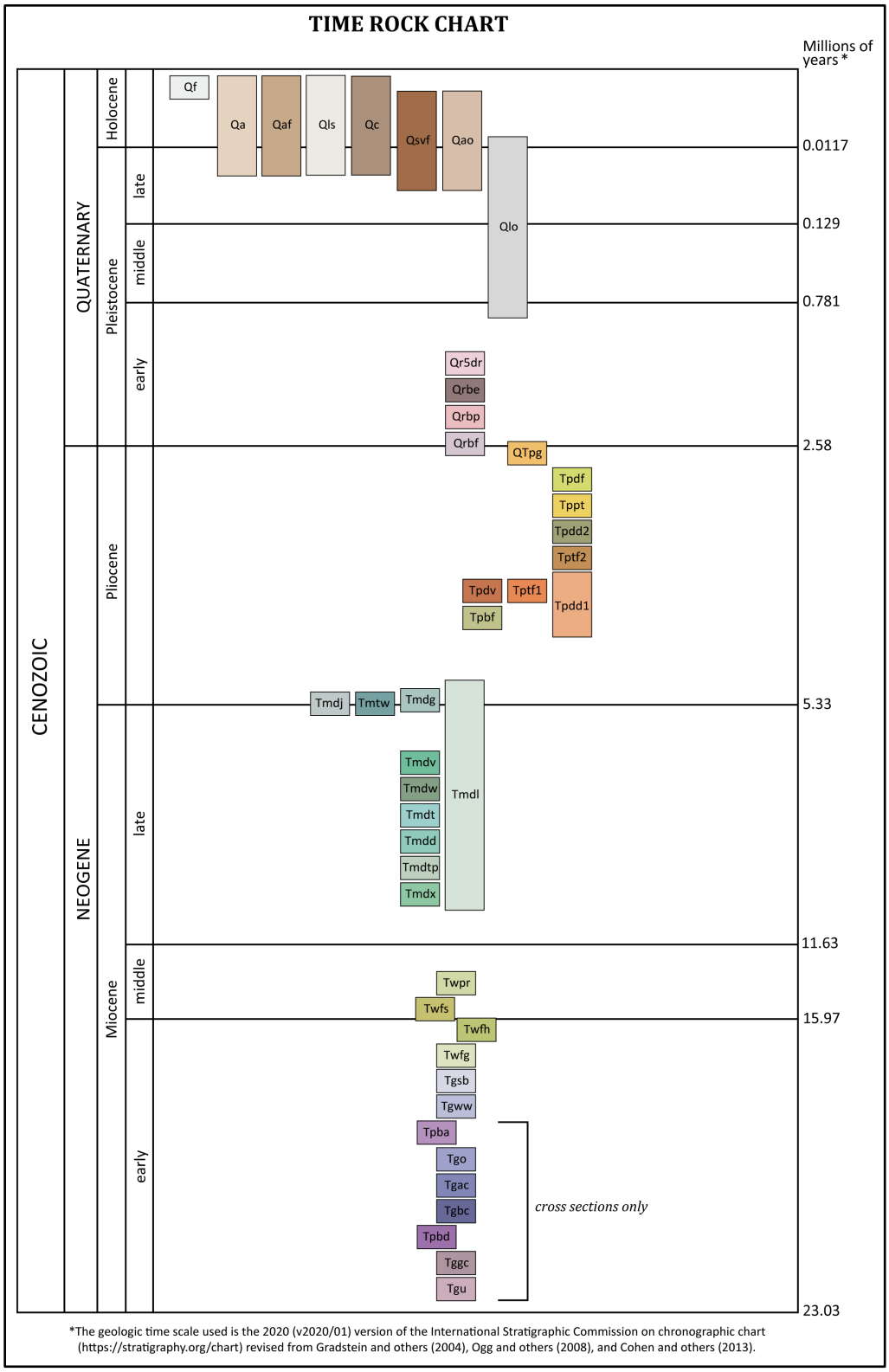

## 6.2 Upper Cenozoic surficial deposits

**Qf** **modern fill and construction material (upper Holocene)—**Artificial or constructed fill deposits of poorly sorted and crudely layered mixed gravel, sand, clay, and other engineered fill (**Figure 6-2**; Plate 1). Deposits mapped as modern fill and construction material in the map area are generally associated with railroad grades, dams and levees, road embankments, causeways, culvert fills, and mined land (**Figure 6-2**; Plates 1, 2, and 3). These deposits usually contain rounded to angular clasts ranging from small pebbles up to several meters across. The orientation of clasts is typically less uniform than is found in naturally occurring imbricated or bedding-parallel gravel. Older fills are likely uncompacted versus newer fills, which are likely engineered and reinforced using geotextiles or retaining structures. The thickness of fill-deposits is as much as 30 m (98 ft). Unit **Qf** is assigned a late Holocene age, ranging in age from the late 1800s to recent times (**Figure 6-1**).

**Figure 6-2. Examples of modern fill and construction material (Qf) in the Dufur area. (a) Road embankment underlying U.S. Highway 197 along Pine Creek Canyon, north of Dufur Gap Road (45.420349, -121.141819). View is looking northeast. (b) Abandoned railroad grade preserved along Pine Creek Canyon, 1.9 km (1.2 mi) west of U.S. Highway 197 (45.400092, -121.164958). View is looking north. The abandoned railroad grade was part of the 66-km-long (41 mi) Great Southern Railroad short-line which ran between The Dalles and Friend (Due and French, 1979). Construction of the rail-line began in 1904 and was completed by 1913. Regular train service along the line came to an end in 1928. Large parts of the railroad grade have been washed out by major floods along Pine Creek. Photo credits: J.D. McClaughry, 2014.**

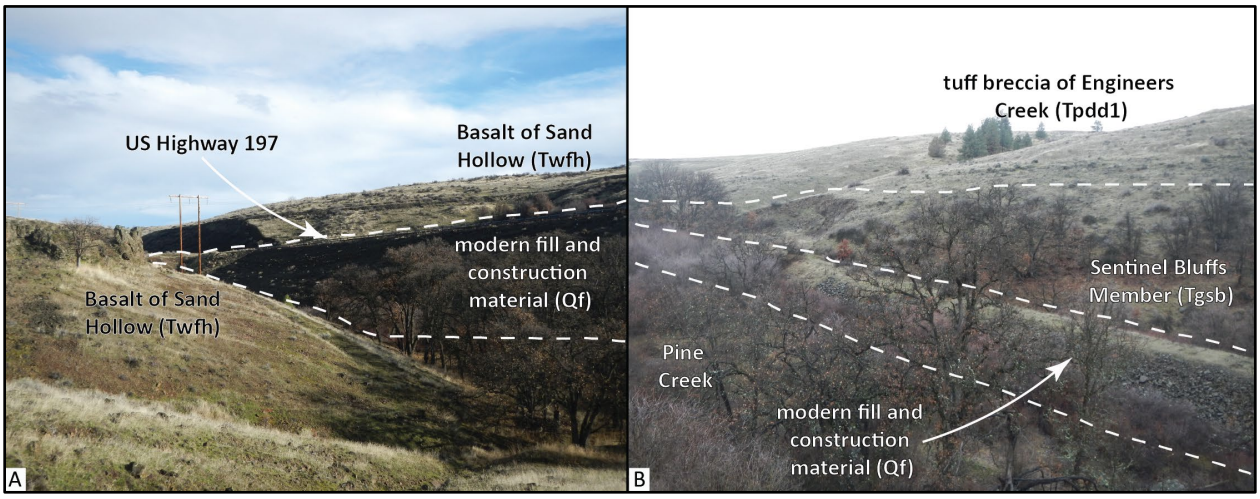


**Qa** **alluvium (Holocene and Upper Pleistocene)—** Unconsolidated, poorly to moderately stratified gravel and sand along streams (**Figure 6-3**; Plates 1, 2, and 3). Thickness of unit **Qa** is generally < 5 to 7 m (16 to 23 ft); bedrock units may be locally exposed in the base of stream channels within areas mapped as unit **Qa**. Unit **Qa** is assigned a Late Pleistocene and Holocene age on the basis of stratigraphic position and a lack of more precise age indications (**Figure 6-1**). Areas mapped as unit **Qa** are known to have been inundated by record floods during 1861, 1964, 1974, 1996, and 2006. They may include deposits containing human-made debris or artifacts, or deposits filling areas known to have been modified by humans such as railroad grades, excavations, roadways, or gravel pits.

**Figure 6-3. Quaternary alluvium (Qa) and fan deposits (Qaf) preserved along Eightmile Creek in the northwest part of the map area (45.460780, -121.234613). View is looking north. Flow of Eightmile Creek is from left to right (west to east) in the photograph. Photo credit: J.D. McClaughry, 2014.**


**Qaf** **fan deposits (Holocene and Upper Pleistocene)—** Unconsolidated, poorly sorted, poorly graded deposits of boulders, cobbles, pebbles, granules, sand, silt, and clay in upland drainages and as fan-shaped accumulations at the transition between low-gradient valley floodplains and steeper uplands (Plates 1, 2, and 3). The unit (**Qaf**) may locally include rapidly deposited talus from rockfall in steep drainages. Individual fans (**Qaf**) generally cover less than 4 hectares (10 acres). The local thickness of alluvial fan deposits is variable but is probably <15 m (50 ft). Unit **Qaf** includes fan deposits of Late Pleistocene and Holocene age (**Figure 6-1**).

**Qls** **landslide deposits (Holocene and Upper Pleistocene)—**Unconsolidated, chaotically mixed masses of rock and soil deposited by landslides, including slumps, slides, earthflows, and rock avalanches (Plates 1, 2, and 3). Deposits (**Qls**) consist of individual slide masses or form large complexes resulting from reactivation of older landslide terrain. Landslide terrain is characterized by sloping hummocky surfaces, closed depressions, springs and wet seeps, and locally, open ground fissures. Tilted trees and trees with bent trunks or disrupted fence lines may be common on the surface. Toes to more recent deposits retain convex-up, fan-shaped morphologies. Slides are often

traceable uphill to head scarps or failure surfaces. In deeper landslides, these head scarps commonly expose bedrock. Single Quaternary landslide complexes (**Qls**) in the map area cover up to 11 acres (4.5 hectares); more commonly slides are less than 2 acres (0.8 hectares). A majority of mapped landslide deposits (**Qls**) are simple rotational or shallow-seated earthflow-type features that occur along major drainages, originating on sparsely vegetated, moderately to steep slopes underlain by weakly consolidated rocks of the Dalles Formation (**Tmdl**) or unconsolidated loess (**Qlo**). Thickness of landslide deposits (**Qls**) is highly varied but may be more than several tens of meters in larger deposits. Landslide deposits range in age from Late Pleistocene to those that have been recurrently active in the Holocene (**Figure 6-1**). Large areas mapped as Quaternary landslide deposits (**Qls**) typically include many discrete deposits of varying age that have not been differentiated here. Landslide deposits are typically referred to as clay, boulders, rock, or rock and clay in water well logs.

**Qc** **colluvium (Holocene and Upper Pleistocene)—**Unconsolidated mixtures of rock and soil deposited in rockfall and talus cones beneath steep slopes (Plates 1, 2, and 3). Thickness of colluvial deposits is highly varied; maximum thickness is several meters. Unit **Qc** is assigned a Late Pleistocene and Holocene age on the basis of stratigraphic position (**Figure 6-1**).

**Qsvf** **silty valley fill (Holocene and Upper Pleistocene)—** Unconsolidated, mostly silt-dominated terraces mapped along intermittent streams draining loess capped uplands in the northeast part of the map area (Plate 3). Unit **Qsvf** is considered to have a Late Pleistocene or Holocene age on the basis of stratigraphic position (**Figure 6-1**).

**Qao** **older alluvium (Holocene and Upper Pleistocene)—**Moderately dissected, unconsolidated, well- to poorly sorted and stratified gravel, sand, silt, and clay deposited in active stream channels and on adjoining flood plains (Plates 1, 2, and 3). These deposits (**Qao**) are recognized and mapped along Eightmile and Fifteenmile Creeks and a number of smaller tributary streams, where deposits reside adjacent to younger, incised drainages filled with younger Quaternary alluvium (**Qa**). Thickness of unit **Qao** probably does not exceed 6 m (20 ft). Unit **Qao** is assigned a Late Pleistocene and Holocene age on the basis of stratigraphic position and a lack of more precise age indications (**Figure 6-1**).

**Qlo** **loess (Holocene and Pleistocene)—**Pale yellowish brown (10YR 6/2), micaceous, quartzo-feldspathic silt and minor amounts of very fine-grained sand and clay mantling upland in the Dufur area (**Figure 6-4a**; Plates 1, 2, and 3). Loess (**Qlo**) typically forms a massive, featureless deposit that has been extensively modified by dry-land agriculture over the past century (**Figure 6-4**). Where the antecedent deposit was originally thin or has been further thinned by tilling, silt may be mixed with larger rock fragments from the underlying bedrock geology. Commonly, the edges of wheat fields constructed in loess (**Qlo**), are characterized by steep 1- to 2-m-high (3.3 to 6.5 ft) embankments created from circular, annual tilling of large fields (**Figure 6-4a**). Long-term residents of the area report that annual tilling in the same circular direction has led to often thicker accumulations of loess (**Qlo**) along the outer edges of fields, in places removing the entire thickness of the unit near the center of fields. Thickness of unit **Qlo** ranges from thin veneers <1 m (3.3 ft) to as much as 6 m (20 ft), on the basis of information reported from well logs; roadcuts may locally show up to 5 m (16.4 ft) of loess in vertical section.

The distribution of loess, (**Qlo**), as mapped here, has been determined on the basis of a combination of field observations, soils mapping by Green (1982), geologic mapping by Waters (1968), 1-m lidar DEMs, and 2014 and 2018 National Agriculture Imagery Program orthophotos (Plates 1, 2, and 3). The distribution portrayed generally follows divisions in the soils map of Green (1982). Areas that Green (1982) described as dominantly silt or silty loam and that are of significant thickness to conceal the underlying bedrock geology, have been mapped as loess (**Qlo**); areas identified as mixtures of silt and rock (e.g., cobbly loam) have been mapped as part of the underlying bedrock geology. Most of the contacts portrayed represent man-modified boundaries, such as field edges, where silt-dominated deposits lie adjacent to or surround rock areas of mixed grain size. Thin and small loess (**Qlo**) deposits have not been mapped where the underlying geology can be reasonably inferred or is known to be present at the surface.

The distribution of loess (**Qlo**) across this part of the Columbia Plateau indicates episodic deposition by southwesterly winds (McDonald and others, 2012). Loess (**Qlo**) deposits in the eastern Middle Columbia Basin are assigned a Pleistocene and Holocene age on the basis of stratigraphic position and may be as old as ~ 600 ka (**Figure 6-1**). Medley (2012) interprets loess deposits and Missoula Flood deposits exposed along U.S. Highway 197 between Dufur and The Dalles to lie above a series of older paleosols that contain pumice correlated to the ~ 600 ka Dibekulewe tuff from Nevada (Cordero, 1997). Pluhar and others (2014) reported paleomagnetically reversed paleosols at the base of U.S. Highway 197 section, so loess in that area may be older than 0.78 Ma. The unit is identified as the Palouse Formation by Waters (1968).

**Figure 6-4. Loess deposits (Qlo) and Mima mounds. (a) Tilled wheat field underlain by loess (Qlo). Note the steep-sided field edges of redistributed loess resulting from circular, annual tilling of large fields. View is looking east from Boyd Market Road (45.470061, -121.082683). (b) Large swaths of ground between tilled loess-dominated wheat fields are capped by Mima mounds. View is looking southeast toward Kingsley from the Friend-Kingsley Market Road (45.348729, -121.223506). Photo credits: J.D. McClaughry, 2014.**

**Unconformity**

## 6.3 Upper Cenozoic volcanic and sedimentary rocks

### 6.3.1 Quaternary and/or upper Pliocene volcanic and sedimentary rocks of the late High Cascades

#### 6.3.1.1 Products of regional Quaternary volcanoes

**Qr5dr** **basaltic andesite of Dog River (lower Pleistocene)—**Basaltic andesite lava flow ($SiO_2$ = 55.88 to 57.56 weight percent; $K_2O$ = 1.08 to 1.24 weight percent; *n* = 20 analyses outside map area) mapped along South Fork Mill Creek in the northwest corner of the map area (**Figure 5-14**, **Figure 5-15**, **Figure 6-5**; **Table 6-1**; Plate 1; Appendix; McClaughry and others, 2020a; J.D. McClaughry unpublished geologic mapping). The basaltic andesite of Dog River (**Qr5dr**) was erupted from an extant cinder cone-capped fissure located south of Mill Creek Buttes, along the Dog River-Mill Creek divide at an altitude of 1,391 m (4,565 ft) (McClaughry and others, 2020a). South of Mill Creek Buttes the lava flow descended into South Fork Mill Creek and flowed northeast as an intracanyon lava flow ~25 km (15.5 mi) to Oak Flat, southwest of The Dalles (Plate 1). A unit **Qr5dr** lava flow also flowed northwest into the Hood River graben and ancestral valley of East Fork Hood River (McClaughry and others, 2020a). Outcrops of unit **Qr5dr** are characterized by a massive rounded form, by broad blocky meter-scale columns, or intervals of thick platy or slabby jointing (**Figure 6-5**). The lava flow typically weathers to subrounded boulders up to 0.5 m (1.6 ft) across or thick, angular slabs up to 2 m (6.6 ft) across. Maximum thickness of unit **Qr5dr** along South Fork Mill Creek is 40 m (131 ft) (Plate 1). Typical hand samples of the basaltic andesite are medium gray (N5), containing 15 to 25 percent (vol.) chalky light gray (N7), distinctly resorbed, euhedral to subhedral, blocky to prismatic, seriate plagioclase microphenocrysts and phenocrysts ≤5 mm (0.2 in), <1 percent (vol.) subhedral olivine microphenocrysts ≤1 mm (0.04 in), <1 percent (vol.), clear, subhedral to anhedral, blocky- to lath-shaped clinopyroxene microphenocrysts <1 mm (0.04 in), and rare subangular to subrounded andesite xenoliths to 1 cm (0.4 in), distributed within a fine-grained hypocrystalline groundmass (**Figure 6-6**). Sieve textures in plagioclase, displayed by corroded and partially resorbed crystals, are common (**Figure 6-6**). Clinopyroxene is common as inclusions in some larger plagioclase phenocrysts. Thin sections contain ~1 to 2 percent (vol.) Fe-Ti oxides.

Unit **Qr5dr** has normal magnetic polarity and is assigned an early Pleistocene age on the basis of stratigraphic position and an $^{40}Ar/^{39}Ar$ age of 1.87 ± 0.02 Ma (groundmass; sample 178 DWFJ 15; McClaughry and others, 2020a) (**Figure 6-1**). A whole rock K-Ar age of 1.7 ± 0.4 Ma (whole rock; sample JA85023) was reported for this unit by Anderson (1987) for a sample collected along South Fork Mill Creek (north of the map area) (**Figure 5-13**; Appendix). The reader should note that the original reported location for sample JA85023 was inadvertently transposed with sample JA85022, with a reported K-Ar age of 3.7 Ma (J.L. Anderson, written commun., 1998, to R.M. Conrey; Appendix). The 3.7 Ma age belongs to the older trachydacite of Fivemile Creek (**Tpdv**) (Plate 1; Appendix). Both samples and their corresponding geochemical and isotopic age-date analyses are herein properly located (**Table 5-1**).

**Figure 6-5. The basaltic andesite of Dog River (Qr5dr) exposed southeast of Mill Creek Buttes in the adjacent Fivemile Butte 7.5' quadrangle, (45.438261, -121.491110). Scale bar is 1 m (3.3 ft) tall. View is looking west. Photo credit: J.D. McClaughry, 2016.**

**Table 6-1. Representative XRF analyses for upper Pliocene and/or early Pleistocene volcanic rocks in the Dufur area.**

| Sample | 390 MCBJ 16 | RC98-190 | 167 DFWJ 15 | 159 DFWJ 15 | 175a WRCN 15 |
|---|---|---|---|---|---|
| **Geographic Area** | South Fk. Mill Creek | Hesslan Canyon | Hesslan Canyon | Owl Creek | Larch Creek |
| **Formation** | Regional volcano | Regional volcano | Regional volcano | Regional volcano | Regional volcano |
| **Map Unit** | Qr5dr | Qrbe | Qrbp | Qrbf | Qrbf |
| **UTM N (NAD 83)** | 5039473 | 5030616 | 5030698 | 5024159 | 5024930 |
| **UTM E (NAD 83)** | 626839 | 627673 | 627515 | 628806 | 632156 |
| **Age (Ma)** | ~1.8 Ma | nd | ~2.35 Ma | 2.57 Ma | ~2.57 Ma |
| **Plate** | na | 1 | 1 | na | 1 |
| **Map Label** | na | G49 | G51 | na | G17 |
| ***Oxides, weight percent*** | | | | | |
| **$SiO_2$** | 56.78 | 51.21 | 48.89 | 56.47 | 55.91 |
| **$Al_2O_3$** | 18.07 | 17.36 | 17.18 | 17.63 | 17.58 |
| **$TiO_2$** | 1.21 | 1.89 | 2.40 | 1.31 | 1.31 |
| **FeO*** | 7.05 | 9.56 | 12.34 | 8.06 | 8.14 |
| **MnO** | 0.12 | 0.17 | 0.19 | 0.12 | 0.13 |
| **CaO** | 7.47 | 8.66 | 8.04 | 6.88 | 7.20 |
| **MgO** | 4.01 | 6.26 | 5.53 | 4.31 | 4.48 |
| **$K_2O$** | 1.11 | 0.80 | 1.07 | 1.18 | 1.13 |
| **$Na_2O$** | 3.92 | 3.68 | 3.83 | 3.80 | 3.87 |
| **$P_2O_5$** | 0.26 | 0.40 | 0.52 | 0.25 | 0.26 |
| **LOI** | 0.17 | nd | nd | nd | 0.57 |
| **Total_I** | 99.36 | nd | 99.83 | 98.93 | 98.71 |
| ***Trace Elements, parts per million*** | | | | | |
| **Ni** | 47 | 95 | 70 | 62 | 66 |
| **Cr** | 60 | 152 | 96 | 99 | 96 |
| **Sc** | 19 | 25 | 23 | 19 | 19 |
| **V** | 162 | 189 | 189 | 156 | 161 |
| **Ba** | 325 | 281 | 229 | 324 | 333 |
| **Rb** | 17 | 3 | 7 | 20 | 17 |
| **Sr** | 770 | 498 | 510 | 497 | 522 |
| **Zr** | 157 | 157 | 231 | 159 | 157 |
| **Y** | 20 | 29 | 36 | 20 | 21 |
| **Nb** | 8.5 | 15.6 | 22.7 | 10.2 | 10.0 |
| **Ga** | 20 | 20 | 21 | 20 | 20 |
| **Cu** | 42 | 52 | 53 | 38 | 40 |
| **Zn** | 70 | 97 | 119 | 84 | 86 |
| **Pb** | 4 | 0 | 2 | 4 | 3 |
| **La** | 19 | 24 | 22 | 17 | 21 |
| **Ce** | 38 | 55 | 49 | 31 | 36 |
| **Th** | 4 | 2 | 2 | 3 | 4 |
| **Nd** | 22 | 0 | 30 | 19 | 23 |
| **U** | 2 | 0 | 2 | 0 | 2 |

Major element determinations have been normalized to a 100-percent total on a volatile-free basis and recalculated with total iron expressed as FeO*; nd - no data or element not analyzed; na - not applicable or no information. LOI, Loss on Ignition; Total_I, original analytical total.

**Figure 6-6. Hand sample and thin section photographs of the basaltic andesite of Dog River (Qr5dr). (a) Typical abundantly plagioclase-phyric hand sample. Scale bar is 2.5 cm (1 in) tall. (b) Thin section of the basaltic andesite of Dog River (Qr5dr) under cross-polarized light (XPL). (c) Same view as in B under plane-polarized light (PPL). Scale bar for thin- section photographs is 7 mm (0.3 in) wide. Photo credit: J.D. McClaughry, 2017.**

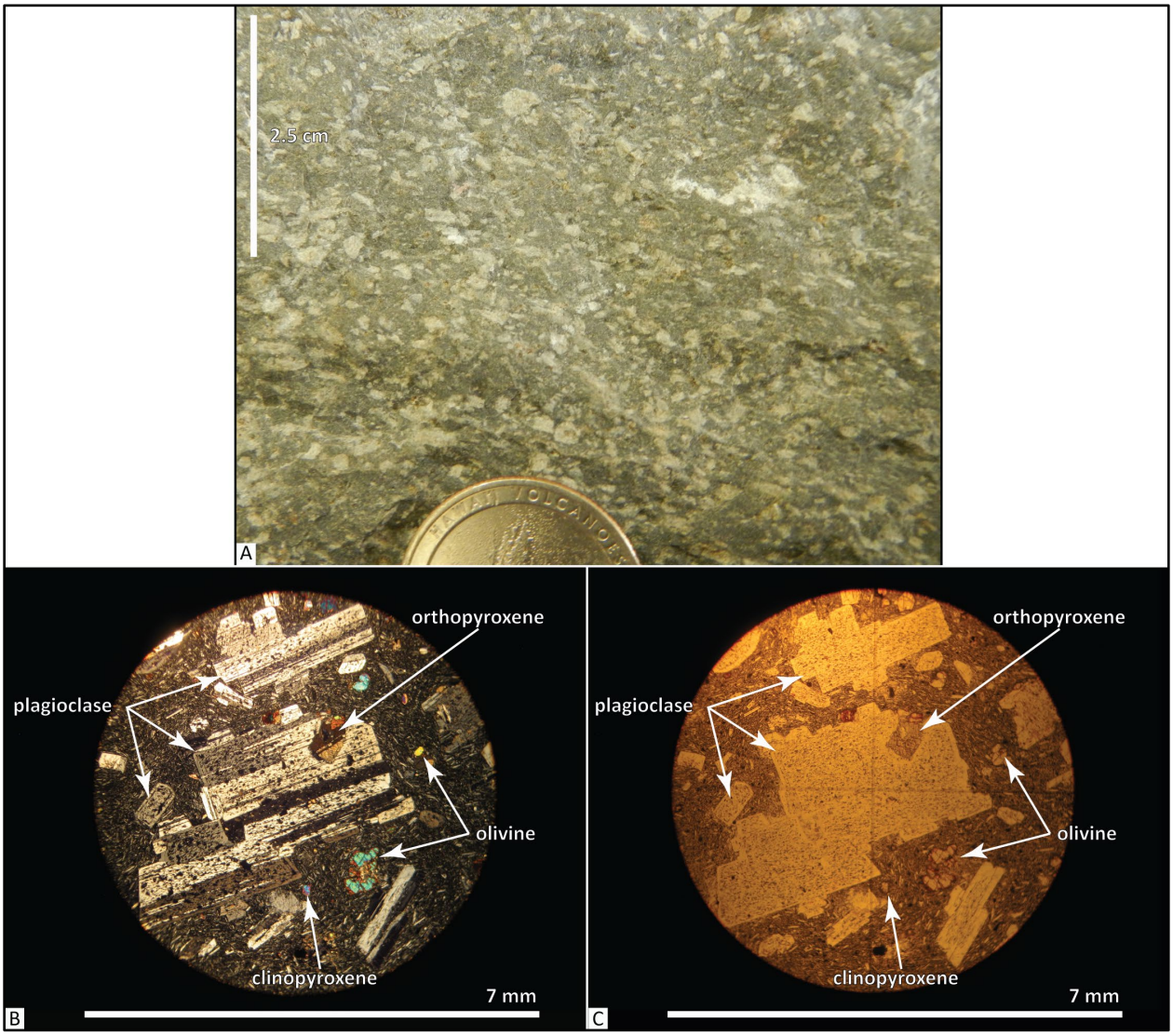


**Qrbe** **basalt of Hesslan Canyon (lower Pleistocene)—**Basalt lava flow ($SiO_2$ = 48.89 to 50.23 weight percent; $K_2O$ = 0.99 to 1.07 weight percent; *n* = 4 analyses [3 outside map area]) with high amounts of titanium ($TiO_2$ = 2.12 to 2.40 weight percent) mapped along Hesslan Canyon in the western part of the map area (**Figure 5-14**, **Figure 5-15**; **Table 6-1**; Plate 1; Appendix; J.D. McClaughry unpublished geologic mapping, 2016). Outcrops of unit **Qrbe** in Hesslan Canyon form the distal snout of an intracanyon lava flow discontinuously exposed ~10.5 km (6.5 mi) west to Bottle Prairie (west of map area; McClaughry and others, 2020a). No outcrops or vent area for the lava flow have been found west of Bottle Prairie. Limited outcrops of unit **Qrbe** are characterized by broad blocky meter-scale columns or intervals of platy jointing. Unit **Qrbe** generally weathers to subangular plates 0.25 to 1 m (0.8 to 3.3 ft) across. Thickness of the lava flow (**Qrbe**) exceeds

32 m (105 ft) in the western part of the map area (Plate 1). Typical hand samples of the basalt are medium light gray (N6) to medium gray (N5) containing 1 to 2 percent (vol.) clear, euhedral, prismatic, seriate plagioclase microphenocrysts and phenocrysts 1 to 2 mm (0.04 to 0.1 in) long and ~3 to 5 percent (vol.) clear to altered yellow-brown, subhedral to anhedral, polygonal- to blocky-shaped, seriate olivine microphenocrysts <1 mm (0.04 in) across, distributed within a fine-grained hypocrystalline groundmass (**Figure 6-7**). Plagioclase phenocrysts occur as single prismatic crystals that commonly have oscillatory and concentric zoning and polysynthetic twins (albite). Olivine microphenocrysts are typically skeletal and are altered to dark yellowish orange (10YR 6/6) iddingsite. Thin sections contain <1 percent (vol.) Fe-Ti oxides.

The basalt has reversed magnetic polarity and is assigned an early Pleistocene age on the basis of stratigraphic position above the 2.35 Ma basalt of Bennett Pass Road (**Qrbp**) (**Figure 6-1**).

**Figure 6-7. Hand sample and thin section photographs of the basalt of Hesslan Canyon (Qrbe). (a) Typical hand sample. Scale bar is 2.5 cm (1 in) tall. (b) Thin section under cross-polarized light (XPL). (c) Same view as in B under plane-polarized light (PPL). Scale bar for thin-section photographs is 7 mm (0.3 in) wide. Photo credit: J.D. McClaughry, 2017.**

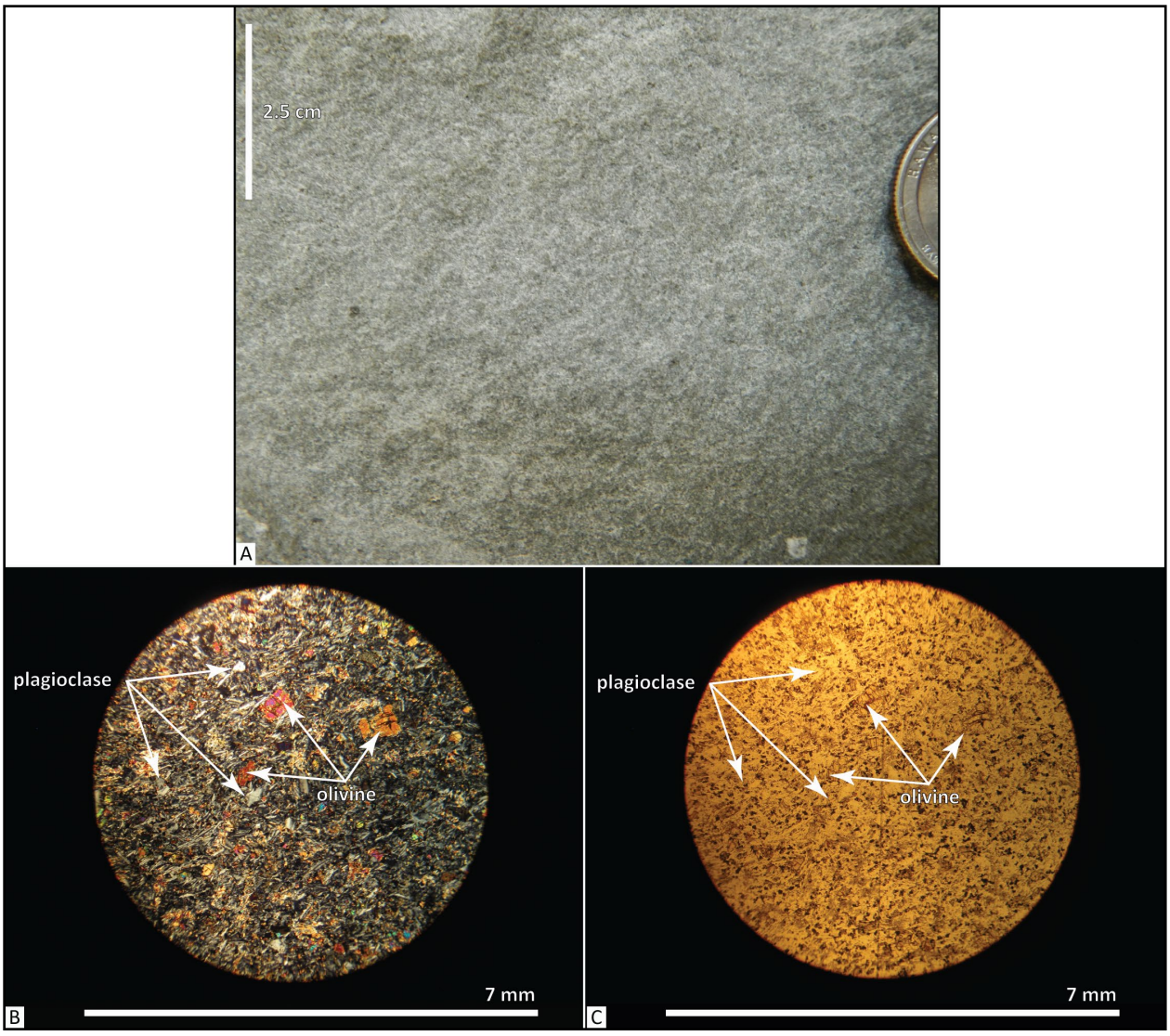

**Qrbp** **basalt of Bennett Pass Road (lower Pleistocene)**—Basalt lava flow ($SiO_2$ = 50.01 to 51.90 weight percent; $K_2O$ = 0.78 to 0.96 weight percent; *n* = 7 analyses [6 outside map area]) mapped at the mouth of Hesslan Canyon in the western part of the map area (**Figure 5-14**, **Figure 5-15**; **Figure 6-8**; **Table 6-1**; Plate 1; Appendix; McClaughry and others, 2020a; J.D. McClaughry unpublished geologic mapping, 2016). Outcrops of unit **Qrbp i**n Hesslan Canyon form the distal snout of an intracanyon lava flow discontinuously exposed ~10.5 km (6.5 mi) west to Bottle Prairie (west of map area) and an additional 6 km (3.7 mi) southwest to High Prairie (McClaughry and others, 2020a). Limited outcrops of unit **Qrbp** are characterized by broad blocky meter-scale columns or intervals of platy jointing (**Figure 6-8**); weathered parts of the flow are characterized by subangular plates 0.25 to 1 m (0.8 to 3.3 ft) across. Thickness of unit **Qrbp** is ≥32 m (105 ft) in Hesslan Canyon. Typical hand samples of the basalt are light gray (N7) to medium dark gray (N4), aphyric to sparsely microporphyritic, containing ≤1 percent (vol.) clear, subhedral to anhedral, prismatic, seriate plagioclase microphenocrysts ≤1 mm (0.04 in) and 2 to 3 percent (vol.) fresh dark greenish yellow (10Y 6/6), subhedral olivine microphenocrysts ≤1 mm (0.04 in), contained within a fine-grained holocrystalline groundmass (**Figure 6-9**). Very rare subhedral olivine phenocrysts occur up to 3 mm (0.1 in). Olivine microphenocrysts are typically skeletal in form and are partially to wholly altered to dark yellowish orange (10YR 6/6) iddingsite. Sieve textures in plagioclase crystals are common. Thin sections contain 1 to 3 percent (vol.), cubic-shaped Fe-Ti oxides.

Unit **Qrbp** has reversed magnetic polarity and is assigned an early Pleistocene age on the basis of stratigraphic position, intracanyon geomorphic setting, and a weighted mean whole rock K-Ar age of 2.35 ± 0.03 Ma for an outcrop at Lookout Mountain (sample S92-H271, Conrey and others, 1996; McClaughry and others, 2020a) (**Figure 6-1**).

**Figure 6-8. The basalt of Bennett Pass Road (Qrbp) cropping out at the mouth of Hesslan Canyon (45.417423, -121.368405). View is looking south. Hammer for scale is 38 cm (15.7 in) long. Photo credit: J.D. McClaughry, 2017.**

**Figure 6-9. Hand sample and thin section photographs of the basalt of Bennett Pass Road (Qrbp). (a) Typical hand sample. Scale bar is 2.5 cm (1 in) tall. (b) Thin section under cross-polarized light (XPL). (c) Same view as in B under plane-polarized light (PPL). Scale bar for thin-section photographs is 7 mm (0.3 in) wide. Photo credit: J.D. McClaughry, 2017.**

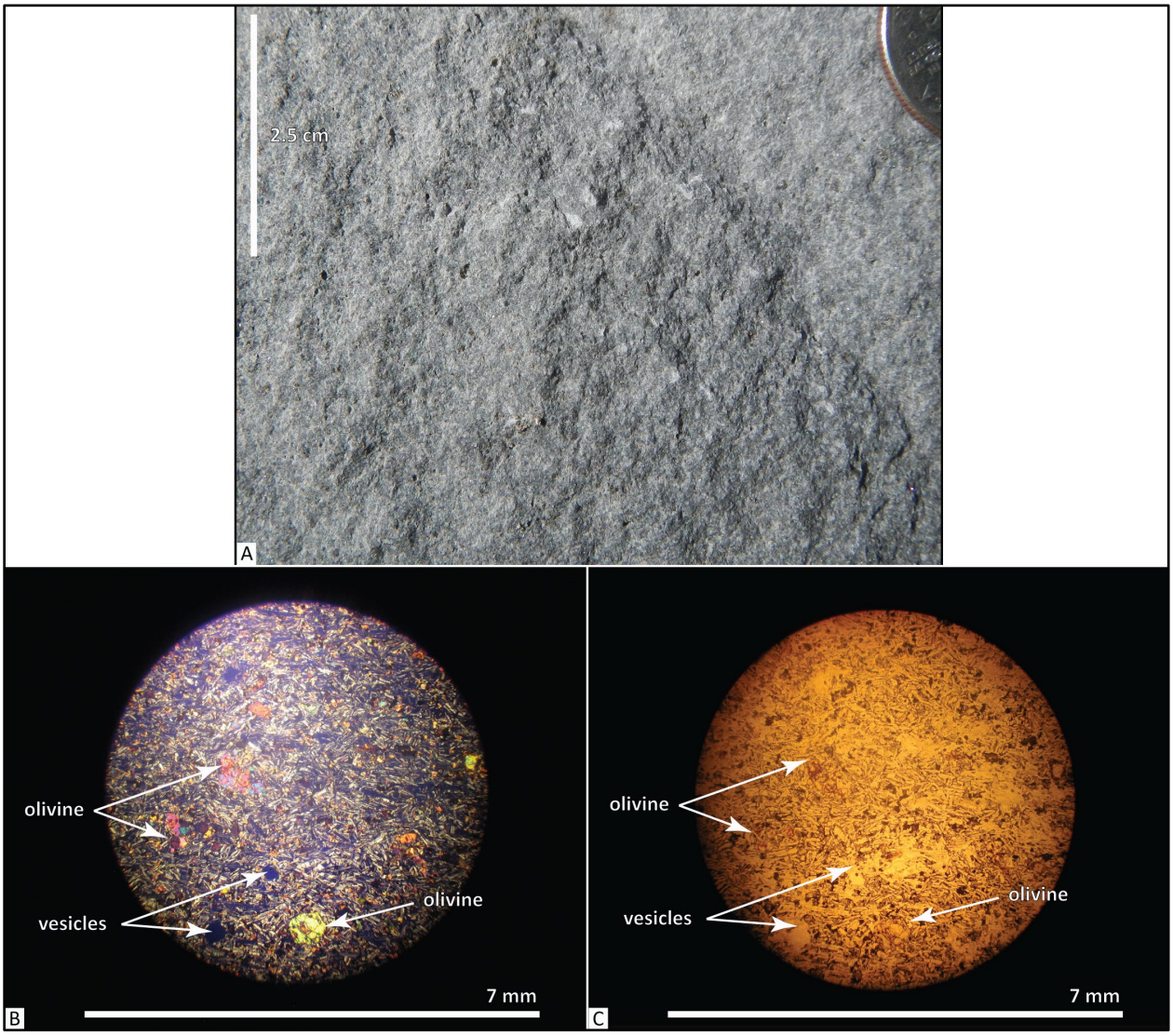


**Qrbf** **basaltic andesite of Flag Point (lower Pleistocene or early Pliocene)**—Basaltic andesite lava flow ($SiO_2$ = 54.79 to 56.61 weight percent; $K_2O$ = 0.98 to 1.38 weight percent; *n* = 14 analyses [12 outside map area]) mapped as an intracanyon lava flow between Larch Creek and Owl Hollow in the southwestern part of the map area (**Figure 5-14**, **Figure 5-15**; **Figure 6-10**; **Table 6-1**; Plate 1; Appendix; J.D. McClaughry unpublished geologic mapping, 2016). Outcrops of unit **Qrbf** south of Larch Creek form the distal snout of an intracanyon lava flow discontinuously exposed ~9 km (5.6 mi) west to Frailey Point (west of map area) and an additional 5 km (3.1 mi) southwest to a vent area at Flag Point (J.D. McClaughry unpublished geologic mapping, 2016). Roadcuts and outcrops of unit **Qrbf** are characterized by a massive rounded form, by broad blocky meter-scale columns, or intervals of platy jointing (**Figure 6-10**). Unit **Qrbf** generally weathers to rounded boulders up to 1 m (3.3 ft) across. Thickness of unit **Qrbf** is ~25 m (82 ft) in the southwest corner

of the map area. Typical hand samples of the basaltic andesite are medium gray (N5) to medium dark gray (N4) basaltic andesite containing 3 to 5 percent (vol.) colorless, euhedral, prismatic, seriate plagioclase microphenocrysts and phenocrysts typically 1 to 2 mm (0.04 to 0.1 in) long (rarely with phenocrysts up to 7 mm [0.3 in] long) and <1 percent (vol.) clear, subhedral to anhedral, polygonal- to blocky-shaped, seriate olivine microphenocrysts <1 mm (0.04 in) across, distributed within a locally diktytaxitic, fine-grained holocrystalline groundmass (**Figure 6-11**). Sieve textures in plagioclase crystals are common. Olivine microphenocrysts are typically skeletal in form and have rare areas or rims altered to dark yellowish orange (10YR 6/6) iddingsite. Thin sections contain 1 to 3 percent (vol.) Fe-Ti oxides and include rare anhedral, embayed clear quartz xenocrysts rimmed by glass and an aggregate of granular pyroxene crystals, which separate it from the groundmass.

Unit **Qrbf** has reversed magnetic polarity and is assigned an early Pliocene or early Pleistocene age on the basis of stratigraphic position and an $^{40}Ar/^{39}Ar$ plateau age of 2.57 ± 0.02 Ma (groundmass; sample 159 DFWJ 15) for outcrops located on the north edge of Owl Hollow, just outside the southwestern part of the map area (**Figure 5-13**, **Figure 6-1**; **Table 5-1;** Appendix). Lithology, chemical composition, and map pattern indicates that **Qrbf** flows were erupted from an extant cinder cone-capped vent underlying the lookout at Flag Point (southwest of the map area; Sherrod and Scott, 1995). Conrey and others (1996) reported a whole rock K-Ar age of 1.92 ± 0.2 Ma (sample RC-DS199A) for basalt underlying the Flag Point lookout.

**Figure 6-10. Basaltic andesite of Flag Point (Qrbf). Knob-forming outcrop of the basaltic andesite of Flag Point (Qrbf) exposed in the headwaters of Larch Creek in the southwestern part of the map area (45.365600, -121.311000). View is looking northeast. Flag Point, the source vent for this flow, lies ~14 km (8.8 mi) southwest of this outcrop. Photo credit: C.A. Niewendorp, 2015.**

**Figure 6-11. Hand sample and thin section photographs of the basaltic andesite of Flag Point (Qrbf). (a) Typical hand sample. Scale bar is 2.5 cm (1 in) tall. (b) Thin section under cross-polarized light (XPL). (c) Same view as in B under plane-polarized light (PPL). Scale bar for thin-section photographs is 7 mm (0.3 in) wide. Photo credit: J.D. McClaughry, 2017.**

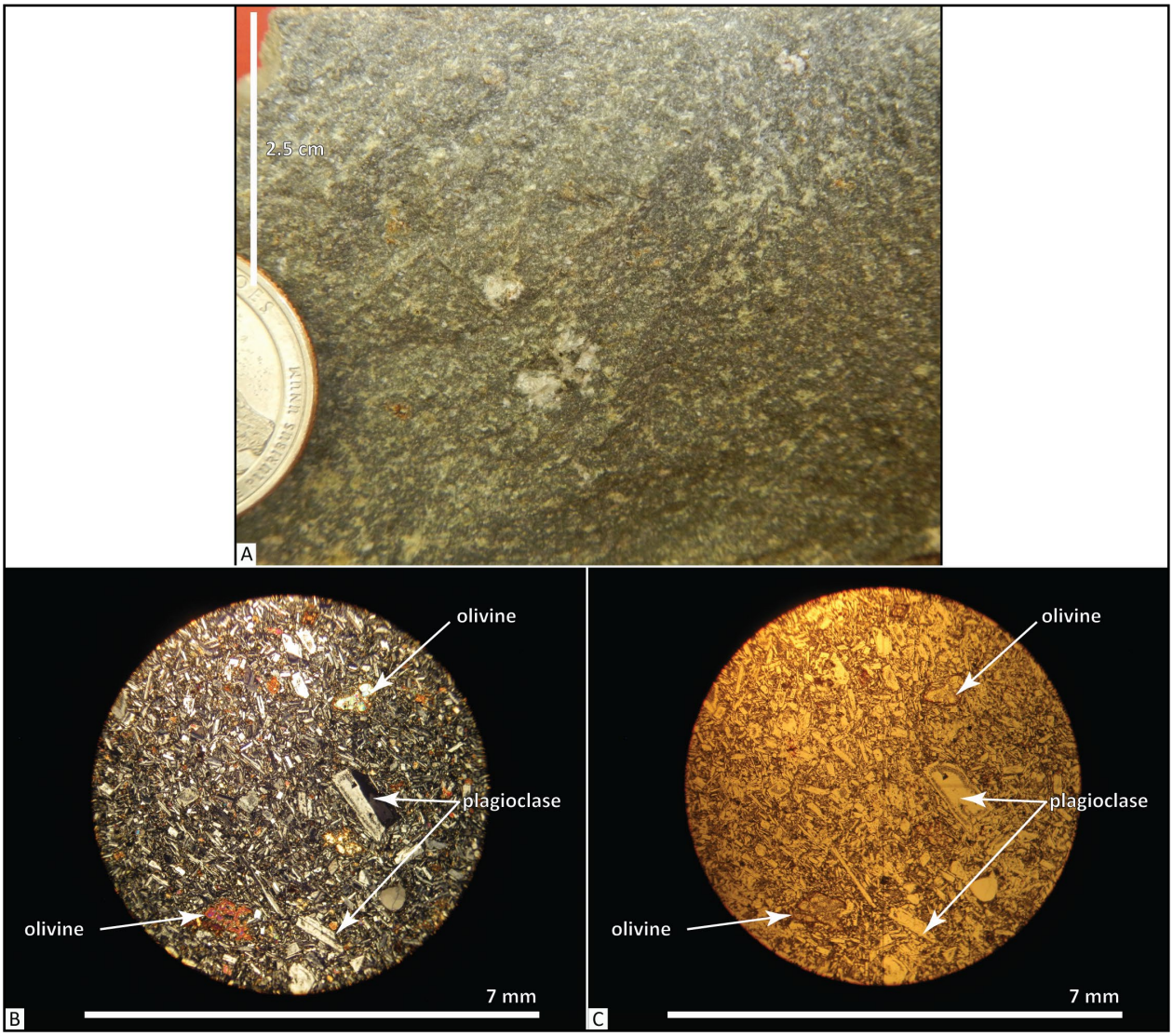

**Disconformity**

### 6.3.2 Pliocene volcanic and sedimentary rocks of the late High Cascades

**QTpg** **sedimentary deposits (lower Pleistocene and/or upper Pliocene)—**Unconsolidated to partially indurated cobble gravel and sand capping older Pliocene units in two parts of the Dufur area. Unit **QTpg** is exposed along Fivemile Creek, where partially indurated gravel and sand is preserved in canyon-restricted lobes above the trachydacite of Fivemile Creek (**Tpdv**) (**Figure 6-12**; Plate 1). Typical thickness of unit **QTpg** along Fivemile Creek is ≤25 m (80 ft). Largely unconsolidated cobble gravel also caps non-welded pumice tuff (**Tppt**) and dacite-clast breccia (**Tpdd1**) along U.S. Highway 197, south of Dufur (**Figure 6-13**; Plate 2). Gravel deposits along U.S. Highway 197 are <2 m (6.6 ft) thick, and are composed dominantly of moderately sorted, clast-supported, subrounded to well-rounded, pebble- to cobble-sized, porphyritic andesitic to dacitic clasts (**Figure 6-13a,b**). The unit is assigned a late Pliocene and/or early Pleistocene age on the basis of stratigraphic position above the ~3.71 Ma tuff breccia of Engineers Creek (**Tpdd1**) and the 3.69 Ma trachydacite of Fivemile Creek (**Tpdv**) (**Figure 6-1**).

**Figure 6-12. Sedimentary deposits (QTpg) exposed along Dutch Flat Road in the northern part of the map area (45.489486, -121.299281). Hammer for scale is 25 cm (10 in) long. View is looking northeast. Photo credit: C.A. Niewendorp, 2015.**

**Figure 6-13. Pumice tuff (Tppt) and gravel (QTpg) exposed on U.S. Highway 197 south of Pine Creek (45.408438, -121.139513). (a) Gravel (QTpg) above non-welded pumice tuff (Tppt). Kneeling person for scale is 1 m (3.3 ft) high. Dashed white line is drawn along the contact. Letter 'B' shows the location of photo B. Letter 'C' shows the location of photo C. View is looking southeast. (b) Clast-supported, moderately sorted, cobble-dominated gravel (QTpg). View is looking southeast. (c) Non-welded pumice tuff (Tppt). Arrows point to individual pumices. Pen is 15 cm (5.5 in) tall. Photo credits: J.D. McClaughry, 2014.**

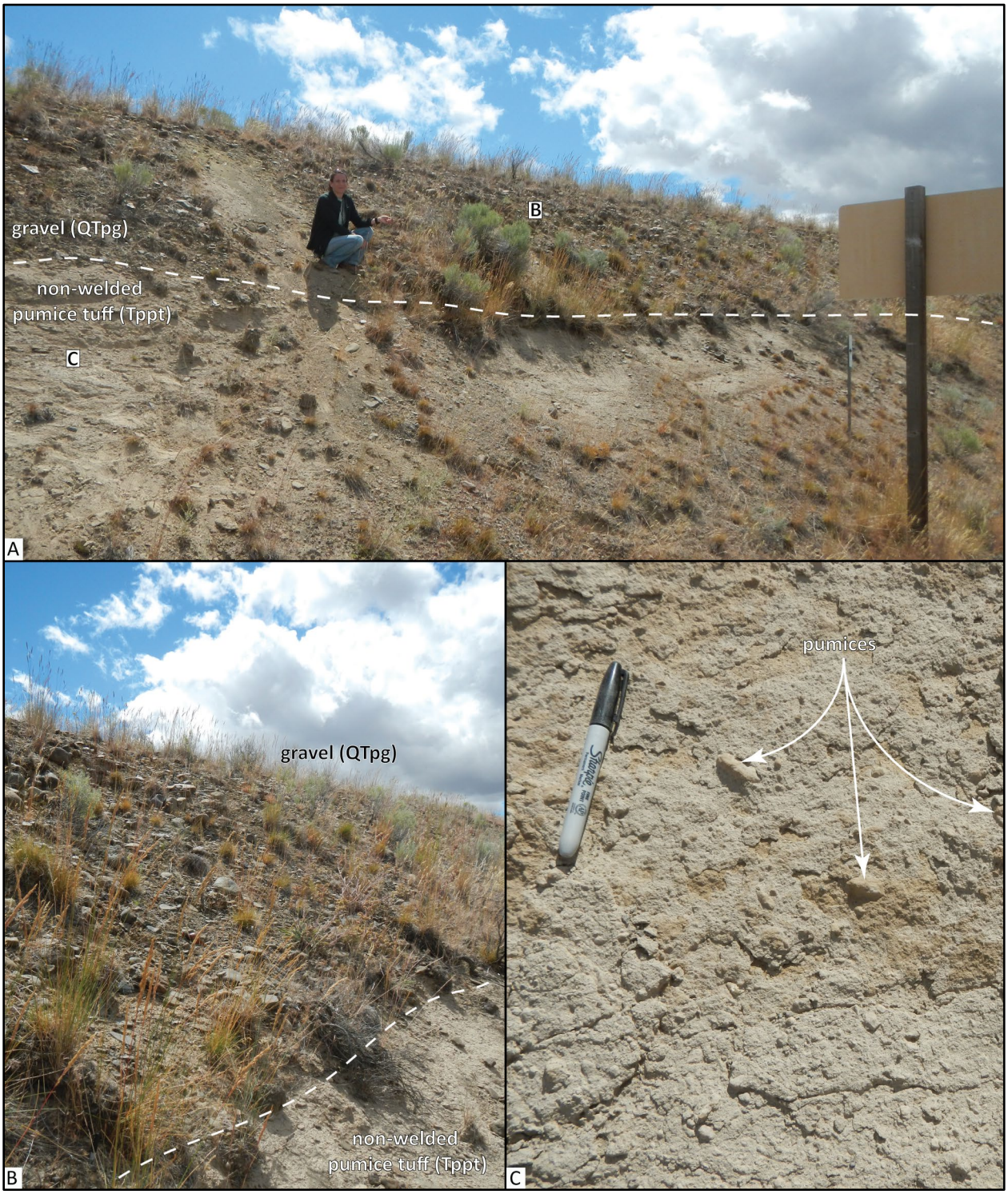

**Tpdf** **dacite of Fifteenmile Creek (upper Pliocene)—**Dacite lava flow ($SiO_2$ = 62.55 to 64.14 weight percent; $K_2O$ = 2.01 to 2.31 weight percent; *n* = 9 analyses [26 outside map area]) capping a narrow ridge between Larch and Fifteenmile Creeks in the southwest corner of the map area (**Figure 5-11**, **Figure 5-12**, **Figure 6-14**; **Table 6-2**; Plate 1; Appendix; McClaughry and others, 2020a). Outcrops of unit **Tpdf** form the distal snout of an intracanyon lava flow discontinuously exposed ~15 km (9.3 mi) west to the headwaters of Fret Creek (west of map area; McClaughry and others, 2020a). A flow-on-flow sequence of compositionally identical dacite lava flows and several prominent N.15°E.- to N.25°E.-striking dacite dikes ($SiO_2$ = 62.55 to 66.26 weight percent; $K_2O$ = 2.01 to 3.01 weight percent; *n* = 19 analyses) mapped as part of unit **Tpdf** in the upper parts of Culvert Creek in the Badger Lake 7.5′ quadrangle mark the vent area (McClaughry and others, 2020a). Unit **Tpdf** crops out as precipitous cliff-forming exposures marked by meter-scale columnar-jointing; columns are often characterized by internal, horizontal platy joint sets. Outcrops weather to meter-scale, subrounded boulders and angular slabs, forming extensive talus slopes beneath cliffs (**Figure 6-14b**). Irregularly shaped gabbro-norite inclusions ($SiO_2$ = 53.85 to 57.77 weight percent; $K_2O$ = 0.72 to 1.88 weight percent; *n* = 7 analyses outside map area), ranging from centimeters up to several meters across, are a conspicuous and distinguishing feature of this unit throughout its outcrop distribution (McClaughry and others, 2020a). Concentration of inclusions ranges from ~5 to ≤50 percent (vol.). The composite thickness of the unit in the map area is ~ 60 to 70 m (197 to 230 ft) (Plate 1). Typical hand samples of the dacite are medium light gray (N6), medium dark gray (N4), light bluish gray (5B 7/1), to medium bluish gray (5B 5/1), containing 10 to 20 percent (vol.) clear to chalky white (N9), euhedral to subhedral, prismatic to blocky, seriate plagioclase microphenocrysts and phenocrysts ≤1 cm (0.4 in), 2 to 3 percent (vol.) grayish black (N2), euhedral to subhedral, blocky to prismatic pyroxene microphenocrysts and phenocrysts ≤ 3 mm (0.1 in) (orthopyroxene > clinopyroxene), and ~2 percent (vol.) plagioclase-pyroxene glomerocrysts ≤6 mm (0.2 in) distributed within a very fine-grained holocrystalline to hypocrystalline groundmass (**Figure 6-15**). Gabbro-norite inclusions are medium light gray (N6) to pale yellowish brown (10YR 6/2) and equigranular, with a mottled medium-grained holocrystalline groundmass of plagioclase and pyroxene (clinopyroxene + orthopyroxene).

Unit **Tpdf** has normal magnetic polarity and is assigned a late Pliocene age on the basis of stratigraphic position and a groundmass $^{40}Ar/^{39}Ar$ plateau age of 3.02 ± 0.02 Ma (groundmass; sample 146 DFWJ 15) obtained from outcrops between Fifteenmile and Larch Creeks in the southwest part of the map area (**Figure 5-13**, **Figure 6-1**; **Table 5-1**; Plate 1; Appendix). The 3.02 Ma age is similar to an older K-Ar age of 2.86 ± 0.06 Ma (plagioclase; sample RCS88-25) reported by Sherrod and Scott (1995) and Gray and others (1996) for a sample from equivalent lava flows mapped near Cold Point, ~7 km (4.3 mi) southwest of the map area.

**Figure 6-14. The dacite of Fifteenmile Creek (Tpdf) exposed in the upper Fifteenmile Creek drainage in the southwestern part of the map area (45.387246, -121.335311). (a) The lava flow (Tpdf) fills a paleochannel incised into underlying monolithologic dacite clast breccia deposits of unit Tpdd1 and Tmdd. View is looking west up Fifteenmile Creek toward Mount Hood. (b) Close-up of cliff-forming outcrops shown in A, showing characteristic massive columnar to platy jointing (45.383368, -121.337802). The location of photograph B corresponds to sample 146 DFWJ 15 with an $^{40}Ar/^{39}Ar$ plateau age of 3.02 ± 0.02 Ma. View is looking north-northwest. Photo credits: C.A. Niewendorp, 2015.**

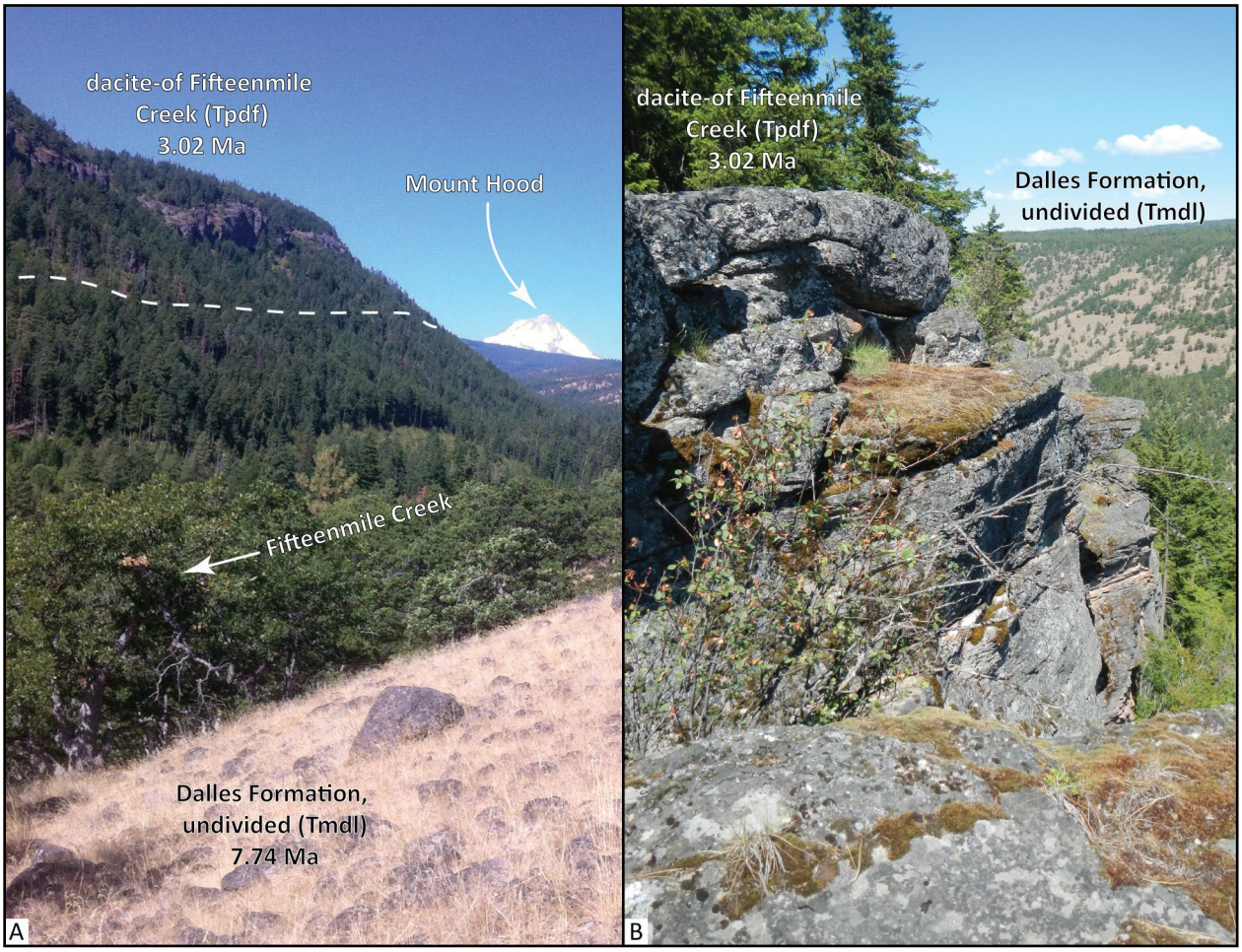

**Table 6-2. Representative XRF analyses for Pliocene volcanic rocks in the Dufur area (part 1 of 2).**

| Sample | 146 DFWJ 15 | 71 DFWJ 15 | 76a DFWJ 14 | 76b DFWJ 14 | 150 DFWJ 15 | 151 DFWJ 15 | 160b DFWJ 15 | 160a DFWJ 15 | 155a DFWJ 15 | 31 DFWJ 15 | 70 DFWJ 15 |
|---|---|---|---|---|---|---|---|---|---|---|---|
| **Geographic Area** | Fifteenmile Creek | Pine Creek | U.S. 197 | U.S. 197 | Larch Creek | Larch Creek | Larch Creek | Larch Creek | Larch Creek | Friend | Pine Creek |
| **Formation** | Pliocene Pleist. volcanics | Pliocene Pleist. volcanics | Pliocene Pleist. volcanics | Pliocene Pleist. volcanics | Pliocene Pleist. volcanics | Pliocene Pleist. volcanics | Pliocene Pleist. volcanics | Pliocene Pleist. volcanics | Pliocene Pleist. volcanics | Pliocene Pleist. volcanics | Pliocene Pleist. volcanics |
| **Map Unit** | Tpdf | Tppt (pumice) | Tppt (pumice) | Tppt (bulk) | Tpdd2 | Tpdd2 | Tptf2 | Tptf2 | Tptf2 | Tpdd1 (clast) | Tpdd1 (clast) |
| **UTM N (NAD 83)** | 5026883 | 5027592 | 5030006 | 5030006 | 5024660 | 5024676 | 5023701 | 5023701 | 5024488 | 5024233 | 5027593 |
| **UTM E (NAD 83)** | 630132 | 640405 | 645611 | 645611 | 629593 | 629633 | 629422 | 629422 | 629570 | 636804 | 640438 |
| **Age (Ma)** | 3.02 Ma | nd | nd | nd | nd | nd | nd | nd | nd | ~3.71 Ma | nd |
| **Plate** | 1 | 2 | 2 | 2 | 1 | 1 | na | na | 1 | 1 | 2 |
| **Map Label** | G37 | G41 | G77 | G78 | G14 | G16 | na | na | G5 | G3 | G42 |
| ***Oxides, weight percent*** | | | | | | | | | | | |
| **$SiO_2$** | 64.14 | 65.93 | 68.19 | 66.50 | 62.86 | 63.05 | 66.77 | 67.19 | 67.29 | 64.12 | 64.49 |
| **$Al_2O_3$** | 16.09 | 18.36 | 15.60 | 16.97 | 15.98 | 15.80 | 16.02 | 16.91 | 15.91 | 15.22 | 16.24 |
| **$TiO_2$** | 0.86 | 0.66 | 0.64 | 0.82 | 1.22 | 1.23 | 0.79 | 0.70 | 0.69 | 1.09 | 0.78 |
| **FeO*** | 5.23 | 5.67 | 4.42 | 5.70 | 6.52 | 6.33 | 5.49 | 4.88 | 5.13 | 6.65 | 5.16 |
| **MnO** | 0.09 | 0.11 | 0.08 | 0.09 | 0.16 | 0.16 | 0.09 | 0.09 | 0.09 | 0.11 | 0.09 |
| **CaO** | 4.90 | 3.20 | 2.27 | 2.46 | 4.01 | 4.06 | 2.45 | 1.98 | 2.21 | 3.69 | 4.50 |
| **MgO** | 2.14 | 1.24 | 0.58 | 0.76 | 1.53 | 1.55 | 0.64 | 0.55 | 0.62 | 1.28 | 1.84 |
| **$K_2O$** | 2.31 | 2.21 | 4.12 | 3.17 | 1.81 | 1.80 | 3.99 | 4.10 | 4.14 | 3.42 | 2.68 |
| **$Na_2O$** | 4.03 | 2.41 | 3.93 | 3.33 | 5.51 | 5.63 | 3.58 | 3.45 | 3.78 | 4.06 | 4.03 |
| **$P_2O_5$** | 0.21 | 0.20 | 0.15 | 0.20 | 0.39 | 0.40 | 0.18 | 0.16 | 0.15 | 0.38 | 0.19 |
| **LOI** | nd | 9.63 | nd | 10.44 | nd | nd | 5.42 | 5.42 | 3.93 | nd | nd |
| **Total_I** | 98.91 | 99.55 | 95.42 | 99.87 | 98.97 | 98.75 | 95.52 | 93.43 | 95.10 | 98.70 | 98.76 |
| ***Trace Elements, parts per million*** | | | | | | | | | | | |
| **Ni** | 25 | 13 | 4 | 23 | 1 | 2 | 3 | 3 | 2 | 1 | 14 |
| **Cr** | 35 | 13 | 4 | 17 | 1 | 1 | 6 | 5 | 3 | 0 | 13 |
| **Sc** | 11 | 8 | 9 | 8 | 15 | 15 | 10 | 10 | 9 | 12 | 11 |
| **V** | 103 | 41 | 16 | 45 | 46 | 45 | 31 | 18 | 19 | 47 | 70 |
| **Ba** | 452 | 645 | 609 | 663 | 449 | 429 | 630 | 622 | 630 | 640 | 546 |
| **Rb** | 52 | 63 | 84 | 69 | 32 | 31 | 85 | 84 | 85 | 72 | 53 |
| **Sr** | 449 | 367 | 187 | 212 | 417 | 423 | 228 | 178 | 192 | 285 | 377 |
| **Zr** | 239 | 334 | 486 | 522 | 267 | 259 | 438 | 525 | 483 | 389 | 241 |
| **Y** | 24 | 108 | 45 | 47 | 37 | 37 | 45 | 46 | 48 | 45 | 30 |
| **Nb** | 13.9 | 18.8 | 27.2 | 33.7 | 20.3 | 19.8 | 26.8 | 29.1 | 27.7 | 26.0 | 16.8 |
| **Ga** | 19 | 26 | 21 | 27 | 24 | 23 | 21 | 23 | 22 | 23 | 20 |
| **Cu** | 16 | 29 | 10 | 43 | 3 | 1 | 19 | 16 | 15 | 19 | 22 |
| **Zn** | 66 | 84 | 79 | 101 | 115 | 115 | 78 | 77 | 68 | 103 | 77 |
| **Pb** | 6 | 2 | 9 | <1 | 6 | 6 | 8 | 8 | 8 | 8 | 8 |
| **La** | 31 | 85 | 39 | 44 | 27 | 28 | 40 | 40 | 42 | 42 | 26 |
| **Ce** | 52 | 65 | 84 | 81 | 57 | 57 | 77 | 87 | 78 | 85 | 52 |
| **Th** | 8 | 16 | 11 | 23 | 3 | 4 | 10 | 12 | 11 | 9 | 6 |
| **Nd** | 24 | nd | 38 | nd | 33 | 32 | 39 | 40 | 42 | 47 | 26 |
| **U** | 3 | 1 | 4 | 1 | 2 | 3 | 2 | 3 | 4 | 4 | 3 |

Major element determinations have been normalized to a 100-percent total on a volatile-free basis and recalculated with total iron expressed as FeO*; nd - no data or element not analyzed; na - not applicable or no information. LOI, Loss on Ignition; Total_I, original analytical total.

*Table 6-2, continued. Select XRF geochemical analyses for Pliocene volcanics in the Dufur area (part 2 of 2).*

| Sample | 98 DFWJ 15 | 265 DFWJ 14 | 372a DFWJ 14 | 372b DFWJ 14 | 202b DFWJ 15 | 269 DFWJ 14 | 373 DFWJ 14 | 168 WRCN 15 | 148 DFWJ 15 | 173 DFWJ 15 | JA85022 ¥ | 172 DFWJ 15 |
|---|---|---|---|---|---|---|---|---|---|---|---|---|
| **Geographic Area** | Pine Creek | Pine Creek | Mays Creek Canyon | Mays Creek Canyon | U.S. 197 | Pine Creek | Mays Creek Canyon | Larch Creek | Larch Creek | Fivemile Creek | Fivemile Creek | Fivemile Creek |
| **Formation** | Pliocene Pleist. volcanics | Pliocene Pleist. volcanics | Pliocene Pleist. volcanics | Pliocene Pleist. volcanics | Pliocene Pleist. volcanics | Pliocene Pleist. volcanics | Pliocene Pleist. volcanics | Pliocene Pleist. volcanics | Pliocene Pleist. volcanics | Pliocene Pleist. volcanics | Pliocene Pleist. volcanics | Pliocene Pleist. volcanics |
| **Map Unit** | Tpdd1 (clast) | Tpdd1 (clast) | Tpdd1 (clast) | Tpdd1 (clast) | Tpdd1 (clast) | Tpdd1 (basal tuff) | Tpdd1 (basal tuff) | Tptf1 | Tptf1 | Tpdv | Tpdv | Tpbf |
| **UTM N (NAD 83)** | 5028439 | 5029062 | 5029749 | 5029749 | 5029001 | 5029200 | 5029826 | 5025270 | 5024595 | 5037478 | 5038928 | 5037452 |
| **UTM E (NAD 83)** | 640916 | 643030 | 644812 | 644812 | 653145 | 643134 | 644838 | 630252 | 629502 | 631449 | 634134 | 631479 |
| **Age (Ma)** | nd | 3.71 Ma | nd | nd | nd | nd | 3.83 Ma | nd | nd | 3.69 Ma | 3.7 | 3.72 |
| **Plate** | 2 | 2 | 2 | 2 | 2 | 2 | 2 | 1 | 1 | 1 | 1 | 1 |
| **Map Label** | G52 | G60 | G72 | G73 | G81 | G65 | G75 | G20 | G8 | G67 | G78 | G65 |
| ***Oxides, weight percent*** | | | | | | | | | | | | |
| **$SiO_2$** | 63.31 | 65.14 | 64.06 | 75.31 | 73.93 | 67.44 | 67.26 | 62.84 | 62.43 | 65.53 | 65.03 | 51.84 |
| **$Al_2O_3$** | 16.65 | 15.24 | 16.29 | 13.52 | 14.60 | 15.21 | 15.79 | 16.55 | 15.94 | 14.90 | 14.87 | 17.64 |
| **$TiO_2$** | 0.81 | 0.92 | 0.86 | 0.09 | 0.15 | 0.48 | 0.82 | 1.24 | 1.31 | 0.93 | 0.92 | 1.72 |
| **FeO*** | 5.50 | 6.18 | 5.47 | 1.49 | 1.33 | 6.53 | 5.45 | 6.72 | 6.69 | 6.31 | 6.28 | 9.54 |
| **MnO** | 0.11 | 0.12 | 0.09 | 0.03 | 0.04 | 0.11 | 0.08 | 0.14 | 0.17 | 0.12 | 0.12 | 0.16 |
| **CaO** | 4.93 | 3.44 | 4.55 | 0.86 | 1.28 | 2.75 | 3.17 | 3.99 | 4.30 | 3.23 | 3.16 | 8.53 |
| **MgO** | 2.14 | 1.18 | 1.99 | 0.05 | 0.08 | 0.76 | 1.10 | 1.28 | 1.64 | 0.95 | 0.80 | 5.59 |
| **$K_2O$** | 2.38 | 3.14 | 2.04 | 4.38 | 3.80 | 3.22 | 2.84 | 2.03 | 1.83 | 3.08 | 3.20 | 0.89 |
| **$Na_2O$** | 3.93 | 4.33 | 4.44 | 4.26 | 4.76 | 3.42 | 3.34 | 4.88 | 5.28 | 4.67 | 5.31 | 3.71 |
| **$P_2O_5$** | 0.25 | 0.31 | 0.22 | 0.02 | 0.03 | 0.08 | 0.14 | 0.34 | 0.42 | 0.29 | 0.29 | 0.39 |
| **LOI** | 1.86 | nd | nd | nd | nd | nd | nd | 2.90 | nd | nd | nd | nd |
| **Total_I** | 99.68 | 97.74 | 99.71 | 99.48 | 99.68 | 94.60 | 92.08 | 96.65 | 98.57 | 98.35 | nd | 99.62 |
| ***Trace Elements, parts per million*** | | | | | | | | | | | | |
| **Ni** | 21 | 1 | 19 | 1 | 6 | 4 | 6 | 7 | 3 | 2 | 4 | 75 |
| **Cr** | 37 | 1 | 17 | 1 | 2 | 6 | 10 | 6 | 0 | 1 | 15 | 68 |
| **Sc** | 9 | 11 | 13 | 2 | 2 | 9 | 11 | 16 | 15 | 13 | 17 | 22 |
| **V** | 78 | 37 | 77 | 5 | 4 | 31 | 74 | 60 | 51 | 21 | 13 | 175 |
| **Ba** | 604 | 664 | 508 | 713 | 748 | 540 | 585 | 433 | 458 | 588 | 602 | 294 |
| **Rb** | 47 | 68 | 51 | 130 | 105 | 62 | 73 | 37 | 31 | 73 | 72 | 10 |
| **Sr** | 419 | 273 | 392 | 62 | 164 | 268 | 249 | 419 | 449 | 254 | 244 | 546 |
| **Zr** | 243 | 411 | 248 | 150 | 219 | 270 | 255 | 258 | 248 | 394 | 357 | 177 |
| **Y** | 31 | 46 | 34 | 36 | 30 | 31 | 34 | 37 | 38 | 47 | 49 | 26 |
| **Nb** | 18.0 | 27.5 | 17.7 | 23.8 | 22.2 | 18.1 | 19.3 | 19.3 | 18.6 | 27.4 | 31.1 | 15.5 |
| **Ga** | 24 | 23 | 20 | 20 | 20 | 20 | 21 | 24 | 22 | 22 | 23 | 20 |
| **Cu** | 27 | 11 | 26 | 7 | 7 | 13 | 13 | 10 | 4 | 23 | 26 | 30 |
| **Zn** | 77 | 100 | 77 | 44 | 59 | 78 | 83 | 118 | 110 | 110 | 107 | 102 |
| **Pb** | 1 | 9 | 8 | 14 | 13 | 9 | 9 | 8 | 6 | 9 | 8 | 2 |
| **La** | 30 | 37 | 35 | 41 | 40 | 26 | 33 | 27 | 32 | 39 | 43 | 13 |
| **Ce** | 57 | 78 | 51 | 77 | 78 | 62 | 64 | 56 | 58 | 82 | 117 | 43 |
| **Th** | 8 | 8 | 6 | 15 | 12 | 9 | 9 | 5 | 5 | 8 | 7 | 1 |
| **Nd** | nd | 39 | 30 | 31 | 33 | 25 | 28 | 31 | 32 | 40 | nd | 24 |
| **U** | 1 | 3 | 1 | 5 | 3 | 3 | 2 | 4 | 1 | 3 | nd | 2 |

Major element determinations have been normalized to a 100-percent total on a volatile-free basis and recalculated with total iron expressed as FeO*; nd - no data or element not analyzed; na - not applicable or no information. LOI, Loss on Ignition; Total_I, original analytical total.

**Figure 6-15. Hand sample and thin section photographs of the dacite of Fifteenmile Creek (Tpdf). (a) Typical abundantly plagioclase hand sample. Scale bar is 2.5 cm (1 in) tall. (b) Thin section under cross-polarized light (XPL). (c) Same view as in B under plane-polarized light (PPL). Scale bar for thin section photographs is 7 mm (0.3 in) wide. Photo credits: J.D. McClaughry, 2015.**

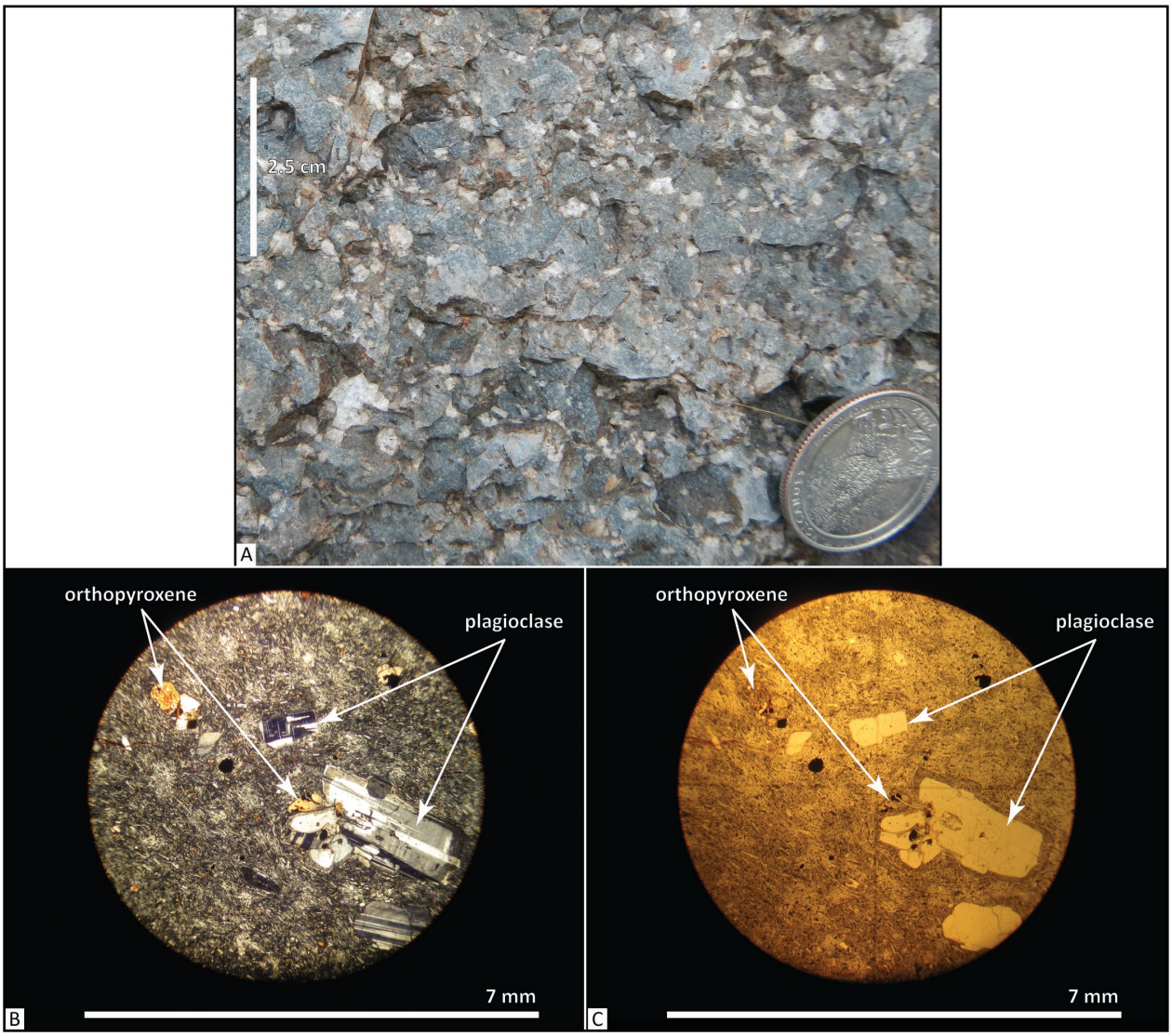


**Tppt** **non-welded pumice tuff (lower Pliocene)—**Non-welded, partially consolidated dacitic tuff ($SiO_2$ = 66.65 weight percent; Zr = 522 ppm; Nb = 33.7 ppm; *n* = 1 analysis) containing pumices of a similar dacitic chemical composition ($SiO_2$ = 65.93 to 68.19 weight percent; Zr = 334 to 486 ppm; Nb = 18.8 to 27.2 ppm; *n* = 2 analyses) (**Figure 5-11**, **Figure 5-12**, **Figure 6-16**; **Table 6-2**; Plates 1 and 2; Appendix). Unit **Tppt** is exposed above monolithologic dacite-clast breccia (**Tpdd1**) and below unconsolidated gravel (**QTpg**) along U.S. Highway 197; the tuff is also mapped above unit **Tpdd1**, ~2 km (1.2 mi) northeast of Friend, where it is recognized by tilled fields containing abundant fragments of pumice (**Figure 6-16**). Unit **Tppt** is <10 m (~33 ft) thick where best exposed along US Highway 197. Typical hand samples of the tuff contain 20 to 40 percent (vol.) very pale orange (10YR 8/2) to very light gray (N8) subrounded to subangular, feldspar-phyric pumices ranging in size from <1 cm (0.4 cm) to 12 cm (4.7 in) across, ~1 to 3 percent (vol.) clear,

subhedral to anhedral and broken, prismatic- to blocky-shaped, seriate plagioclase microphenocrysts 0.5 to 1 mm (0.02 to 0.04 in) in length, <1 percent (vol.) pale greenish yellow (10Y 8/2), euhedral to anhedral, prismatic- to lath-shaped and broken orthopyroxene and clinopyroxene crystals (orthopyroxene > clinopyroxene) <0.5 mm (0.02 in) across, rare quartz, and ~1 to 2 percent (vol.) fine- to very fine-grained crystalline lithic fragments up to 1 cm (0.4 cm), contained within a groundmass of very pale orange (10YR 8/2), poorly sorted very fine- to coarse-grained crystal-ash.

The tuff (**Tppt**) has normal magnetic polarity and is assigned an early Pliocene age on the basis of stratigraphic position above the ~3.71 tuff breccia of Engineers Creek (**Tpdd1**) (**Figure 6-1**). Pumice tuff making up this unit shares a similar chemical composition and stratigraphic position to the upper unit of the tuff of Friend (**Tptf2**) but lacks the conspicuous dark gray (N3) pumices that distinguish unit **Tptf2**.

**Figure 6-16. Non-welded pumice tuff (Tppt) and the lower unit of the tuff breccia of Engineers Creek (Tpdd1). (a) Scattered pumices covering the upper surface of unit Tpdd1 tuff breccia, southwest of the intersection of Larch and Pine Creeks (45.387762, -121.20644). Dashed white line shows the approximate contact between non-welded pumice tuff (Tppt) and tuff breccia (Tpdd1). Hammer for scale is 38 cm (15 in) long. View is looking north. (b) Tuff breccia (Tpdd1) exposed on the plateau between Pine and Larch Creeks (45.387764, -121.206018). The tuff breccia is most commonly exposed as fields of scattered boulders. Person for scale in the left side of the photograph is 1.6 m (5.2 ft tall). Photo credits: J.D. McClaughry, 2014.**

**Tpdd2** **tuff breccia of Engineers Creek, upper unit (lower Pliocene)**—Matrix- to clast-supported boulder breccia capping narrow, topographically inverted, east-west-trending ridges south of Larch Creek, in the southwest part of the map area (**Figure 6-17**). Unit **Tpdd2** lies across or is inset into the upper unit of the tuff of Friend (**Tptf2**). The tuff breccia (**Tpdd2**) is composed of angular to subrounded, nearly monolithologic-appearing grayish black (N2), plagioclase-phyric volcanic clasts typically 30 to 50 cm (11.8 to 19.7 in) across. Clasts within this unit have variable textures ranging from highly fractured to those that are glassy, flow banded, highly vesiculated, or characterized by breadcrust textures (**Figure 6-18**). Outcrops of the unit are rare; instead, unit **Tpdd2** is exposed as surfaces of boulders intermixed with coarse-grained sandy to gravelly soils (**Figure 6-17**). Clasts sampled from the breccia have trachyandesitic to trachydacitic chemical compositions ($SiO_2$ = 59.84 to 63.05 weight percent; $K_2O$ = 1.56 to 1.83 weight percent; *n* = 5 analyses) with relatively high amounts of niobium (Nb = 18.6 to 21.3 ppm) and zirconium (Zr = 248 to 252 ppm) (**Figure 5-11**, **Figure 5-12**; **Table 6-2**; Plate 1; Appendix). The upper surface of the boulder-rich deposit is locally mantled by scattered very pale orange (10 YR 8/2) pumices. Thickness of the unit is <12 m (40 ft) (Plate 1). Typical hand samples of clasts are medium dark gray (N4) (weathered surfaces are grayish orange pink [5YR 7/2]) and distinctly porphyritic, similar to those clasts in unit **Tppd1** lower in the section. Clasts in unit **Tppd2** are typically characterized by 20 to 30 percent (vol.) prismatic to blocky plagioclase microphenocrysts and phenocrysts up to 5 mm (0.2 in) long distributed within a very fine-grained hypocrystalline groundmass.

Unit **Tppd2** is assigned an early Pliocene age on the basis of stratigraphic position directly above the 3.68 Ma upper unit of the tuff of Friend (**Tptf2**) (**Figure 6-1**). The upper age limit of unit **Tppd2** is constrained by the 2.57 Ma basaltic andesite of Flag Point (**QTbf**) which flowed down a paleochannel incised into both the tuff breccia (**Tppd2**) and upper unit of the tuff of Friend (**Tptf2**). The upper tuff breccia (**Tppd2**) is nearly identical in clast lithology to the lower tuff breccia (**Tpdd1**) but is herein subdivided on the basis of stratigraphic position relative to the upper unit of the tuff of Friend (**Tptf2**).

**Figure 6-17. Boulder-covered surface of the upper unit of the tuff breccia of Engineers Creek (Tpdd2) exposed above the upper unit of the tuff of Friend (Tptf2) between Larch Creek and Owl Hollow (45.363606, -121.344748). Hammer for scale is 38 cm (15 in) long. View is looking north-northwest. Photo credit: J.D. McClaughry, 2015.**

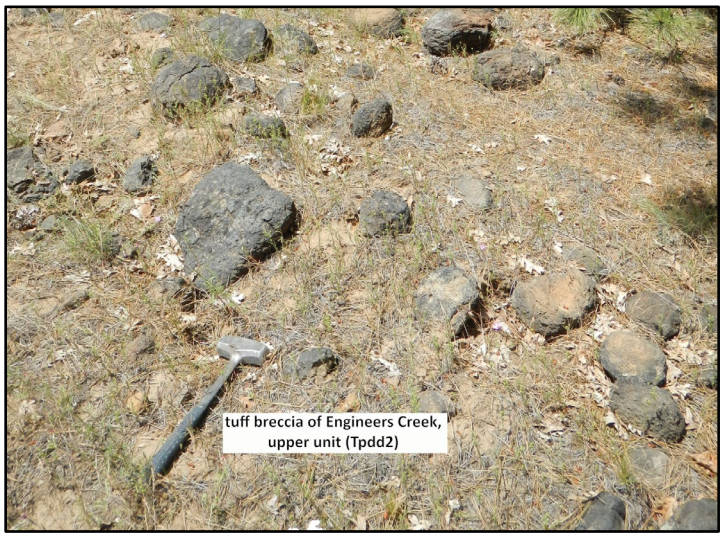

**Figure 6-18. Clast textures from the upper unit of the tuff breccia of Engineers Creek (Tpdd2), west of Friend. (a) Glassy, fractured, breadcrust-textured block. (b) Highly vesiculated dacite block. Scale bar in A and B is 10 cm (3.9 in) high. (c) Flow-banded dacite block. Pen magnet for scale is 12 cm (4.7 in) long. Blocks shown in A, B, and C are from the site shown in Figure 6-17 (45.363606, -121.344748). Photo credits: J.D. McClaughry, 2015.**


**Tptf2** **tuff of Friend, upper unit (lower Pliocene)**—Weakly to moderately welded, pumice-rich and plagioclase-phyric trachydacitic tuff ($SiO_2$ = 64.83 to 67.94 weight percent; $K_2O$ = 3.13 to 4.02 weight percent; Zr = 393 to 438 ppm; Nb = 24.6 to 29.4 ppm; La = 31 to 43 ppm, and Ce = 75 to 108 ppm; *n* = 7 analyses, bulk tuff) mapped interbedded with the tuff breccia of Engineers Creek (**Tpdd1**, **Tpdd2**) in the southwestern part of the map area (**Figure 5-11**, **Figure 5-12**, **Figure 6-19**, **Figure 6-20**; **Table 6-2**; Plate 1; Appendix). The tuff (**Tptf2**) is well exposed between Larch and Pine Creeks, forming prominent cliffs, hoodoos, caverns, and precipitous spires (**Figure 6-19**). Outcrops typically display cavernous weathering, eroding to meter-scale, subrounded boulders, angular slabs, angular chips, and fine-grained crystal-rich soils. The composite thickness of the unit in the map area exceeds 100 m (331 ft) (Plate 1). The tuff (**Tptf2**) is readily distinguished in the field by conspicuous dark gray (N3) pumices, pumiceous lapilli, and bombs as large as 30 cm

(11.8 in) across (**Figure 6-20a**). Pumices are of similar trachydacitic chemical composition to the bulk tuff ($SiO_2$ = 67.04 to 67.81 weight percent; $K_2O$ = 3.73 to 4.14 weight percent; Zr = 456 to 525 ppm; Nb = 25.8 to 29.1 ppm; La = 38 to 42 ppm, and Ce = 78 to 87 ppm; *n* = 5 analyses, pumice) (**Figure 5-11**, **Figure 5-12**, **Table 6-2**; Plate 1; Appendix). The upper unit (**Tptf2**) of the tuff of Friend is similar in texture to the lower unit (**Tptf1**), but is differentiated on systematic geochemical variations, containing higher amounts of $SiO_2$, Nb, Zr, La, and Ce (**Table 6-2**; Appendix). Typical hand samples of the tuff are light olive gray (5Y 5/2) to pale yellowish brown (10YR 6/2) and dark yellowish brown (10YR 4/2) moderately to weakly welded, moderately to well-indurated, and sparsely microporphyritic containing clear, broken, subhedral to anhedral, prismatic to blocky seriate plagioclase microphenocrysts and phenocrysts 0.5 to 2 mm (0.02 to 0.1 in) in length, <1 percent (vol.) pale greenish yellow (10Y 8/2), broken, euhedral to anhedral, prismatic- to lath-shaped orthopyroxene and clinopyroxene (orthopyroxene ≥ clinopyroxene) microphenocrysts <0.5 mm (0.02 in) across, ~10 percent (vol.) dark gray (N3) oblate to slightly flattened banded pumices, and ~5 percent (vol.) fine- to very fine-grained medium light gray (N6) to medium dark gray (N4) dacite lithics, contained within a groundmass of devitrified cuspate glass shards and ash (**Figure 6-20c,d**).

Unit **Tpft2** has normal magnetic polarity and is assigned an early Pliocene age on the basis of stratigraphic position and an $^{40}Ar/^{39}Ar$ plateau age of 3.68 ± 0.02 Ma (plagioclase; sample 154 DFWJ 15), for a sample from upper Larch Creek (**Figure 5-13**, **Figure 6-1**; **Table 5-1**; Plate 1; Appendix). The tuff of Friend (**Tptf1**, **Tpft2**) is indistinguishable in age and compositionally similar to a suite of silicic volcanic rocks described at nearby Gordon Butte (~17 km [10.6 mi] southwest) and Graveyard Butte (~22.8 km [14.2 mi] south-southwest) by Westby (2014). Westby (2014) reports ages for rhyolites at Gordon and Graveyard Buttes, ranging between 3.6 and 3.8 Ma.

**Figure 6-19. Hoodoos in the upper unit of the tuff of Friend (Tptf2) in upper Larch Creek, in the southwestern part of the map area (45.345683, -121.334705). View is looking northwest. Photo credit: J.D. McClaughry, 2015.**

**Figure 6-20. Hand sample and thin section photographs of the upper unit of the tuff of Friend (Tptf2). (a) Close-up view of pumice-rich tuff from the outcrop at sample site 154 DFWJ 15 (45.362131, -121.341900). A sample from this outcrop returned an $^{40}Ar/^{39}Ar$ plateau age of 3.68 ± 0.02 Ma. Note the abundance of dark gray (N3) pumices. Quarter for scale bar is 2.5 cm (1 in) across. (b) Close-up view of pumice- and lithic-rich tuff from similar Tptf2 outcrops along USFS Road 2730 (outside map area). These outcrops contain distinctly porphyritic, black (N1) dacitic lithic clasts similar to those found in tuff breccia of units Tpdd1 and Tpdd2 (45.354873, -121.347697). Increments on the scale bar are 1 cm (0.4 in). (c) Representative thin section of unit Tptf2 under cross- polarized light (XPL). (d) Same view as in C under plane-polarized light (PPL). Scale bar for thin section photographs is 7 mm (0.3 in) wide. Photo credits: J.D. McClaughry, 2015, 2016.**

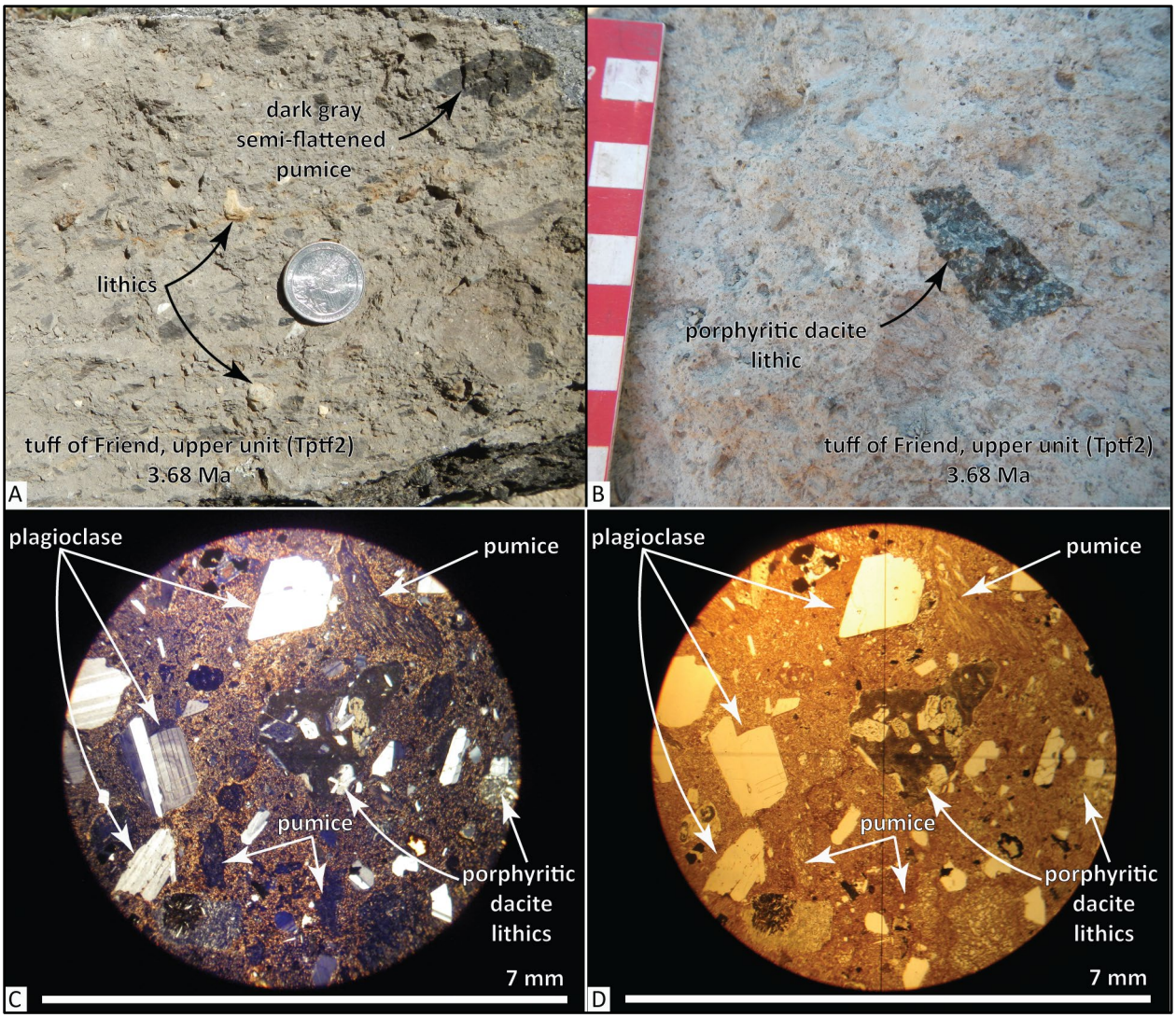


**Tpdd1** **tuff breccia of Engineers Creek, lower unit (lower Pliocene)**—Matrix- to clast-supported boulder breccia and basal pumice tuff mapped in an east-to northeast-oriented outcrop belt between upper Fifteenmile Creek, the headwaters of Larch Creek, Dufur, and Rice (**Figure 6-21**, **Figure 6-22**, **Figure 6-23, Figure 6-24**, , **Figure 6-25**; Plates 1, 2, and 3). Unit **Tpdd1** is mapped ~5.6 km (3.5 mi) west of the map area into the upper reach of Cedar Creek (J.D. McClaughry unpublished geologic mapping, 2016) and ~13 km (8 mi) west into the headwaters of Engineers Creek, along

the eastern escarpment of the Hood River graben (McClaughry and others, 2020a). Between Cedar Creek and the confluence of Larch and Pine Creeks unit **Tpdd1** caps a broad plateau where it is interbedded with the tuff of Friend (**Tptf1**, **Tptf2**) (**Figure 6-21**). Northeast of the confluence of Larch and Pine Creeks the deposit is confined within a paleochannel partly coincident with modern Pine Creek Canyon (Plates 1 and 2). Between Dufur Gap Road and U.S. Highway 197 the unit diverges from modern Pine Creek canyon and fills a paleochannel inset into the CRBG (Plate 2). East and downstream of U.S. Highway 197 unit **Tpdd1** caps a narrow, topographically inverted plateau-forming paleochannel extending northeast to Rice (**Figure 6-21**; Plates 2 and 3). In areas lacking outcrop the distribution of unit **Tpdd1** is identified by fields of scattered, angular to subrounded, medium dark gray (N4) to black (N1) andesite and dacite boulders and coarse-grained sandy to gravelly soils. Typical thickness of unit **Tpdd1** is variable, ranging from ~70 to 100 m (230 to 328 ft) west of Friend to ~20 m (66 ft) east of U.S. Highway 197 (**Figure 6-21**; Plates 1, 2, and 3). Unit **Tpdd1** lies across or is inset into the older CRBG or Dalles Formation along its length (**Figure 6-22a**; Plates 1, 2, and 3). This typically well-defined contact is locally associated with an intervening matrix-supported conglomerate composed entirely of CRBG clasts (**Figure 6-26**).

Breccia beds are typically massively bedded, very poorly sorted, and matrix supported, with localized clast-supported areas (**Figure 6-22a**, **Figure 6-24**). Unit **Tpdd1** contains a texturally similar, but chemically diverse assemblage of dense to vesiculated and fractured, angular to subangular clasts of medium dark gray (N4) to black (N1) porphyritic andesite, trachyandesite, dacite, and trachydacite ($SiO_2$ = 58.91 to 65.14 weight percent; $K_2O$ = 2.00 to 3.42 weight percent; Nb = 14.2 to 27.5 ppm; Zr = 239 to 411 ppm; *n* = 22 analyses) (**Figure 5-11**, **Figure 5-12**, **Figure 6-27**; **Table 6-2**; Plates 1 and 2; Appendix). The breccia also includes very sparse angular clasts of light brownish gray (5YR 6/1) to very pale orange (10YR 8/2), flow-banded rhyolite ($SiO_2$ = 73.93 to 75.31 weight percent; $K_2O$ = 3.80 to 4.38 weight percent; Nb = 22.2 to 23.8 ppm; Zr = 150 to 219 ppm; *n* = 2 analyses), and black (N1) perlitic obsidian nodules (**Figure 5-11**, **Figure 5-12**; **Table 6-2**; Plate 2; Appendix). Several clast samples obtained in the upper part of Larch Creek and near Rice are plagioclase-porphyritic, low-potassium andesite and dacite ($SiO_2$ = 60.37 to 63.98 weight percent; $K_2O$ = 0.88 to 1.67 weight percent; Nb = 5.2 to 9.5 ppm; Zr = 108 to 151 ppm; *n* = 3 analyses) more typical of the older Dalles Formation (Plates 1 and 3; Appendix). No clasts derived from the CRBG, which directly underlies unit **Tpdd1** along much of its course, have been found. The maximum observed clast size in the deposit is ~5.2 m (17.1 ft) at the confluence of Pine and Larch Creeks, where the flow transitions from a plateau mantling deposit to one confined within Pine Creek (**Figure 6-28**; Plate 1). The average size of the ten largest observed clasts at all outcrops is ~2.6 m (8.6 ft). Maximum clast size over the length of the unit reduces toward the east.

Typical samples of clasts show slight textural variations but are largely a similar medium dark gray (N4) to black (N1) and distinctly plagioclase porphyritic (**Figure 6-27**). Clasts contain ~20 to 25 percent (vol.) clear, subhedral to anhedral, prismatic to blocky, seriate plagioclase microphenocrysts and phenocrysts ≤5 mm (0.2 in), <1 percent (vol.) grayish black (N2), euhedral to subhedral, prismatic- to lath-shaped orthopyroxene and clinopyroxene microphenocrysts ≤1 mm (0.04 in) (orthopyroxene > clinopyroxene), and <1 percent (vol.) plagioclase-pyroxene glomerocrysts between 2 mm and 7 mm (0.1 and 0.3 in) across, contained within a fine- to medium-grained hypocrystalline groundmass (**Figure 6-27c,d**).

Clasts are typically supported by a yellowish gray (5Y 7/2) to grayish orange pink (5YR 7/2), poorly sorted matrix composed of ~10 percent (vol.) angular to subrounded, medium dark gray (N4) to dark gray (N3), fine- to very fine-grained crystalline andesite or dacite lithics, and ~10 percent (vol.) chalky white (N9) pumice fragments up to 3 cm (1.2 in) across. Clasts are contained within a very fine-grained tuffaceous sandstone composed of ~20 to 30 percent (vol.) poorly sorted, clear, euhedral to anhedral and broken, very angular prismatic to blocky plagioclase crystals <0.5 mm (0.02 in) across, ~2 percent (vol.) grayish black (N2) anhedral, stubby orthopyroxene crystals up to 2 mm (0.1 in), and ~5 percent (vol.) very angular to cuspate brown colored glass shards (**Figure 6-27b,e,f**).

A weakly consolidated, non-welded dacitic pumice tuff ($SiO_2$ = 67.26 to 67.44 weight percent; $K_2O$ = 2.84 to 3.22 weight percent; Nb = 18.1 to 19.3 ppm; Zr = 255 to 270 ppm; *n* = 3 analyses) is locally preserved at the base of unit **Tppd1** (**Figure 5-11**, **Figure 5-12**, **Figure 6-29**; **Table 6-2**; Plate 2; Appendix). In exposures along Dufur Gap Road, near the northern margin of the filled Pine Creek paleochannel, the contact between breccia and pumice tuff is gradational; the breccia matrix here incorporates fragments of the underlying pumice tuff (**Figure 6-22a,c**). Typical hand samples of the tuff are very pale orange (10YR 8/2) to yellowish gray (5Y 7/2) and poorly to moderately indurated, containing ~45 to 85 percent (vol.) chalky white (N9) to very light gray (N8) angular to subrounded aphyric to pyroxene microporphyritic pumices ranging from 0.5 to 3 cm (0.02 to 1.2 in) across, 2 to 5 percent (vol.) subangular, gray, andesite to dacite rock fragments up to 1 cm (0.4 in) across, 1 to 2 percent (vol.) subrounded, perlitic glass fragments up to 1 mm (0.04 in) across, ~1 to 2 percent (vol.) clear poorly sorted, subhedral to anhedral and broken, prismatic to blocky plagioclase microphenocrysts and phenocrysts <2 mm (0.1 in) in length, <1 percent (vol.) pale greenish yellow (10Y 8/2), anhedral, prismatic- to lath-shaped and broken, orthopyroxene and clinopyroxene (orthopyroxene > clinopyroxene) microphenocrysts <0.2 mm (0.008 in) across, and rare anhedral, colorless quartz up to 0.5 mm (0.02 in) across, contained within a groundmass of devitrified ash (**Figure 6-29b,c**). The tuff groundmass is locally altered to sericite.

Unit **Tpdd1** is assigned an early Pliocene age on the basis of stratigraphic position beneath the 3.02 Ma dacite of Fifteenmile Creek and 3.68 upper unit of the tuff of Friend (**Tptf2**), and isotopic ages (**Figure 6-1**). A sample of the non-welded pumice tuff, defining the base of unit **Tpdd1** in Mays Canyon, has an $^{40}Ar/^{39}Ar$ plateau age of 3.83 ± 0.01 Ma (plagioclase, sample 373 DFWJ 14) (**Figure 5-13**, **Table 5-1**; Plate 2; Appendix). A single clast obtained from unit **Tpdd1** has an $^{40}Ar/^{39}Ar$ plateau age of 3.71 ± 0.02 Ma (plagioclase, sample 265 DFWJ 14) (**Figure 5-13**, **Table 5-1**; Plate 2; Appendix). Unit **Tpdd1** in the Dufur area is considered equivalent to the tuff breccia of Engineers Creek (unit Tpdd of McClaughry and others, 2020a) mapped along the eastern escarpment of the Hood River graben on the basis of comparable stratigraphic position beneath the 3.02 Ma dacite of Fifteenmile Creek (**Tpdf**) and inclusion of texturally and chemically similar clasts. Similar to unit **Tpdd1** in the Dufur area, the tuff breccia of Engineers Creek in the Hood River graben escarpment contains clasts of andesite, trachydacite, and rhyolite ($SiO_2$ = 63.53 to 69.43 weight percent; $K_2O$ = 2.29 to 3.12 weight percent; *n* = 5 analyses) with relatively high amounts of niobium (Nb = 19.6 to 29.9 ppm) and zirconium (Zr = 194 to 430 ppm) (McClaughry and others, 2020a). Collectively, mapped breccia deposits between Engineers Creek and Rice define an ~50-km-long (31 mi) early Pliocene paleochannel (**Figure 6-21**). The source area for the tuff breccia of Engineers Creek is presumed to lie within the Hood River graben.

**Figure 6-21. Distribution of the lower unit of the tuff breccia of Engineers Creek (Tpdd1) between the headwaters of Fifteenmile Creek, Friend, Dufur, and Rice. The inferred source area is located an additional 15 km (9.3 mi) west of site 244b DFWJ 15 along East Fork Hood River (out of figure view). Red arrows represent sample sites for size measurements of clasts shown in Figure 6-28a. Thin red line is the channel profile illustrated in Figure 6-28b. Base map is a Google Earth™ image, with an oblique view looking north toward The Dalles and the Columbia River.**

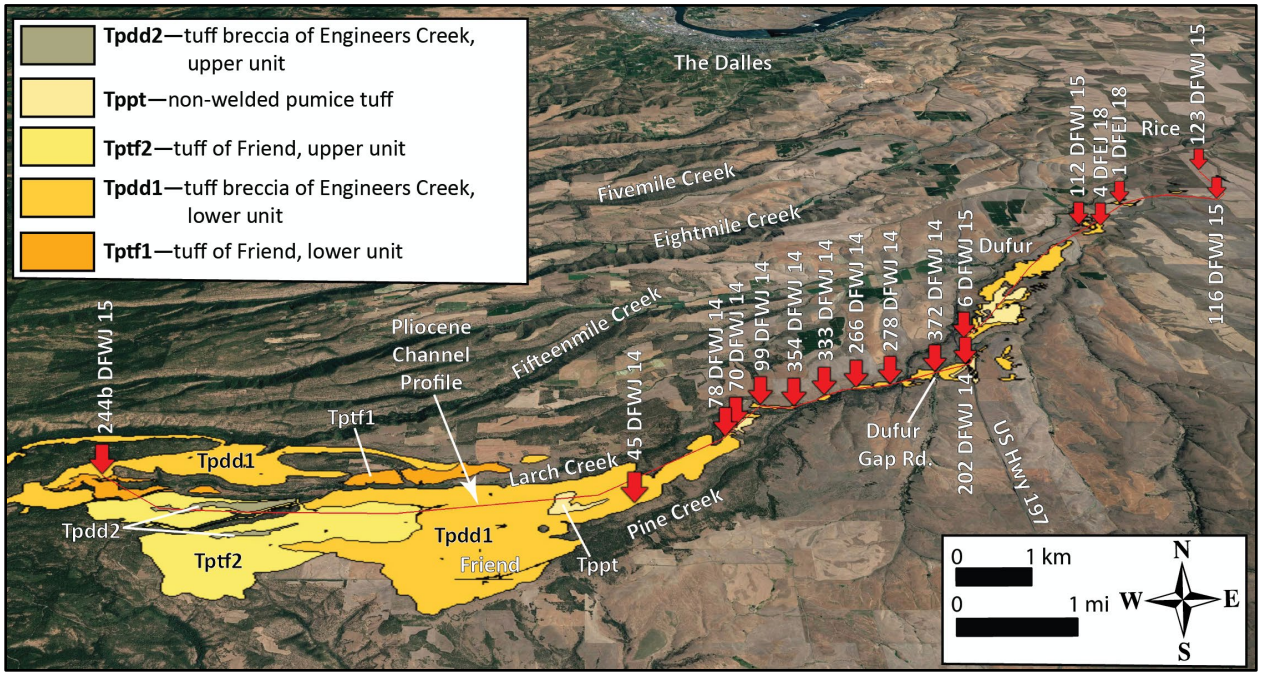

**Figure 6-22. Lower unit of the tuff breccia of Engineers Creek (Tpdd1). (a) Outcrop of the tuff breccia of Engineers Creek (Tpdd1) exposed along Dufur Gap Road (45.40666, -121.149181). The east end of the outcrop is near part of the paleochannel margin, which controlled the emplacement distribution of the breccia and underlying pumice tuff. The early Pliocene paleochannel here was cut through basalt flows of the Frenchman Springs Member (Twfh, Twfg) of the CRBG. The mega clast shown in photograph A measures ~2.5 m (8.2 ft) m in long-axis dimension. Letter 'B' shows the location of photo B. Letter 'C' shows the location of photo C. Letter 'X' shows the location of Figure 6-23. (b) Matrix-supported breccia deposit near the east end of the outcrop shown in A. Clasts are supported in a pumiceous tuff matrix, derived from the underlying pumice tuff in C. (c). Pumice tuff exposed along the paleochannel margin and near the base of the dacite-clast breccia deposit. The pumice tuff is progressively reworked and mixed into the breccia toward the interior and top of the deposit. The location of photograph C corresponds to sample 373 DFWJ 14, which has an $^{40}Ar/^{39}Ar$ plateau age of 3.83 ± 0.01 Ma. Hammer for scale in A, B, and C is 38 cm (15 in) long. Photo credits: J.D. McClaughry, 2014.**

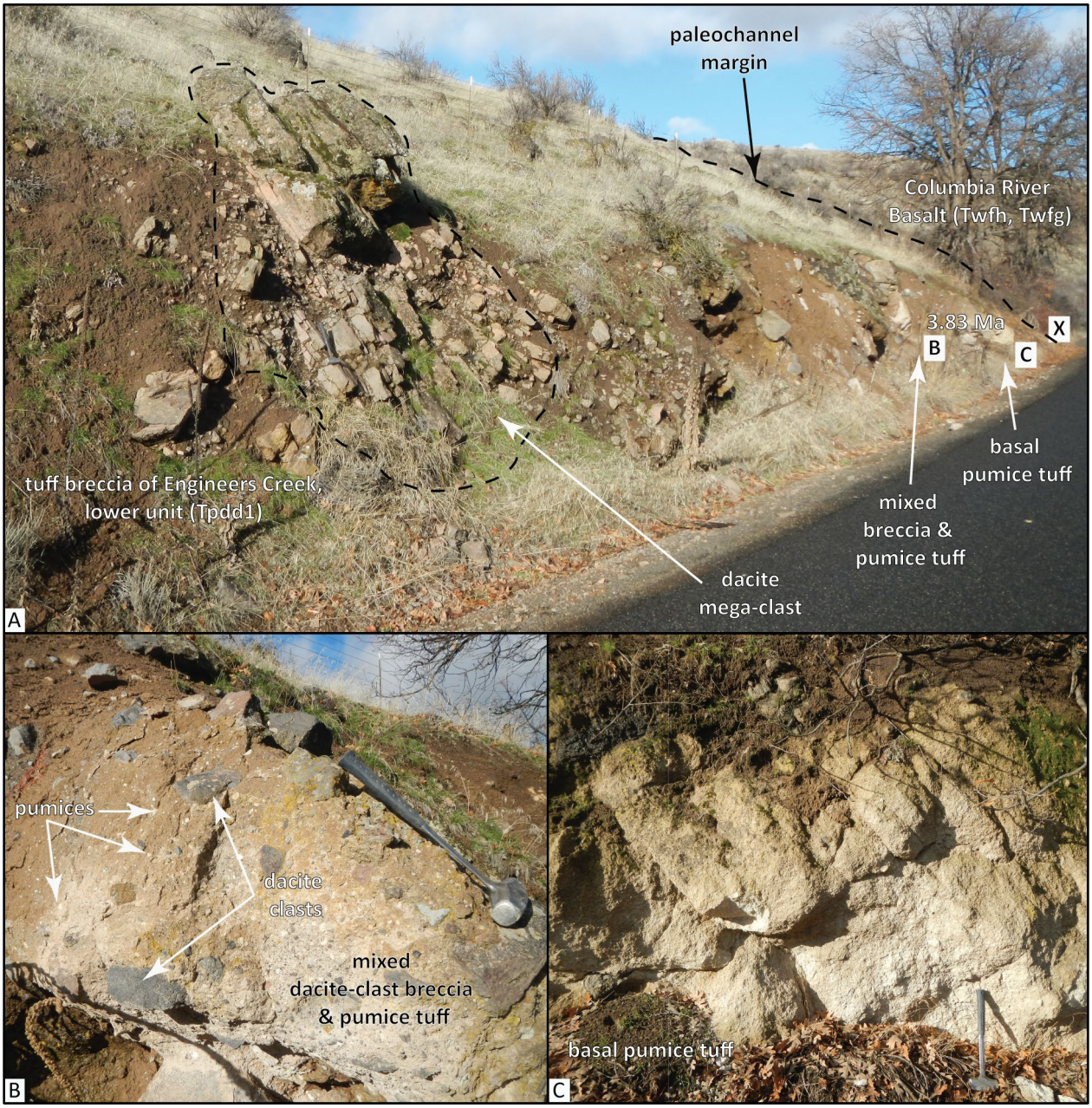

**Figure 6-23. Ridges and drainages underlain by the lower unit of the tuff breccia of Engineers Creek (Tpdd1), in the headwaters of Larch Creek, east of USFS Road 4421, in the southwestern part of the map area (45.372980, -121.361587). Boulders in this part of the deposit are dominantly black (N1) porphyritic andesite and dacite that typically exceed 1 m (3.3 ft) in long-axis dimension. Arrow points to 1 m (3.3 ft) long ruler. View is looking northwest. Photo credit: J.D. McClaughry, 2015.**


**Figure 6-24. Clast-supported lower unit of the tuff breccia of Engineers Creek (Tpdd1) along Dufur Gap Road (45.40616, -121.149415). Arrow points to 1 m (3.3 ft) tall shovel for scale near lower-center part of the photograph. A dacite clast from the nearby exposures of the deposit within Pine Creek Canyon has returned an $^{40}Ar/^{39}Ar$ plateau age of 3.71 ± 0.02 Ma (sample 265 DFWJ 14).**

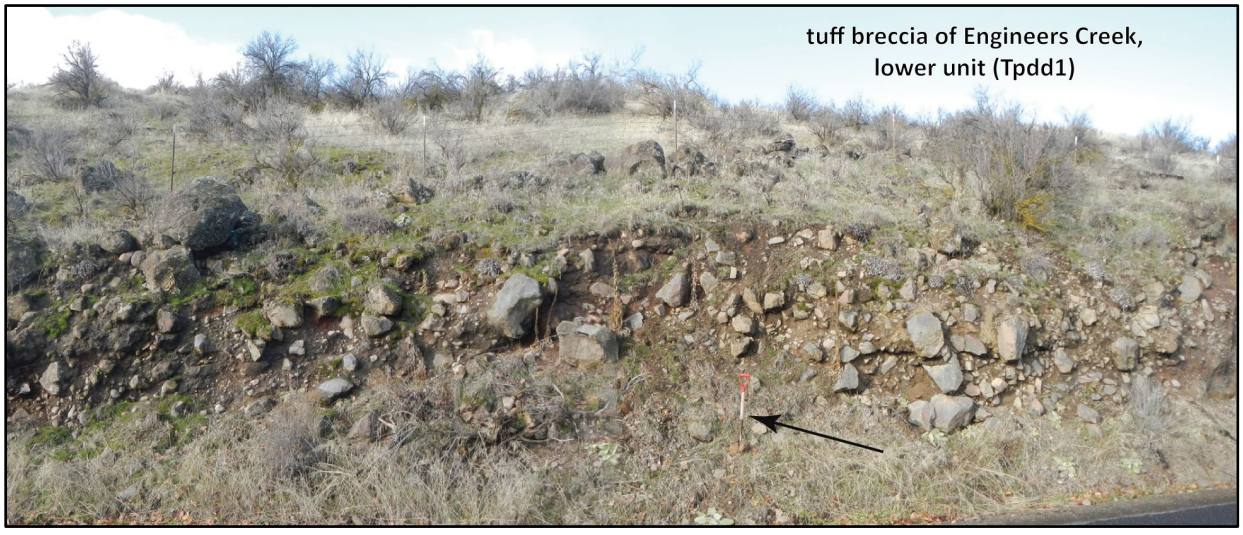

**Figure 6-25. Boulders weathering out of the lower unit of the tuff breccia of Engineers Creek (Tpdd1), north of Adkisson Road in the northeast part of the map area (45.48175, -121.064213). Person for scale on the left side of the photograph is 1.8 m (5.8 ft) tall. View is looking southeast toward Mount Hood. Photo credit: J.D. McClaughry, 2018.**


**Figure 6-26. Matrix-supported conglomerate composed completely of clasts of Columbia River Basalt, preserved in the base of the early Pliocene paleochannel along Dufur Gap Road (45.407117, -121.149081). Hammer for scale bar is 25 cm (9.8 in) long. Location of this exposure is shown by the 'X' marked in Figure 6-22a. Photo credit: J.D. McClaughry, 2014.**

**Figure 6-27. Hand samples from the lower unit of the tuff breccia of Engineers Creek (Tpdd1). (a) Typical clasts are black (N1) to medium dark gray (N4) and distinctly porphyritic. (b) Matrix samples contain angular to subrounded, medium dark gray (N4) to dark gray (N3), crystalline andesite or dacite and chalky white (N9) pumices in a fine-grained sandstone. Scale bar in both A and B is 2.5 cm (1 in). (c) Thin section of a dacite clast under cross-polarized light (XPL). (d) Same view as in C under plane-polarized light (PPL). (e) Thin section of the matrix under cross-polarized light (XPL). (f) Same view as in E under plane-polarized light (PPL). Scale bar for C-F is 7 mm (0.3 in). Photo credits: J.D. McClaughry, 2015.**

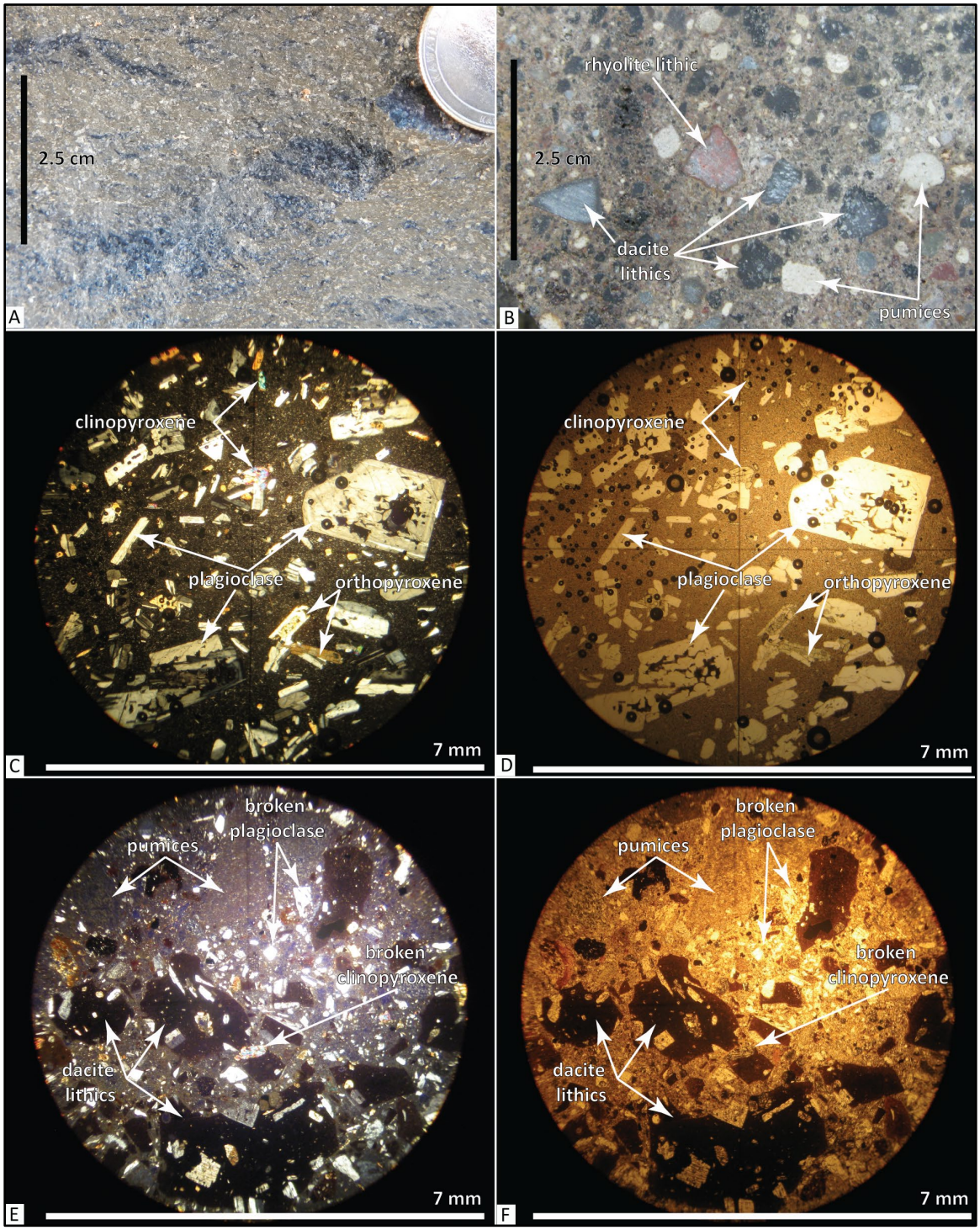

**Figure 6-28. Clast distribution and channel gradient for the tuff breccia of Engineers Creek (Tpdd1). (a) Histogram showing the downstream distribution of the largest clast-sizes and average size of the ten largest clasts from fifteen studied outcrops of unit Tpdd1. The vertical axis is the maximum or average clast size measured in meters (m). The horizontal axis is the distance (flowing east to west) from an inferred vent or origination area located near East Fork Hood River. The largest mega clasts (exceeding 4.7 m (15.4 ft) in long-axis) are found on the plateau near Friend and at the confluence of Pine and Larch Creeks. (b) Graph showing the gradient profiles of the base of unit Tpdd1 (blue line), modern Pine Creek (red line), and Fifteenmile Creek (green line; downstream of the mouth of Pine Creek). The vertical axis is the elevation in feet above sea level. The horizontal axis is the distance (flowing east to west) from the inferred East Fork Hood River source area. The modern channels of Pine and Fifteenmile Creeks follow a similar gradient to that preserved by the Pliocene paleochannel. Horizontal scales in both A and B are equivalent and correspond to the mapped geology, sample sites, and profile line shown in Figure 6-21.**

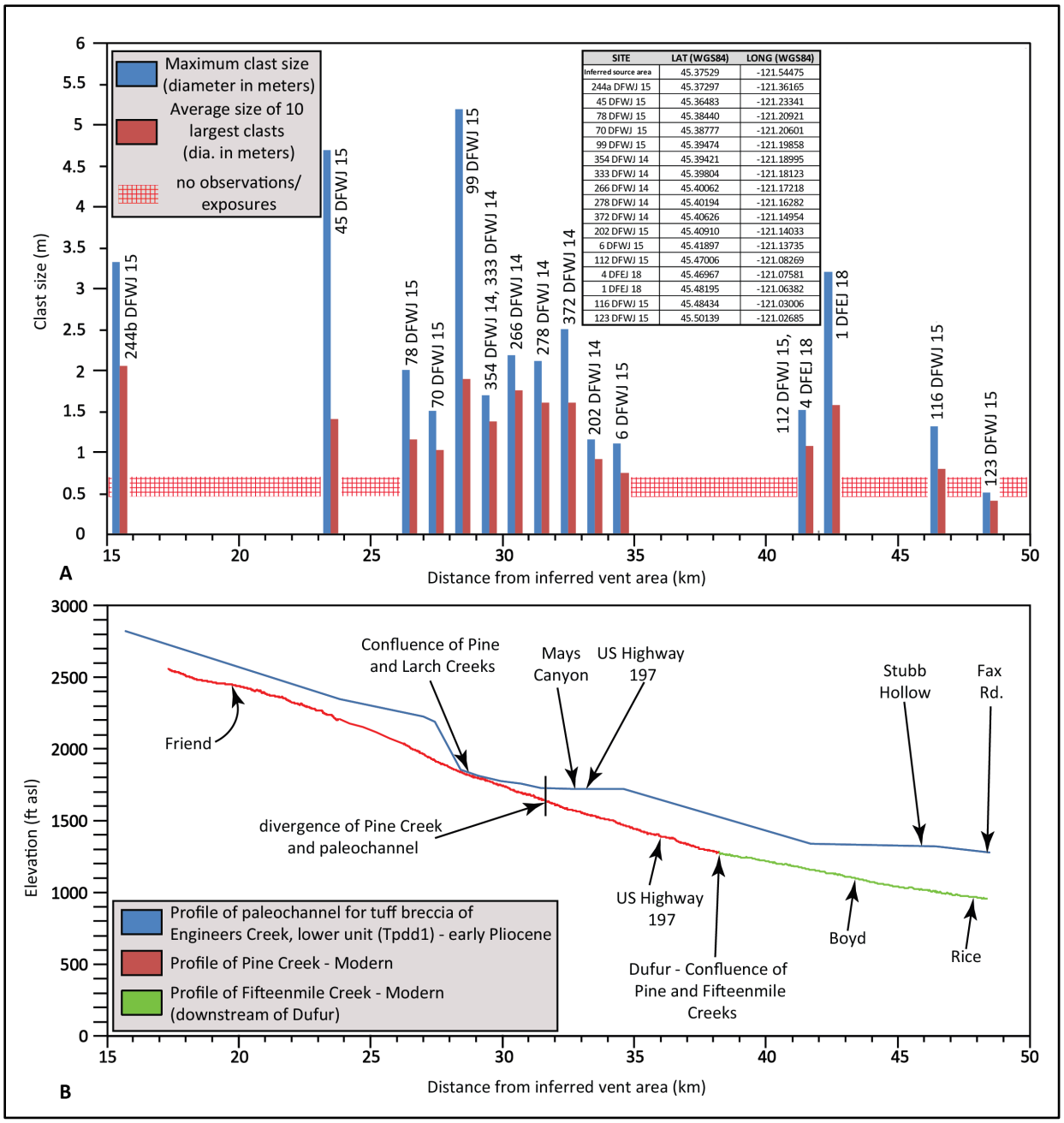


| SITE | LAT (WGS84) | LONG (WGS84) |
|---|---|---|
| Inferred source area | 45.37529 | -121.54475 |
| 244a DFWJ 15 | 45.37297 | -121.36165 |
| 45 DFWJ 15 | 45.36483 | -121.23341 |
| 78 DFWJ 15 | 45.38440 | -121.20921 |
| 70 DFWJ 15 | 45.38777 | -121.20601 |
| 99 DFWJ 15 | 45.39474 | -121.19858 |
| 354 DFWJ 14 | 45.39421 | -121.18995 |
| 333 DFWJ 14 | 45.39804 | -121.18123 |
| 266 DFWJ 14 | 45.40062 | -121.17218 |
| 278 DFWJ 14 | 45.40194 | -121.16282 |
| 372 DFWJ 14 | 45.40626 | -121.14954 |
| 202 DFWJ 15 | 45.40910 | -121.14033 |
| 6 DFWJ 15 | 45.41897 | -121.13735 |
| 112 DFWJ 15 | 45.47006 | -121.08269 |
| 4 DFEJ 18 | 45.46967 | -121.07581 |
| 1 DFEJ 18 | 45.48195 | -121.06382 |
| 116 DFWJ 15 | 45.48434 | -121.03006 |
| 123 DFWJ 15 | 45.50139 | -121.02685 |

**Figure 6-29. Pumice tuff at the base of the lower unit of the tuff breccia of Engineers Creek (Tpdd1). (a) Outcrop exposed at the base of unit Tpdd1 along the northern edge of Pine Creek Canyon, ~2.5 km (1.5 mi) west of U.S. Highway 197 (45.401685, -121.171129). The black dashed line shows the approximate contact between the pumice tuff and boulder-dominated breccia. The arrow points to a blue portable fluxgate magnetometer for scale, which is 23 cm (9 in) across. (b) A hand sample of the tuff obtained from the same outcrop as in A, is marked by an abundance of chalky white (N9) pumices. Pencil for scale is 15 cm (6 in) long. (c) Thin sections of the pumice tuff are characterized by a variety of volcanic lithic fragments and broken, prismatic- to blocky-shaped plagioclase microphenocrysts and phenocrysts, contained within a groundmass of devitrified ash. Scale bar is 7 mm (0.3 in) in width. Photo credits: J.D. McClaughry, 2014.**

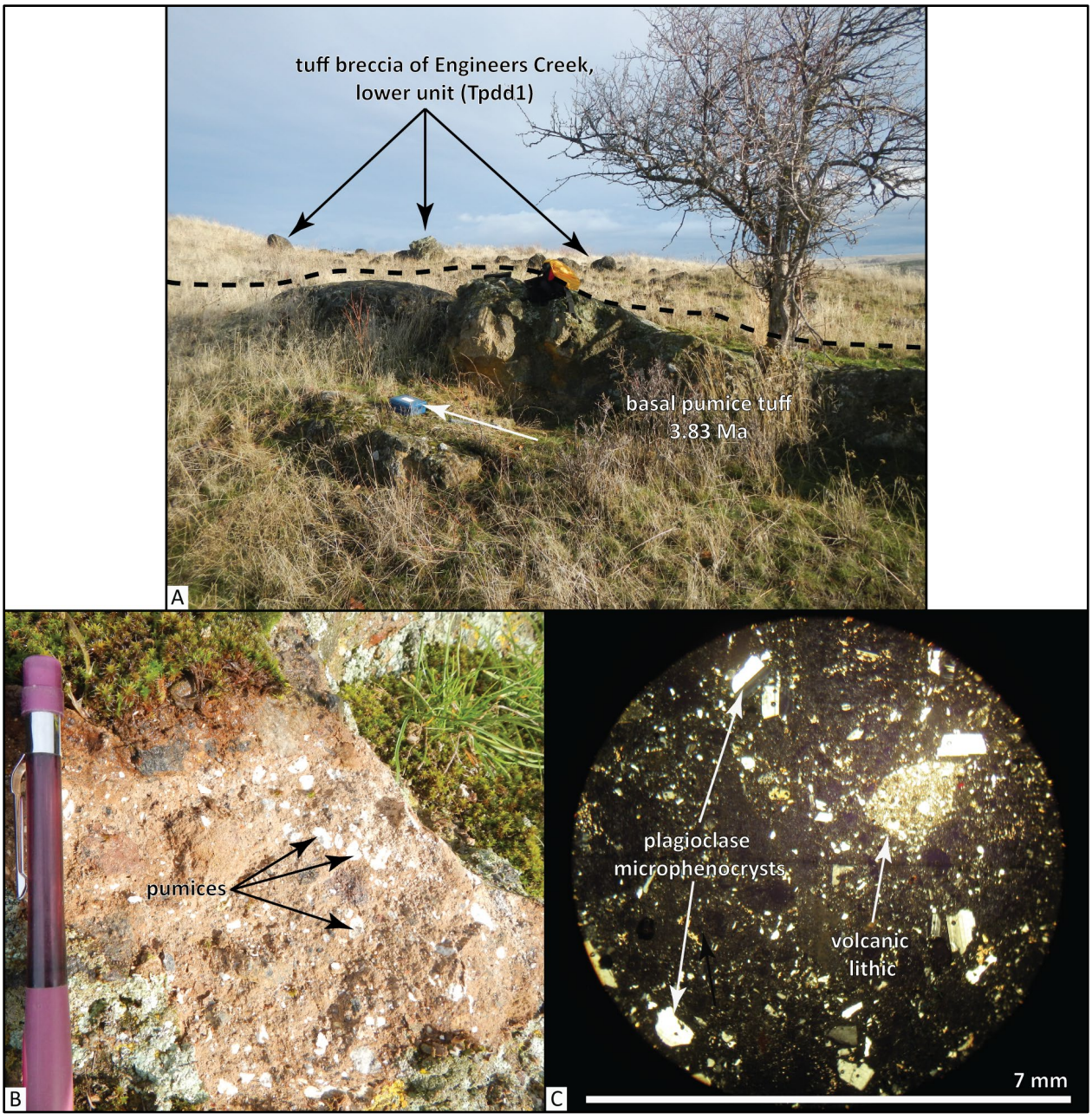

**Tptf1** **tuff of Friend, lower unit (lower Pliocene)**—Non- to moderately welded, pumice-rich and plagioclase-microphyric andesite to dacite tuff ($SiO_2$ = 61.76 to 63.79 weight percent; $K_2O$ = 1.67 to 2.64 weight percent; Zr = 211 to 258 ppm; Nb = 15.0 to 19.3 ppm; La = 23 to 31 ppm, and Ce = 48 to 57 ppm; *n* = 6 analyses, bulk tuff) mapped along Larch Creek (**Figure 5-11**, **Figure 5-12**, **Figure 6-30a**; **Table 6-2**; Plate 1; Appendix). The lower unit of the tuff of Friend (**Tptf1**) sits on the Dalles Formation (**Tmdt**, **Tmdd**) and CRBG (**Twfh**); the tuff (**Tptf1**) is overlain by the upper unit of the tuff of Friend (**Tptf2**) and the lower unit of the tuff breccia of Engineers Creek (**Tpdd1**) (Plate 1). Unit **Tptf1** crops out as prominent cliffs and hoodoos that weather to meter-scale, subrounded boulders, angular slabs and chips, and sandy soils (**Figure 6-30a**). The thickness of unit **Tptf1** ranges between 30 and 61 m (100 and 200 ft) (Plate 1). Similar to the upper unit (**Tptf2**), the lower unit (**Tptf1**) contains conspicuous dark gray (N3) pumices, lapilli, and bombs ≥10 cm (4 in) across (**Figure 6-30b**). Pumices are of similar trachydacite chemical composition to the bulk tuff ($SiO_2$ = 63.39 weight percent; $K_2O$ = 1.85 weight percent; Zr = 258 ppm; Nb = 19.0 ppm; La = 26 ppm, and Ce = 54 ppm; *n* = 1 analyses, pumice) (**Figure 5-11**, **Figure 5-12**). Unit **Tptf1** is similar in texture to unit **Tptf2**, but is differentiated on geochemistry, containing lesser amounts of $SiO_2$, Nb, Zr, La, and Ce (**Table 6-2**; Plate 1; Appendix). Typical hand samples of the tuff are light olive gray (5Y 5/2) to pale yellowish brown (10YR 6/2) and dark yellowish brown (10YR 4/2), non- to weakly welded, moderately to well-indurated, and sparsely microporphyritic containing ~1 to 2 percent (vol.) lath-shaped to blocky and broken plagioclase microphenocrysts <1 mm (0.04 in), ~10 to 20 percent (vol.) dark gray (N3) oblate to slightly flattened pumices, and ~5 percent (vol.) medium light gray (N6) to medium dark gray (N4) dacite lithics, contained within a devitrified ash matrix (**Figure 6-30b**).

Unit **Tptf1** has normal magnetic polarity and is assigned an early Pliocene age on the basis of stratigraphic position beneath the 3.68 Ma upper unit of the tuff of Friend (**Tptf2**) (**Figure 6-1**; Plate 1).

**Figure 6-30. Lower unit of the tuff of Friend (Tptf1). (a) Spire-forming outcrop of the lower unit of the tuff of Friend (Tptf1) exposed in the headwaters of Larch Creek (45.370600, -121.357000). View is looking west. (b) Pumice- and lithic-rich tuff (Tptf1) from outcrops along Larch Creek, with porphyritic, dark gray (N3) dacitic pumices (45.368816, -121.334956). Scale bar is 10 cm (4 in) tall. Photo credits: J.D. McClaughry, 2015.**

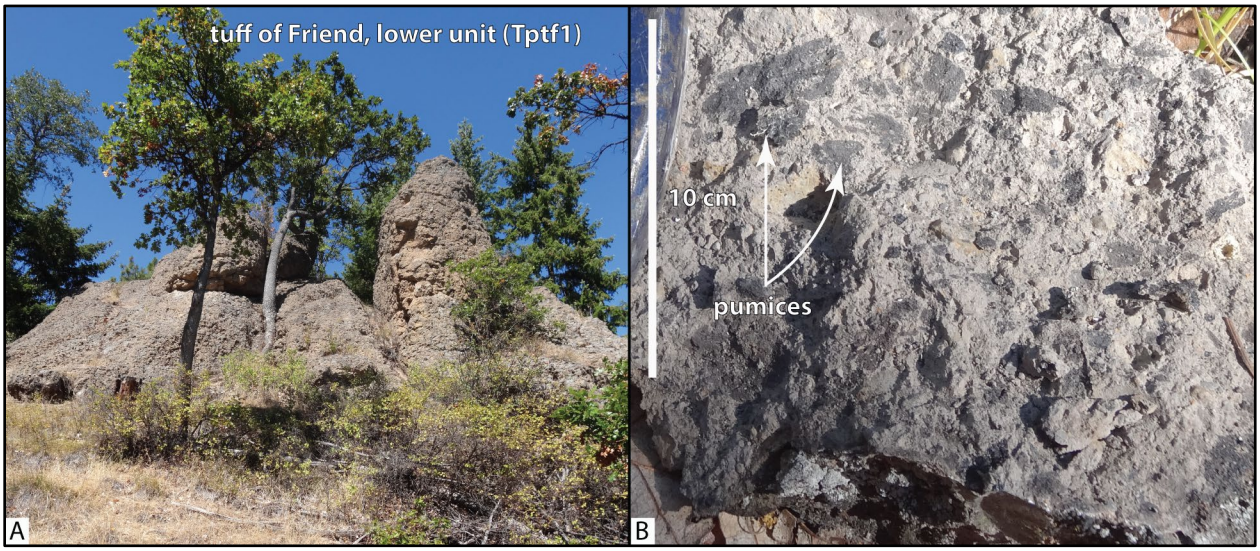

**Tpdv** **trachydacite of Fivemile Creek (lower Pliocene)—**Trachydacite lava flow ($SiO_2$ = 64.09 to 66.07 weight percent; $K_2O$ = 2.76 to 3.36 weight percent; Nb = 24.8 to 31 ppm; Zr = 356 to 421 ppm; *n* = 20 analyses [6 outside map area]) mapped as an intracanyon lava flow along Fivemile Creek in the northwestern part of the map area (**Figure 5-11**, **Figure 5-12**, **Figure 6-31**; **Table 6-2**; Plate 1; Appendix). Mapping over the larger Middle Columbia Basin indicates unit **Tpdv** extends from western exposures on East Fork Hood River and south of Mill Creek Buttes (McClaughry and others, 2020a) northeast ~30 km (18.6 mi) downstream to outcrops along Fivemile Creek at Pleasant Ridge Road (2.5 km [1.6 mi] northeast of map area, The Dalles South 7.5′ quadrangle; **Figure 1-2**, **Figure 5-4**). Unit **Tpdv** crops out as prominent cliffs and benches marked by massive to meter-scale columnar-joints and irregular zones of horizontal platy jointing (**Figure 6-31**). The common bench and rise topography associated with outcrops along Fivemile Creek and intervening vesicular horizons may indicate that two chemically identical and age-equivalent intracanyon lava flows are present within the unit. Outcrops weather to meter-scale, angular subrounded boulders and angular plates forming extensive talus slopes beneath cliffs. Composite thickness of unit **Tpdv** is ≥90 m (296 ft) in the canyon of Fivemile Creek (Plate 1). Unit **Tpdv** is locally capped by sedimentary deposits of unit **QTpg** (**Figure 6-31**). Typical hand samples of the trachydacite are dark gray (N3) containing 1 to 2 percent (vol.) clear, subhedral to anhedral, prismatic to blocky, seriate plagioclase microphenocrysts and phenocrysts ≤3 mm (0.1 in), ~1 percent grayish black (N2) (vol.) euhedral to subhedral, prismatic- to lath-shaped pyroxene microphenocrysts ≤1 mm (0.04 in) (orthopyroxene ≥ clinopyroxene), and ≤1 percent plagioclase-pyroxene microglomerocrysts ≤1 mm (0.1 in), distributed within a very fine grained holocrystalline to hypocrystalline groundmass (**Figure 6-32**).

Unit **Tpdv** has reversed magnetic polarity and is assigned an early Pliocene age on the basis of stratigraphic position and an $^{40}Ar/^{39}Ar$ plateau age of 3.69 ± 0.02 Ma (groundmass; sample 173 DFWJ 15) obtained from the outcrops in Fivemile Canyon (**Figure 5-13**, **Figure 6-1**; **Table 5-1**; Plate 1; Appendix). The 3.69 Ma $^{40}Ar/^{39}Ar$ age is indistinguishable from a K-Ar age of 3.7 ± 0.2 Ma (whole rock; sample JA85022) previously reported by Anderson (1987) for a sample collected along the south side of Fivemile Creek (**Table 5-1**; Plate 1; Appendix), 3.3 km (1.9 mi) east of sample 173 DFWJ 15. The reader should note that the original reported location for sample JA85022 was inadvertently transposed with sample JA85023, with a reported K-Ar age of 1.7 Ma (J.L. Anderson, written commun., 1998, to R.M. Conrey). Both samples and their corresponding geochemical and isotopic ages are herein properly located (**Table 5-1**; Plate 1).

**Figure 6-31. Trachydacite of Fivemile Creek (Tpdv). (a) Intracanyon, cliff-forming outcrops of the trachydacite of Fivemile Creek (Tpdv), inset into late Miocene and early Pliocene Dalles Formation (Tmdl) and overlain by sedimentary deposits of unit QTpg (45.478649, -121.324042). View is looking south. (b) Trachydacite (Tpdv) cliffs along Upper Fivemile Road in the northern part of the map area (45.477707, -121.318601). A sample from this outcrop returned an $^{40}Ar/^{39}Ar$ plateau age of 3.69 ± 0.02 Ma (sample 173 DFWJ 15). View is looking southwest. (c) Columnar-jointed outcrop of the trachydacite of Fivemile Creek (Tpdv) along USFS Road 1722 in the northwestern part of the map area (45.466261, -121.362867). Arrow points to hammer for scale, which is 38 cm (15 in) long. View is looking to the northwest. Photo credits: C.A. Niewendorp and J.D. McClaughry, 2015.**

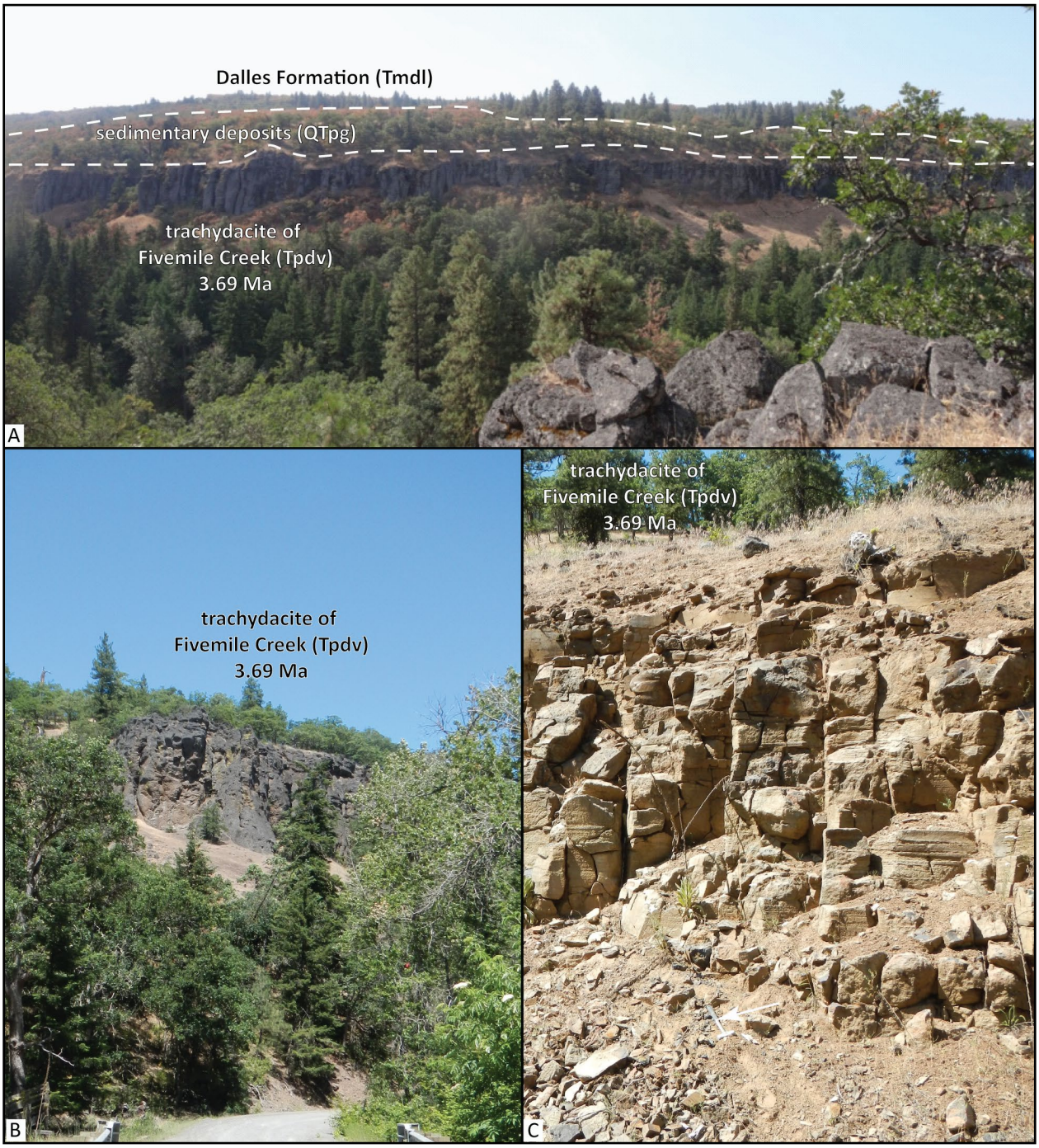

**Figure 6-32. Hand sample and thin section photographs of the trachydacite of Fivemile Creek (Tpdv). (a) Typical hand sample. Scale bar is 2.5 cm (1 in) tall. (b) Thin section under cross-polarized light (XPL). (c) Same view as in B under plane-polarized light (PPL). Scale bar for thin section photographs is 7 mm (0.3 in) wide. Photo credits: J.D. McClaughry, 2016.**

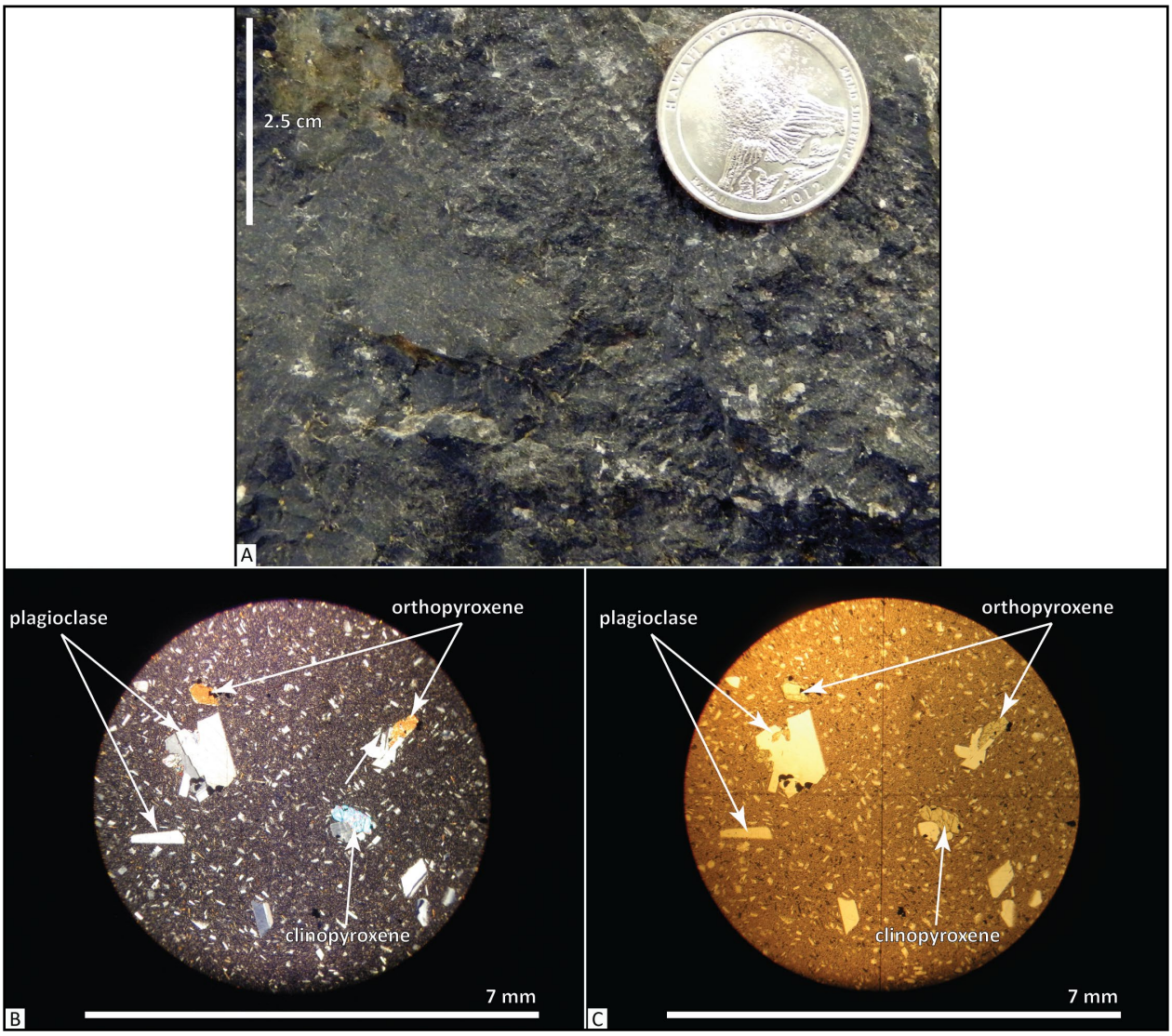


**Tpbf** **basalt (lower Pliocene)**—Intracanyon basalt lava flow ($SiO_2$ = 51.83 weight percent; $K_2O$ = 0.89 weight percent; *n* = 1 analysis) exposed in a single outcrop along Upper Fivemile Road in the northwestern part of the map area (**Figure 5-11**, **Figure 5-12**, **Figure 6-33**; **Table 6-2**; Plate 1; Appendix). The extent of unit **Tpbf** to the west or east of this outcrop along Upper Fivemile Road, is not known. Unit **Tpbf** is characterized by blocky meter-scale columns and intervals of platy jointing, and weathers to rounded boulders up to 1 m (3.3 ft) across (**Figure 6-33**). Thickness of unit **Tpbf** is unknown as the base of the unit is not exposed. Typical hand samples of the basalt are light gray (N7) to medium light gray containing 3 to 5 percent (vol.) clear, euhedral, prismatic, seriate plagioclase microphenocrysts and phenocrysts ≤5 mm (0.2 in) long, 1 to 3 percent (vol.) unaltered pale greenish yellow (10Y 8/2) to dark yellowish orange (10YR 6/6), subhedral to anhedral, blocky, seriate iddingsitized olivine microphenocrysts <1 mm (0.04 in) across, <1

percent (vol.) grayish black (N2), subhedral to anhedral, blocky- to lath-shaped, clinopyroxene microphenocrysts <1 mm (0.04 in) across, and sparse glomerocrysts of plagioclase, olivine, pyroxene, and Fe-Ti oxides ≤1 cm (0.4 in) across, contained within a holocrystalline groundmass (**Figure 6-34**).

Unit **Tpbf** has reversed magnetic polarity and is assigned an early Pliocene age on the basis of stratigraphic position beneath the 3.69 Ma trachydacite of Fivemile Creek and an $^{40}Ar/^{39}Ar$ plateau age of 3.72± 0.02 Ma (groundmass; sample 172 DFWJ 15) (**Figure 5-13**, **Figure 6-1**; **Table 5-1**; Plate 1; Appendix).

**Figure 6-33. Intracanyon lava flows, including the trachydacite of Fivemile Creek (Tpdv) and basalt (Tpbf) exposed along Fivemile Creek in the northern part of the map area (45.478213, -121.317775). The location of the photograph corresponds to samples 172 DFWJ 15 (Tpbf) and 173 DFWJ 15 (Tpdv). Sample 172 DFWJ 15 (Tpbf) returned an $^{40}Ar/^{39}Ar$ plateau age of 3.72 ± 0.02 Ma, while sample 173 DFWJ 15 (Tpdv) returned an $^{40}Ar/^{39}Ar$ plateau age of 3.69 ± 0.02 Ma. Lower arrow points to iPad for scale, which is 25 cm (9.8 in) tall. View is looking north. Photo credit: J.D. McClaughry, 2015.**

**Figure 6-34. Hand sample and thin section photographs of basalt (Tpbf). (a) Typical hand sample. Scale bar is 2.5 cm (1 in) tall. (b) Thin section under cross-polarized light (XPL). (c) Same view as in B under plane-polarized light (PPL). Scale bar for thin section photographs is 7 mm (0.3 in) wide. Photo credits: J.D. McClaughry, 2016.**

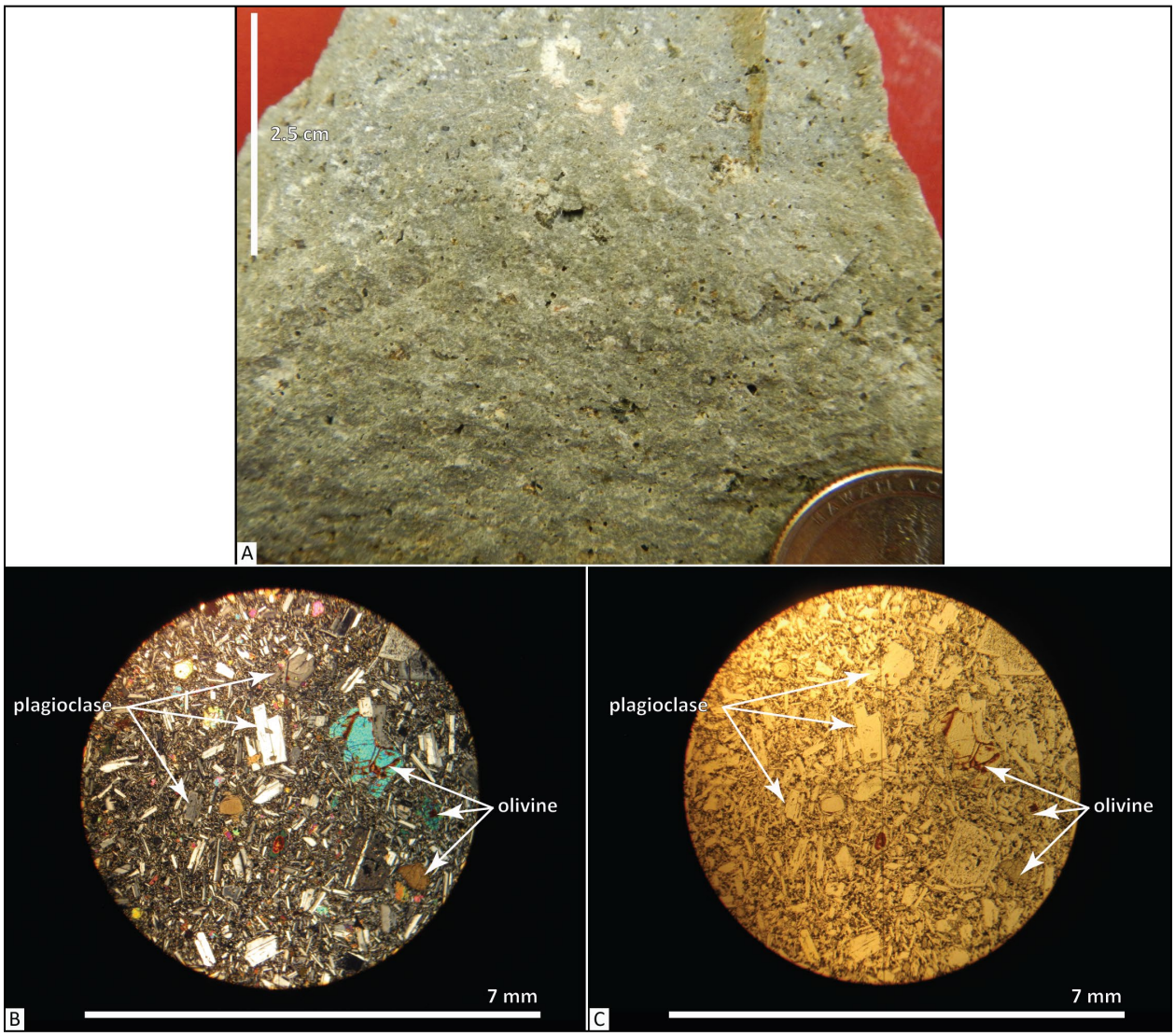

**Disconformity**

### 6.3.3 Lower Pliocene and upper Miocene volcanic and sedimentary rocks of the early High Cascades

#### 6.3.3.1 Dalles Formation

**Tmdl** **Dalles Formation, undivided (lower Pliocene and upper Miocene)—**Moderately to well-indurated, pale yellowish brown (10YR 6/2), medium gray (N5) to very light gray (N8) boulder breccia, fluvial conglomerate and sandstone, tuffaceous siltstone, and pumice-, ash-, and lithic-tuff, broadly exposed above the CRBG in the Dufur area (**Figure 6-35**, **Figure 6-36**, **Figure 6-37**). A majority of beds within the Dalles Formation (**Tmdl**) are often thin, discontinuous, texturally indistinct, and occur at a scale too small to map separately and are therefore grouped here. Thickness of unit **Tmdl** in the Dufur area is ≥343 m (1,000 ft).

Breccia beds are typically well-exposed, forming erosionally resistant ledges along canyon walls (**Figure 6-35b**, **Figure 6-36**). Where breccia beds are deeply weathered, surfaces are mantled by meter-scale boulders, intermixed with coarse-grained sandy soils (**Figure 6-35c,d**). Breccia is typically matrix-supported with localized clast-supported areas. The deposits range from monolithologic to heterolithologic, dominated by a variety of medium light gray (N6) to pale blue (5B 6/2) and pale purple (5P 6/2), subrounded to subangular clasts of plagioclase and two-pyroxene (± hornblende) andesite and dacite. Clasts are typically enclosed in a matrix composed of volcanic lithics, pumice, partly altered volcanic glass, and plagioclase and pyroxene crystals. Locally, breccia is interbedded with massive to planar stratified sandstone and pebble conglomerate deposited by hyperconcentrated flood-flows, tuff deposited by pyroclastic flows and falls, and lenticular bedded, massive to trough- and planar-cross bedded, pebble- to cobble-rich conglomerate, pebbly sandstone, and sandstone and massive to laminated tuffaceous siltstone deposited in fluvial environments (**Figure 6-37**). Fluvial conglomerate in the Dufur area is locally exposed consisting of 3- to 15-m-thick (9.9- to 49-ft), typically lenticular beds, containing moderately to well-sorted, well-rounded cobbles and pebbles derived from Cascadian volcanic sources and the underlying CRBG (**Figure 6-37**). Exotic metamorphic clasts or non-Cascadian clasts were not found in fluvial deposits in the map area. Northeast of the map area, in the Petersburg 7.5′ quadrangle, the Dalles Formation as presently mapped, includes fluvial facies with an inferred Deschutes River provenance (**Figure 1-2**). These strata contain clasts thought to be derived from older Tertiary volcanic sources unique to parts of Central Oregon (e.g., John Day and Clarno Formations; Cannon and O'Connor, 2019).

Unit **Tmdl** is assigned a late Miocene and early Pliocene age, ranging between ~8.8 and 5 Ma, on the basis of stratigraphic position, numerous isotopic ages in the Middle Columbia Basin, and vertebrate and leaf fossils (**Figure 6-1**). Equivalent to the Dalles Formation as defined by Condon (1874).

**Figure 6-35. Typical landscapes developed on the Dalles Formation (Tmdl) in the Dufur area. (a) The Dalles Formation (Tmdl) in the Dufur Area caps northeast-elongated ridges that parallel modern drainages, including Fifteenmile, Eightmile, and Fivemile Creeks. The view is looking west toward Mount Hood from the cell towers located just northwest of the city of Dufur (45.457938, -121.140224). (b) Drainages incised into the Dalles Formation (Tmdl) and perpendicular to the northeast trend of ridges, locally reveal well-exposed stratigraphic sections, characterized by bench- and cliff-forming outcrops. The view is looking north toward the cell towers located just northwest of the city of Dufur (45.456720, -121.134821). (c) The Dalles Formation is typically mantled by thin soils and surfaces vegetated by grasses, small shrubs, and locally oak forests. The view is looking east toward the city of Dufur (45.433430, -121.186507). Arrow points to person for scale who is 1.6 m (5.2 ft) tall. (d) Small boulder piles are often discontinuously exposed where wheat fields have been developed over thin soils (45.403779, -121.181616). Photo credits: J.D. McClaughry, 2014.**

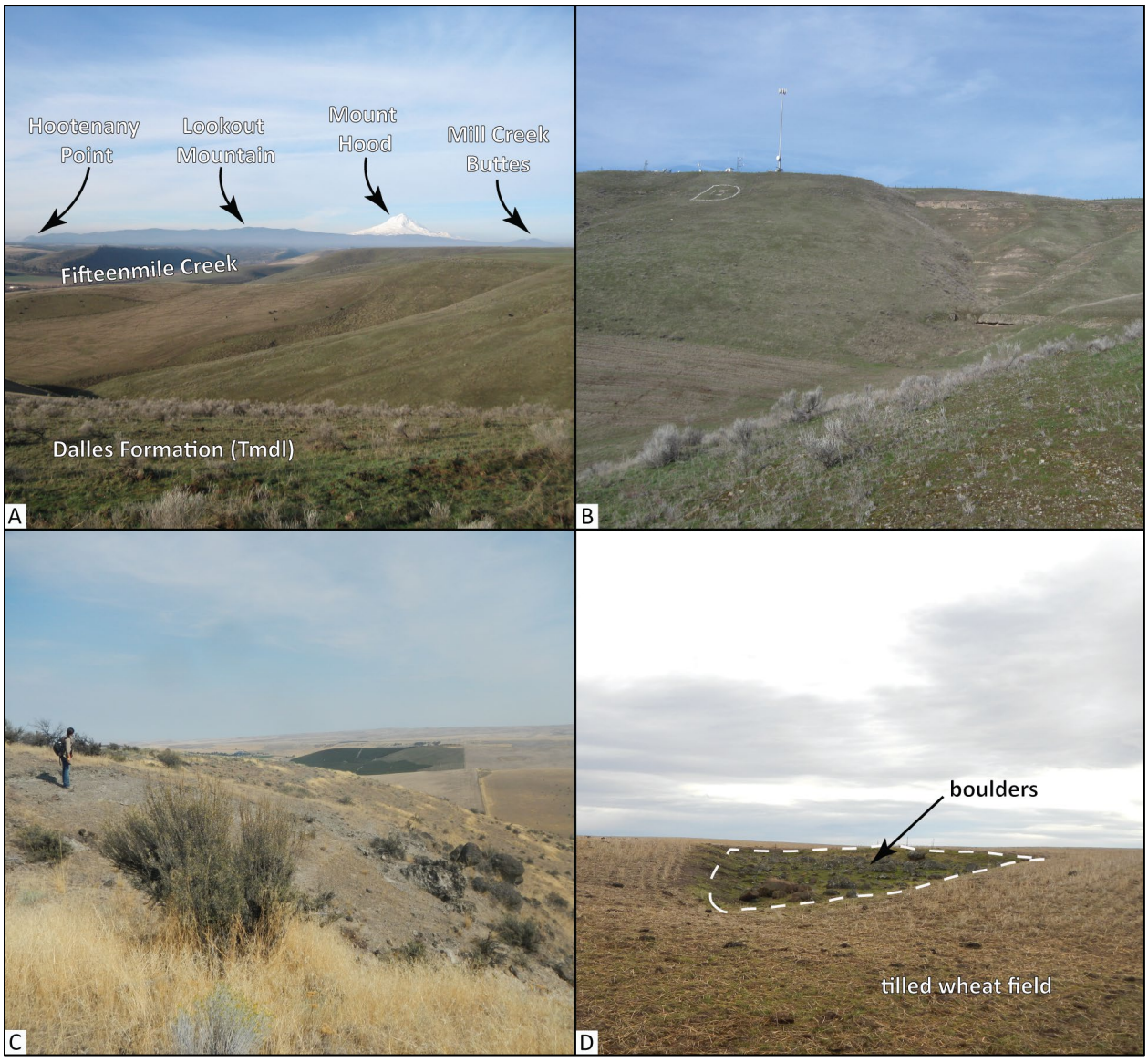

**Figure 6-36. Typical landscapes developed on the Dalles Formation (Tmdl) in the Dufur area. (a) The Dalles Formation (Tmdl) is composed largely of stacked successions of boulder breccia, pebbly sandstone, and sandstone. The image direction looking north from cliff-forming outcrops of the dacite of Fifteenmile Creek shown in Figure 6-14a (45.383368, -121.337802). (b) Sparsely vegetated, layered beds of boulder breccia, pebbly sandstone, and sandstone exposed along Upper Eightmile Road in the northeast part of the map area. The view is looking north from the Upper Eightmile Road (45.460501, -121.260001). Photo credits: C.A. Niewendorp, 2015.**

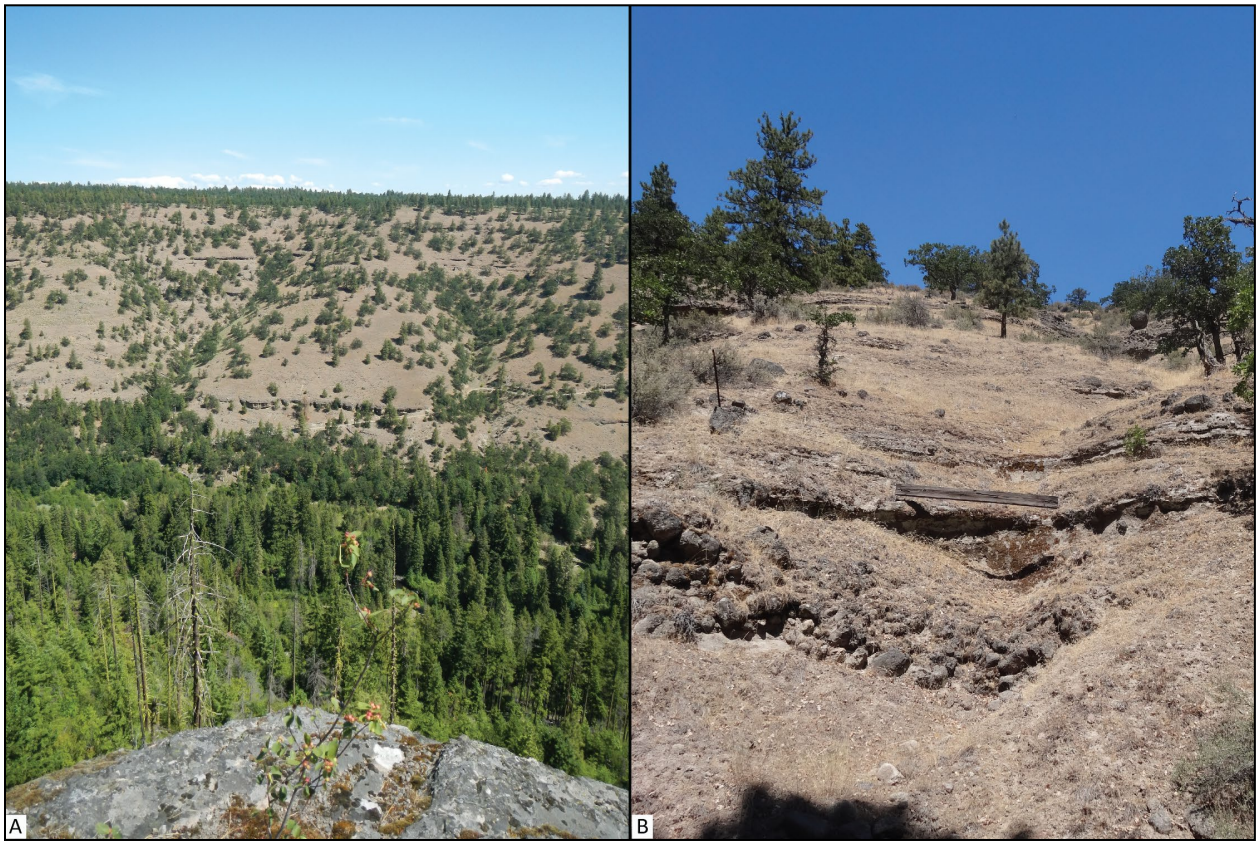


**Figure 6-37. Examples of typical Dalles Formation (Tmdl) outcrops (*image on following page*). (a) Massive boulder breccia (Tmdd) overlying cross-bedded pebbly sandstone of the Dalles Formation (Tmdl) on the north side of Fifteenmile Creek, west of the city of Dufur (45.449764, -121.158558). Overhanging ledges, formed between erosionally resistant upper units and more easily eroded lower units, are a common feature of the Dalles Formation (Tmdl) in the Dufur area. The dashed white line shows the sharp, planar contact between the two units. Person for scale is 1.6 m (5.2 ft) tall. (b) Cross-bedded pebbly sandstone typical of fluvial facies in the Dalles Formation (45.449652, -121.158199). iPad for scale is 25 cm (9.8 in) tall. (c) Well-exposed section of planar-stratified pebble breccia and massively bedded pumiceous breccia overlain by massively bedded ash tuff on the south side of Eightmile Creek (45.473502, -121.175479). The 'Y' corresponds to the location for photo D. Person for scale is 1.6 m (5.2 ft) tall. (d) Pumice-rich, matrix-supported deposit typical of debris-flow facies in the Dalles Formation (Tmdl) (45.473502, -121.175479). Colored increments on the Jacob's Staff are 10 cm (4 in). (e) Planar-stratified sandstone and pebble conglomerate exposed near the base of the Dalles Formation (Tmdl) in Rail Hollow (45.412417, -121.200820). Pen for scale is 15 cm (5.9 in) tall. (e) Massive boulder breccia overlying fluvial pebble-cobble conglomerate on the north side of Henderson Hollow (45.433239, -121.186308). Person kneeling for scale is about 1 m (3.3 ft) high. Photo credits: J.D. McClaughry, 2014.**

**Figure 6-37. (Examples of The Dalles Formation (Tmdl) – *caption on previous page*)**

**Table 6-3. Representative XRF analyses for the late Miocene and early Pliocene Dalles Formation in the Dufur area (part 1 of 3).**

| Sample | 95b WRCN 15 | 67 WRCN 15 | 70 WRCN 15 | 71 WRCN 15 | 53 WRCN 15 | 208 DFWJ 15 | 66 DFWJ 14 | 30 DFWJ 15 | 158 DFWJ 15 | 168 DFWJ 15 | 291 DFWJ 14 |
|---|---|---|---|---|---|---|---|---|---|---|---|
| **Geographic Area** | Ramsey Creek | Rail Hollow | Rail Hollow | Rail Hollow | South Fk. Fivemile Creek | Eightmile Creek | Eightmile Creek | Friend | Owl Hollow | Hesslan Canyon | Eightmile Creek |
| **Formation** | Dalles Formation | Dalles Formation | Dalles Formation | Dalles Formation | Dalles Formation | Dalles Formation | Dalles Formation | Dalles Formation | Dalles Formation | Dalles Formation | Dalles Formation |
| **Map Unit** | Tmdl (clast) | Tmdl (clast) | Tmdl (clast) | Tmdl (clast) | Tmdl (clast) | Tmdl (clast) | Tmdl (pumice) | Tmtw | Tmdj | Tmdv | Tmdw |
| **UTM N (NAD 83)** | 5032760 | 5033590 | 5033680 | 5033910 | 5035560 | 5037173 | 5038163 | 5024197 | 5024270 | 5030972 | 5035066 |
| **UTM E (NAD 83)** | 636126 | 628004 | 627961 | 627326 | 627976 | 642607 | 643059 | 636779 | 627455 | 627123 | 637284 |
| **Age (Ma)** | nd | nd | nd | nd | nd | nd | nd | 5.27 | nd | ~ 7.7 Ma | 7.91 Ma |
| **Plate** | 1 | 1 | 1 | 1 | 1 | 2 | 2 | 1 | 1 | na | 2 |
| **Map Label** | G52 | G55 | G56 | G57 | G58 | G127 | G128 | G2 | G4 | na | G124 |
| ***Oxides, weight percent*** | | | | | | | | | | | |
| **$SiO_2$** | 64.66 | 65.41 | 64.51 | 63.08 | 62.04 | 64.75 | 73.48 | 73.13 | 64.69 | 63.95 | 64.29 |
| **$Al_2O_3$** | 16.93 | 17.18 | 16.92 | 17.40 | 17.99 | 18.81 | 15.35 | 15.21 | 17.78 | 17.27 | 15.72 |
| **$TiO_2$** | 0.64 | 0.70 | 0.72 | 0.80 | 0.82 | 0.66 | 0.22 | 0.15 | 0.67 | 0.73 | 0.97 |
| **FeO*** | 4.70 | 4.57 | 4.92 | 5.48 | 5.33 | 4.28 | 2.41 | 1.99 | 4.98 | 5.05 | 5.70 |
| **MnO** | 0.08 | 0.08 | 0.07 | 0.08 | 0.09 | 0.08 | 0.06 | 0.06 | 0.06 | 0.08 | 0.09 |
| **CaO** | 4.94 | 4.95 | 5.05 | 5.34 | 5.81 | 5.06 | 2.31 | 1.25 | 4.70 | 5.36 | 4.06 |
| **MgO** | 2.16 | 1.35 | 1.98 | 2.33 | 2.58 | 1.77 | 0.57 | 0.16 | 1.59 | 1.93 | 1.98 |
| **$K_2O$** | 1.92 | 1.49 | 1.39 | 1.19 | 1.02 | 1.08 | 2.77 | 3.51 | 1.28 | 1.22 | 2.85 |
| **$Na_2O$** | 3.84 | 4.11 | 4.27 | 4.15 | 4.19 | 3.40 | 2.74 | 4.48 | 4.12 | 4.23 | 4.13 |
| **$P_2O_5$** | 0.12 | 0.16 | 0.15 | 0.15 | 0.14 | 0.11 | 0.09 | 0.05 | 0.16 | 0.17 | 0.20 |
| **LOI** | 2.05 | 1.40 | 0.71 | 0.93 | 0.48 | 6.84 | nd | 1.50 | nd | 2.90 | nd |
| **Total_I** | 97.06 | 97.57 | 98.56 | 98.72 | 98.59 | 93.24 | 91.28 | 100.25 | 97.77 | 96.65 | 99.92 |
| ***Trace Elements, parts per million*** | | | | | | | | | | | |
| **Ni** | 18 | 16 | 16 | 21 | 19 | 24 | 3 | 8 | 18 | 17 | 17 |
| **Cr** | 22 | 29 | 26 | 26 | 31 | 22 | 4 | 11 | 35 | 28 | 19 |
| **Sc** | 12 | 10 | 11 | 13 | 13 | 10 | 3 | 1 | 10 | 10 | 12 |
| **V** | 84 | 91 | 84 | 104 | 98 | 50 | 7 | 6 | 74 | 79 | 92 |
| **Ba** | 363 | 349 | 322 | 290 | 270 | 288 | 453 | 790 | 398 | 375 | 510 |
| **Rb** | 41 | 32 | 28 | 24 | 17 | 22 | 49 | 100.2 | 24 | 22 | 71 |
| **Sr** | 368 | 618 | 459 | 416 | 551 | 412 | 267 | 170 | 431 | 493 | 332 |
| **Zr** | 168 | 143 | 160 | 139 | 118 | 145 | 148 | 250 | 154 | 155 | 341 |
| **Y** | 16 | 11 | 22 | 23 | 11 | 15 | 13 | 33.2 | 16 | 14 | 34 |
| **Nb** | 9.0 | 8.0 | 8.9 | 8.6 | 5.8 | 8.3 | 8.5 | 29.9 | 9.4 | 9.8 | 16.5 |
| **Ga** | 20 | 20 | 19 | 19 | 19 | 20 | 16 | 25.2 | 21 | 20 | 18 |
| **Cu** | 27 | 19 | 43 | 33 | 17 | 37 | 10 | 21 | 31 | 21 | 45 |
| **Zn** | 59 | 62 | 69 | 65 | 63 | 69 | 45 | 58 | 69 | 83 | 66 |
| **Pb** | 6 | 4 | 5 | 4 | 5 | 8 | 8 | 14 | 6 | 6 | 9 |
| **La** | 19 | 22 | 24 | 34 | 12 | 16 | 21 | 48 | 32 | 21 | 42 |
| **Ce** | 33 | 34 | 31 | 39 | 23 | 38 | 34 | 93 | 37 | 36 | 57 |
| **Th** | 5 | 5 | 4 | 4 | 2 | 6 | 6 | 19.2 | 4 | 2 | 9 |
| **Nd** | 13 | 18 | 29 | 32 | 12 | 16 | 13 | nd | 31 | 20 | 38 |
| **U** | 1 | 2 | 2 | 2 | 1 | 2 | 1 | 1.7 | 0 | 1 | 3 |

Major element determinations have been normalized to a 100-percent total on a volatile-free basis and recalculated with total iron expressed as FeO*; nd - no data or element not analyzed; na - not applicable or no information. LOI, Loss on Ignition; Total_I, original analytical total. Sample 600 MCBJ 16 is located outside the study area, in the Fivemile Butte 7.5′ quadrangle.

*Table 6-3, continued. Select XRF geochemical analyses for late Miocene and early Pliocene Dalles Formation in the Dufur area (part 2 of 3).*

| **Sample** | 177 WRCN 15 | 169 WRCN 15 | 29 DFWJ 14 | 37 DFWJ 14 | 378 DFWJ 14 | 276 DFWJ 15 | 151 WRCN 15 | 153 WRCN 15 | 144 WRCN 15 | 155 WRCN 15 | 319 DFWJ 15 |
|---|---|---|---|---|---|---|---|---|---|---|---|
| **Geographic Area** | Larch Creek | Larch Creek | Winslow Road | Rail Hollow | Henderson Hollow | Fifteenmile Creek | Larch Creek | Larch Creek | Larch Creek | Larch Creek | Rail Hollow |
| **Formation** | Dalles Formation | Dalles Formation | Dalles Formation | Dalles Formation | Dalles Formation | Dalles Formation | Dalles Formation | Dalles Formation | Dalles Formation | Dalles Formation | Dalles Formation |
| **Map Unit** | Tmdt | Tmdt | Tmdt | Tmdt | Tmdt | Tmdt | Tmdd (clast) | Tmdd (clast) | Tmdd (clast) | Tmdd (clast) | Tmdd (clast) |
| **UTM N (NAD 83)** | 5025030 | 5025360 | 5027344 | 5028892 | 5030100 | 5032000 | 5025630 | 5025660 | 5025770 | 5025830 | 5030169 |
| **UTM E (NAD 83)** | 632022 | 630061 | 638107 | 637332 | 637686 | 639196 | 629334 | 629333 | 628416 | 629277 | 640420 |
| **Age (Ma)** | ~8.07 Ma | ~8.07 Ma | 8.07 Ma | nd | nd | nd | ~8.75 Ma | ~8.75 Ma | ~8.75 Ma | ~8.75 Ma | ~8.75 Ma |
| **Plate** | 1 | 1 | 2 | 2 | 2 | 2 | 1 | 1 | 1 | 1 | 2 |
| **Map Label** | G19 | G22 | G36 | G61 | G86 | G106 | G28 | G29 | G30 | G31 | G84 |
| ***Oxides, weight percent*** | | | | | | | | | | | |
| **$SiO_2$** | 65.79 | 64.03 | 63.20 | 63.10 | 62.36 | 63.62 | 64.11 | 66.21 | 64.17 | 67.35 | 64.46 |
| **$Al_2O_3$** | 16.76 | 17.70 | 17.69 | 18.44 | 19.14 | 17.35 | 17.04 | 16.60 | 16.96 | 16.19 | 17.55 |
| **$TiO_2$** | 0.71 | 0.76 | 0.73 | 0.75 | 0.77 | 0.66 | 0.71 | 0.63 | 0.71 | 0.59 | 0.73 |
| **FeO*** | 5.09 | 5.14 | 5.01 | 5.22 | 5.32 | 4.89 | 4.76 | 4.22 | 4.79 | 4.25 | 5.01 |
| **MnO** | 0.10 | 0.09 | 0.09 | 0.10 | 0.10 | 0.11 | 0.08 | 0.06 | 0.09 | 0.06 | 0.13 |
| **CaO** | 4.55 | 5.12 | 5.50 | 5.35 | 5.75 | 5.44 | 5.21 | 4.63 | 4.98 | 4.12 | 4.88 |
| **MgO** | 1.05 | 1.73 | 2.28 | 1.72 | 1.39 | 2.30 | 2.15 | 1.66 | 2.19 | 1.37 | 1.58 |
| **$K_2O$** | 1.66 | 1.62 | 1.27 | 1.33 | 1.17 | 1.82 | 1.39 | 1.69 | 1.44 | 1.89 | 2.09 |
| **$Na_2O$** | 4.14 | 3.65 | 4.08 | 3.84 | 3.86 | 3.66 | 4.39 | 4.17 | 4.51 | 4.01 | 3.40 |
| **$P_2O_5$** | 0.16 | 0.15 | 0.15 | 0.15 | 0.13 | 0.16 | 0.16 | 0.13 | 0.15 | 0.18 | 0.19 |
| **LOI** | 2.05 | 2.44 | nd | nd | nd | 2.75 | 0.75 | 1.05 | 0.82 | 1.44 | 3.79 |
| **Total_I** | 97.19 | 97.45 | 99.32 | 97.15 | 96.60 | 100.13 | 98.25 | 98.19 | 98.57 | 98.12 | 99.91 |
| ***Trace Elements, parts per million*** | | | | | | | | | | | |
| **Ni** | 17 | 18 | 21 | 21 | 19 | 16 | 21 | 18 | 20 | 17 | 24 |
| **Cr** | 26 | 28 | 32 | 31 | 30 | 65 | 35 | 28 | 36 | 25 | 47 |
| **Sc** | 10 | 12 | 11 | 13 | 12 | 10 | 12 | 10 | 12 | 9 | 9 |
| **V** | 87 | 86 | 94 | 87 | 85 | 81 | 83 | 89 | 70 | 60 | 90 |
| **Ba** | 408 | 395 | 337 | 318 | 316 | 367 | 370 | 356 | 382 | 506 | 444 |
| **Rb** | 37 | 33 | 16 | 22 | 19 | 38 | 24 | 38 | 27 | 44 | 44 |
| **Sr** | 403 | 418 | 522 | 512 | 569 | 428 | 438 | 420 | 416 | 391 | 385 |
| **Zr** | 155 | 161 | 135 | 142 | 133 | 161 | 149 | 138 | 149 | 137 | 211 |
| **Y** | 14 | 16 | 11 | 14 | 14 | 15 | 12 | 10 | 13 | 13 | 19 |
| **Nb** | 10.0 | 9.8 | 7.5 | 8.1 | 7.5 | 10.1 | 10.0 | 8.3 | 9.1 | 9.3 | 10.5 |
| **Ga** | 20 | 20 | 20 | 21 | 20 | 22 | 19 | 19 | 20 | 19 | 22 |
| **Cu** | 26 | 21 | 20 | 37 | 42 | 18 | 31 | 36 | 31 | 25 | 49 |
| **Zn** | 77 | 74 | 65 | 65 | 63 | 68 | 72 | 74 | 67 | 68 | 66 |
| **Pb** | 8 | 6 | 4 | 6 | 5 | <1 | 5 | 6 | 4 | 6 | <1 |
| **La** | 23 | 23 | 15 | 17 | 17 | 26 | 16 | 16 | 18 | 23 | 26 |
| **Ce** | 43 | 42 | 31 | 40 | 33 | 42 | 37 | 36 | 35 | 37 | 47 |
| **Th** | 5 | 5 | 5 | 3 | 4 | 8 | 5 | 5 | 4 | 5 | 11 |
| **Nd** | 20 | 19 | 16 | 16 | 14 | nd | 16 | 19 | 18 | 18 | nd |
| **U** | 2 | 2 | 1 | 1 | 2 | 1 | 2 | 3 | 2 | 2 | 1 |

Major element determinations have been normalized to a 100-percent total on a volatile-free basis and recalculated with total iron expressed as FeO*; nd - no data or element not analyzed; na - not applicable or no information. LOI, Loss on Ignition; Total_I, original analytical total.

*Table 6-3, continued. Select XRF geochemical analyses for late Miocene and early Pliocene Dalles Formation in the Dufur area (part 3 of 3).*

| **Sample** | 263 DFWJ 15 | 212 DFWJ 14 | 232 DFWJ 14 | 102 DFWJ 14 | 13a DFWJ 15 | 317 DFWJ 15 |
|---|---|---|---|---|---|---|
| **Geographic Area** | Fifteenmile Creek | Fifteenmile Creek | Fifteenmile Creek | Fifteenmile Creek | Fifteenmile Creek | Rail Hollow |
| **Formation** | Dalles Formation | Dalles Formation | Dalles Formation | Dalles Formation | Dalles Formation | Dalles Formation |
| **Map Unit** | Tmdd (clast) | Tmdd (clast) | Tmdd (clast) | Tmdd (clast) | Tmdd (clast) | Tmdp |
| **UTM N (NAD 83)** | 5031921 | 5033078 | 5033173 | 5034874 | 5035350 | 5030172 |
| **UTM E (NAD 83)** | 638492 | 642673 | 639934 | 644240 | 645630 | 640464 |
| **Age (Ma)** | ~8.75 Ma | 8.75 Ma | nd | nd | nd | nd |
| **Plate** | 2 | 2 | 2 | 2 | 2 | 2 |
| **Map Label** | G105 | G117 | G119 | G123 | G125 | G85 |
| ***Oxides, weight percent*** | | | | | | |
| **$SiO_2$** | 61.72 | 66.14 | 62.90 | 64.25 | 65.64 | 61.07 |
| **$Al_2O_3$** | 18.54 | 16.06 | 17.61 | 17.25 | 16.75 | 18.91 |
| **$TiO_2$** | 0.69 | 0.62 | 0.71 | 0.65 | 0.58 | 1.21 |
| **FeO*** | 5.15 | 4.45 | 5.21 | 4.62 | 4.22 | 7.54 |
| **MnO** | 0.12 | 0.08 | 0.10 | 0.09 | 0.08 | 0.10 |
| **CaO** | 5.82 | 4.55 | 5.61 | 5.24 | 4.84 | 5.11 |
| **MgO** | 2.41 | 2.08 | 2.50 | 2.17 | 1.96 | 1.25 |
| **$K_2O$** | 1.41 | 2.22 | 1.41 | 1.77 | 1.90 | 1.46 |
| **$Na_2O$** | 3.97 | 3.67 | 3.80 | 3.84 | 3.88 | 3.16 |
| **$P_2O_5$** | 0.16 | 0.13 | 0.14 | 0.14 | 0.15 | 0.17 |
| **LOI** | 1.88 | nd | nd | nd | 2.62 | 7.29 |
| **Total_I** | 99.89 | 97.46 | 98.50 | 98.03 | 100.27 | 99.65 |
| ***Trace Elements, parts per million*** | | | | | | |
| **Ni** | 23 | 16 | 20 | 17 | 18 | 18 |
| **Cr** | 49 | 26 | 30 | 24 | 40 | 59 |
| **Sc** | 11 | 11 | 13 | 11 | 8 | 18 |
| **V** | 87 | 77 | 85 | 82 | 69 | 132 |
| **Ba** | 392 | 361 | 364 | 370 | 420 | 384 |
| **Rb** | 33 | 49 | 32 | 39 | 41 | 39 |
| **Sr** | 446 | 373 | 422 | 405 | 380 | 403 |
| **Zr** | 190 | 149 | 151 | 156 | 172 | 192 |
| **Y** | 16 | 14 | 15 | 17 | 18 | 20 |
| **Nb** | 8.9 | 8.6 | 8.3 | 9.1 | 8.8 | 10.3 |
| **Ga** | 23 | 18 | 19 | 20 | 21 | 23 |
| **Cu** | 36 | 19 | 30 | 13 | 23 | 59 |
| **Zn** | 60 | 59 | 62 | 60 | 53 | 72 |
| **Pb** | <1 | 7 | 5 | 7 | <1 | <1 |
| **La** | 26 | 18 | 19 | 20 | 26 | 22 |
| **Ce** | 42 | 32 | 34 | 34 | 51 | 35 |
| **Th** | 8 | 7 | 5 | 5 | 4 | 12 |
| **Nd** | nd | 15 | 15 | 17 | nd | nd |
| **U** | <0.5 | 3 | 0 | 2 | <0.5 | 1 |

Major element determinations have been normalized to a 100-percent total on a volatile-free basis and recalculated with total iron expressed as FeO*; nd - no data or element not analyzed; na - not applicable or no information. LOI, Loss on Ignition; Total_I, original analytical total.

**Tmdg** **plateau-capping conglomerate (lower Pliocene and/or upper Miocene)—**Moderately to well-sorted, consolidated to lithified cobble conglomerate capping ridges between Japanese Hollow on the north and Pine Creek on the south (**Figure 6-38**, **Figure 6-39**; Plates 1 and 2). Exposures are typically limited to roadcuts, roadbeds, rock pits, tilled fields, and small excavations (**Figure 6-38, Figure 6-39**) More commonly the unit weathers to a surface of scattered, well-rounded, ellipsoid-shaped cobbles (**Figure 6-38**, **Figure 6-39**). The conglomerate is dominated by medium light gray (N6) to pale blue (5B 6/2) and pale purple (5P 6/2) clasts of plagioclase and two-pyroxene (± hornblende) andesite and dacite of Cascadian provenance (e.g., Dalles Formation) and lesser amounts of Columbia River Basalt. No lithologies (e.g., metamorphic rocks or older Tertiary volcanic rocks), that might suggest a Columbia Basin or Deschutes River provenance, have been found in unit **Tmdg** in the Dufur area. Unit **Tmdg** is assigned a late Miocene and/or early Pliocene age on the basis of stratigraphic position (**Figure 6-1**).

**Figure 6-38. Cobble conglomerate (Tmdl) capping the ridge between Fifteenmile Creek and Henderson Hollow (45.432874, -121.192471). The tilled wheat field is developed in a thin soil horizon of loess (Qlo) that here overlies the conglomerate (Tmdg). Person for scale is 1.6 m (5.2 ft) tall. View is looking northeast. Photo credit: J.D. McClaughry, 2014.**

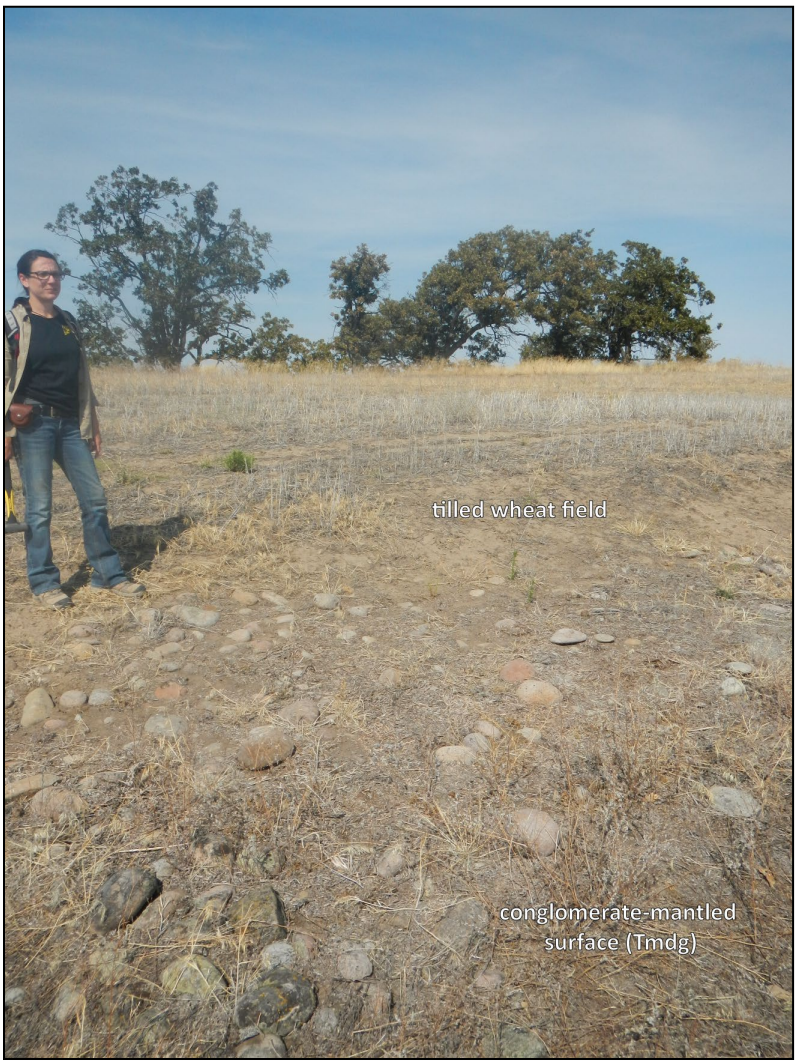

**Figure 6-39. Conglomerate (Tmdl) capping the Dalles Formation. (a) Boulder-cobble conglomerate (Tmdl) on Pleasant Ridge Road in the northwest corner of the map area (45.461487, -121.288600). Arrow points to hammer for scale, which is 38 cm (15 in) long. View is looking northeast. (b) Cobble conglomerate exposed at the edge of a tilled field, north of Pine Creek (45.404264, -121.174500). Camera case for scale is 12 cm (4.7 in) across. Photo credits: J.D. McClaughry, 2015.**


**Tmtw** **welded rhyolite tuff (lower Pliocene)**—Welded, lithophysal rhyolite tuff ($SiO_2$ = 73.13 weight percent; $K_2O$ = 3.51 weight percent; Zr = 250 ppm; Nb = 29.9 ppm; *n* = 1 analysis) mapped 1.6 km (1 mi) northeast of Friend (**Figure 6-40**; **Table 6-3**; Plate 1; Appendix). The tuff (**Tmtw**) is poorly exposed only as a broken surface mantle. Thickness of unit **Tmtw** is unknown. Typical hand samples of the tuff are very light gray (N8) to medium light gray (N6) and pinkish gray (5YR 8/1) to light brownish gray (5YR 6/1) (**Figure 6-40a**). The tuff is sparsely porphyritic with ~1 to 2 percent (vol.) clear, subhedral to anhedral and broken, prismatic to blocky plagioclase phenocrysts ≤3 mm (0.1 in) in length, and <1 percent (vol.) subhedral to anhedral, lath-shaped and broken, pale greenish yellow (10Y 8/2) orthopyroxene and clinopyroxene (orthopyroxene > clinopyroxene) phenocrysts up to 2 mm (0.1 in), contained within a eutaxitic groundmass of crystallites, ash, and devitrified glass (**Figure 6-40b,c**). A eutaxitic groundmass fabric is defined by crystallites aligned parallel to and wrapping around larger microphenocrysts. The tuff also contains single spherulites up to 1 mm (0.04 in).

Unit **Tmtw** is assigned an early Pliocene age on the basis of an $^{40}Ar/^{39}Ar$ inverse isochron age of 5.13 ± 0.76 (plagioclase; 30 DFWJ 15) (**Table 5-1**, **Figure 6-1**; Plate 1; Appendix). The original data yielded no good plateau age, but adjustment of the age spectrum, considering the inverse isochron $^{40}Ar/^{36}Ar$ intercept value, yields a revised plateau age of 5.27 ± 0.46 Ma. The restricted outcrop distribution of the rhyolitic tuff may indicate that the unit is a deeply eroded topographic high in the upper part of the Dalles Formation subsequently buried by boulder-rich block-and-ash-flow deposits of unit **Tpdd1** around 3.7 Ma. Alternatively, outcrops of the rhyolitic tuff could be interpreted as a notable mega-block rafted and contained within the younger **Tpdd1** deposit. The latter interpretation would be consistent with occasional clasts of similar composition rhyolite and rhyolitic welded tuff observed within block-and-ash-flow deposits of unit **Tpdd1** and

the absence of rhyolitic tuff exposed along the contact between the older CRBG units and the younger unit **Tpdd1** in nearby canyons (Plates 1 and 2).

**Figure 6-40. Hand sample and thin section photographs of welded rhyolite tuff (Tmtw). (a) Typical hand sample of devitrified, welded tuff. Scale bar is 5 cm (2 in) across. (b) Thin section under cross-polarized light (XPL). (c) Same view as in B under plane-polarized light (PPL) showing characteristic eutaxitic banding, plagioclase microphenocrysts, and local zones of sericite alteration. Scale bar for thin section photographs is 7 mm (0.3 in) wide. Photo credit: J.D. McClaughry, 2015, 2016.**

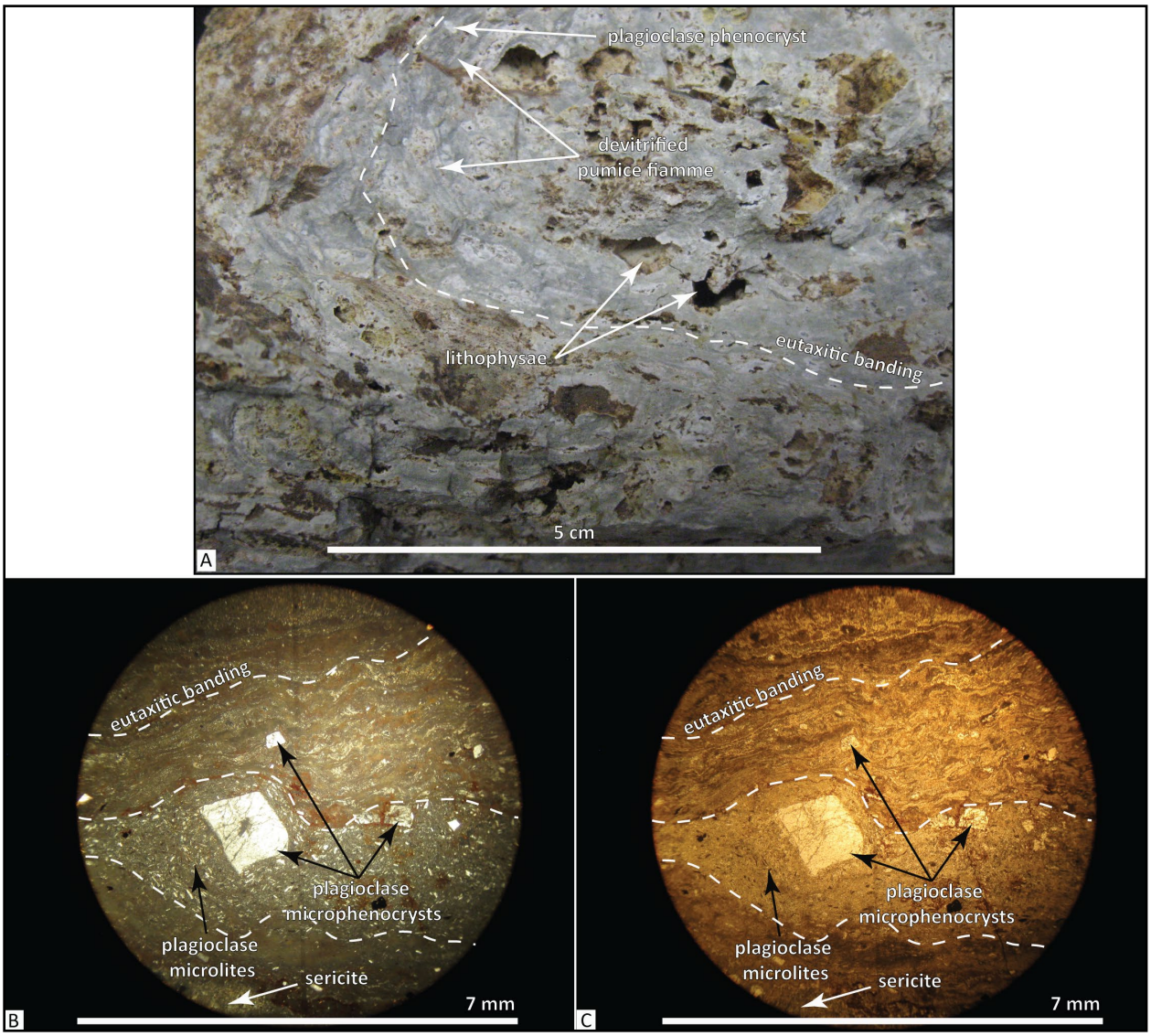


**Tmdj** **dacite of Jordan Butte (lower Pliocene or upper Miocene)**—Andesite and dacite lava flows ($SiO_2$ = 62.26 to 64.69 weight percent; $K_2O$ = 1.02 to 1.28 weight percent; *n* = 2 analyses) mapped on the north side of Owl Hollow along USFS Road 2730 in the southwest part of the map area (**Figure 6-41**; **Table 6-3**; Plate 1; Appendix). Outcrops exposed here are correlative with chemically and lithologically similar lava flows that underlie Jordan Butte, ~4 km (2.5 mi) southwest of the map area (Sherrod and Scott, 1995). Roadcuts and outcrops of unit **Tmdj** are characterized by blocky

meter-scale columns or intervals of platy jointing (**Figure 6-41**); unit **Tmdj** generally weathers to rounded boulders up to 1 m (3.3 ft) across. Thickness of the unit **Tmdj** in the map area is >25 m (82 ft). Typical hand samples of the andesite and dacite are light gray (N7) to medium light gray (N4), containing ~3 to 5 percent (vol.), clear to chalky light gray (N7), prismatic to blocky, seriate plagioclase microphenocrysts and phenocrysts up to 1 cm (0.4 in) long, ~1 percent (vol.) fresh black (N1), subhedral to anhedral, prismatic- to lath-shaped, seriate orthopyroxene and clinopyroxene microphenocrysts and phenocrysts (orthopyroxene > clinopyroxene) <2 mm (0.1 in) in length, and sparse microglomerocrysts of plagioclase, pyroxene, glass, and Fe-Ti oxides <1 mm (0.1 in) across, contained within a hypohyaline groundmass (**Figure 6-42c,d**).

Unit **Tmdj** has normal magnetic polarity and is assigned a late Miocene age on the basis of stratigraphic position (**Figure 6-1**). Bunker and others (1982) reported a K-Ar age of 5.28 ± 0.5 Ma (whole rock; sample 109-WB) for andesite lava flows exposed along USFS Road 27 and Jordan Creek (south of the map area, 5.3 km [3.3 mi] east of Jordan Butte). Sherrod and Scott (1995) interpreted this outcrop to be correlative with lithologically similar lava flows exposed at nearby Jordan Butte. However, the isotopically dated andesite lava flows exposed along Jordan Creek are chemically dissimilar from the dacite lava flows that form the main mass of Jordan Butte (J.D McClaughry unpublished geologic mapping, 2016). Geochemical sampling and mapping along USFS Road 27, north of Jordan Creek, indicates that dacite lava flows chemically identical to the main part of Jordan Butte stratigraphically overlie isotopically dated andesite exposed just to the south. Therefore, the dacite of Jordan Butte, as defined here, is likely younger than 5.28 Ma.

**Figure 6-41. Dacite of Jordan Butte (Tmdj) in Owl Quarry, just southwest of the map area along USFS Road 2730 (45.359292, -121.380478). Hammer for scale is 38 cm (15 in) long. View is looking north. Photo credit: J.D. McClaughry, 2015.**

**Figure 6-42. Hand sample and thin section photographs of the dacite of Jordan Butte (Tmdj). (a) Typical hand sample. Scale bar is 2.5 cm (1 in) tall. (b) Thin section under cross-polarized light (XPL). (c) Same view as in B under plane-polarized light (PPL). Scale bar for thin section photographs is 7 mm (0.3 in) wide. Photo credits: J.D. McClaughry, 2016.**

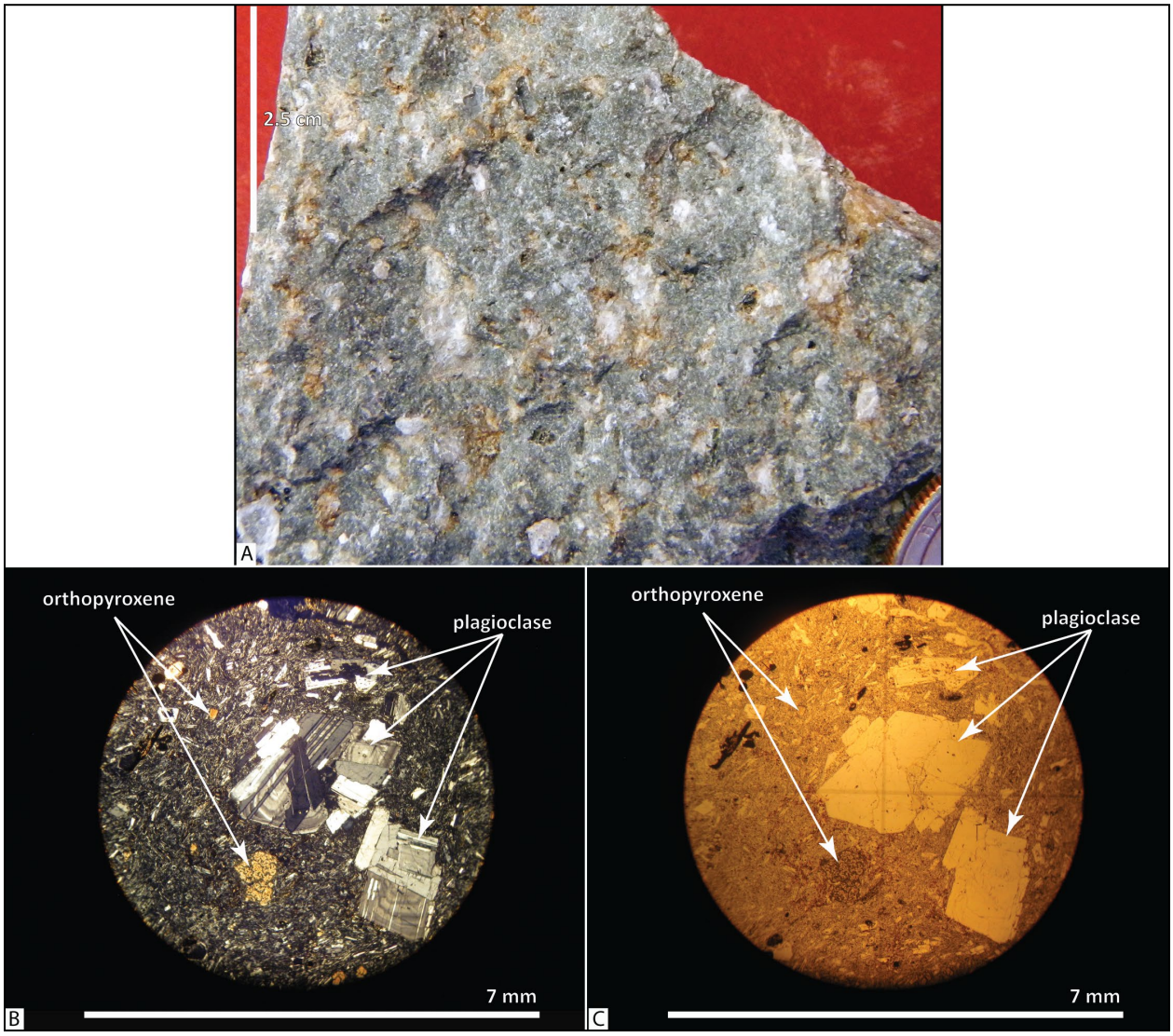


**Tmdv** **dacite of Fivemile Butte, lower flows and domes (upper Miocene)—**Sequence of dacite lava flows and/or domes ($SiO_2$ = 62.78 to 64.70 weight percent; 1.17 to 1.48 weight percent $K_2O$, *n* = 15 analyses, [15 outside map area]) mapped on top of the narrow ridge between Eightmile Creek and Hesslan Canyon in the western part of the map area (**Figure 6-43**; **Table 6-3**; Plate 1; Appendix). Outcrops of the dacite (**Tmdv**) are mapped west ~12 km (7.5 mi) to areas underlying Fivemile Butte, Perry Point, and the headwaters of Dog River in the Fivemile Butte and Dog River 7.5′ quadrangles (McClaughry and others, 2020a; J.D. McClaughry unpublished geologic mapping, 2016). Roadcuts and outcrops are characterized by a massive, rounded form, by broad blocky meter-scale columns, or intervals of vertical platy jointing (**Figure 6-43**). Unit **Tmdv** weathers to meter-scale, subrounded boulders and angular plates, forming extensive talus slopes beneath cliffs. Thickness of unit **Tmdv** in the map area is ~40 m (131 ft) (Plate 1). Typical hand samples of

the dacite are medium gray (N5) to medium dark gray (N4), containing ~3 to 5 percent (vol.), clear to chalky light gray (N7), euhedral, prismatic to blocky, seriate plagioclase microphenocrysts and phenocrysts ≤1 cm (0.4 in) long and ≤1 percent (vol.) fresh grayish black (N2) pyroxene microphenocrysts and phenocrysts ≤2 mm (0.1 in) (orthopyroxene ≥ clinopyroxene), distributed within a very fine-grained holocrystalline to hypocrystalline groundmass.

The dacite (**Tmdv**) has both normal and reversed magnetic polarity outcrops. Unit **Tmdv** is assigned a late Miocene age on the basis of stratigraphic position and a K-Ar age of 7.71 ± 0.17 Ma (plagioclase; sample RC S88-23) obtained by Gray and others (1996) for an outcrop in the saddle between Perry Point and Fivemile Butte (west of map area) (**Figure 6-1**). The dacite of Fivemile Butte (**Tmdv**) is interpreted to be younger than the dacite of Wolf Run (**Tmdw**) on the basis of isotopic ages; no outcrops exposing the contact between the two units are known in the map area or adjacent Fivemile Butte 7.5′ quadrangle (J.D. McClaughry unpublished geologic mapping, 2016).

**Figure 6-43. Dacite of Fivemile Butte (Tmdv) exposed north of Hesslan Canyon along USFS Road 4460 in the west part of the map area (45.420712, -121.375165). View is looking northwest. Photo credit: J.D. McClaughry, 2015.**

**Figure 6-44. Hand sample and thin section photographs of the dacite of Fivemile Butte (Tmdv). (a) Typical abundantly plagioclase porphyritic hand sample. Scale bar is 2.5 cm (1 in) tall. (b) Thin section under cross-polarized light (XPL). (c) Same view as in B under plane-polarized light (PPL). Scale bar for thin section photographs is 7 mm (0.3 in) wide. Photo credit: J.D. McClaughry, 2016.**

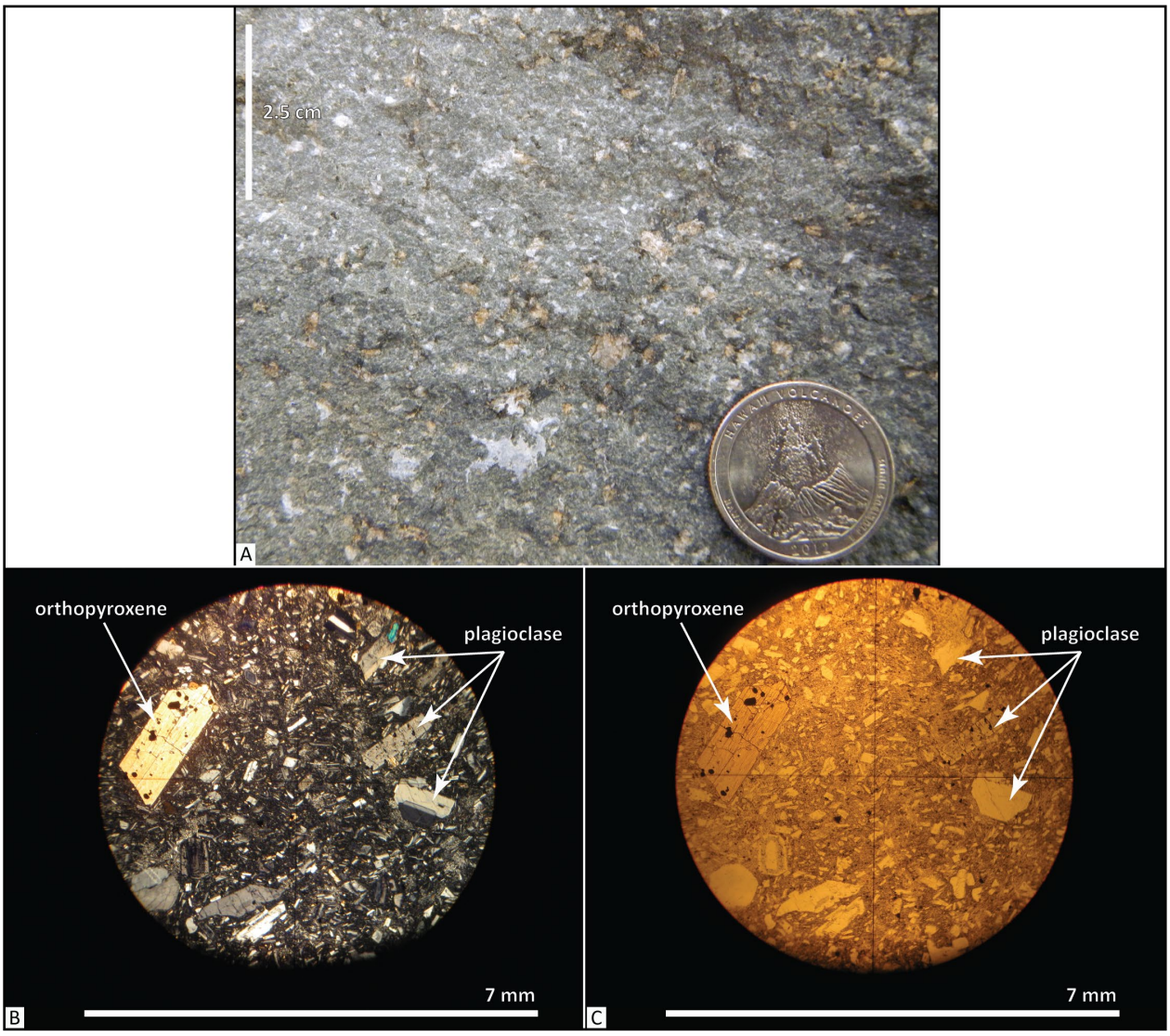

**Tmdw** **dacite of Wolf Run (upper Miocene)—**Dacite lava flow ($SiO_2$ = 63.49 to 65.11 weight percent; $K_2O$ = 2.76 to 2.96, *n* = 13 analyses [8 outside map area]) mapped capping a northeast-trending ridge between Wolf Run and Eightmile Creek in the northwest part of the map area (**Figure 6-45**, **Figure 6-46**; Table 6-3; Plates 1 and 2; Appendix). Unit **Tmdw** has a unique chemical composition for a lava flow of Dalles Formation age with relatively higher potassium ($K_2O$ >2.5 weight percent) and higher amounts of niobium (Nb = 15.7 to 17.6 ppm) and zirconium (Zr = 319 to 341 ppm) (**Table 6-3**; Appendix). The chemically distinct lava flow forms an important stratigraphic marker in the Middle Columbia Basin, reaching ~24 km (15 mi) eastward from the headwaters of Eightmile Creek in the eastern escarpment of the Hood River graben to the intersection of Eightmile Creek and Wolf Run as a topographically inverted intracanyon lava flow overlying volcaniclastic rocks in the Dalles Formation (**Tmdl**) (Plates 1 and 2; McClaughry and others, 2020a). A vent area for the lava flow has not been determined and no outcrops of the unit are known west of the single mapped exposure in the East Fork Hood River area (McClaughry and others, 2020a). Unit **Tmdw** forms prominent cliff-forming exposures marked by meter-scale columnar-jointing (**Figure 6-45a**); outcrops weather to subrounded boulders, forming extensive talus slopes beneath cliff-forming outcrops (**Figure 6-45b,c**). Vesicles are commonly lined by masses of white to pink zeolite minerals. Thickness of unit **Tmdw** between Wolf Run and Eightmile Creek is ~70 m (230 ft). Typical hand samples of the dacite are medium gray (N5) to medium dark gray (N4), containing 20 to 30 percent (vol.) clear to chalky white (N9), subhedral to anhedral, prismatic to blocky, seriate plagioclase microphenocrysts and phenocrysts ≤5 mm (0.2 in), ≤1 percent (vol.) grayish black (N2), euhedral to subhedral, prismatic pyroxene microphenocrysts and phenocrysts ≤2 mm (0.1 in) (orthopyroxene ≥ clinopyroxene), and <1 percent (vol.) plagioclase-pyroxene glomerocrysts ≤3 mm (0.1 in), contained within a very fine-grained holocrystalline to hypocrystalline groundmass (**Figure 6-47**).

Unit **Tmdw** has normal magnetic polarity and is assigned a late Miocene age on the basis of stratigraphic position and an $^{40}Ar/^{39}Ar$ age plateau age of 7.91 ± 0.08 Ma (plagioclase; sample 291 DFWJ 14) for a sample collected from outcrops at the intersection of Wolf Run and Eightmile Creek (**Table 5-1**, **Figure 6-1**; Appendix; Plate 2). Bunker and others (1982) and Bela (1982) report a comparable, but less precise K-Ar age of 8.2 ± 0.8 Ma (whole rock; sample 103-WB) collected from this unit a short distance southwest of Camp Baldwin (west of map area; J.D. McClaughry unpublished geologic mapping, 2016).

**Figure 6-45. Dacite of Wolf Run (Tmdw). (a) Ridge-capping intracanyon flow of the dacite of Wolf Run (Tmdw) inset into Dalles Formation (Tmdl) sedimentary strata between Wolf Run and Eightmile Creek. View is looking west toward Mount Hood (45.473448, -121.175467). The letter X (45.456121, -121.243660) marks the location of sample 291 DFWJ 14, which has an $^{40}Ar/^{39}Ar$ age plateau age of 7.91 ± 0.08 Ma. Photo credit: J.D. McClaughry, 2014.**

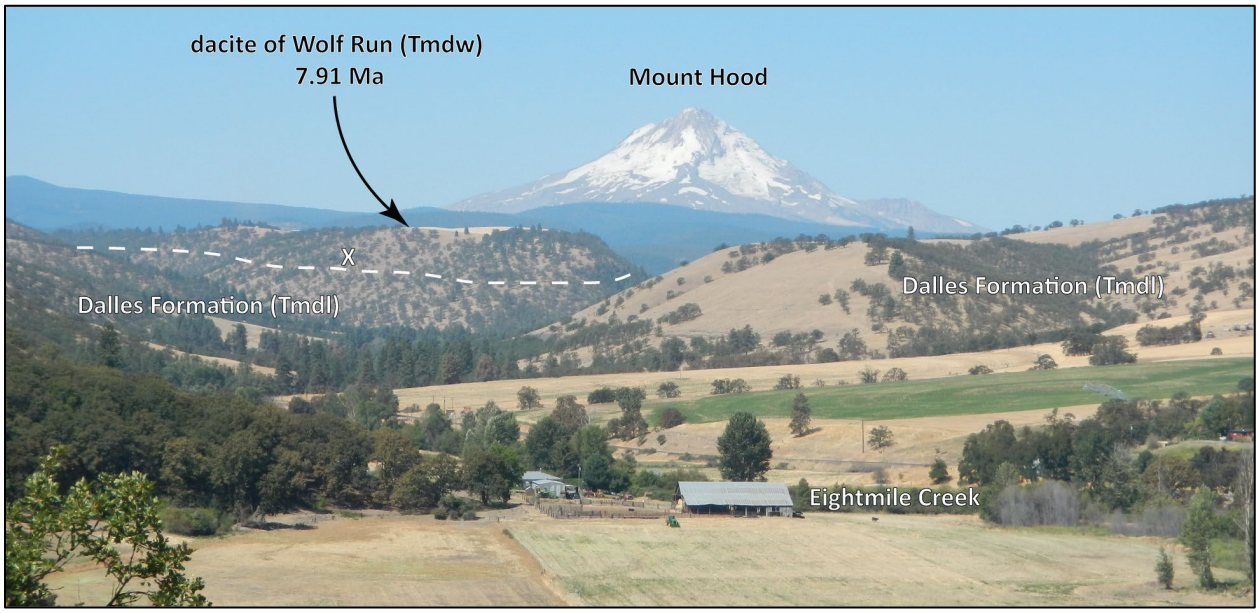

**Figure 6-46. Blocky, columnar-jointed dacite of Wolf Run (Tmdw) exposed along Wolf Run Road in the west-central part of the map area (45.437949, -121.284151). Arrow points to hammer for scale, which is 38 cm (15 in) long. View is looking north. Photo credit: J.D. McClaughry, 2015.**

**Figure 6-47. Hand sample and thin section photographs of the dacite of Wolf Run (Tmdw). (a) Typical abundantly plagioclase porphyritic hand sample. Scale bar is 2.5 cm (1 in) wide. (b) Thin section under cross-polarized light (XPL). (c) Same view as in B under plane-polarized light (PPL). Scale bar for thin section photographs is 7 mm (0.3 in) wide. Photo credit: J.D. McClaughry, 2015.**

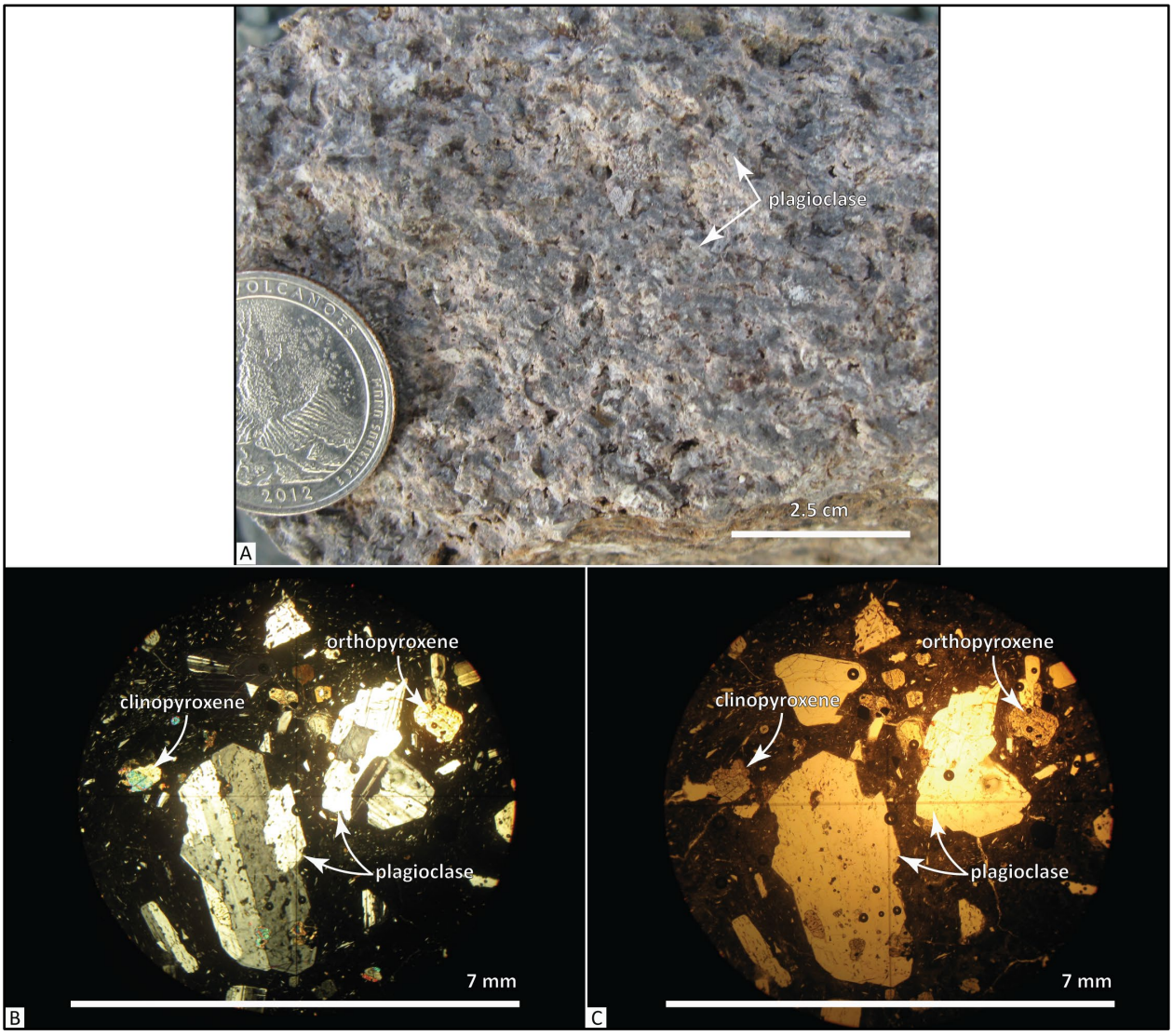


**Tmdt** **tuff of Rail Hollow (upper Miocene)—**Non-welded andesite to dacite tuff ($SiO_2$ = 61.53 to 65.79 weight percent; $K_2O$ = 0.89 to 1.82 weight percent; Zr = 127 to 193 ppm; Nb = 6.9 to 19.1 ppm; *n* = 14 analyses) mapped above the tuff breccia of Fifteenmile Creek (**Tmdd**) between Fifteenmile and Larch Creeks in the southwest part of the Dufur area (**Figure 6-48**; **Table 6-3**; Plates 1 and 2; Appendix). Exposures are limited to roadcuts, roadbeds, and excavations, where the tuff is characterized by indistinct bedding or irregular columnar jointing (**Figure 6-48**). Unit **Tmdt** is typically crystal-ash dominated but contains areas of concentrated pumices with subrounded pumices up to 5 cm (2 in) across (**Figure 6-49**). The unit commonly weathers to a surface scattered with meter-scale boulders. Tuff in the upper parts of unit **Tmdt** may be reworked. Typical hand samples of the tuff are yellowish gray (5Y 7/2) to very light gray (N8), light gray

(N7), and medium light gray (N6), containing ~2 to 5 percent rounded to flattened, white (N9) to very light gray (N8) pumices, ~2 percent subrounded, light gray (N7) dacite lithic fragments, ~25 to 35 percent (vol.), clear, euhedral to anhedral and broken, prismatic to blocky, seriate plagioclase microphenocrysts and phenocrysts up to 4 mm (0.2 in), ~2 percent (vol.) moderate brown (5YR 3/4) euhedral to anhedral, prismatic- to lath-shaped and broken hornblende phenocrysts up to 2 mm (0.1 in), and ~1 to 2 percent (vol.) euhedral to anhedral, prismatic- to lath-shaped and broken, moderate olive brown (5Y 4/4) orthopyroxene and clinopyroxene (orthopyroxene > clinopyroxene) microphenocrysts ≤1 mm (0.04 in), contained within a groundmass of devitrified ash (**Figure 6-50**).

Unit **Tmdt** has normal magnetic polarity and is assigned a late Miocene age on the basis of stratigraphic position and an $^{40}Ar/^{39}Ar$ plateau age of 8.07 ± 0.10 Ma (hornblende; sample 29 DFWJ 14) for a sample collected from outcrops along Rail Hollow Road (**Table 5-1**, **Figure 6-1**; Plate 2; Appendix).

**Figure 6-48. Non-welded, plagioclase- and hornblende-phyric crystal-ash tuff (Tmdt) exposed along Rail Hollow (45.399969, -121.245288). The iPad for scale is 25 cm (9.8 in) tall. A sample from this outcrop has an $^{40}Ar/^{39}Ar$ plateau age of 8.07 ± 0.10 Ma. View is looking north. Photo credit: J.D. McClaughry, 2014.**

**Figure 6-49. Block of non-welded pumice tuff (Tmdt) excavated along Rail Hollow Road in the eastern part of the map area (45.381763, -121.252999). Hammer is 40 cm (15.7 in) tall. Photo credit: C.A. Niewendorp, 2015.**

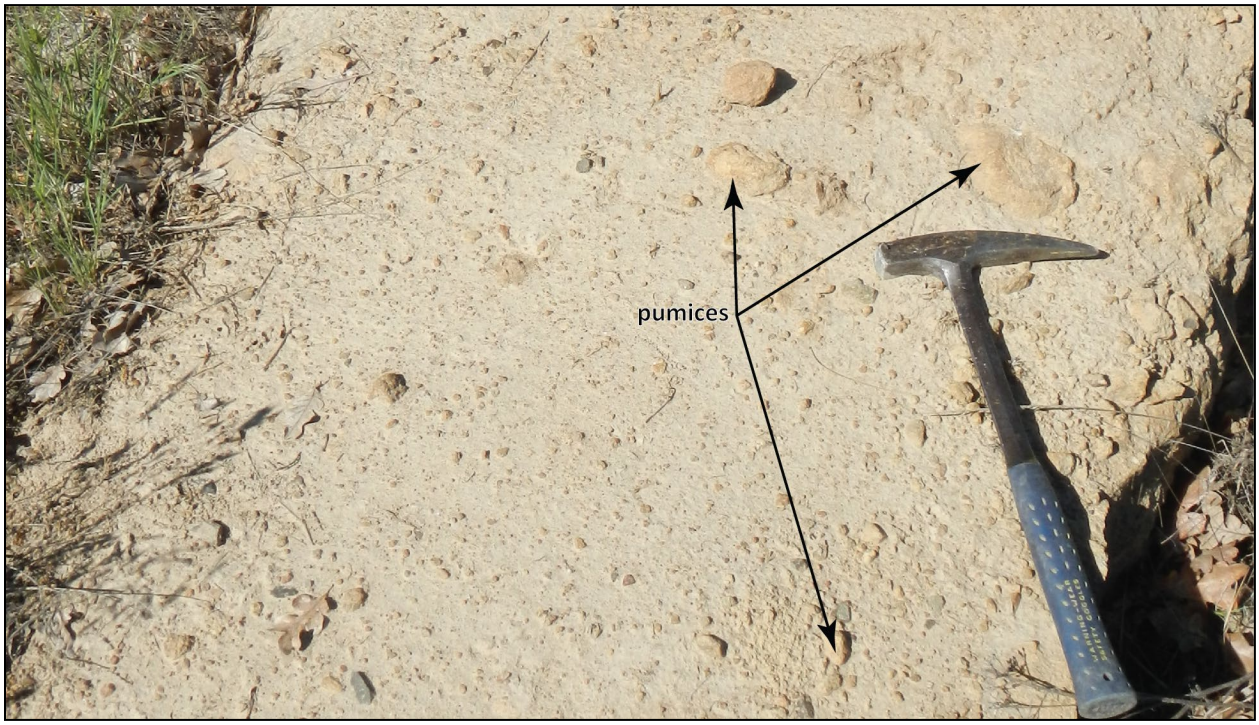

**Figure 6-50. Hand sample and thin section photographs of the tuff of Rail Hollow (Tmdt). (a) Typical abundantly plagioclase- and hornblende-porphyritic hand sample. Scale bar is 2.5 cm (1 in) tall. (b) Thin section under cross-polarized light (XPL). (c) Same view as in B under plane-polarized light (PPL). Scale bar for thin section photographs is 7 mm (0.3 in) wide. Photo credits: J.D. McClaughry, 2015.**

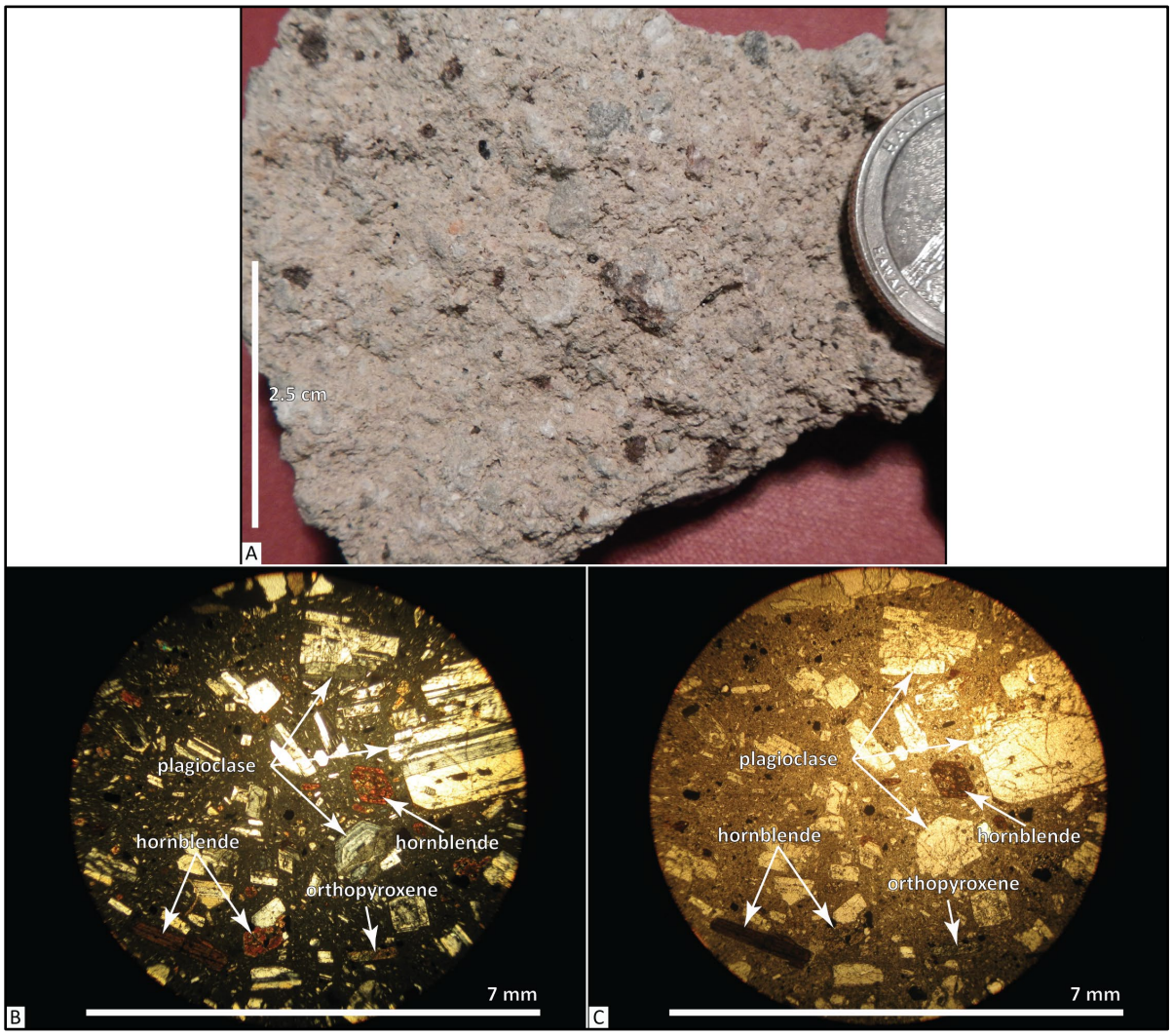

**Tmdd** **tuff breccia of Fifteenmile Creek (upper Miocene)—**Matrix- to clast-supported, cliff-forming boulder breccia exposed along Fifteenmile Creek between the west edge of the map area and the city of Dufur (**Figure 6-51**, **Figure 6-52**; Plates 1 and 2). Breccia beds are typically massively bedded, very poorly sorted, and matrix supported, with localized clast-supported areas. Clasts are typically angular to subrounded, dense to pumiceous, accounting for 50 to 60 percent (vol.) of the deposit. Maximum observed clast size is ~ 2.0 m (6.6 ft); average size of the largest observed clasts at all outcrops is ~1.2 m (3.9 ft). Unit **Tmdd** typically contains a texturally similar, but chemically diverse assemblage unaltered, very light gray (N8) to medium dark gray (N4) and grayish orange-pink (5YR 7/2) hornblende-porphyritic andesite and dacite ($SiO_2$ = 61.72 to 67.35 weight percent; $K_2O$ = 1.39 to 2.22 weight percent; Nb = 8.3 to 10.5 ppm; Zr = 137 to 211 ppm; *n* = 12 analyses) (**Table 6-3**; Appendix). Typical hand samples of unit **Tmdd** clasts contain ~10 to 25 percent (vol.) clear euhedral to anhedral, prismatic to blocky, seriate plagioclase microphenocrysts and phenocrysts up to 6 mm (0.2 in) in length, ~5 to 10 percent (vol.) dark reddish brown (10R 3/4) euhedral to anhedral, prismatic- to lath-shaped, seriate hornblende microphenocrysts and phenocrysts up to 7 mm (0.3 in), and 1 to 3 percent (vol.) dark gray (N2) pyroxene microphenocrysts and phenocrysts up to 2 mm (0.1 in) (orthopyroxene > clinopyroxene), distributed within a fine- to medium-grained hypocrystalline groundmass (**Figure 6-53**). Clasts are typically enclosed by a very light gray (N8) to grayish orange pink (5YR 7/2), poorly sorted, coarse-grained tuffaceous sandstone matrix composed of angular to subrounded, very light gray (N8) to medium dark gray (N4), and grayish orange-pink (5YR 7/2) porphyritic dacite lithics and plagioclase grains. The matrix component typically accounts for 40 to 50 percent (vol) of the deposit.

Unit **Tmdd** is assigned a late Miocene age on the basis of stratigraphic position and an $^{40}Ar/^{39}Ar$ plateau age of 8.75 ± 0.05 Ma (hornblende; sample 212 DFWJ 14) determined for a sample from a single boulder clast collected from outcrops at the Henderson Pioneer Cemetery **Table 5-1**, **Figure 6-1**; Plate 2; Appendix). Along Fifteenmile Creek, in the Wolf Run 7.5′ quadrangle, the unit directly underlies lahar deposits (**Tmdl**) containing a clast with a reported K-Ar age of 7.74 ± 0.16 Ma (plagioclase; sample S88-24; Gray and others, 1996) (**Table 5-1**; Plate 1; Appendix).

**Figure 6-51. Tuff breccia of Fifteenmile Creek (Tmdd) exposed at the mouth of Henderson Hollow (45.436822, -121.175752). A single boulder collected from this outcrop returned an $^{40}Ar/^{39}Ar$ plateau age of 8.75 ± 0.05 Ma. Arrow points to hammer for scale, which is 38 cm (15 in) long; person at the right of the photograph is 1.6 m (5.2 ft) tall. View is looking north. Photo credit: J.D. McClaughry, 2014.**

**Figure 6-52. Tuff breccia of Fifteenmile Creek (Tmdd) exposed on the north side of Fifteenmile Creek canyon, in the southwest part of the map area (45.387535, -121.336587). View is looking north. Photo credit: J.D. McClaughry, 2015.**

**Figure 6-53. Hand sample and thin section photographs of the tuff breccia of Fifteenmile Creek (Tmdd). (a) Typical abundantly plagioclase- and hornblende-porphyritic hand sample. Scale bar is 2.5 cm (1 in) tall. (b) Thin section under cross-polarized light (XPL). (c) Same view as in B under plane-polarized light (PPL). Scale bar for thin section photographs is 7 mm (0.3 in) wide. Photo credits: J.D. McClaughry, 2015.**

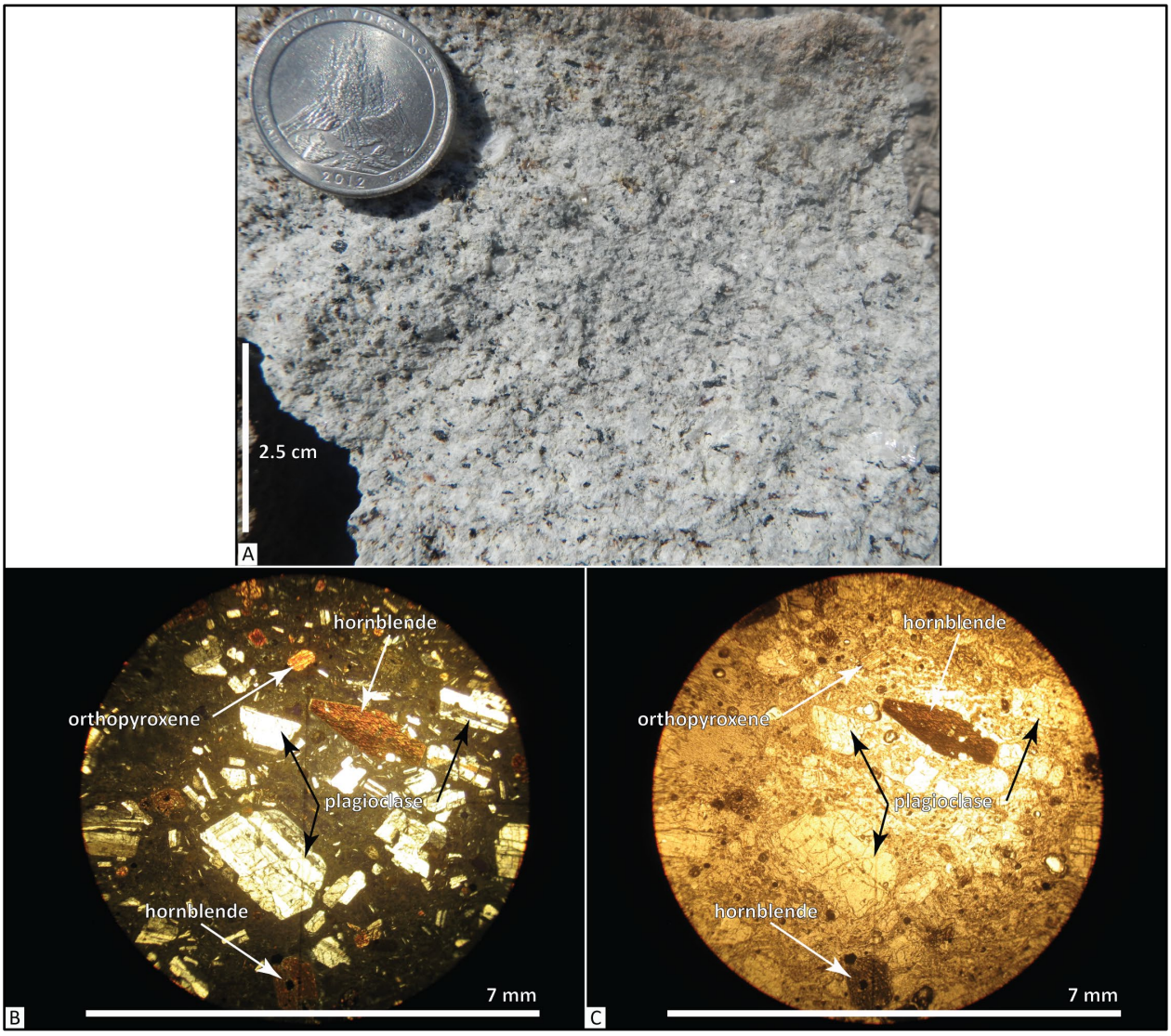


**Tmdtp** **pumice tuff (upper Miocene)—**Non-welded andesite to dacite pumice tuff ($SiO_2$ = 60.11 to 64.14 weight percent; $K_2O$ = 1.29 to 1.58 weight percent; Zr = 156 to 221 ppm; Nb = 8.4 to 10.8 ppm; *n* = 6 analyses) discontinuously exposed beneath the tuff breccia of Fifteenmile Creek (**Tmdd**) along Rail Hollow and Fifteenmile Creek in the central part of the map area (**Figure 6-54**; Plates 1 and 2). Exposures are typically limited to roadcuts, roadbeds, and small excavations (**Figure 6-54a**). Typical hand samples of the tuff are very pale orange (10YR 8/2) to pale yellowish brown (10YR 6/2) and pinkish gray (5YR 8/1) with abundant subrounded, white (N9) to very light gray (N8), hornblende-phyric pumices up to 5 cm (1.2 in), contained within a semi-consolidated ash groundmass (**Figure 6-54b**). Pumices are characteristically porphyritic, containing 2 to 3 percent (vol.) blocky to prismatic, dark reddish brown (10R 3/4) hornblende and clear plagioclase phenocrysts up to 2 mm (0.1in).

The tuff is assigned a late Miocene age on the basis of stratigraphic position beneath the ≤8.75 Ma tuff breccia of Fifteenmile Creek (**Tmdd**) and above the ~15.9 Ma Basalt of Sentinel Gap (**Twfs**) (**Figure 6-1**).

**Figure 6-54. Non-welded pumice tuff (Tmdtp). (a) Unit Tmdtp is discontinuously exposed beneath tuff breccia of Fifteenmile Creek (Tmdd) and above the Basalt of Sentinel Gap (Twfs), along Rail Hollow Road (45.410964, -121.204928). Arrow points to hammer for scale, which is 38 cm (15 in) tall. View is looking northeast. (b) Typical hand samples of the tuff are very pale orange (10YR 8/2) to pale yellowish brown (10YR 6/2) and pinkish gray (5YR 8/1) with abundant subrounded, white (N9) to very light gray (N8), hornblende-phyric pumices up to 5 cm (1.2 in) across. Scale bar is 2 cm (1 in) tall. Photo credits: J.D. McClaughry, 2014.**

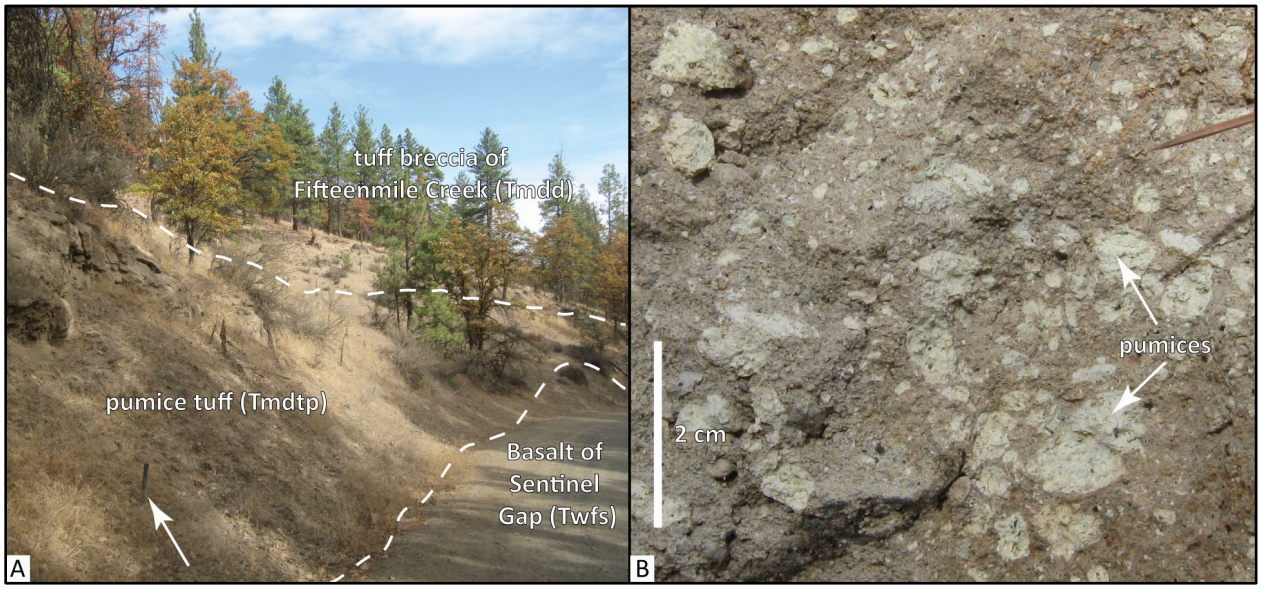


**Tmdx** **heterolithologic andesite- and dacite-clast breccia (upper Miocene)—**Heterolithologic cobble-boulder breccia mapped on both the north and south sides of Eightmile Creek between the mouth of Wolf Run on the west and Endersby on the east (**Figure 6-55**; Plate 1). The breccia typically crops out as precipitous cliffs, characterized by vertical joint sets and hoodoo-style weathering (**Figure 6-55a**). Many slopes underlain by the breccia weather to fields of subrounded boulders and coarse-grained, sandy to rocky soils (**Figure 6-55b**). Thickness of unit **Tmdx** ranges between 15 and 40 m (49 and 131 ft). Breccia beds are typically massive, very poorly sorted, and matrix-supported, with localized clast-supported domains. Interbedded channel-forms of planar stratified sandstone occur locally. Clasts are typically subrounded, black (N1), medium dark gray (N4), very light gray (N8), to grayish orange pink (5YR 7/2), aphyric to porphyritic andesite and dacite making up 50 to 60 percent (vol.) of the deposit. Maximum observed clast size is ~1.5 m (4.9 ft); average size of the largest observed clasts at all outcrops is ~1.0 m (3.3 ft). Clasts are typically enclosed by a very light gray (N8) to grayish orange pink (5YR 7/2), poorly sorted, coarse-grained sandstone composed of angular to subrounded, very light gray (N8) to medium dark gray (N4) and grayish orange pink (5YR 7/2) aphyric to porphyritic andesite and dacite lithics, pumice, and plagioclase grains. The matrix component typically accounts for 40 to 50 percent (vol) of the deposit.

The unit is assigned a late Miocene age on the basis of stratigraphic position near the base of the Dalles Formation (**Figure 6-1**).

**Figure 6-55. Heterolithologic andesite- and dacite-clast boulder breccia (Tmdx). (a) Cliff-forming breccia (Tmdx) mapped along Eightmile Creek, in the northern part of the map area (45.474198, -121.179821). View is looking southwest. (b) Massively bedded, very poorly sorted, matrix- to clast-supported, heterolithologic andesite- and dacite-clast boulder breccia (Tmdx) exposed near Endersby, in the northeastern part of the map area (45.486859, -121.138396). Fence post in the foreground is about 1 m (3.3 ft) tall. View is looking north. Photo credits: J.D. McClaughry, 2014.**

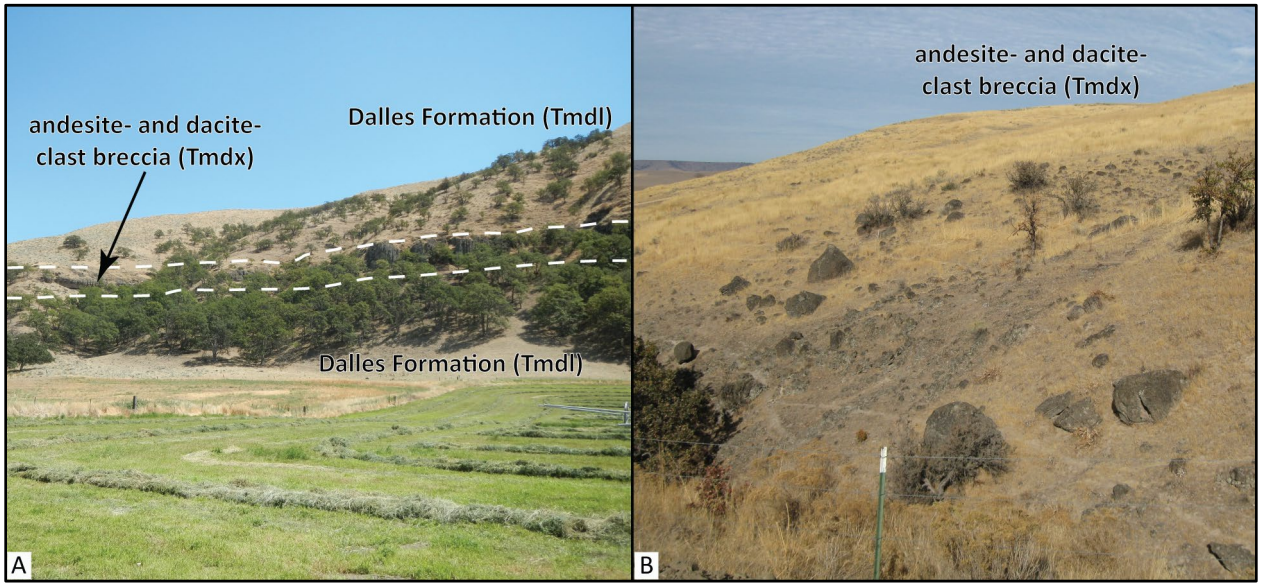


**Angular unconformity to disconformity**

## 6.3.4 Middle and Lower Miocene volcanic and sedimentary rocks

### 6.3.4.1 Columbia River Basalt Group

### 6.3.4.2 Wanapum Basalt

The Wanapum Basalt in the Dufur area consists of lava flows assigned to the Priest Rapids and Frenchman Springs members. Effusion of the Wanapum Basalt produced over 12,175 km$^3$ (2,920 mi$^3$) of lava flows that covered an area exceeding 87,400 km$^2$ (33,745 mi$^2$) (Rediel and others, 2013). Composite thickness of the Wanapum Basalt in the map area is ≤174 m (571 ft) (Plates 1, 2, and 3).

### 6.3.4.3 Priest Rapids Member

The Priest Rapids Member forms the upper part of the Wanapum Basalt in the Dufur area, unconformably overlying the Frenchman Springs Member (Plate 3). The Priest Rapids member consists of two flows assigned to the Lolo and Rosalia chemical types, which are differentiated on the basis of lithology and geochemistry (**Figure 5-7**; **Figure 6-56**; Wright and others, 1973; Camp, 1981; Anderson, 1987; Anderson and Vogt, 1987). Priest Rapids lava flows are distinguished from other CRBG units by their

relatively high concentrations of magnesium, titanium ($TiO_2$ > 3.50 weight percent), iron, and phosphorous (**Table 6-4**; Appendix). Lava flows in the Priest Rapids Member also have reversed magnetic polarity, which serves to distinguish these flows from adjacent units (Swanson and others, 1979b). The Priest Rapids Member was erupted at ~15.9 Ma (Kasbohm and Schoene, 2018) from linear dike systems in the Clearwater Embayment of western Idaho and flowed west (Camp, 1981), covering most of the north and central parts of the Columbia Plateau. These flows were largely confined as intracanyon flows as they traversed the area of the present-day Cascade Range (Anderson and Vogt, 1987) (**Figure 5-6**). Effusion of the Priest Rapids Member produced over 2,800 $km^3$ (672 $mi^3$) of lava that covered an area exceeding 57,300 $km^2$ (22,123 $mi^2$) (Swanson and others, 1979b, Camp, 1981; Tolan and others, 1989). The maximum thickness of the Priest Rapids Member in the Dufur area is ~11 m (36 ft) (Plate 3).

**Twpr** **Basalt of Rosalia (middle Miocene)**—High-titanium, aphyric to sparsely plagioclase-phyric basalt ($SiO_2$ = 51.28 weight percent; $TiO_2$ = 3.77 weight percent; *n* = 1 analysis), poorly exposed above the Basalt of Sentinel Gap (**Twfs**) in the uplands between Dry Creek and Jameson Canyon, northeast of the city of Dufur (**Figure 5-7**; **Table 6-4**; Plate 3; Appendix). The Basalt of Rosalia (**Twpr**) is distinguished from older lava flows in the Frenchman Springs Member on the basis of reversed magnetic polarity and relatively higher amounts of titanium (avg $TiO_2$ = 3.74 weight percent) and phosphorous (avg $P_2O_5$ = 0.81 weight percent) and lesser amounts of chromium (avg Cr = 5 ppm) (*n* = 33 analyses in Middle Columbia Basin; **Figure 5-10**; Madin and McClaughry, 2019; McClaughry and others, 2020a; J.D. McClaughry unpublished geologic mapping). The Basalt of Rosalia (**Twpr**) crops out as indistinct ledges characterized by blocky columns ≤2 m (6.5 ft) across and vertical platy joint sets. North of the map area, unit **Twpr** is commonly marked by the presence of pillow lava enclosed in a palagonite matrix. Maximum thickness of unit **Twpr** in the map area is 11 m (35 ft) on the east side of Dry Canyon. Unit **Twpr** flows thin and pinch out ~1 km (0.6 mi) south of the northern boundary of the Dufur East 7.5′ quadrangle (Plate 3); the unit thickens to the north toward The Dalles and Biggs, where composite flow thickness ranges between ~25 and 30 m (80 to 100 ft) (Madin and McClaughry, 2019). Typical hand samples of the basalt are generally aphyric, but Anderson (1987) reported that yellow-colored plagioclase phenocrysts and glomerocrysts 3 mm to 1 cm across (0.1 to 0.4 in) are sparsely distributed throughout the unit elsewhere. The groundmass is fine to medium grained with equant to acicular plagioclase and equant olivine microphenocrysts.

The Basalt of Rosalia (**Twpr**) has reversed magnetic polarity. Unit (**Twpr**) is assigned a middle Miocene age on the basis of U/Pb dating of an ash between the Basalt of Rosalia and the Basalt of Lolo, which provided an age of 15.895 ± 0.019 Ma (Kasbohm and Schoene, 2018; **Figure 5-7**, **Figure 6-1**). Equivalent to the Rosalia chemical type of Wright and others (1973).

**Table 6-4. Representative XRF analyses for the CRBG in the Dufur area (part 1 of 2).**

| Sample | 122 DFWJ 15 | 132 WRCN 15 | 141a DFWJ 14 | 103b DFWJ 14 | 112 WRCN 15 | 369 DFWJ 14 | 367 DFWJ 14 | 366 DFWJ 14 | 365 DFWJ 14 | 103a DFWJ 14 |
|---|---|---|---|---|---|---|---|---|---|---|
| **Geographic Area** | Fax Road | Fifteenmile Creek | Dufur | Fifteenmile Creek | Fifteenmile Creek | Pine Creek | Pine Creek | Pine Creek | Pine Creek | Fifteenmile Creek |
| **Formation** | Wanapum Basalt | Wanapum Basalt | Wanapum Basalt | Wanapum Basalt | Wanapum Basalt | Wanapum Basalt | Wanapum Basalt | Wanapum Basalt | Wanapum Basalt | Wanapum Basalt |
| **Map Unit** | Twpr | Twfs | Twfs | Twfs | Twfh | Twfh | Twfh | Twfh | Twfh | Twfh |
| **UTM N (NAD 83)** | 5040327 | 5027060 | 5033740 | 5036220 | 5027780 | 5031195 | 5031139 | 5031055 | 5031012 | 5036197 |
| **UTM E (NAD 83)** | 654265 | 630617 | 646229 | 648347 | 633172 | 645017 | 645071 | 645063 | 645098 | 648326 |
| **Age (Ma)** | na | na | na | na | na | na | na | na | na | na |
| **Plate** | outside map | 1 | 1 | 3 | 1 | 2 | 2 | 2 | 2 | 3 |
| **Map Label** | na | G38 | G121 | DE102 | G141 | G94 | G92 | G90 | G88 | DE101 |
| ***Oxides, weight percent*** | | | | | | | | | | |
| **$SiO_2$** | 51.28 | 51.48 | 49.69 | 51.91 | 51.59 | 49.14 | 50.98 | 51.59 | 51.46 | 51.91 |
| **$Al_2O_3$** | 13.39 | 13.07 | 15.48 | 13.16 | 13.46 | 13.23 | 13.63 | 13.45 | 13.35 | 13.72 |
| **$TiO_2$** | 3.78 | 3.08 | 3.65 | 3.11 | 2.88 | 2.92 | 3.07 | 2.95 | 2.89 | 3.03 |
| **FeO*** | 14.33 | 14.91 | 15.03 | 14.16 | 14.12 | 14.37 | 14.49 | 14.18 | 14.47 | 13.54 |
| **MnO** | 0.21 | 0.22 | 0.21 | 0.22 | 0.22 | 0.41 | 0.22 | 0.21 | 0.23 | 0.21 |
| **CaO** | 8.80 | 8.02 | 8.34 | 8.18 | 8.23 | 11.17 | 8.61 | 8.70 | 8.38 | 9.30 |
| **MgO** | 3.52 | 4.30 | 3.08 | 4.26 | 4.55 | 4.23 | 4.42 | 4.46 | 4.56 | 3.56 |
| **$K_2O$** | 1.21 | 1.36 | 0.68 | 1.46 | 1.28 | 1.23 | 1.22 | 1.26 | 1.29 | 1.29 |
| **$Na_2O$** | 2.67 | 2.96 | 3.14 | 2.91 | 3.10 | 2.77 | 2.82 | 2.63 | 2.81 | 2.88 |
| **$P_2O_5$** | 0.81 | 0.60 | 0.71 | 0.62 | 0.56 | 0.53 | 0.55 | 0.57 | 0.55 | 0.56 |
| **LOI** | nd | 0.36 | nd | 0.00 | 1.57 | nd | nd | nd | nd | nd |
| **Total_I** | 96.50 | 98.58 | 95.69 | 99.86 | 97.67 | 96.44 | 98.96 | 96.43 | 98.66 | 97.40 |
| ***Trace Elements, parts per million*** | | | | | | | | | | |
| **Ni** | 17 | 19 | 16 | 16 | 25 | 19 | 19 | 18 | 19 | 19 |
| **Cr** | 6 | 15 | 19 | 16 | 37 | 36 | 39 | 40 | 39 | 41 |
| **Sc** | 39 | 36 | 41 | 37 | 37 | 35 | 38 | 35 | 38 | 38 |
| **V** | 426 | 440 | 437 | 439 | 406 | 403 | 442 | 408 | 404 | 424 |
| **Ba** | 705 | 604 | 701 | 598 | 563 | 580 | 572 | 504 | 553 | 531 |
| **Rb** | 35 | 36 | 9 | 39 | 33 | 26 | 30 | 30 | 30 | 32 |
| **Sr** | 315 | 306 | 361 | 314 | 311 | 329 | 328 | 321 | 320 | 335 |
| **Zr** | 223 | 199 | 235 | 213 | 182 | 162 | 174 | 176 | 181 | 185 |
| **Y** | 53 | 44 | 46 | 45 | 40 | 36 | 41 | 40 | 41 | 39 |
| **Nb** | 17.2 | 14.4 | 17.9 | 16.4 | 13.7 | 12.7 | 14.2 | 13.0 | 13.9 | 14.0 |
| **Ga** | 23 | 21 | 24 | 21 | 21 | 20 | 21 | 21 | 20 | 21 |
| **Cu** | 24 | 26 | 23 | 27 | 31 | 26 | 25 | 27 | 30 | 29 |
| **Zn** | 161 | 149 | 169 | 151 | 141 | 128 | 143 | 133 | 136 | 140 |
| **Pb** | 5 | 7 | 6 | 7 | 6 | 5 | 5 | 5 | 6 | 5 |
| **La** | 29 | 28 | 33 | 30 | 26 | 25 | 24 | 23 | 23 | 25 |
| **Ce** | 70 | 65 | 65 | 64 | 56 | 49 | 52 | 54 | 54 | 54 |
| **Th** | 4 | 5 | 6 | 4 | 3 | 3 | 4 | 5 | 4 | 6 |
| **Nd** | 41 | 35 | 38 | 36 | 33 | 29 | 29 | 31 | 31 | 30 |
| **U** | 3 | 2 | 2 | 2 | 2 | 2 | 2 | 3 | 2 | 1 |

Major element determinations have been normalized to a 100-percent total on a volatile-free basis and recalculated with total iron expressed as FeO*; nd - no data or element not analyzed; na - not applicable or no information. LOI, Loss on Ignition; Total_I, original analytical total.

*Table 6-4, continued. Select XRF analyses for the CRBG in the Dufur area (part 2 of 2).*

| **Sample** | 140 DFWJ 14 | 263 DFWJ 14 | 208 DFWJ 14 | 190 DFWJ 15 | 144 DFWJ 14 | 152 DFWJ 14 | 12 DFWJ 14 | 179 DFWJ 14 | 112 DFWJ 14 |
|---|---|---|---|---|---|---|---|---|---|
| **Geographic Area** | Pine Creek | Pine Creek | Long Hollow | Friend | U.S. 197 | Dufur Gap Road | Dufur Gap Road | Dry Creek | Butler Canyon |
| **Formation** | Wanapum Basalt | Wanapum Basalt | Wanapum Basalt | Grande Ronde Basalt | Grande Ronde Basalt | Grande Ronde Basalt | Grande Ronde Basalt | Grande Ronde Basalt | Grande Ronde Basalt |
| **Map Unit** | Twfg | Twfg | Twfg | Tgsb | Tgsb | Tgsb | Tgsb | Tgww | Tgww |
| **UTM N (NAD 83)** | 5027905 | 5029073 | 5029589 | 5021935 | 5025704 | 5023448 | 5024473 | 5028452 | 5017805 |
| **UTM E (NAD 83)** | 644132 | 642908 | 652251 | 629349 | 645499 | 643641 | 643260 | 649337 | 643992 |
| **Age (Ma)** | na | na | na | na | na | na | na | na | na |
| **Plate** | 2 | 2 | 3 | outside map | 2 | 2 | 2 | 3 | outside map |
| **Map Label** | G45 | G62 | DE75 | na | G23 | G7 | G11 | DE68 | na |
| ***Oxides, weight percent*** | | | | | | | | | |
| **$SiO_2$** | 50.74 | 51.13 | 51.09 | 54.92 | 54.84 | 54.43 | 53.62 | 55.57 | 56.30 |
| **$Al_2O_3$** | 13.20 | 13.59 | 13.25 | 14.53 | 14.50 | 14.37 | 13.92 | 13.49 | 13.54 |
| **$TiO_2$** | 3.04 | 3.20 | 3.13 | 1.78 | 1.95 | 1.79 | 1.97 | 2.12 | 2.12 |
| **FeO*** | 15.36 | 14.35 | 15.12 | 10.74 | 10.98 | 11.34 | 12.48 | 12.69 | 11.86 |
| **MnO** | 0.24 | 0.26 | 0.22 | 0.18 | 0.18 | 0.22 | 0.21 | 0.21 | 0.21 |
| **CaO** | 8.31 | 8.82 | 7.86 | 8.56 | 8.91 | 8.52 | 8.56 | 7.21 | 7.15 |
| **MgO** | 4.45 | 4.01 | 4.42 | 4.64 | 4.35 | 4.71 | 4.73 | 3.46 | 3.39 |
| **$K_2O$** | 1.21 | 1.25 | 1.28 | 1.32 | 1.04 | 1.18 | 1.17 | 1.64 | 2.01 |
| **$Na_2O$** | 2.85 | 2.80 | 3.02 | 3.01 | 2.94 | 3.12 | 3.00 | 3.27 | 3.06 |
| **$P_2O_5$** | 0.61 | 0.60 | 0.61 | 0.31 | 0.31 | 0.33 | 0.33 | 0.35 | 0.36 |
| **LOI** | nd | nd | 0.00 | nd | nd | nd | nd | 0.00 | nd |
| **Total_I** | 98.58 | 98.37 | 98.66 | 99.68 | 97.44 | 98.96 | 99.27 | 98.73 | 98.62 |
| ***Trace Elements, parts per million*** | | | | | | | | | |
| **Ni** | 17 | 15 | 14 | 14 | 13 | 22 | 14 | 5 | 6 |
| **Cr** | 13 | 13 | 10 | 35 | 35 | 33 | 34 | 5 | 5 |
| **Sc** | 36 | 36 | 37 | 35 | 38 | 35 | 36 | 33 | 33 |
| **V** | 404 | 434 | 413 | 312 | 321 | 308 | 317 | 354 | 350 |
| **Ba** | 532 | 601 | 553 | 553 | 469 | 576 | 485 | 643 | 645 |
| **Rb** | 27 | 27 | 32 | 33 | 25 | 27 | 30 | 46 | 49 |
| **Sr** | 327 | 347 | 312 | 329 | 325 | 324 | 315 | 318 | 322 |
| **Zr** | 187 | 176 | 179 | 161 | 161 | 168 | 168 | 178 | 185 |
| **Y** | 39 | 40 | 41 | 33 | 36 | 36 | 36 | 37 | 40 |
| **Nb** | 14.4 | 13.7 | 13.7 | 10.5 | 11.5 | 11.2 | 12.2 | 12.8 | 13.1 |
| **Ga** | 20 | 20 | 21 | 22 | 21 | 20 | 20 | 23 | 21 |
| **Cu** | 26 | 25 | 28 | 25 | 31 | 25 | 29 | 9 | 11 |
| **Zn** | 153 | 140 | 144 | 115 | 118 | 118 | 122 | 131 | 131 |
| **Pb** | 6 | 5 | 4 | 5 | 6 | 5 | 6 | 7 | 9 |
| **La** | 23 | 24 | 21 | 23 | 18 | 19 | 20 | 24 | 27 |
| **Ce** | 57 | 54 | 57 | 43 | 40 | 48 | 48 | 56 | 53 |
| **Th** | 5 | 4 | 4 | 4 | 2 | 4 | 4 | 6 | 6 |
| **Nd** | 30 | 31 | 31 | 25 | 23 | 26 | 26 | 29 | 30 |
| **U** | 1 | 1 | 1 | 2 | 1 | 2 | 1 | 2 | 1 |

Major element determinations have been normalized to a 100-percent total on a volatile-free basis and recalculated with total iron expressed as FeO*; nd - no data or element not analyzed; na - not applicable or no information. LOI, Loss on Ignition; Total_I, original analytical total.

#### 6.3.4.4 Frenchman Springs Member

The Frenchman Springs Member forms the lower part of the Wanapum Basalt in the Dufur area, consisting of 3 to 5 individual lava flows. On the basis of texture, phenocryst distribution, and geochemistry, these lava flows are divided from oldest to youngest into the Ginkgo (**Twfg**), Sand Hollow (**Twfh**), and Sentinel Gap (**Twfs**) basalt (**Figure 5-7**; **Figure 6-56**; **Table 6-4, Table 6-5**; Plates 1, 2, and 3; Beeson and others, 1985; Martin and others, 2013). Frenchman Springs lava flows are distinguished from other CRBG units by large, widely scattered to locally abundant plagioclase phenocrysts and high titanium contents ($TiO_2$ = ~2.9 to 3.06 weight percent) (Beeson and others, 1985, 1989; **Figure 5-10a-b**; **Table 6-4, Table 6-5**; Appendix). Upper lava flows (**Twfs**, **Twfh**) in the Frenchman Springs Member have normal magnetic polarity, while those in the lower part of the member (**Twfg**) have excursional polarity. The Frenchman Springs Member was erupted between 15.9 and 16.0 Ma on the basis of U/Pb ages obtained from silicic tuff interbeds between basalt flows on the Columbia Plateau by Kasbohm and Schoene (2018). These lava flows overlie the Vantage Member of the Ellensburg Formation (**Figure 5-7**) and the Sentinel Bluffs Member (**Tgsb**) at the top of the Grande Ronde Basalt; they are overlain by reversed-polarity lava flows of the ~15.9 Ma Priest Rapids Member, forming the upper part of the Wanapum Basalt (**Twpr**) (**Figure 5-7**; Plates 1, 2, and 3). Frenchman Springs Member lava flows were erupted from a northerly-striking vent system in eastern Washington and northern Oregon (Kuehn, 1995) and flowed west down an ancestral paleoslope (**Figure 5-6**). Effusion of the Frenchman Springs Member produced over 7628 $km^3$ (1830 $mi^3$) of lava that covered an area exceeding 72,595 $km^2$ (28,029 $mi^2$) (Martin and others, 2013). Composite thickness of the Frenchman Springs Member in the Dufur area is ≤163 m (533 ft) (**Figure 6-56**; Plates 1, 2, and 3). The Frenchman Springs Member is subdivided in the map area into:

**Figure 6-56. Detailed stratigraphic section of water well WASC 50922 in the Dufur area (*image on following page*). Water Well WASC 50922 is located in Rail Hollow in the central part of the map area (45.424545, -121.180221). The original descriptive log and analytical results can be retrieved from the USGS Oregon Water Science Center at (*http://or.water.usgs.gov/projs_dir/crbg/data/wells/wasc_50922/index.html*). Additional data about well construction and groundwater levels for WASC 50922 is available online from OWRD (*https://apps.wrd.state.or.us/apps/gw/gw_info/gw_info_report/gw_details.aspx?gw_site_id=675*).**

**Figure 6-56. (Detailed stratigraphic section of water well WASC 50922 –** ***caption on previous page*****)**

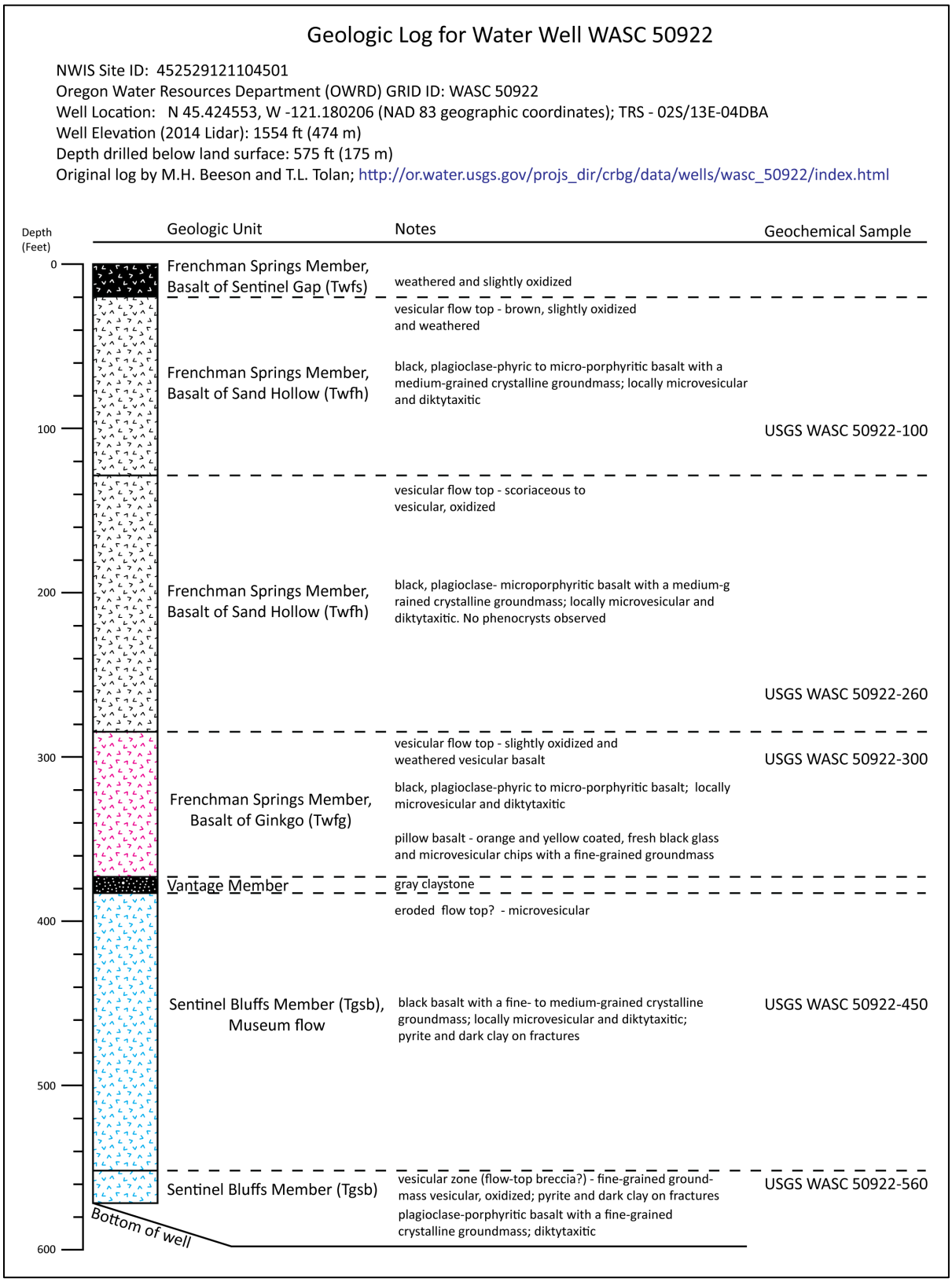

**Table 6-5. Representative XRF analyses for CRBG from water well WASC 50922. See Figure 6-56 for a detailed well log.**

| Sample | †USGS WASC 50922-100 | †USGS WASC 50922-260 | †USGS WASC 50922-300 | †USGS WASC 50922-450 | †USGS WASC 50922-560 |
|---|---|---|---|---|---|
| **Geographic Area** | Rail Hollow | Rail Hollow | Rail Hollow | Rail Hollow | Rail Hollow |
| **Formation** | Wanapum Basalt | Wanapum Basalt | Wanapum Basalt | Grande Ronde Basalt | Grande Ronde Basalt |
| **Map Unit** | Twfh | Twfh | Twfg | Tgsb | Tgsb |
| **UTM N (NAD 83)** | 5031725 | 5031725 | 5031725 | 5031725 | 5031725 |
| **UTM E (NAD 83)** | 642364 | 642364 | 642364 | 642364 | 642364 |
| **Age (Ma)** | na | na | na | na | na |
| **Plate** | 2 | 2 | 2 | 2 | 2 |
| **Map Label** | G100 | G101 | G102 | G103 | G104 |
| ***Oxides, weight percent*** | | | | | |
| **$SiO_2$** | 51.41 | 51.56 | 51.76 | 54.30 | 55.59 |
| **$Al_2O_3$** | 13.46 | 13.44 | 14.03 | 14.41 | 15.26 |
| **$TiO_2$** | 2.96 | 3.01 | 3.34 | 1.75 | 1.96 |
| **FeO*** | 14.28 | 14.39 | 12.99 | 11.50 | 9.56 |
| **MnO** | 0.22 | 0.22 | 0.19 | 0.18 | 0.17 |
| **CaO** | 8.15 | 8.20 | 9.41 | 8.51 | 9.08 |
| **MgO** | 4.67 | 4.41 | 3.56 | 4.92 | 4.02 |
| **$K_2O$** | 1.31 | 1.28 | 1.14 | 1.07 | 1.08 |
| **$Na_2O$** | 2.96 | 2.92 | 2.93 | 3.03 | 2.97 |
| **$P_2O_5$** | 0.58 | 0.57 | 0.65 | 0.32 | 0.30 |
| **LOI** | nd | nd | nd | nd | nd |
| **Total_I** | nd | nd | nd | nd | nd |
| ***Trace Elements, parts per million*** | | | | | |
| **Ni** | 16 | 19 | 19 | 14 | 15 |
| **Cr** | 43 | 50 | 20 | 46 | 45 |
| **Sc** | 38 | 36 | 37 | 35 | 38 |
| **V** | 427 | 430 | 454 | 306 | 332 |
| **Ba** | 558 | 606 | 551 | 532 | 563 |
| **Rb** | nd | nd | nd | nd | nd |
| **Sr** | 314 | 317 | 339 | 313 | 340 |
| **Zr** | 187 | 183 | 189 | 159 | 163 |
| **Y** | 38 | 39 | 39 | 31 | 33 |
| **Nb** | nd | nd | nd | nd | nd |
| **Ga** | nd | nd | nd | nd | nd |
| **Cu** | 24 | 25 | 25 | 28 | 31 |
| **Zn** | 125 | 123 | 130 | 105 | 112 |
| **Pb** | nd | nd | nd | nd | nd |
| **La** | 25 | 25 | 26 | 22 | 20 |
| **Ce** | 63 | 58 | 63 | 48 | 47 |
| **Th** | 4 | 4 | 4 | 4 | 3 |
| **Nd** | 27 | 25 | 23 | 23 | 20 |
| **U** | nd | nd | nd | nd | nd |

Major element determinations have been normalized to a 100-percent total on a volatile-free basis and recalculated with total iron expressed as FeO*; nd - no data or element not analyzed; na - not applicable or no information. LOI, Loss on Ignition; Total_I, original analytical total. †Data from Oregon Water Science Center, https://or.water.usgs.gov/projs_dir/crbg/data/wells/wasc_50922/index.html

**Twfs** **Basalt of Sentinel Gap (middle or early Miocene)—**High-titanium basalt and basaltic andesite ($SiO_2$ = 49.69 to 54.12 weight percent; $TiO_2$ =2.92 to 3.65 weight percent; *n* = 25 analyses) mapped beneath the Dalles Formation (**Tmdl**) and above the Basalt of Sand Hollow (**Twfh**) (**Figure 5-7**, **Figure 6-56**, **Figure 6-57**; **Table 6-4**; Plates 1, 2, and 3; Appendix). The mapped distribution of the Basalt of Sentinel Gap (**Twfs**) is confined to Fifteenmile Creek in the Wolf Run 7.5′ quadrangle (Plate 1, cross sections), north of Pine Creek in the Dufur West 7.5′ quadrangle (Plate 2, cross sections), and the northern half of the Dufur East 7.5′ quadrangle (Plate 3, cross section). A few isolated remnants of the Basalt of Sentinel Gap (**Twfs**) crop out along Tygh Ridge in the southeast and northeast part of the Dufur East and Sherars Bridge 7.5′ quadrangles, respectively (Plate 3, cross section). The Basalt of Sentinel Gap (**Twfs**) is distinguished from the underlying Basalt of Sand Hollow (**Twfh**) on the basis of relatively higher amounts of titanium (avg $TiO_2$ = 3.09 weight percent) and phosphorous (avg $P_2O_5$ = 0.63 weight percent) and lesser amounts of chromium (avg Cr = 14 ppm) (*n* = 71 analyses in Middle Columbia Basin; **Figure 5-10b-d**; **Table 6-4**; Appendix; Madin and McClaughry, 2019; McClaughry and others, 2020a; J.D. McClaughry unpublished geologic mapping). The Basalt of Sentinel Gap (**Twfs**) is distinguished from the overlying Priest Rapids Member on the basis of geochemistry and magnetic polarity (**Figure 5-10b-d**; **Table 6-4**; Appendix). Exposures of unit **Twfs** in the Dufur area are typically restricted to roadcuts and outcrops located in the bottoms of stream, drainages (**Figure 6-58**). Outcrops are typically characterized by well-defined colonnade jointing and/or platy jointing (**Figure 6-58**). Where the upper part of the unit (**Twfs**) is exposed, outcrops are characterized by 0.2- to 2-m-thick (0.7 to 6.6 ft) vesicular flow lobes. Thickness of unit **Twfs** in the Dufur area is ≤50 m (165 ft), thickening to the north and east (**Figure 6-56**; Plates 1, 2, and 3). Typical hand samples of the basalt are medium dark gray (N4) to dark gray (N2) and aphyric to very sparsely porphyritic with <1 percent (vol.) clear to pale yellowish orange (10YR 8/6), euhedral to subhedral, prismatic- to lath-shaped and blocky, seriate plagioclase microphenocrysts and phenocrysts ≤7 mm (0.3 in) (~1 phenocryst/$m^2$) and <2 percent (vol.) grayish black (N2) clinopyroxene microphenocrysts, enclosed within a fine-grained holocrystalline to hypocrystalline groundmass of plagioclase, intergranular clinopyroxene, Fe-Ti oxides, and intersertal glass (**Figure 6-59**).

The Basalt of Sentinel Gap (**Twfs**) has normal magnetic polarity and an early to middle Miocene age bracketed by U/Pb dates of 15.895 ± 0.019 Ma for ash between the overlying Basalt of Rosalia (**Twpr**) and Basalt of Lolo (Priest Rapids Member), and 16.066 ± 0.04 Ma for ash between the older Basalt of Ginkgo (**Twfg**) and the Sentinel Bluffs Member **(Tgsb)** (Kasbohm and Schoene, 2018; **Figure 5-7**, **Figure 6-1**). Equivalent to the Sentinel Gap flows of Mackin (1961) and Beeson and others (1985) and flows of Union Gap of Powell (1982).

**Figure 6-57. Quarry along Fifteenmile Creek exposing the contact between the upper part of the Basalt of Sand Hollow (Twfh) and the lower part of the Basalt of Sentinel Gap (Twfs)(45.463529, -121.102708). View is looking to the northeast. The 'X' corresponds to the location for photo D shown in Figure 6-60. The 'Y' corresponds to the location for photo B shown in Figure 6-58. Arrow points to iPad for scale, which is 25 cm (9.8 in) tall. Photo credit: J.D. McClaughry, 2014.**

**Figure 6-58. Well-developed columnar jointing is typical for the Basalt of Sentinel Gap (Twfs) in the Dufur area. (a) Columnar-jointed outcrop along Fifteenmile Creek at the Boyd Market Road crossing near Boyd (45.479181, -121.080812). Arrow points to hammer for scale, which is 38 cm (15 in) tall. View is looking northeast. (b) Columnar-jointed quarry exposure along Fifteenmile Creek (45.463749, -121.102430). Arrow points to iPad for scale, which is 25 cm (9.8 in) tall. View is looking northeast. (c) Platy-jointed basalt exposed along Rail Hollow Road (45.409756, -121.207045). View is looking north. Photo credits: J.D. McClaughry, 2014.**

**Figure 6-59. Hand sample and thin section photographs of the Basalt of Sentinel Gap (Twfs). (a) Typical hand sample. Scale bar is 2.5 cm (1 in) tall. (b) Thin section under cross-polarized light (XPL). (c) Same view as in B under plane-polarized light (PPL). Scale bar for thin section photographs is 7 mm (0.3 in) wide. Photo credits: J.D. McClaughry, 2015.**

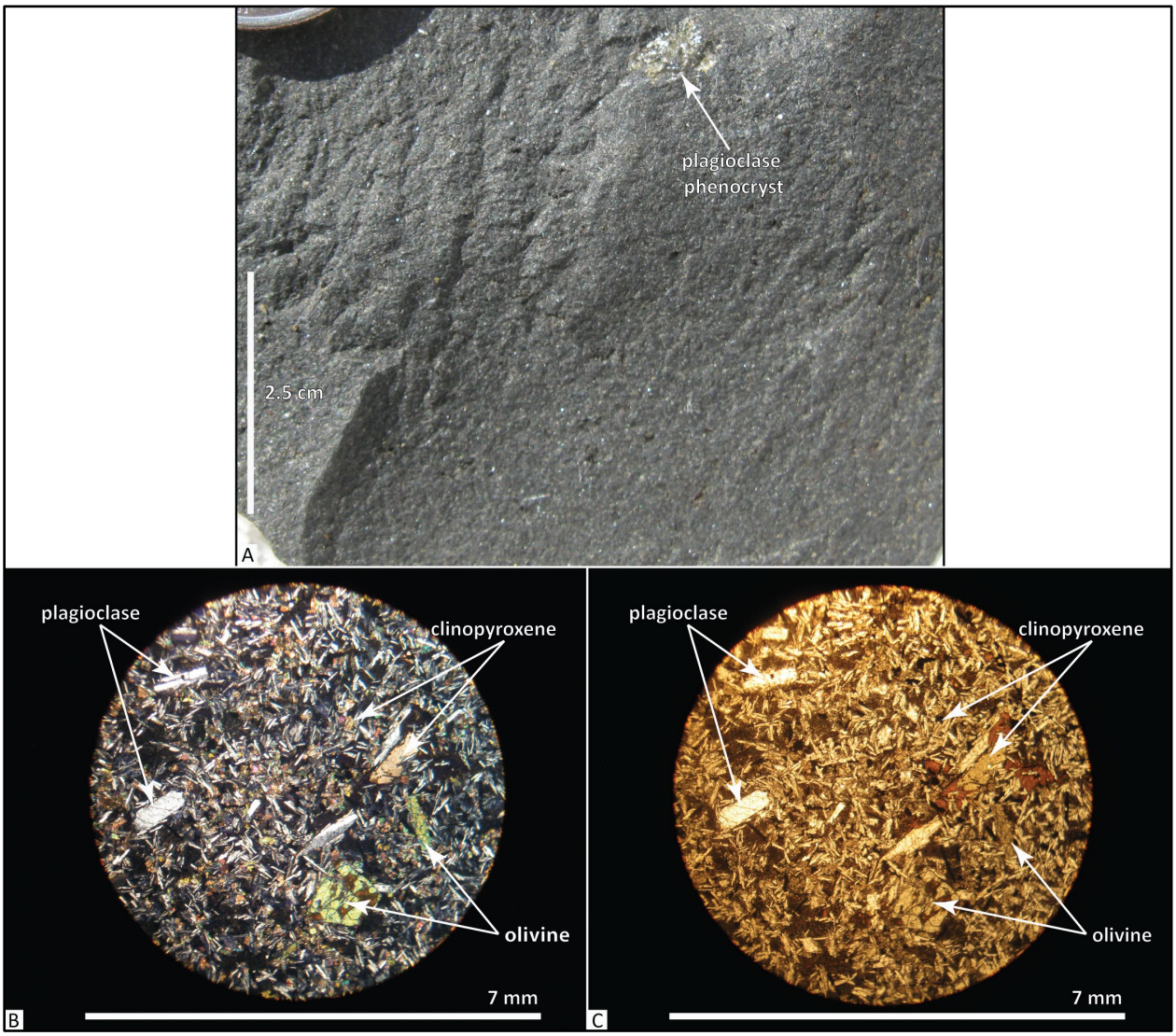


**Twfh** **Basalt of Sand Hollow (middle or early Miocene)—**High-titanium basalt and basaltic andesite ($SiO_2$ = 49.14 to 53.72 weight percent; $TiO_2$ = 2.85 to 3.27 weight percent; *n* = 108 analyses) lying stratigraphically beneath the Basalt of Sentinel Gap (**Twfs**) and above the Basalt of Ginkgo (**Twfg**) and Sentinel Bluffs Member (**Tgsb**) (**Figure 5-7**, **Figure 6-56**, **Figure 6-57**; **Table 6-4**, **Table 6-5**; Plates 1, 2, and 3; Appendix). The Basalt of Sand Hollow (**Twfh**) is mapped along Fifteenmile Creek in the Wolf Run 7.5′ quadrangle (Plate 1, cross sections) and south and east of Rail Hollow in the Dufur West 7.5′ quadrangle and northern part of the Postage Stamp Butte 7.5′ quadrangle (Plate 2, cross sections). Unit **Twfh** is widely mapped across the Dufur East 7.5′ quadrangle, northern part of the Sherars Bridge 7.5′ quadrangle, and northwest part of the Summit Ridge 7.5′ quadrangle, southeast of Fifteenmile Creek (Plate 3). The Basalt of Sand Hollow (**Twfh**) is distinguished from other Frenchman Springs units on the basis of sparsely distributed plagioclase

phenocrysts and relatively lower amounts of titanium (avg $TiO_2$ = 2.97 weight percent) and phosphorous (avg $P_2O_5$ = 0.56 weight percent) and higher amounts of chromium (avg Cr = 38 ppm) (n = 156 analyses in Middle Columbia Basin; **Figure 5-10b-d**; **Table 6-4**; Appendix; Madin and McClaughry, 2019; McClaughry and others, 2020a; J.D. McClaughry unpublished geologic mapping, 2016). Thickness of unit **Twfh** in the Dufur area ranges between ~20 m (66 ft) along U.S. Highway 197 in the southern part of the map area to ~81 m (266 ft) in the subsurface beneath Rail Hollow (Plate 1, Well - WASC 50922; **Figure 6-56**; Appendix). Unit **Twfh** is ~67 m (220 ft) thick in Well WASC 51672 northeast of Dufur.

The Basalt of Sand Hollow (**Twfh**) consists of two flow units in the Dufur area (**Figure 6-60a**). The lower Sand Hollow flow (**Twfh**) in the Dufur area is aphyric to very sparsely porphyritic, characterized by a well-developed platy to blocky colonnade jointing (**Figure 6-60b**). Where the flow is deeply weathered, slopes underlain by the Basalt of Sand Hollow (**Twfh**) are mantled by subrounded boulders, generally <1.5 m (4.9 ft) in diameter. Typical hand samples from the lower lava flow are pale blue (5B 6/2) to medium dark gray (N4) and aphyric to very sparsely porphyritic (~1 phenocryst/$m^2$) and microporphyritic. The basalt contains 1 to 2 percent (vol.) yellow brown (5YR 5/6) to very pale orange (10YR 8/2), euhedral to subhedral, prismatic- to lath-shaped and blocky, plagioclase phenocrysts up to 7 mm (0.3 in) in length, 1 to 2 percent (vol.) conspicuous blocky to lath-shaped plagioclase microphenocrysts, and ≤1 percent clinopyroxene microphenocrysts ≤1 mm (0.04 in), enclosed within a fine-grained equigranular hypocrystalline groundmass of plagioclase, intergranular clinopyroxene, minor opaques, and intersertal to hyalophitic glass (**Figure 6-61a**, **c**, **d**). Very rare olivine microphenocrysts, ranging from 0.2 to 0.5 (0.008 to 0.02 in) mm across, are also present.

The upper Sand Hollow lava flow (**Twfh**) in the Dufur area is distinctly plagioclase porphyritic, characterized by a meter-scale, blocky columnar jointing and irregular platy jointing (**Figure 6-60a,b,c**). Where the flow is deeply weathered, slopes underlain by the upper Basalt of Sand Hollow flow (**Twfh**) are mantled by subrounded boulders, generally <1.5 m (4.9 ft) in diameter. A distinct flow-top zone, up to 25 m (82 ft) thick, is commonly present. The topmost part of the upper **Twfh** lava flow is characterized by massive, 0.5 to 2 m (1.6 to 6.6 ft)-thick, layered flow lobes containing abundant stretched vesicles, vesicle sheets, pods, and cylinders (**Figure 6-60c-d**). Typical hand samples from uppermost part of the upper **Twfh** lava flow are medium dark gray (N4) to dark gray (N2) and abundantly porphyritic and microporphyritic (**Figure 6-61b**). The basalt contains 3 to 5 percent (vol.) yellow brown (5YR 5/6) to very pale orange (10YR 8/2), euhedral to subhedral, prismatic to lath-shaped, plagioclase phenocrysts and glomerocrysts up to 2 cm (0.8 in), 2 to 3 percent (vol.) conspicuous blocky to lath-shaped plagioclase microphenocrysts, and ≤1 percent clinopyroxene microphenocrysts ≤1 mm (0.04 in), enclosed within a diktytaxitic, fine-grained holocrystalline groundmass of plagioclase, intergranular clinopyroxene, and minor Fe-Ti oxides (**Figure 6-61e**,**f**).

The Basalt of Sand Hollow (**Twfh**) has normal magnetic polarity and an early or middle Miocene age bracketed by U/Pb dates of 15.895 ± 0.019 Ma for ash between the overlying Basalt of Rosalia and Basalt of Lolo (Priest Rapids Member) and 16.066 ± 0.04 Ma for ash between the older Basalt of Ginkgo and the Sentinel Bluffs Member **(Tgsb)** (Kasbohm and Schoene, 2018; **Figure 5-7**, **Figure 6-1**). Equivalent to the Sand Hollow flows of Mackin (1961) and Beeson and others (1985) and the Kelly Hollow flow of Powell (1982).

**Figure 6-60. The Basalt of Sand Hollow (Twfh) in the Dufur area. (a) The Basalt of Sand Hollow (Twfh) in the Dufur area consists of two aphyric to very sparsely plagioclase-phyric flows; the upper part of the upper flow is typically abundantly plagioclase-phyric (45.418436, -121.139615). View is looking west. (b) Platy-jointed Basalt of Sand Hollow (Twfh) exposed along Upper Fifteenmile Creek Road near Taylor Grade (45.397718, -121.274199). Arrow points to hammer for scale, which is 38 cm (15 cm) long. View is looking north. (c) Abundantly plagioclase-phyric flow top to the Basalt of Sand Hollow (Twfh) characterized by thin, vesicular pahoehoe flow lobes exposed along U.S. Highway 197 (45.440148, -121.131843). Arrow points to hammer for scale, which is 38 cm (15 cm) long. View is looking east. (d) Pahoehoe flow lobes marking the upper part of the Basalt of Sand Hollow along Fifteenmile Creek (45.463529, -121.102708). iPad for scale is 25 cm (9.8 in) tall. View is looking north. Photo credits: J.D. McClaughry, 2014.**

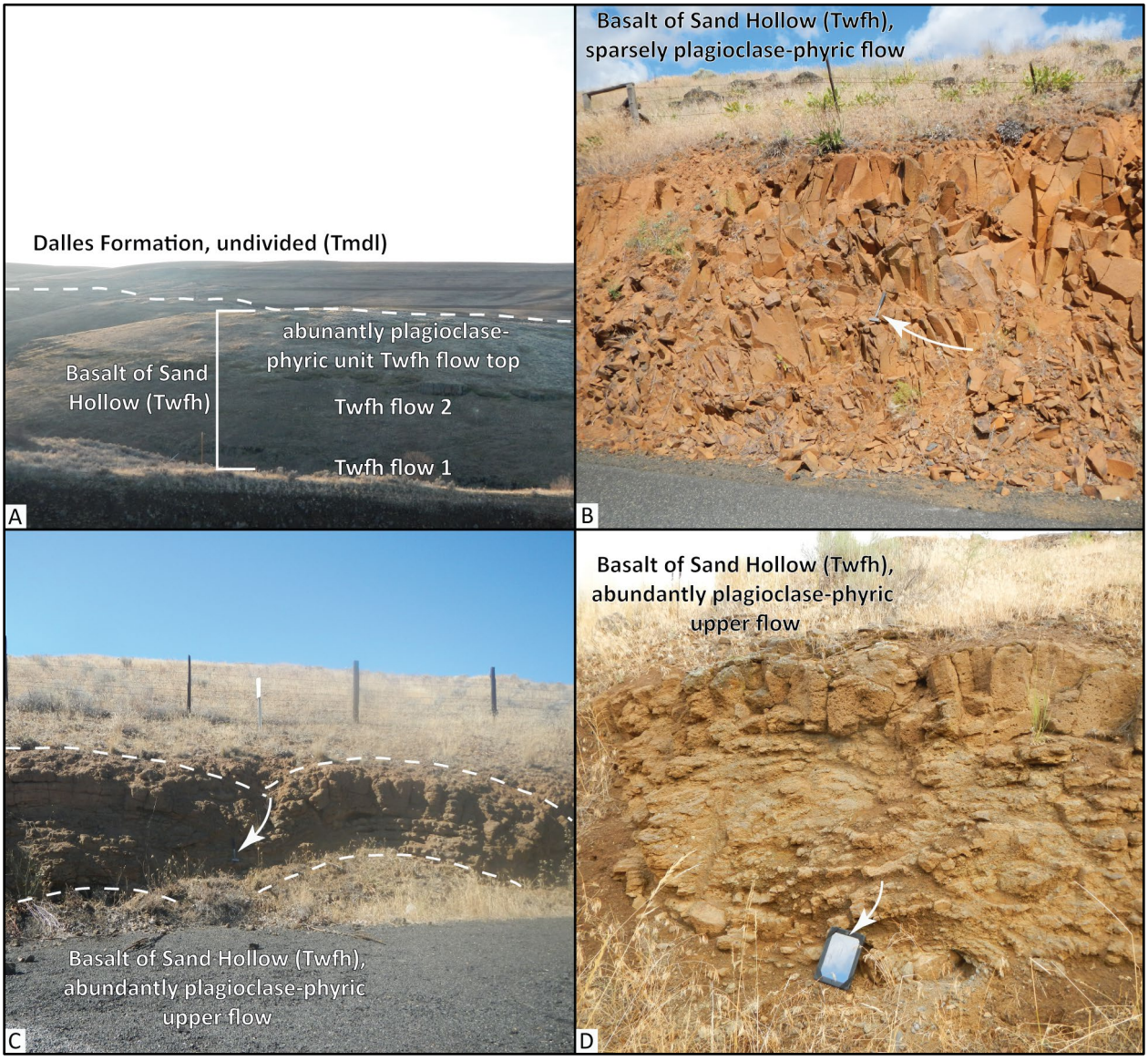

**Figure 6-61. Hand sample and thin section photographs of the Basalt of Sand Hollow (Twfh). (a) Typical hand sample of the lower flow in unit Twfh. (b) Typical hand sample of the upper part of unit Twfh. Scale bars for hand sample photographs in A and B are 2.5 cm (1 in) tall. (c) Thin section of hand sample in A under cross-polarized light (XPL). (d) Same view as in C under plane-polarized light (PPL). (e) Thin section of hand sample in B under cross-polarized light (XPL). (f) Same view as in e under plane-polarized light (PPL). Scale bar for thin section photographs is 7 mm (0.3 in) wide. Photo credits: J.D. McClaughry, 2015.**

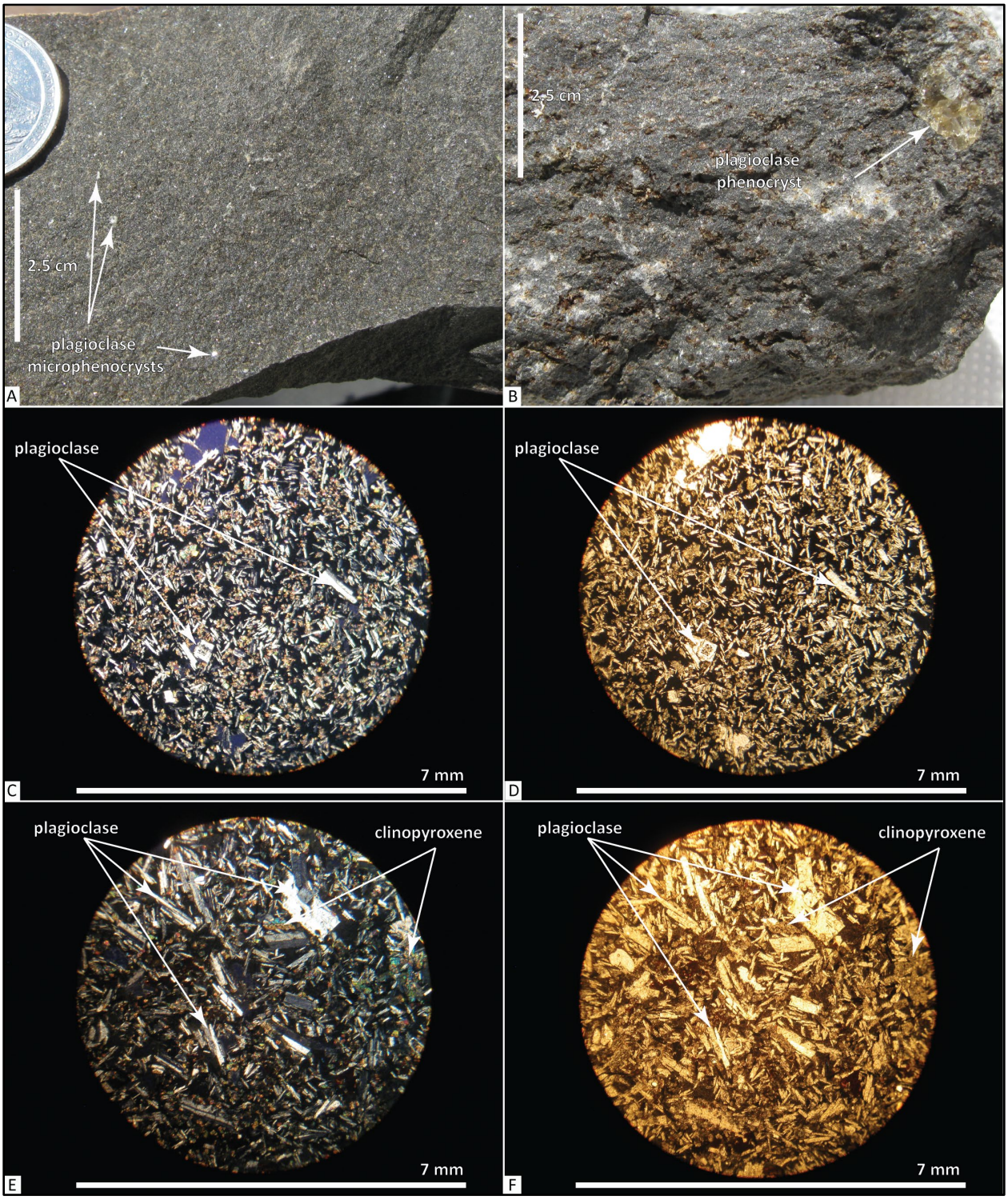

**Twfg** **Basalt of Ginkgo (middle or lower Miocene)—**High-titanium basalt ($SiO_2$ = 50.67 to 52.76 weight percent; $TiO_2$ = 3.04 to 3.36 weight percent; *n* = 41 analyses) mapped beneath the Basalt of Sand Hollow (**Twfh**) and above the Sentinel Bluffs Member (**Tgsb**) (**Figure 5-7**, **Figure 6-56**, **Figure 6-62**; **Table 6-4**, **Table 6-5**; Plates 2, and 3; Appendix). The Basalt of Ginkgo (**Twfg**) is not exposed in the Wolf Run 7.5′ quadrangle or northern part of the Friend 7.5′ quadrangle as the depth of erosion there does not penetrate beneath the overlying Basalt of Sand Hollow (**Twfh**) (Plate 1, cross sections). Eastward into the Dufur West 7.5′ quadrangle and northern half of the Postage Stamp Butte 7.5′ quadrangle, the Basalt of Ginkgo (**Twfg**) is mapped south from Larch and Pine creeks to Tygh Ridge and the head of Butler Canyon (Plate 2, cross sections). Unit **Twfg** is widely exposed in the Dufur East 7.5′ quadrangle, northern part of the Sherars Bridge 7.5′ quadrangle, and northwest part of the Summit Ridge 7.5′ quadrangle, where erosional windows along a number of deeply incised canyons south of Mays Canyon Creek and Dry Creek reveal older lava flows beneath the Basalt of Sand Hollow (**Twfh**) (Plate 3, cross section). The Basalt of Ginkgo (**Twfg**) is distinguished from other Frenchman Springs units (**Twfs**, **Twfh**) on the basis of abundant plagioclase phenocrysts and relatively high amounts of titanium (avg $TiO_2$ = 3.18 weight percent) and phosphorous (avg $P_2O_5$ = 0.62 weight percent) and lower amounts of chromium (avg Cr = 14 ppm) (*n* = 62 samples; **Figure 6-56**, **Figure 6-62b,c**; **Figure 5-10b-d**; **Table 6-4**, **Table 6-5**; Appendix; Madin and McClaughry, 2019; McClaughry and others, 2020a; J.D. McClaughry unpublished geologic mapping, 2015).

Unit **Twfg** is typically not well exposed in the map area, tending to form talus-covered or boulder-armored slopes with rounded boulders 0.5- to 1-m (1.6 to 3.3 ft) across. In eastern areas, outcrops of unit **Twfg** are characterized by meter-scale blocky columnar jointing (**Figure 6-62a**). The uppermost part of unit **Twfg** is characterized by massive, 0.5- to 2-m (1.6 to 6.6 ft) thick, layered lava flow lobes containing abundant stretched vesicles, vesicle sheets, pods, and cylinders. Thickness of unit **Twfg** in the Dufur area ranges between ~20 m (66 ft) at the head of Butler Canyon and in Pine Creek Canyon to ~27 m (89 ft) in the subsurface beneath Rail Hollow (Plate 1; Well - WASC 50922; **Figure 6-56**). The unit is ~46 m (150 ft) thick in water well WASC 51672 northeast of Dufur (Plate 3; Appendix). Typical hand samples of the basalt are medium dark gray (N4) to dark gray (N2) and abundantly porphyritic and microporphyritic containing ~3 to 5 percent (vol.) yellow brown (5YR 5/6) to very pale orange (10YR 8/2), euhedral to subhedral, prismatic to lath-shaped, plagioclase phenocrysts and glomerocrysts ≤3 cm (1.2 in) and conspicuous blocky to lath-shaped plagioclase microphenocrysts (**Figure 6-63a**). Phenocrysts and microphenocrysts are distributed within an inequigranular holocrystalline groundmass of plagioclase, intergranular clinopyroxene, and minor Fe-Ti oxides (**Figure 6-63b,c**). The Basalt of Ginkgo (**Twfg**) may be aphyric to depths of 5 to 10 m (16.4 to 32.8 ft) from upper lava flow surfaces (Anderson, 1987).

The Basalt of Ginkgo (**Twfg**) has excursional magnetic polarity and an early or middle Miocene age bracketed by U/Pb dates of 15.895 ± 0.019 Ma for ash between the overlying Basalt of Rosalia (**Twpr**) and Basalt of Lolo (Priest Rapids Member) and 16.066 ± 0.04 Ma for ash between the Basalt of Ginkgo (**Twfg**) and the Sentinel Bluffs Member (**Tgsb**) (Kasbohm and Schoene, 2018; **Figure 5-7**, **Figure 6-1**). Equivalent to the Ginkgo flows of Mackin (1961) and Beeson and others (1985).

Note that in this report and set of geologic maps we have not mapped the Basalt of Ginkgo (**Twfg**) separately from the stratigraphically, texturally, and chemically similar Basalt of Silver Falls presumed to be present in the Dufur area by Beeson and others (1985) and Martin and others (2013). The two units are distinguished by some other workers on the basis of subtle

differences in sample texture and slight variations in phosphorous (Ginkgo avg $P_2O_5$ = 0.69 weight percent, *n* = 342 analyses; Silver Falls avg $P_2O_5$ = 0.62 weight percent, *n* = 57 analyses) and magnesium (Ginkgo avg MgO = 3.92 weight percent; Silver Falls avg MgO = 4.06 weight percent) (see Beeson and others, 1985; Martin and others, 2013). However, all other major and trace elements in the two units are remarkably similar, rock sample textures are not diagnostic, and paleomagnetic separation of the two units is ambiguous. These problems led Martin and others (2013) to raise the question: "Are the Basalt of Ginkgo and the Basalt of Silver Falls separate units or is the Basalt of Silver Falls a variant of the more voluminous Ginkgo Basalt". We therefore map this stratigraphic interval in the Dufur area as the more widespread and voluminous Basalt of Ginkgo (**Twfg**) and retain the earlier name defined by Mackin (1961).

**Figure 6-62. Outcrop and hand sample photographs of the Basalt of Ginkgo (Twfg). (a) Roadcut exposures of the Basalt of Ginkgo (Twfg), such as this example along Easton Canyon Road are typically characterized by meter-scale blocky columnar jointing (45.437938, -121.050544). (b) The Basalt of Ginkgo (Twfg) is distinguished in the field on the basis of abundant, large plagioclase phenocrysts (45.437938, -121.050544). Pen for scale is 15 cm (5.9 in) tall. (c) Amber-colored plagioclase phenocrysts and glomerocrysts up to 3 cm (1.2 in) across are common within the unit (45.435891, -121.045796). Quarter is 2.5 cm (1 in) across. Photo credits: J.D. McClaughry, 2015.**

**Figure 6-63. Hand sample and thin section photographs of the Basalt of Ginkgo (Twfg). (a) Typical porphyritic and microporphyritic hand sample, with 3 to 5 percent plagioclase phenocrysts and glomerocrysts up to 2 cm (0.8 in) in length. Scale bar is 2.5 cm (1 in) tall. (b) Thin section under cross-polarized light (XPL). (c) Same view as in B under plane-polarized light (PPL). Scale bar for thin section photographs is 7 mm (0.3 in) wide. Photo credits: J.D. McClaughry, 2015.**

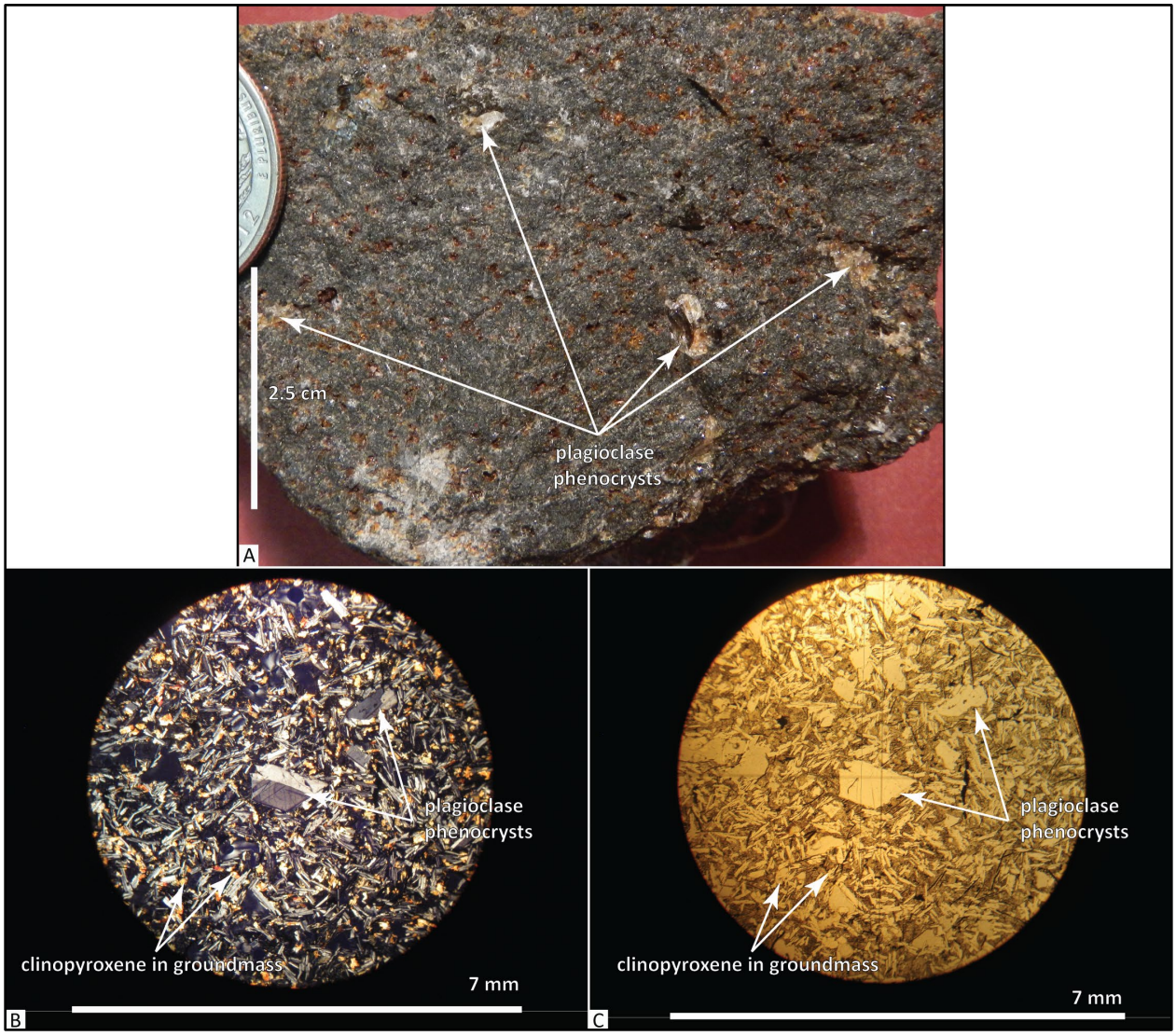

**Disconformity—Vantage Member of the Ellensburg Formation**

### 6.3.4.5 Vantage Member of the Ellensburg Formation

The Grande Ronde-Wanapum Basalt contact is readily mapped across the Columbia Plateau and through the Columbia Gorge on the basis of rock texture and distinctly different chemical compositions of the two units (**Figure 5-7**, **Figure 5-10a-b**, **Figure 6-56**; **Table 6-4**, **Table 6-5**; Appendix). At many localities across the region the contact is further distinguished by the presence of a thin (<several meters) and discontinuous sedimentary interval known as the Vantage Member of the Ellensburg Formation (Swanson and others, 1979b; Beeson and others, 1989; Reidel and others, 2013). Outcrops exposing the Vantage Member in the Dufur area are very rare, restricted to a few roadcuts. The few Vantage outcrops observed are characterized by either moderate yellowish brown (10YR 5/4), fine-grained (fU) mica-bearing lithic sandstone or basalt-clast cobble gravel (**Figure 6-64**). Thickness of the Vantage Member in the Dufur area is probably less than 4 m (13 ft) on the basis of outcrop observations and log information from water well WASC 50922 (**Figure 6-56**; Plate 2). Distribution of the Vantage Member in this area is discontinuous and too thin to display on Plates 1, 2, and 3. Equivalent to the Vantage Member of the Ellensburg Formation (Swanson and others, 1979b) and the Vantage Sandstone of Reidel and others (2013).

**Figure 6-64. The Vantage Member of the Ellensburg Formation locally marks the contact between the Grande Ronde Basalt and the Wanapum Basalt in the Dufur area. (a) Moderate yellowish brown (10YR 5/4) fine-grained (fU) mica-bearing lithic sandstone (45.342120, -121.161435). Shovel for scale is 1 m (3.28 ft) tall. (b) Basalt-clast cobble gravel (45.418597, -121.074681). Scale bar in the photograph is 1 m (3.28 ft) tall. Photo credits: J.D. McClaughry, 2015.**

#### 6.3.4.6 Grande Ronde Basalt

The upper part of the Grande Ronde Basalt is the stratigraphically lowest exposed geologic unit in the Dufur area (**Figure 5-7**, **Figure 6-56**; Plates 1, 2, and 3; Appendix). These lava flows, erupted between 16.572 ± 018 Ma (base of R1 magnetostratigraphic unit) and 16.066 ± 0.04 Ma (Vantage Horizon), are the thickest, most voluminous formation of the CRBG (**Figure 5-7**; 66 percent of total volume erupted; Camp and others, 2003; Camp and Ross, 2004; Kasbohm and Schoene, 2018). Effusion of the Grand Ronde Basalt from vents and fissures in the eastern and southeastern parts of the Columbia Plateau, produced over 150,400 km$^3$ (36,082 mi$^3$) of lava flows that covered an area exceeding 169,600 km$^2$ (65,482 mi$^2$) (**Figure 5-6**; Tolan and others, 1989; Reidel and others, 1989; Barry and others, 2010; Reidel and Tolan, 2013). The Grand Ronde Basalt spans at least four paleomagnetic zones and has been stratigraphically subdivided into the R1, N1, R2, N2 magnetostratigraphic units by Swanson and others (1979b) (**Figure 5-7**). The Grande Ronde Basalt mapped in the Dufur area consists of lava flows assigned to the Sentinel Bluffs (**Tgsb**) and Winter Water (**Tgww**) members; farther to the south in Butler Canyon, deeper exposed parts of the section include lava flows assigned to the Ortley (**Tgo**), Armstrong Canyon (**Tgac**), and Buttermilk Canyon (**Tgbc**) members of the N2 magnetostratigraphic unit and the Grouse Creek member (**Tggc**) of the R2 magnetostratigraphic unit (**Figure 5-7**; Hagstrum and others, 2010).

Grande Ronde Basalt lava flows are generally monotonously fine-grained, aphyric, and petrographically non-distinctive. Chemical compositions also have a relatively narrow range, but precise analyses of major and trace elements can be used to correlate individual flows on a regional basis, when used in conjunction with careful geologic mapping (**Figure 5-10a-b**; **Table 6-5**; Appendix; Swanson and others, 1981; Reidel and others, 1989, Tolan and others, 1989; Hooper, 2000; Wells and others, 2009; Hagstrum and others, 2010). Grande Ronde lava flows are distinguished from the overlying Wanapum Basalt by the local presence of the intervening Vantage Member of the Ellensburg Formation (Swanson and others, 1979b), the conspicuous absence of large plagioclase phenocrysts and glomerocrysts, and significantly lesser titanium contents (**Figure 5-10a-b**; **Table 6-4**, **Table 6-5**; Appendix; Hooper, 2000; Tolan and others, 2009b). Composite thickness of the Grande Ronde Basalt in the Dufur area exceeds 330 m (1,082 ft) (Plates 1, 2, and 3).

The Grande Ronde Basalt is subdivided in the map area into the following units:

##### 6.3.4.6.1 *Normal-polarity (N2) magnetostratigraphic unit*

The N2 magnetostratigraphic unit is the youngest Grande Ronde Basalt magnetostratigraphic unit, made up of chemically distinctive lava flow packages that cover an area of ~114,500 km$^2$ (44,208 mi$^2$) **Figure 5-7**). The estimated volume of the N2 magnetostratigraphic unit is ~35,300 km$^3$ (8,469 mi$^3$) (Reidel and Tolan, 2013). The N2 magnetostratigraphic unit is locally subdivided into the following units:

**Tgsb** **Sentinel Bluffs Member (lower Miocene)—**Basaltic andesite lava flows ($SiO_2$ = 53.30 to 55.19 weight percent; $TiO_2$ =1.74 to 2.06 weight percent; *n* = 79 analyses) mapped beneath the Frenchman Springs Member (**Twfg**, **Twfh**, **Twfs**) and above the Winter Water Member (**Tgww**) in the Dufur area (**Figure 5-7**, **Figure 5-10a-b**, **Figure 6-56**, **Figure 6-65**; **Table 6-5**; Plates 1, 2, and 3; Appendix). The Sentinel Bluffs Member (**Tgsb**) is mapped over a small area southeast of the Mays Canyon Creek fault in the northern part of the Friend 7.5′ quadrangle (Plate 1, cross sections). Eastward into the Dufur West 7.5′ quadrangle and northern half of the Postage Stamp Butte 7.5′ quadrangle, the Sentinel Bluffs Member (**Tgsb**) is mapped southeast from Pine Creek to Tygh Ridge and the head of Butler Canyon (Plate 2, cross sections). Unit **Tgsb** is widely exposed in the Dufur East 7.5′ quadrangle, northern part of the Sherars Bridge 7.5′ quadrangle, and

northwest part of the Summit Ridge 7.5′ quadrangle, where erosional windows along a number of deeply incised canyons south of Mays Canyon Creek and Dry Creek reveal older lava flows beneath the Basalt of Ginkgo (**Twfg**) (Plate 3, cross section). The Sentinel Bluffs Member (**Tgsb**) is distinguished from other members of the Grande Ronde Basalt on the basis of lithology and higher contents of magnesium (avg MgO = 4.99 weight percent; 139 analyses in Middle Columbia Basin = 4.99 weight percent; **Figure 5-10a-b**; **Table 6-5**; Madin and McClaughry, 2019; McClaughry and others, 2020a; J.D. McClaughry unpublished geologic mapping). Unit **Tgsb** is composed of thin lava flow lobes, generally <5 to 20 m thick (16.4 to 65.6 ft), that are characterized by well-developed vesicular flow tops and basal flow breccia (**Figure 6-65a,b**). Flow interiors are typically characterized by massive meter-scale colonnade jointing with lesser hackly entablatures (**Figure 6-65c,d**). The Sentinel Bluffs Member (**Tgsb**) is generally more resistant to erosion than the overlying Basalt of Ginkgo (**Twfg**), tending to form cliffs and steep slopes (**Figure 6-65d**). The base of the Sentinel Bluffs Member (**Tgsb**) is not exposed in the Dufur area, west of the city of Dufur (Plates 1 and 2); southeast of Dufur the lower contact of the unit with the older Winter Water Member (**Tgww**) is exposed in Dry Creek canyon. A minimum thickness for the Sentinel Bluffs Member of ~54 m (180 ft) is indicated from water well WASC 50922 in Rail Hollow (**Figure 6-56**; Plate 1; Appendix). Maximum thickness of the Sentinel Bluffs Member in Butler Canyon (south of map area), along Dry Creek, and in water well WASC 51672 is 125 m (410 ft). Typical hand samples of the basalt are medium light gray (N6) to medium gray (N5) and aphyric to very sparsely microporphyritic containing ≤2 percent (vol.) clear, euhedral, prismatic to blocky, plagioclase microphenocrysts distributed within an equigranular fine-grained diktytaxitic hypocrystalline groundmass of plagioclase, intergranular clinopyroxene, minor Fe-Ti oxides, and intersertal glass (**Figure 6-66**). Minor amounts of olivine microphenocrysts are also present in some lava flows.

The Sentinel Bluffs Member (**Tgsb**) has normal magnetic polarity and is assigned an early Miocene age bracketed by U/Pb dates of 16.066 ± 0.04 Ma for ash from the overlying Vantage Horizon and 16.254 ± 0.034 Ma for ash between the Wapshilla Ridge and Meyer Ridge Members of the underlying R2 magnetostratigraphic unit (Kasbohm and Schoene, 2018; **Figure 5-7**, **Figure 6-1**). The Sentinel Bluffs Member (**Tgsb**) was erupted from a northerly trending vent system in eastern Washington and northern Oregon and flowed west down an ancestral paleoslope (**Figure 5-6**; Tolan and others, 2009b; Reidel and Tolan, 2013). Effusion of the Sentinel Bluffs Member produced ~10,150 $km^3$ (2,435 $mi^3$) of lava flows that covered an area exceeding 167,700 $km^2$ (64,749 $mi^2$) (Reidel and Tolan, 2013). Equivalent to the high-MgO flows of Wright and others (1973), the Sentinel Bluffs unit of Reidel and others (1989), and the Sentinel Bluffs Member of Reidel and Tolan (2013).

**Figure 6-65. The Sentinel Bluffs Member (Tgsb) in the Dufur area. (a) Steeply north-dipping, thin flows of the Sentinel Bluffs Member (Tgsb) cropping out along U.S. Highway 197, south of Dufur (45.370525, -121.142174). Flows here are deformed along the Dry Creek monocline. Person at the left of the photograph is 1.6 m (5.2 ft) tall. (b) Thin, vesicular pahoehoe flow lobes in the Sentinel Bluffs Member (Tgsb) exposed at the south end of the outcrop shown in A (45.369921, -121.141985). Hammer for scale is 38 cm (15 cm) long. (c) Massive to columnar-jointed Sentinel Bluffs basalt (Tgsb) exposed along Long Hollow Market Road (45.407290, -121.058217). Arrow points to hammer for scale, which is 38 cm (15 cm) long. (d) Cliff-forming, hackly jointed flow in the Sentinel Bluffs Member (Tgsb) exposed along Dry Creek (45.400028, -121.094468). Photo credits: J.D. McClaughry, 2014.**

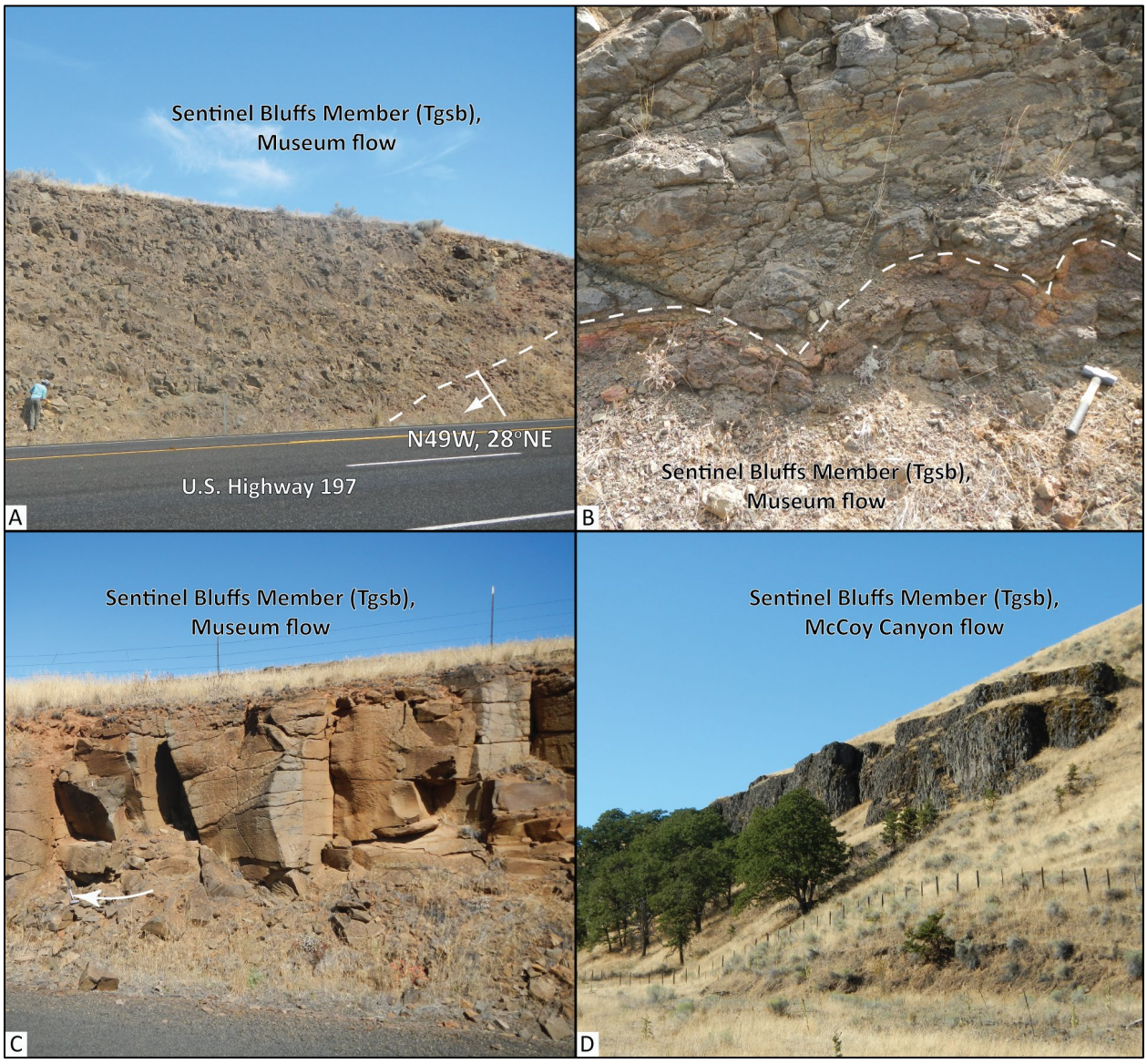

**Figure 6-66. Hand sample and thin section photographs of the Sentinel Bluffs Member (Tgsb). (a) Typical aphyric to very sparsely microporphyritic hand sample of upper Sentinel Bluffs Member. (b) Thin section of the sample in A under cross- polarized light (XPL). (c) Hand sample of basalt exposed in the middle part of the Sentinel Bluffs Member. (d) Thin section of the sample in C under cross- polarized light (XPL). (e) Hand sample of the lowermost exposed Sentinel Bluffs Member. (f) Thin section of the sample in E under cross- polarized light (XPL). Scale bar for hand sample photographs is 2.5 cm (1 in) tall. Scale bar for all thin sections is 7 mm (0.3 in) in width. Photo credits: J.D. McClaughry, 2015.**

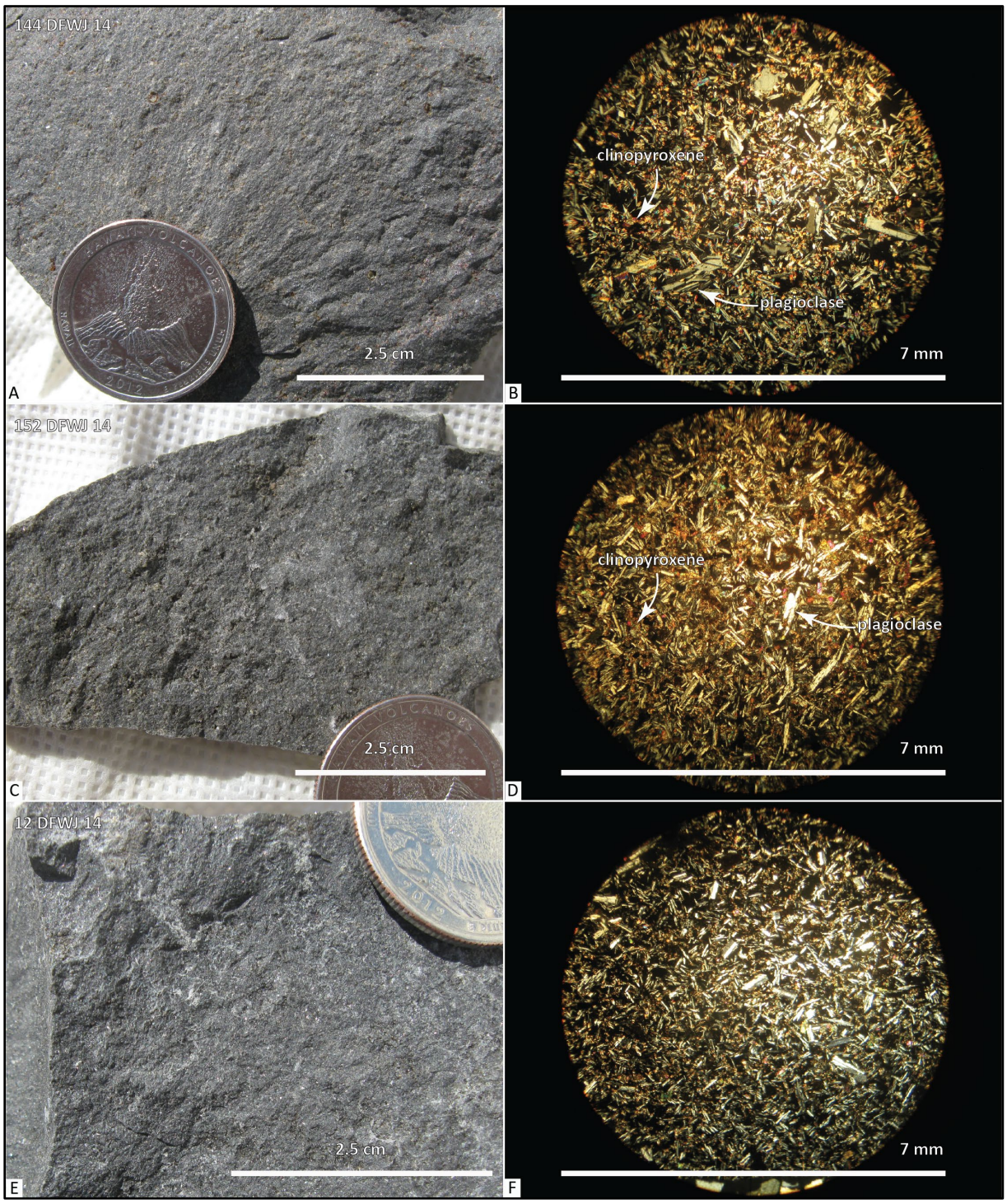

**Tgww** **Winter Water Member (lower Miocene)—**Basaltic andesite lava flow ($SiO_2$ = 55.19 to 56.43 weight percent; $TiO_2$ =2.02 to 2.12 weight percent; *n* = 16 analyses) mapped below the Sentinel Bluffs Member (**Tgsb**) along Dry Creek in the southeast part of the map area (**Figure 5-7**, **Figure 5-10a-b**, **Figure 6-67**, **Figure 6-68**; **Table 6-5**; Plate 3; Appendix). The Winter Water Member (**Tgww**) is also exposed beneath the Sentinel Bluffs Member (**Tgsb**) and above a basaltic andesite flow of the Prineville Basalt (**Tpba**) in Butler Canyon along U.S. Highway 197, just south of the map area (**Figure 6-1**; Plates 1, 2, and 3, cross sections; Hagstrum and others, 2010; M.J. Sawlan and J.T. Hagstrum, written commun., 2015). Unit **Tgww** is chemically distinguished from the underlying Ortley member (**Tgo**) by higher amounts of titanium (avg $TiO_2$ = 2.10 weight percent) and from the overlying Sentinel Bluffs Member (**Tgsb**) by lesser amounts of magnesium (avg MgO = 3.43 weight percent) (*n* = 38 analyses in the Middle Columbia Basin; **Figure 5-10a-b**; **Table 6-5**; Appendix; J.D. McClaughry unpublished geologic mapping, 2015, 2016). Outcrops in the map area are typically hackly jointed and are composed of irregular, narrow (5 to 15 cm [2 to 5.9 in] wide) columns that extend across horizontal, vesicle-rich bands (**Figure 6-67**). Partially emptied lava tubes, up to 0.5 m (1.6 ft) across, are present near the base of unit in Dry Canyon (**Figure 6-68**; Plate 3). Talus slopes beneath outcrops are typically composed of gray and gray-brown, angular, equidimensional fragments up to 10 cm (3.9 in) in diameter. Thickness of the Winter Water Member (**Tgww**) along Dry Creek is >40 m (131 ft), but the base of the unit is not exposed in that area (Plate 3). The thickness of the Winter Water Member (**Tgww**) is ~58.5 m (192 ft) in Butler Canyon (Hagstrum and others, 2010; M.J. Sawlan and J.T. Hagstrum, written commun., 2015). Typical hand samples of the Winter Water Member (**Tgww**) are medium dark gray (N4) to dark gray (N2), aphyric to very sparsely microporphyritic and glomeroporphyritic, containing 1 to 2 percent (vol.) clear, euhedral, prismatic plagioclase microphenocrysts and v-shaped or radial, spoked glomerocrysts <2 mm (0.1 in) across, contained within an inequigranular hypocrystalline groundmass of plagioclase, intergranular clinopyroxene, intersertal glass, and minor opaques Fe-Ti oxides (**Figure 6-69**). Conspicuous plagioclase phenocrysts and glomerocrysts are diagnostic field characteristics which distinguishes this unit from other lava flows in the N2 magnetostratigraphic unit (Reidel and others, 1989; Wells, personal commun., 2011). Tolan (1982) indicated that glomerocrysts and phenocrysts may be less abundant within the entablature portion of the flow.

The Winter Water Member (**Tgww**) has normal magnetic polarity and is assigned an early Miocene age bracketed by U/Pb dates of 16.066 ± 0.04 Ma for ash from the overlying Vantage Horizon and 16.254 ± 0.034 Ma for ash between the Wapshilla Ridge and Meyer Ridge Members of the underlying R2 magnetostratigraphic unit (Kasbohm and Schoene, 2018; **Figure 5-7**, **Figure 6-1**). Equivalent to the Winter Water flow of Powell (1978), the Winter Water unit of Reidel and others (1989), and the Winter Water Member of Reidel and Tolan (2013).

**Figure 6-67. The Winter Water Member (Tgww) cropping out along Fargher Road in the upper part of Dry Creek (45.345916, -121.097398). Unit Tgww flows here directly overlie thin beds of siltstone and are characterized by irregular, narrow columns and hackly jointing. View is looking east. Photo credit: H.H. Herinckx, 2017.**

**Figure 6-68. Partially emptied lava tubes near the base of the Winter Water Member (Tgww) along Fargher Road in the upper part of Dry Creek. (45.345916, -121.097398). Red-dashed lines outline partially emptied lava tubes. Scale bar is 0.5 m (1.6 ft) tall. View is looking east. Photo credit: H.H. Herinckx, 2017.**

**Figure 6-69. Hand sample and thin section photographs of the Winter Water Member (Tgww). (a) Typical aphyric hand sample. Scale bar is 2.5 cm (1 in) tall. (b) Thin section under cross-polarized light (XPL). (c) Same view as in B under plane-polarized light (PPL). Scale bar for thin section photographs is 7 mm (0.3 in) wide. Photo credits: J.D. McClaughry, 2018.**

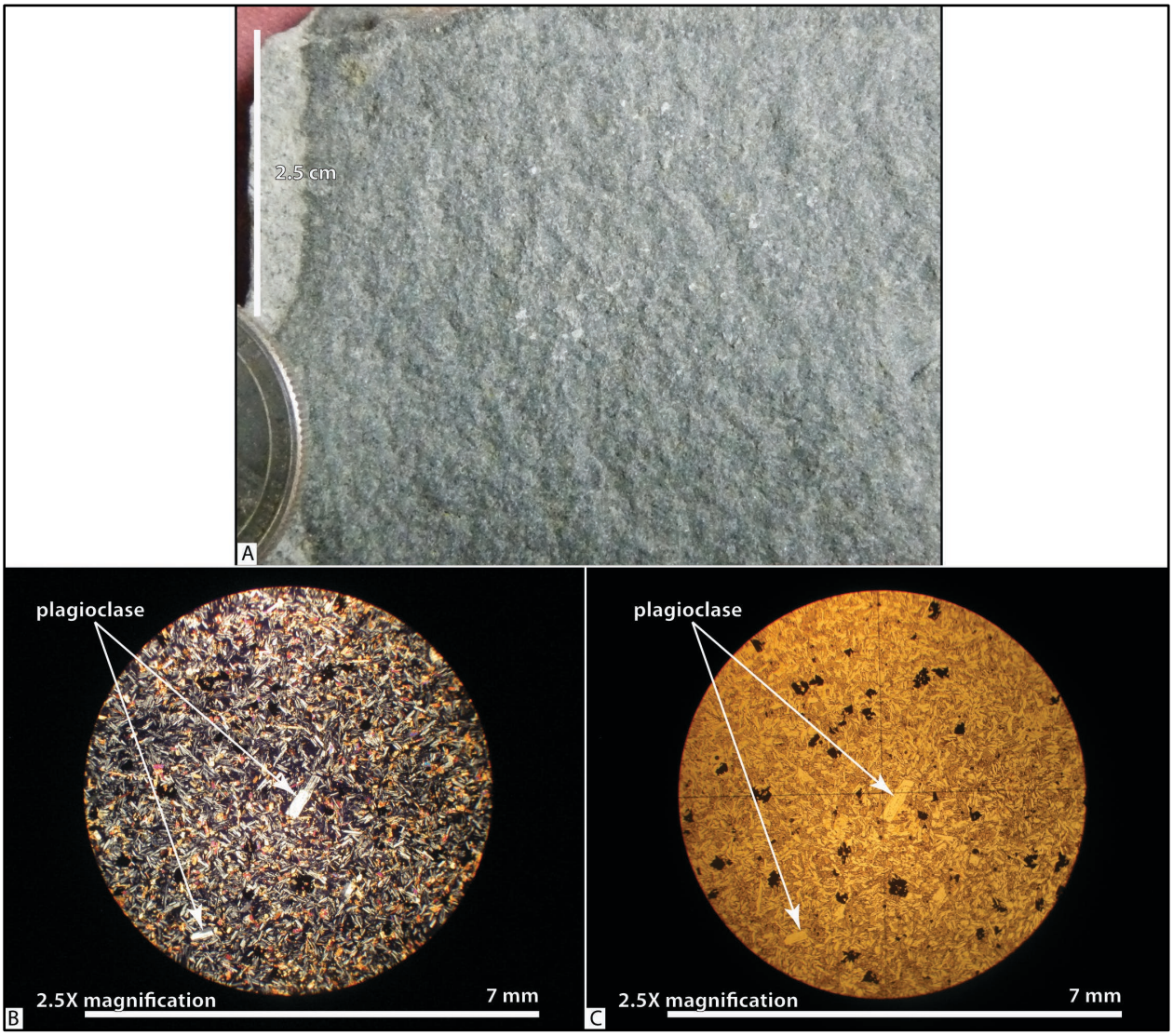


***NOTE***— The Winter Water Member (**Tgww**) is the stratigraphically lowest unit mapped in the Dufur area. The CRBG units (**Tgo**, **Tgac**, **Tgbc**, **Tggc**, **Tgu**, **Tpba**, **Tpbd**) discussed below are not mapped in the study area but are shown in the subsurface of geologic cross sections displayed on Plates 1, 2, and 3 and in the Time Rock chart shown in **Figure 6-1**. Subsurface interpretation of the distribution of geologic units displayed in cross sections beneath the Winter Water Member (**Tgww**) in the Dufur area is interpreted on the basis of unpublished geologic mapping and measured stratigraphic sections provided by M.J. Sawlan and J.T. Hagstrum (written commun., 2015) in Butler Canyon south of the map area. The precise northern limit of some CRBG units shown in the subsurface of geologic cross sections on Plates 1, 2, and 3 is not known.

**Tgo** **Ortley member (lower Miocene) (cross sections only)—**Medium dark gray (N4) to grayish black (N2), aphyric, iron-rich basaltic andesite exposed in Butler Canyon. Lava flows of the Ortley member (**Tgo**) in Butler Canyon lie directly beneath a basaltic andesite flow of the Prineville Basalt (**Tpba**) and reach a composite thickness there of ~55.5 m (182 ft) (**Figure 6-1**; Plates 1, 2, and 3, cross sections; Hagstrum and others, 2010; M.J. Sawlan and J.T. Hagstrum, written commun., 2015). Samples obtained from the Ortley Member (**Tgo**) across the Middle Columbia Basin have a basaltic andesite chemical composition with ~55.93 weight percent $SiO_2$, ~1.99 weight percent $TiO_2$, ~3.58 weight percent MgO, and ~0.33 weight percent $P_2O_5$ (*n* = 29 analyses; **Figure 5-10a-b**; McClaughry and others, 2012; J.D. McClaughry unpublished geologic mapping 2015, 2016); analyses of the unit in the Middle Columbia Basin are comparable to those obtained to the east on the Columbia Plateau ($SiO_2$ = ~56.30 weight percent, $TiO_2$ = ~1.98 weight percent, MgO = ~3.52 weight percent, and $P_2O_5$ = ~0.34 weight percent; avg of 239 analyses reported by Reidel and Tolan, 2013).

The Ortley member (**Tgo**) has normal magnetic polarity and is assigned an early Miocene age bracketed by U/Pb dates of 16.066 ± 0.04 Ma for ash from the overlying Vantage Horizon and 16.254 ± 0.034 Ma for ash between the Wapshilla Ridge and Meyer Ridge Members of the underlying R2 magnetostratigraphic unit (Kasbohm and Schoene, 2018; **Figure 5-7**, **Figure 6-1**). Equivalent to the low-MgO flows of Wright and others (1973), the Ortley unit of Reidel and others (1989), and the Ortley member of Reidel and Tolan (2013).

**Tgac** **Armstrong Canyon member (lower Miocene) (cross sections only)—**Medium dark gray (N4) to grayish black (N2), rarely to sparsely plagioclase phyric, iron-rich basaltic andesite exposed in Butler Canyon. A single lava flow of the Armstrong Canyon member (**Tgac**) is exposed beneath the Ortley Member (**Tgo**) in Butler Canyon and reaches a composite thickness there of ~60 m (197 ft) (**Figure 6-1**; Plates 1, 2, and 3, cross sections; Hagstrum and others, 2010; M.J. Sawlan and J.T. Hagstrum, written commun., 2015). Samples obtained from the Armstrong Canyon member (**Tgac**) across the Columbia Plateau have a basaltic andesite chemical composition with ~55.37 weight percent $SiO_2$, ~1.87 weight percent $TiO_2$, ~4.16 weight percent MgO, and ~0.31 weight percent $P_2O_5$ (Average of 150 analyses reported by Reidel and Tolan, 2013).

The Armstrong Canyon member (**Tgac**) has normal magnetic polarity and is assigned an early Miocene age bracketed by U/Pb dates of 16.066 ± 0.04 Ma for ash from the overlying Vantage Horizon and 16.254 ± 0.034 Ma for ash between the Wapshilla Ridge and Meyer Ridge Members of the underlying R2 magnetostratigraphic unit (Kasbohm and Schoene, 2018; **Figure 5-7**, **Figure 6-1**). Equivalent to the Armstrong Canyon unit of Reidel and others (1989) and the Armstrong Canyon member of Reidel and Tolan (2013).

**Tgbc** **Buttermilk Canyon member (lower Miocene) (cross sections only)—**Medium dark gray (N4) to grayish black (N2), rarely to sparsely plagioclase phyric, iron-rich basaltic andesite exposed in Butler Canyon. A single lava flow of the Buttermilk Canyon member (**Tgbc**) is exposed beneath the Armstrong Canyon member (**Tgac**) in Butler Canyon and reaches a composite thickness there of ~30 m (98 ft) (**Figure 6-1**; Plates 1, 2, and 3, cross sections; Hagstrum and others, 2010; M.J. Sawlan and J.T. Hagstrum, written commun., 2015). Samples obtained from the Buttermilk Canyon member (**Tgbc**) across the Columbia Plateau have a basaltic andesite chemical composition with ~55.19 weight percent $SiO_2$, ~2.19 weight percent $TiO_2$, ~3.57 weight percent MgO, and ~0.38 weight percent $P_2O_5$ (Average of 10 analyses reported by Reidel and Tolan, 2013).

The Buttermilk Canyon member (**Tgbc**) has normal magnetic polarity and is assigned an early Miocene age bracketed by U/Pb dates of 16.066 ± 0.04 Ma for ash from the overlying Vantage Horizon and 16.254 ± 0.034 Ma for ash between the Wapshilla Ridge and Meyer Ridge Members of the underlying R2 magnetostratigraphic unit (Kasbohm and Schoene, 2018; **Figure 5-7**, **Figure 6-1**). Unit **Tgbc** is equivalent to the Buttermilk Canyon member of Hagstrum and others (2010) and Reidel and Tolan (2013).

#### 6.3.4.6.2 *Reversed-polarity (R2) magnetostratigraphic unit*

The R2 magnetostratigraphic unit is the most aerially extensive Grande Ronde Basalt magnetostratigraphic unit, made up of chemically distinctive lava flow packages that cover an area of ~117,730 km$^2$ (45,456 mi$^2$). The estimated volume of the R2 magnetostratigraphic unit is ~56,000 km$^3$ (13,435 mi$^3$) (Reidel and Tolan, 2013). Kasbohm and Schoene (2018) indicate that a majority of the R2 unit ranges in age between 16.288 ± 0.046 Ma and 16.210 ± 0.047 Ma (**Figure 5-7**). The R2 magnetostratigraphic unit is locally subdivided into the following units:

**Tggc** **Grouse Creek member (lower Miocene) (cross section only)—**Black (N1) to medium bluish gray (5B 5/1), aphyric to rarely plagioclase phyric, iron-rich basaltic andesite exposed in Butler Canyon. Lava flows of the Grouse Creek member (**Tggc**) exposed in Butler Canyon lie directly beneath Bowman Dam chemical type flows of the Prineville Basalt (**Tpbd**) and reach a composite thickness there of ~62.6 m (205 ft) (**Figure 6-1**; Plates 1, 2, and 3, cross sections; Hagstrum and others, 2010; M.J. Sawlan and J.T. Hagstrum, written commun., 2015). The base of the Grouse Creek member (**Tggc**) is not exposed in Butler Canyon. Samples obtained from the Grouse Creek member (**Tggc**) across the Middle Columbia Basin have a basaltic andesite chemical composition with ~55.97 weight percent $SiO_2$, ~1.96 weight percent $TiO_2$, ~3.72 weight percent MgO, and ~0.33 weight percent $P_2O_5$ (*n* = 11 analyses; **Figure 5-10a-b**; McClaughry and others, 2012; J.D. McClaughry unpublished geologic mapping); analyses of the unit in the Middle Columbia Basin are comparable to those obtained to the east on the Columbia Plateau ($SiO_2$ = ~55.75 weight percent, $TiO_2$ = ~2.03 weight percent, MgO = ~3.51 weight percent, and $P_2O_5$ = ~0.34 weight percent; avg of 150 analyses reported by Reidel and Tolan, 2013). The Grouse Creek member (**Tggc**) has transitional reversed magnetic polarity and can be recognized by a steep magnetic inclination (-85°) (Wells and others, 2009).

The Grouse Creek member (**Tggc**) is assigned an early Miocene age bracketed by U/Pb dates of 16.066 ± 0.04 Ma for ash from the overlying Vantage Horizon and 16.254 ± 0.034 Ma for ash between the underlying Wapshilla Ridge and Meyer Ridge Members of the R2 magnetostratigraphic unit (Kasbohm and Schoene, 2018; **Figure 5-7**, **Figure 6-1**). Unit **Tggc** lava flows are chemically and lithologically similar to those in the Ortley Member (**Tgo**) but are distinguished on the basis of magnetic polarity. These flows (**Tggc**) are distinguished from the older Wapshilla Ridge Member on the basis of lesser amounts of $TiO_2$. Equivalent to the Grouse Creek flows of Ross (1978), the Grouse Creek unit of Reidel and others (1989), and the Grouse Creek member of Reidel and Tolan (2013).

**Tgu** **Grande Ronde Basalt, undivided (lower Miocene) (cross section only)—**Older flows of the Grande Ronde Basalt that lie stratigraphically below the Grouse Creek member (**Tggc**) but are not exposed either in the map area or in Butler Canyon. The base of the Grouse Creek member (**Tggc**) is not

exposed in Butler Canyon and is therefore queried on geologic cross sections (**Figure 6-1**; Plates 1, 2, and 3, cross sections).

#### 6.3.4.7 Prineville Basalt

The Prineville Basalt is a geographically restricted, but chemically distinctive CRBG unit that covers an area of ~11,440 km$^2$ (4,417 mi$^2$) in central and north-central Oregon (**Figure 6-1**; Plates 1, 2, and 3, cross sections). The estimated volume of the Prineville Basalt is ~590 km$^3$ (142 mi$^3$) (Reidel and others, 2013). Several lava flows of the Prineville Basalt are interbedded with the Grande Ronde Basalt in Butler Canyon (Hagstrum and others, 2010; M. Sawlan and J. Hagstrum, written commun., 2015) and are subdivided into the following units:

**Tpba** **Prineville Basalt, basaltic andesite (lower Miocene) (cross section only)—**Medium dark gray (N4) to grayish black (N2), aphyric to sparsely plagioclase-microporphyritic, iron-rich basalt and basaltic andesite lava flows exposed in Butler Canyon. Basaltic andesite lava flows of the Prineville Basalt (**Tpba**) in Butler Canyon lie directly beneath the Winter Water Member (**Tgww**) and reach a composite thickness of ~47.5 m (156 ft) (**Figure 6-1**; Plates 1, 2, and 3, cross sections; Hagstrum and others, 2010; M.J. Sawlan and J.T. Hagstrum, written commun., 2015). Samples obtained from upper lava flows of the Prineville Basalt have a basaltic to basaltic andesite and basaltic trachyandesite chemical compositions with ~54.81 weight percent $SiO_2$, ~2.57 weight percent $TiO_2$, ~3.36 weight percent MgO, ~1.41 weight percent $P_2O_5$, and ~2159 ppm Ba (avg of 11 analyses reported by Smith, 1986; Hooper and others, 1993; Lite and Gannett, 2002; McClaughry and others, 2009). Basaltic andesite lava flows of the Prineville Basalt have normal magnetic polarity (Hooper and others, 1993). Hooper and others (1993) correlate the Bowman Dam chemical type of the Prineville Basalt with the normal-polarity (N2) magnetostratigraphic unit of the Grande Ronde Basalt. The basalt is distinguished geochemically from similarly aged lava flows of the Grande Ronde Basalt by relatively higher amounts of titanium and remarkably high incompatible element concentrations of phosphorous and barium.

The Prineville Basalt (**Tpba**) is assigned an early Miocene age bracketed by U/Pb dates of 16.066 ± 0.04 Ma for ash from the overlying Vantage Horizon and 16.254 ± 0.034 Ma for ash between the underlying Wapshilla Ridge and Meyer Ridge Members of the R2 magnetostratigraphic unit (Kasbohm and Schoene, 2018; **Figure 5-7**, **Figure 6-1**). Equivalent to the Prineville Basalt as defined by Uppuluri (1974), Smith (1986), Tolan and others (1989), and Hooper and others (1993).

**Tpbd** **Prineville Basalt, Bowman Dam chemical type (lower Miocene) (cross section only)—**Medium dark gray (N4) to grayish black (N2), aphyric to sparsely plagioclase-microporphyritic, iron-rich basalt and basaltic andesite lava flows exposed in Butler Canyon. Bowman Dam chemical type Prineville Basalt (**Tpbd**) lava flows lie directly beneath the Buttermilk Canyon member (**Tgbc**) and reach a composite thickness of ~57 m (187 ft) in Butler Canyon (**Figure 6-1**; Plates 1, 2, and 3, cross sections; Hagstrum and others, 2010; M.J. Sawlan and J.T. Hagstrum, written commun., 2015). Samples obtained from Bowman Dam chemical type lava flows (**Tpbd**) have basaltic to basaltic andesite and basaltic trachyandesite chemical compositions with ~51.78 weight percent $SiO_2$, ~2.71 weight percent $TiO_2$, ~4.25 weight percent MgO, ~1.39 weight percent $P_2O_5$, and ~2075 ppm Ba (average of 49 analyses reported by Smith, 1986; Hooper and others, 1993; Lite and Gannett, 2002, McClaughry and others, 2009). The unit (**Tpbd**) is distinguished geochemically

from similarly aged lava flows of the Grande Ronde Basalt by relatively higher amounts of titanium and remarkably high incompatible element concentrations of phosphorous and barium. Lower Bowman Dam chemical type lava flows (**Tpbd**) have reversed magnetic polarity, while the upper flow at the type section at Bowman Dam south of Prineville has normal magnetic polarity (Hooper and others, 1993). Hooper and others (1993) correlate the Bowman Dam chemical type of the Prineville Basalt (**Tpbd**) with the uppermost part of the reversed-polarity (R2) magnetostratigraphic unit and lowest part of the normal-polarity (N2) magnetostratigraphic unit of the Grande Ronde Basalt.

The Prineville Basalt (**Tpbd**) is assigned an early Miocene age bracketed by U/Pb dates of 16.066 ± 0.04 Ma for ash from the overlying Vantage Horizon and 16.254 ± 0.034 Ma for ash between the underlying Wapshilla Ridge and Meyer Ridge Members of the R2 magnetostratigraphic unit (Kasbohm and Schoene, 2018; **Figure 5-7**, **Figure 6-1**). Unit **Tpbd** is equivalent to the Prineville Basalt as defined by Uppuluri (1974), Smith (1986), Tolan and others (1989), and Hooper and others (1993).

# 7.0 STRUCTURE

## 7.1 Introduction

Geologic structure in the Dufur area is defined by the mapped distribution of geologic units, faults, topographic lineaments (as observed in 1-m lidar DEMs and 10-m DEMs), folds, and bedding attitudes (Plates 1, 2, and 3; Appendix). Primary structural features (e.g., slickensides or fault breccia) were rarely observed in the field. Fault zones, such as those shown on Plates 1, 2, and 3 are recognized on the basis of offset geologic contacts (**Figure 7-1**), small-scale offsets observed in roadcut and natural exposures, missing units, topographic lineaments and linear alignments of drainages as indicators of possible movement, breccia zones (**Figure 7-2**), and structure contours generated from subsurface lithologic data obtained from water well logs (**Figure 7-3**).

Problems in recognizing faults in the Dufur area are attributed to a number of factors. Many CRBG flows, especially in the upper part of the Grande Ronde Basalt and Wanapum Basalt flowed onto and infilled irregular flow- or structurally deformed surfaces. Determining fault piercing points in such irregularly layered units is problematic. In some cases, where strike-slip faults cut CRBG units, distinct fault planes are not readily apparent. Instead observed deformation is apparently accommodated by often diffuse shear across and around massive columnar cooling joint sets (**Figure 7-2**). Difficulties recognizing faults in the Dalles Formation arise as 1) lateral facies changes in the formation can be abrupt; 2) fault planes are not expected to be well preserved in moderately to weakly indurated strata; 3) those faults actually observed often have small offsets (< several cm in some cases) (**Figure 7-1**); 4) separation of beds can be difficult to determine in the field; and 5) areas of distinctly contrasting lithologies (e.g., Dalles Formation versus CRBG) are rarely exposed along stream drainages in the map area.

Remote sensing of the locations of faults and bed offsets in the Dalles Formation is improved through the use of enhanced 1-m lidar DEMs, processed using the Sky-View Factor computation tool (Zakšek and others, 2011; see discussion of Sky-View tool in *Orientation Points* in the Appendix). Sky-View visualizes hillshade models using diffuse illumination, overcoming the common problem of direct illumination, which can obscure linear objects that lie parallel to the direction of the light source and saturation of shadow areas.

**Figure 7-1. Faults cutting sandstone and pebbly sandstone in the Dalles Formation (Tmdl) along Eightmile Road in the northwest part of the map area. Dalles sedimentary beds here are cut by several small-offset (< 5 cm [2 in]), down-on-the east normal faults(45.461593, -121.250972). Dashed lines are fault planes. Solid line is a bedding contact. Arrows show relative offset of faults. iPad for scale is 25 cm (9.8 in) across. View is looking north. Photo credit: C.A. Niewendorp, 2015.**

**Figure 7-2. Fault breccia in Columbia River Basalt in the Dufur area. (a) A boudin-like zone of brecciated basalt intervening along the boundaries of columnar joint sets in the upper part of the Basalt of Sand Hollow (Twfh) along lower Pine Creek near Dufur (45.440301, -121.131046). (b) Planar zone of brecciated basalt cutting across columnar joint sets in the upper part of the Basalt of Sand Hollow (Twfh) in lower Pine Creek near Dufur (45.440629, -121.130771). Hammer for scale in both photographs is 25 cm (9.8 in) tall. Photo credits: J.D. McClaughry, 2016.**

**Figure 7-3. Structure contour map of the upper surface of the Basalt of Sentinel Gap (Twfs) in the Dufur West 7.5′ quadrangle (Plate 1). Contours are derived from surface and water well elevation points (yellow circles with black centers). Black contour lines represent 10-ft structure contours; red lines are 100-ft index contours. Contours were generated from using ArcToolbox/Spatial Analyst Tools/Interpolation/Spline with Barriers and are contained within the geodatabase feature class IsoStructureLines. Underlying slope gradient map colors range from white (high elevations) to orange (low elevations).**

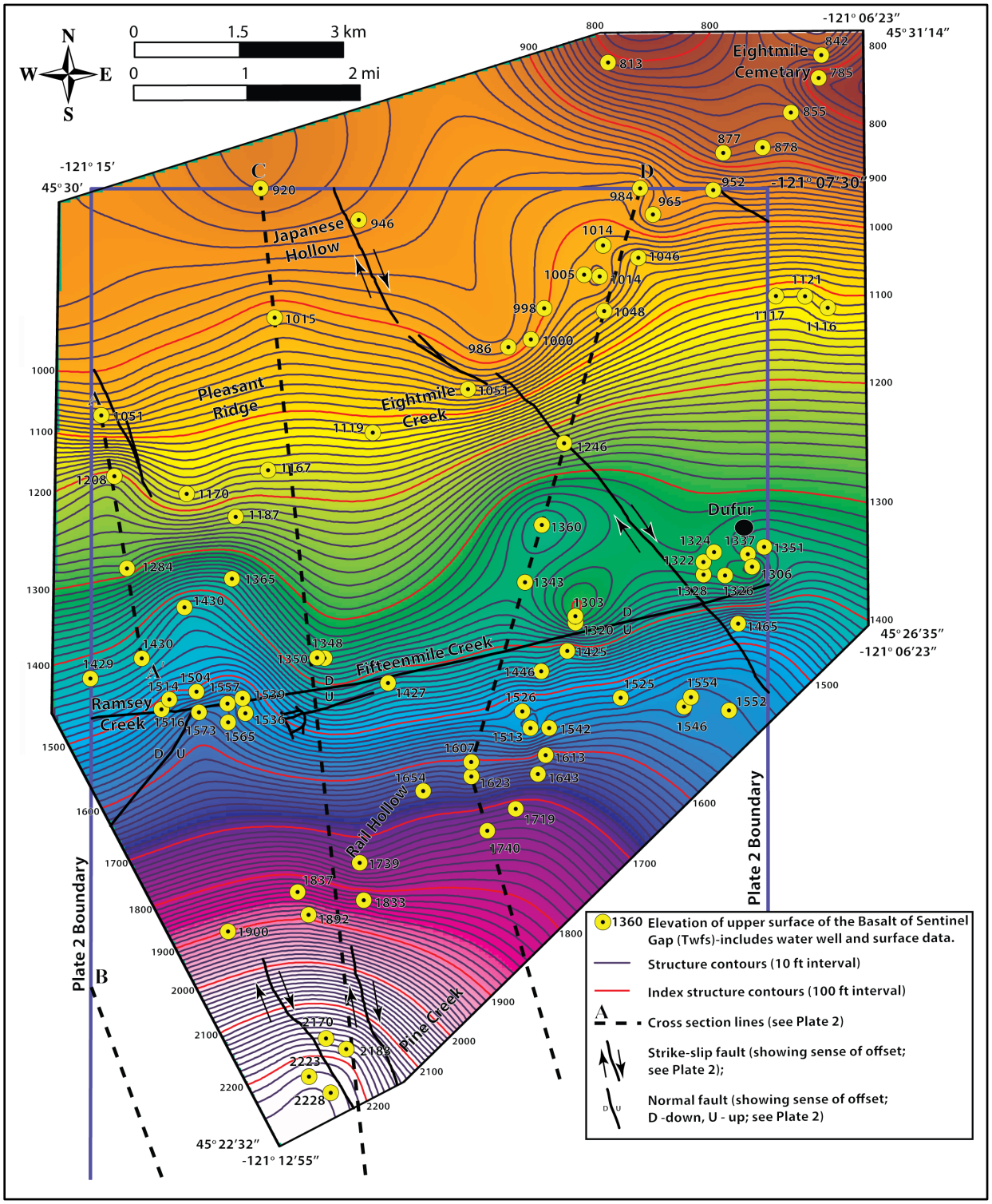

## 7.2 Yakima Fold Belt

The CRBG, Dalles Formation, and to a much lesser extent younger late Pliocene sedimentary and volcanic rocks in the Dufur area are broadly folded into a series of east-northeast-trending folds. These structures are related to deformation occurring within the Yakima Fold Belt, a broad zone of regional east-west- to northeast-trending asymmetric folds covering much of the western and west-central Columbia Plateau and extending west beneath the Cascade Range (**Figure 5-2**; see discussion of the Yakima Fold Belt in section 5.1; Swanson and others, 1979b, 1981; Anderson, 1987; Watters, 1989; Reidel and Campbell, 1989; Tolan and Reidel, 1989, Tolan and others, 2009a; Anderson and others, 2013). Please refer to the detailed discussion of the Yakima Fold Belt in Section 5 of this report.

### 7.2.1 Yakima Fold Structures in the Dufur Area

The Dufur area lies in a moderately to little deformed structural area situated between asymmetric, locally overturned and faulted Yakima Fold Belt anticlinal ridges/uplifts centered on The Dalles on the north and Tygh Ridge on the south (**Figure 5-3**). The exposed stack of CRBG lava flows in the map area is characterized by a shallow, 1˚ to 3˚ regional northward dip, with flows gently warped by closely spaced, open folds (Plates 1, 2, and 3, cross sections). Folds in the CRBG in the map area have wavelengths on the order of 0.5 to 2.5 km (0.3 to 1.6 mi). North of Fifteenmile and Pine creeks, the Dalles Formation thickens filling a northward deepening synclinal trough (Plates 1, 2, and 3, cross sections). This thickened section of Dalles Formation largely buries the CRBG, obscuring the structural character of the older units. Dalles Formation units have near-horizontal to shallow-dipping (1° to 6°) bedding orientations and have broad folds with axes paralleling the major drainages of Fivemile, Eightmile, and Fifteenmile Creeks (Plates 1, 2, and 3, cross sections). Fold wavelengths in the Dalles Formation are similar to that observed in the CRBG on the order of 0.5 to 2.5 km (0.3 to 1.6 mi). Contrary to the general 1˚ to 3˚ regional northward dip of CRBG, many lidar-derived orientations for the Dalles Formation in the Wolf Run, Dufur West, and Dufur East 7.5′ quadrangles indicate complex, generally east-northeast-striking and southward-dipping individual beds. This contrast may be due in part to original complex depositional contacts created during aggradation and outbuilding of the late Miocene arc-adjacent alluvial plain above the CRBG, complex post-deposition folding, and/or problems arising from field or lidar-based orientation measurements taken on shallow-dipping flow surfaces.

The CRBG lava flows are abruptly deformed into a northeast- to east-trending monocline in the southern part of the Dufur area (Plate 2, cross sections B-B', C-C', and D-D'). This monocline, herein referred to as the Dry Creek monocline, was identified through detailed geologic mapping of CRBG flows, an abrupt break and steepening of topography recognized in 1-m lidar DEMs, and substantial steepening of bedding orientation of CRBG flows across the structure (up to 28° NE.) (**Figure 6-65a**). Part of the abrupt linear steepening on the northside of the Dry Creek monocline is inferred to have been aided by a steeply dipping reverse fault, herein referred to as the Mays Canyon Creek fault (Plate 2). Evidence for this fault includes (1) a generally northeast- to east-striking lineament that cuts across the southern part of the map area, (2) geologic mapping that places older units above younger units, (3) thinning and absence of stratigraphic units across the fault trace, (4) and surface manifestations of fossil hot-springs along the inferred fault trace (Plate 2, cross sections B-B', C-C', and D-D').

Evidence for the absence of stratigraphic units can be found between Hix Road and mile marker 19 on U.S. Highway 197 south of Dufur (Plate 2). In this part of the Dufur area, the younger Basalt of Sand Hollow (**Twfh**) sits directly on the Sentinel Bluffs Member (**Tgsb**). The Basalt of Ginkgo (**Twfg**), typically found between units **Twfh** and **Tgsb** in the Dufur area, is conspicuously missing. The local absence of the Basalt

of Ginkgo (**Twfg**) may be due to structural deformation and localized uplift of the area associated with the Mays Creek Canyon fault and the Dry Creek monocline during the time intervening between Grande Ronde and Frenchman Springs eruptions **Figure 5-7**; Plate 2). This structural topography, generated concurrently with or closely following the end of Grande Ronde eruptions, appears to have controlled the distribution of Ginkgo lava flows (**Twfg**) across this part of the map area. Thinning, folding, and faulting of the Basalt of Sand Hollow (**Twfh**) indicates structural uplift along the Dry Creek monocline persisted at least through latest part of Frenchman Springs eruptions (~15.9 Ma) (**Figure 5-7**; Plate 2).

Subtly north-dipping flows of the CRBG are also warped along the Tygh Ridge monocline, mapped along Tygh Ridge in the northern part of the Sherars Bridge 7.5′ quadrangle (Plate 3). CRBG flows cropping out north of Old Tygh Road have dip orientations from 1° to 2° N., typical of the observed regional dip. South of Old Tygh Road, across the Tygh Ridge monocline, the orientations of CRBG flows (**Twfh**, **Twfg**) steepens abruptly to 7° to 9° N. (Plate 3, cross section A-A′).

East-northeast-striking folds in the Dufur area are locally segmented by N. 20° W.- to N. 30° W-striking strike-slip faults. Previous workers in the Columbia River Gorge (Anderson, 1987; Anderson and others, 2013) and on the Columbia Plateau (Reidel and Campbell, 1989) have referred to these types of fold-segmenting faults as wrench faults. Spatial relationships between folds, thrust faults, and strike-slip faults indicate a mutual development of all three components during progressive deformational phases, occurring in the Yakima Fold Belt from the middle Miocene and into the Quaternary (Anderson, 1987; Anderson and others, 2013).

Northwest-southeast-striking faults in the map area appear to have become active in latest Frenchman Springs time (~15.9 Ma), with some offset of the CRBG stack occurring prior to deposition of the Dalles Formation, beginning in the late Miocene (~9 Ma). Further structural disruption of the Dalles Formation and younger early Pliocene units and topographic lineaments cutting obliquely across Dalles Formation-capped plateaus indicate that northwest-southeast-striking faults remained periodically active into the Pliocene. Activity along these faults could extend to the present time, but no direct evidence supporting such interpretations has yet been documented.

## 7.3 Faulting in the Wolf Run and Friend 7.5′ quadrangles (Plate 1)

A northeast-striking normal fault (N.20°E. to N.30°E.) can be traced from Fifteenmile Creek near the southern edge of the Wolf Run 7.5′ quadrangle to the quadrangle's northeastern corner. At its southern end, Sherrod and Scott (1995) mapped a strand of this fault crossing Fifteenmile Creek and also recognized a normal down-on-the-east sense of slip. This fault is believed to extend over a distance of ~15.3 km (9.5 mi) and is recognized on the basis of offsets (down-on-the-east) in Dalles Formation strata observed in a roadcut exposure (e.g., Walston Grade Road) on Fivemile Creek, bed offsets observed and mapped in 1-m lidar DEMs and Sky-View lidar hillshade models, and offset rock ledges along stream channels. This fault strand continues at least 3.1 mi (4.9 km) northeasterly into the adjacent The Dalles South 7.5′ quadrangle.

North of Pleasant Ridge and Fivemile Creek, in the northern part of the Wolf Run 7.5′ quadrangle, traces of fault strands are recognized in 1-m lidar DEMs and Sky-View lidar hillshade models. These fault strands are mapped by the presence of linear topographic features. A normal down-on-the-east sense of offset is suggested for the north-south-striking fault that is parallel to Dutch Flat Road. This fault strand continues northward into the adjacent Brown Creek 7.5′ quadrangle, where it ties in with the Maupin fault system (**Figure 1-2**). The Maupin fault is a major, high-angle right-lateral strike-slip to oblique-slip fault

zone in this part of north-central Oregon, discontinuously traced between the Columbia River, Tygh Ridge, and Maupin (**Figure 5-3**; Anderson and others, 2013).

Between Old Friend Road and Camp Friend Road and along the northern side of Larch Creek, in the southern part of the map area, short north-striking faults cut the tuff breccia of Engineers Creek (**Tpdd1**). These faults are recognized by subtle topographic lineaments and contorted ridges recognized in 1-m lidar DEMs and Sky-View lidar hillshade models. Normal faulting is suggested by offset of some ridges. Continuation of these faults to the south into the tuff of Friend (**Tptf1, Tptf2**) is unknown, as distinct topographic lineaments appear to die out.

Topographic lineaments cutting obliquely across plateaus underlain by the 7.91 Ma dacite of Wolf Run (**Tmdw**) and the 3.02 Ma dacite of Fifteenmile Creek (**Tpdf**) indicate that faults in the Wolf Run and Friend area have been active through the latest Pliocene. A N.30°W.-striking fault strand appears to offset the latter in the southern part of the map area while a north-south-striking normal fault (slip to the east) strand cuts the former. Activity along these faults could extend to the present time, but no stratigraphic relationships or direct evidence supporting such interpretations is yet documented.

## 7.4 Faulting in the Dufur West and Postage Stamp Butte 7.5′ quadrangles (Plate 2)

Several northwest-striking faults are mapped through Dalles Formation and CRBG units in the Dufur West and Postage Stamp Butte 7.5′ quadrangles (Plate 2).

Between Pleasant Ridge and Dufur, in the north-central part of the map area, a northwest-southeast-striking right-lateral strike-slip fault cuts the Dalles Formation and CRBG (Plate 2). The fault is recognized on the basis of offsets in Dalles strata observed in a roadcut exposure on Fivemile Creek (north of the map area, Dalles South 7.5' quadrangle; **Figure 1-2**), bed offsets observed and mapped in 1-m lidar DEMs and Sky-View lidar hillshade models in the northern part of the map area, and offset ledges along stream channels (e.g., north embankment of Fifteenmile Creek, Plate 2). Southeast of the city of Dufur, along US Highway 197, the trace of the fault is recognized by subtle topographic lineaments crossing ridges, the juxtaposition of different CRBG flow units, and localized areas of scattered calcite float along the fault trace. Diffuse brecciated shear zones and boudin-like features within otherwise undisturbed columnar-jointed basalt exposed in the base of Pine Creek suggest the probable location of the fault trace southeast of U.S. Highway 197 (**Figure 7-2**). The fault cannot be traced further than Mays Canyon Creek, southeast of U.S. Highway 197 (Plate 3).

Three N.30°W.-striking, right-lateral strike-slip fault strands, herein referred to as the Pine Creek fault zone, offset CRBG in the area between Larch and Pine Creeks in the southwest part of the Dufur West and northwest part of the Postage Stamp Butte 7.5′ quadrangles (Plate 2). The relationship of fault strands to topography, suggests vertical or near-vertical fault strands. The eastern and middle strands in the Pine Creek fault zone are mapped over distances of 6 and 7.5 km (3.7 to 4.7 mi), respectively, between Winslow Road and Mays Canyon (Plate 2). Right-lateral separation of the **Twfh**/**Twfg** and **Twfg**/**Tgsb** contacts along the eastern strand is ~24 m (80 ft), while mapping shows a right-lateral offset of ~49 m (160 ft) along the middle strand. Apparent down-on-the-east offset of CRBG contacts is ~9 m (30 ft) along the eastern strand, while down-on-the-east offset along the middle strand is ~20 m (66 ft). The westernmost strand in the Pine Creek fault zone is mapped over a distance of ~4 km (2.5 mi), between Winslow Road and the southwest corner of the map area (Plate 2). Mapped right-lateral offset of the **Twfh**/**Twfg** contact along the western fault strand, south of Pine Creek is ~40 m (131 ft). Late Miocene and Pliocene units (**Tmdt**; **Tpdd1**) capping plateaus between Rail Hollow and Pine Creek are similarly offset by right-lateral

displacement along the western fault strand, with horizontal separation of ~27 m (90 ft). Continuation of the Pine Creek fault zone to areas northwest or southeast of that shown on Plate 2 is unknown.

### 7.4.1 Fifteenmile Creek fault zone

The Fifteenmile Creek fault zone is an east-west-striking and north-dipping normal fault zone paralleling Fifteenmile Creek and mapped for a length of ~13.4 km (8.3 mi) between the central part of the Wolf Run 7.5′ quadrangle on the west (Plate 1) and the city of Dufur on the east (Plate 2, cross sections C-C′, D-D′). The western part of the Fifteenmile Creek fault zone apparently splays with an east-west-striking strand projecting west of the confluence of Fifteenmile Creek and Ramsey Creek, into the Wolf Run 7.5′ quadrangle. This east-west-striking strand of the Fifteenmile Creek fault zone terminates on the west against a N.20°E.- to N.30°E-striking normal fault reaching across the Wolf Run 7.5′ quadrangle between Fifteenmile Creek and Fivemile Creek (Plate 1). An additional down-on-the-northwest normal fault strand strikes ~N.35°E., paralleling Fifteenmile Creek for a distance of ~6 km (3.7 mi) southwest from the confluence of Fifteenmile Creek and Ramsey Creek. The eastern part of the Fifteenmile fault zone is inferred to terminate against a major right-lateral strike-slip fault crossing Fifteenmile Creek, just west of the city of Dufur. The fault zone is recognized and mapped on the basis of the linear trend of Fifteenmile and Ramsey creeks, and the distinct linear trend of topographic features running along the south side of both aforementioned streams. The Fifteenmile Creek fault zone is composed of a series of high-angle, north-dipping fault strands that offset CRBG flows and younger units in the Dalles Formation, including unit **Tmdd**. Analysis of structure contours drawn on the basis of OWRD water well lithologic log data (http://apps.wrd.state.or.us/apps/gw/well_log/; Appendix) reveals closely spaced contours coinciding with down on the north offset of the upper surface of the CRBG (**Twfs**)in the Fifteenmile Creek fault zone. Vertical offset of the upper CRBG surface along the main fault strand ranges between ~18 to 30 m (60 to 100 ft) (**Figure 7-3**; Plate 1). Detailed geologic mapping also indicates a subsidiary (conjugate?) northeast-southwest-trending fault strand, paralleling upper Fifteenmile Creek in the extreme western part of the map area that offsets the Basalt of Sand Hollow (**Twfh**) and Dalles Formation breccia (**Tmdd**) in a down-on-the-northwest sense. Apparent cumulative offset along this fault strand may be as much as 24 to 30 m (78 to 100 ft). Relative offset along the east-west-striking fault strand, portrayed west of the confluence of Fifteenmile Creek and Ramsey Creek is unknown.

A recent bulldozer cut up the elongated ridge along the south side of Dufur Valley Road, ~1.6 km (1 mi) east of the confluence of Ramsey Creek, revealed the Fifteenmile Creek fault zone is associated with a 320-m-wide (146 ft) zone of fault disruption (Plate 2). The zone of disruption is characterized by chaotically sheared tuff (**Tmdt**) and conglomerate (**Tmdg**) units that cap the top of the ridge. The stratigraphic sequence of conglomerate (**Tmdg**) over tuff (**Tmdt**) that characterizes the top of the ridge, is repeated multiple times downsection (north) through the fault zone indicating probable offset by several ~N.20°E.-striking fault strands with a down-on-the-northwest normal sense of offset. Fracture planes in the zone are locally infilled by pervasive calcite veining and contain shear fabrics. Units lower in the Dalles stratigraphic section (e.g., **Tmdl** and **Tmdd**), outcropping on either side of the fault zone are completely missing or buried between faults strands from the top of the ridge to the level of Fifteenmile Creek. The fault zone has likely undergone multiple episodes of movement, with the latest fault movement in the Pleistocene. Evidence for late-stage movement is found against steep topographic slopes on the south side of Fifteenmile Creek, where unconsolidated gravels banked against older strata host minor offsets and are cut locally by calcite mineralized and slickensided planes. Recent movement may also be indicated by the nature of the south slopes themselves (between the mouth of Ramsey Creek and Rail Hollow) as they are

characterized by a very sharp, linear, and steep geomorphic expression (~60°), atypical of the erosional habit of other landscapes underlain by the Dalles Formation in the Dufur area (Plate 1, cross section C-C').

## 7.5 Faulting in the Dufur East, Sherars Bridge, and Summit Ridge 7.5' quadrangles (Plate 3)

Few faults were recognized and mapped within the Dufur East, Sherars Bridge, and Summit Ridge 7.5′ quadrangles (Plate 3). The contacts between the CRBG flows in these quadrangles are planar, have a 1° to 3° regional northward dip, and show little to no evidence of significant vertical offset. A calculated regional dip determined from cross section A-A′ has an average strike of N30°E, and a dip of 2.5° NW. The Mays Canyon Creek reverse fault and the north-northwest-striking right-lateral strike-slip fault crossing U.S. Highway 197 south of Dufur, are projected into the Dufur East 7.5′ quadrangle. No geologic evidence was found to draw these fault strands farther east than Dry Canyon (Plate 3). Also, two N.45°W.-striking faults are projected into the northwest corner of the Dufur East 7.5′ quadrangle on the basis of geologic mapping in the Petersburg 7.5′ quadrangle (J. O'Connor, written commun., 2016; **Figure 1-2**) and topographic lineaments observed in 1-m lidar DEMs and 10-m DEMs. The eastern of the two fault strands offset the **Twfs/Twfh** contact as the fault crosses Fifteenmile Creek (Plate 3). Mapping does not indicate the continuation of the eastern fault strand south of Dry Creek.

# 8.0 GEOLOGIC HISTORY

Late Cenozoic volcanic and sedimentary rocks and surficial deposits mapped in the Dufur area provide a partial record of the volcanic, depositional, and deformational history east of the axis of the Cascades volcanic arc since the early Miocene (**Figure 5-2**, **Figure 5-4**, **Figure 5-5**).

## 8.1 Early Miocene (~16.6 to 16.0 Ma)

The first lava flows of the CRBG to enter the Columbia Trans-Arc Lowland on their way to the Pacific coast were part of the Grande Ronde Basalt, erupted between 16.572 ± 0.18 and 16.066 ± 0.04 Ma (**Figure 5-7**, **Figure 6-1**; Kasbohm and Schoene, 2018). The earliest lava flows, including the Grouse Creek (**Tggc**), Buttermilk Canyon (**Tgbc**), Armstrong Canyon (**Tgac**), and Ortley (**Tgo**) members erupted in eastern parts of the Columbia Plateau and flowed westward, following pre-CRBG ancestral Columbia River channels, which were probably located along the northern edge of the Columbia Trans-Arc Lowland (**Figure 5-6**, **Figure 5-7**, **Figure 6-1**; Plates 1, 2, and 3; Beeson and others, 1989, Wells and others, 2009). Several lava flows of the Prineville Basalt (**Tpbd**, **Tpba**), interbedded with the lower part of the Grande Ronde Basalt, in Butler Canyon, were erupted from yet to be discovered vent locations, likely located south of Prineville in central Oregon (150 km [93 mi] south-southeast of Dufur (**Figure 5-6**; Smith, 1986; Hooper and others, 1993; McClaughry and others, 2009). Lava flows in the Grande Ronde Basalt are locally separated by thin, discontinuous sedimentary interbeds, indicating brief intervals of erosion and deposition between eruptions.

Subsequent lava flows of Grand Ronde Basalt, including those of the Winter Water (**Tgww**) and Sentinel Bluffs (**Tgsb**) members locally overlie or grade into intervals of pillow lava and hyaloclastite (**Figure 5-7**, **Figure 6-1**). Winter Water (**Tgww**) flows largely overwhelmed topographic lows that had formed on older Grande Ronde Basalt units, forming a relatively uniform distribution of lava flows across the lowland. The

youngest part of the Grande Ronde Basalt, the Sentinel Bluffs Member (**Tgsb**), largely flowed across a relatively muted terrain covering the most extensive area of any CRBG unit (Beeson and others, 1989). Emplacement of the Sentinel Bluffs Member (**Tgsb**) was followed by an eruptive hiatus and a period of erosion on the upper surface of the CRBG, leaving a regionally widespread unconformity known as the Vantage Member of the Ellensburg Formation (**Figure 6-64**). Ancestral Columbia River channels developed through the Columbia Trans-Arc Lowland above this unconformity creating new pathways for younger CRBG flows to reach western Oregon (**Figure 5-6**).

## 8.2 Early to Middle Miocene (~16.0 to 15.9 Ma)

The Basalt of Ginkgo (**Twfg**) was the first lava flow of the Frenchman Springs Member of the Wanapum Basalt to reach from the Columbia Plateau into the Dufur area, where lava flows were directed along developing synclines in the Yakima Fold Belt (**Figure 5-7**, **Figure 6-1**, **Figure 6-62**; Beeson and others, 1989). The conspicuous absence of the Vantage Member and Basalt of Ginkgo (**Twfg**) intervening between the older Sentinel Bluffs Member (**Tgsb**) and younger Basalt of Sand Hollow (**Twfh**) in the northern part of the Postage Stamp Butte 7.5' quadrangle (**Figure 1-2**; Plate 2) is evidence for localized uplift along the Dry Creek monocline and associated Mays Creek Canyon fault (Plate 2). This structural topography, generated concurrently with or closely following the end of Grand Ronde Basalt time (**Figure 5-7**), appears to have controlled the distribution of Ginkgo lava flows (**Twfg**) across this part of the map area. Fold deformation and structural offset of the Basalt of Sand Hollow (**Twfh**) indicates structural uplift along the Dry Creek monocline persisted at a minimum through latest Frenchman Springs time (~15.9 Ma) (**Figure 5-7**). Elsewhere, between Mosier (~32 km [20 mi] northwest of Dufur) and the Willamette Valley of western Oregon, the lava flow encountered the canyon of the ancestral Columbia River, as suggested by the common occurrence of pillows and hyaloclastite at the base of the unit in those areas (McClaughry and others, 2012). Subsequent lava flows of the Basalt of Sand Hollow (**Twfh**) covered a more extensive area than earlier Ginkgo lava flows (**Twfg**) (**Figure 5-7**, **Figure 6-1**, **Figure 6-60**; Barry and others, 2010). Sentinel Gap lava flows (**Twfs**), forming the upper part of the Frenchman Springs Member in the area, were confined to the northern part of the Columbia Trans-Arc Lowland and forced the ancestral Columbia River to establish a new course along the axis of the Mosier syncline (**Figure 5-7**, **Figure 6-1**, **Figure 6-59**; Beeson and others, 1989; Tolan and others 2009a; McClaughry and others, 2012). Lava flows in the Frenchman Springs Member are locally separated by thin and discontinuous sedimentary interbeds, indicating intervals of erosion between eruptions.

Eruption of the last of the Frenchman Springs lava flows was followed by an ≤170,000-year lull in CRBG volcanism and ensuing period of erosion and sedimentation across the Columbia Trans-Arc Lowland (**Figure 5-6**). Continued deformation and uplift of Yakima Fold Belt anticlines and reoccupation and downcutting by ancestral channels of the Columbia River across the lowland generated a ~1- to 2-km-wide (0.6 to 1.2 mi) deep river canyon that was incised through the Frenchman Springs Member (**Twfs**, **Twfh**, **Twfg**) and into the Sentinel Bluffs Member (**Tgsb**) in areas west and north of Dufur (Anderson and Vogt, 1987; McClaughry and others, 2012). Lava flows of the Basalt of Rosalia (**Twpr**) of the Priest Rapids Member of the Wanapum Basalt were partly confined to this paleocanyon as they traversed the area of the present day Cascade Range around 15.9 Ma (**Figure 5-6**, **Figure 6-1**; Anderson and Vogt, 1987; McClaughry and others, 2012; Madin and McClaughry, 2019). As lava flows filled the channel they spread into more aerially extensive overflow areas south of The Dalles. Overtopping of the paleochannel by the Basalt of Rosalia (**Twpr**) forced the ancestral Columbia River northward (Tolan and Beeson, 1984). The last of the CRBG flows to enter the Columbia River Gorge was the Pomona Member of the Saddle

Mountains Basalt (McClaughry and others, 2012). This chemically distinct flow was erupted around 12 Ma during a period (~13.8 Ma to 6 Ma) of significant tectonism, canyon incision, and waning volcanism and deposition of thick sedimentary interbeds between more infrequent CRBG eruptions.

## 8.3 Late Miocene to early Pliocene (~8.8 to 5 Ma)

Following ~4 to 7 m.y. of erosion and structural deformation, regional CRBG volcanism was replaced across the Middle Columbia Basin by early High Cascades volcanism focused along the crest of the Cascades volcanic arc in areas underlying and east of present day Mount Hood (**Figure 5-2**, **Figure 5-4**; McClaughry and others, 2020a). Early High Cascades volcanoes in the Mount Hood area produced deposits of the ~8.8 to 5 Ma Dalles Formation, a succession of low- to medium $K_2O$, calc-alkaline lava flows and domes, pyroclastic rocks, bedded andesitic and dacitic lithic block-and-ash flow and laharic deposits, hyperconcentrated flood-flow deposits, and fluvial deposits (**Figure 5-4**, **Figure 5-5**, **Figure 5-11**, **Figure 6-1**; Plates 1, 2, and 3, cross sections). The Dalles Formation was emplaced across a broad constructional volcanic highland along the axis of the Cascades volcanic arc and in a northeast-sloping arc-adjacent volcanic plain stretching ~40 km (25 mi) from Mount Hood northeast to the Columbia River (**Figure 5-4**). In the Hood River graben, along the axis of the Cascades volcanic arc, the Dalles Formation is characterized by interlayered vent-proximal lava flows and domes, hypabyssal intrusions, block-and-ash flow deposits, and ash-flow tuff (McClaughry and others, 2020a). Distal arc-adjacent volcanic plain deposits mapped eastward to The Dalles and Dufur, become increasingly rich in thick sections of block-and-ash-flow deposits, volcanogenic debris flow (lahar) deposits, hyperconcentrated flood-flow deposits, and ash-flow tuff, interbedded with horizons of fluvial conglomerate, sandstone, and siltstone (**Figure 5-4**). These lithologic associations indicate a transition from volcanic dominated highlands on the west to axial stream-dominated drainage systems on the east (**Figure 5-4**).

Early construction of the distal part of the volcanic apron in the Dufur area between ~9 and 8 Ma was characterized by the deposition of ash-flow units (**Tmdtp**, **Tmdt**; **Figure 6-48**, **Figure 6-49**, **Figure 6-54**), and block-and-ash flow units (**Tmdd** and parts of **Tmdl**; **Figure 6-51**, **Figure 6-52**) that buried underlying CRBG units. Inter-eruption cycles were dominated by the deposition of heterolithologic debris flows (**Tmdx** and parts of **Tmdl**; **Figure 6-55**), hyperconcentrated flood-flows (**Tmdl**), and fluvial gravels and sands (**Tmdl**; **Figure 6-35**, **Figure 6-36**, **Figure 6-37**). Generation and distal runout of Dalles Formation lahars into the Dufur area (>25 km [15.5 mi] from western source areas along the axis of the Cascades volcanic arc requires: 1) an adequate water source; 2) abundance of unconsolidated debris, such as pyroclastic-flow and -fall deposits; 3) steep slopes and substantial relief at the source; and 4) a triggering mechanism, such as volcanic eruptions or other process such as torrential rains or melting of snow and ice (Vallance, 1999). The nearly monolithologic clast assemblage, inclusion of large pumiceous clasts, association of breccia (**Tmdd**) with bracketing tuffs (**Tmdtp**, **Tmdt**) of similar chemical and mineralogical composition, and similar isotopic ages of breccia blocks and tuffs, suggest a primary pyroclastic flow origin for some cycles of units and direct association with volcanic eruption(s). At the extreme distal edge of the volcanic apron, Cascades-derived Dalles Formation units interfinger with sediment of Deschutes River provenance (Cannon and O'Connor, 2019). During periods of voluminous volcanic and sediment production (e.g., **Tmdtp**, **Tmdd**, **Tmdt**), Dalles Formation facies may have dominated even the ancestral Deschutes River system.

Construction of the volcanic apron in the Dufur area, between ~8.8 and 5 Ma, was accompanied by the emplacement of several canyon-filling lava flow sequences (**Tmdj**, **Tmdv**, **Tmdw**; Plates 1 and 2). The distinctly plagioclase-porphyritic dacite of Wolf Run (**Tmdw**), erupted at 7.91 Ma, fills a narrow

paleocanyon incised into older Dalles Formation (**Tmdl**) strata across the northwest part of the map area (**Figure 6-45**, **Figure 6-46**; Plates 1 and 2). Unit **Tmdw** has been traced from its distal exposure near Dufur on the east, west to the High Prairie area along the eastern escarpment of the Hood River graben (McClaughry and others, 2020a). The dacite of Fivemile Butte (**Tmdv**), erupted at ~7.7 Ma, fills a narrow paleocanyon between its source area at Fivemile Butte and Hesslan Canyon in the west part of the map area (**Figure 6-43**; Plate 1; McClaughry and others, 2020a; J.D. McClaughry unpublished geologic mapping, 2016). The dacite of Jordan Butte (**Tmdv**), erupted at ~5 Ma, fills a narrow paleocanyon between its source area at Jordan Butte and the southwest part of the map area (**Figure 6-41**; Plate 1; J.D. McClaughry unpublished geologic mapping, 2016).

Discontinuously exposed cobble conglomerate (**Tmdg**) capping many plateaus in the Dufur area mark the end of aggradation associated with Dalles Formation volcanism and a transition to post-eruption entrenchment of fluvial systems draining volcanic highlands on the west (**Figure 6-39**, **Figure 6-38**). Continued tectonic warping, associated with development of the Yakima Fold Belt in post-Dalles Formation time, deformed the Dalles Formation in the Dufur area into a series of very broad open folds (Plates 1, 2, and 3, cross sections). Dalles Formation outcrops, coincident with Yakima anticlinal uplifts and thrust faults in other parts of the Middle Columbia Basin (e.g., Mosier, The Dalles, East Fork Hood River area), show more severe deformation, with locally tight folds and steeply inclined strata (dips up to 50°; McClaughry and others, 2012; McClaughry and others, 2020a).

## 8.4 Pliocene and early Pleistocene (~4.2 to 2.5 Ma)

The Pliocene and early Pleistocene interval between 4.2 and 2.5 Ma signaled a key period in the volcanic and structural evolution of the late High Cascades of north-central Oregon and the nearby Dufur area (**Figure 5-2**). Intra-arc faulting initiated during the Pliocene and early Pleistocene along north-northwest-striking normal or normal oblique-slip faults and north-south-striking normal faults led to the formation of the north-striking Hood River graben along the axis of the High Cascades volcanic arc (McClaughry and others, 2012; McClaughry and others, 2013; McClaughry and others, 2020a). Development of the southern part of the Hood River graben along East Fork Hood River was temporally and spatially associated with the eruption of a compositionally diverse suite of volcanic rocks (basalt to rhyolite). In contrast to the relatively wide regional distribution of Early High Cascades rocks of the Dalles Formation, younger Pliocene and early Pleistocene volcanics were increasingly confined to the structural low of the Hood River graben (**Figure 5-4**; McClaughry and others, 2020a). Distribution of these rocks was controlled by a combination of constructional volcanic topography on remnant Dalles Formation volcanoes, northeast-striking stream channels incised into the Dalles Formation arc-adjacent volcaniclastic apron extending east through Dufur, and structural relief created along active faults in the Hood River graben.

Post-Dalles Formation volcanism in the Dufur area is recorded by a narrow interval of activity, with volcanics emplaced between 3.83 and 3.68 Ma. Pliocene medium-to high-potassium andesite to dacite and trachydacite units markedly contrast with the dominantly low-potassium andesite and dacites characterizing the older Dalles Formation (**Figure 5-2**, **Figure 5-11**, **Figure 5-12**). The earliest post-Dalles volcanism in the Dufur area is recorded by ash-flow tuff (**Tpdd1** [basal tuff]), the tuff breccia of Engineers Creek (**Tpdd1**, **Tpdd2**), and sequence-capping pumice tuff (**Tppt**) (**Figure 6-1**, **Figure 6-16**, **Figure 6-17**, **Figure 6-21**, **Figure 6-22**, **Figure 6-29**; Plates 1, 2, and 3). These units formed as explosive volcanic eruptions in or directly adjacent to the eastern escarpment of the Hood River graben created a sequence of pumiceous ash flows (**Tpdd1** [basal tuff], **Tppt**) and block-and-ash flows (**Tpdd1** [breccia], **Tpdd2**) that poured east across a broad plateau now underlying the ghost town of Friend (**Figure 5-2**,

**Figure 6-21**, **Figure 6-28**; Plate 1; McClaughry and others, 2020a). On the plateau, northwest of Friend, block-and-ash flow breccia beds (**Tpdd1**) were emplaced between 3.83 and 3.68 Ma, closely in space and time with the 3.68 Ma tuff of Friend, a markedly thick sequence of trachydacite, pumice-lithic pyroclastic flow deposits (**Tptf1**, **Tptf2**). At the confluence of Pine and Larch Creeks, block-and-ash flows (**Tpdd1**) cascaded into and were confined downstream within a steep-sided northeast-striking Pine Creek paleochannel (**Figure 6-21**, **Figure 6-22**, **Figure 6-28**; Plate 2). Intermixing of primary pyroclastic material with clasts derived from the underlying Dalles Formation in distal parts of the **Tpdd1** deposit, east of Dufur, suggests that primary pyroclastic flows transitioned to more sediment-laden and erosive lahars downstream. Unit **Tpdd1** breccia extends at least 50 km (25 mi) from correlative deposits along Engineers Creek in the eastern escarpment of the Hood River graben (unit Tpdd of McClaughry and others, 2020a) downstream to distal deposits cropping out near Rice (Plate 3 and Petersburg 7.5′ quadrangle; **Figure 1-2**, **Figure 5-2**, **Figure 6-21**, **Figure 6-28**; Plates 1, 2, and 3; McClaughry and others, 2020a).

The long runout distance >10 km (6.2 mi) from the inferred source area in the Hood River graben is atypical of most world-wide cited examples of block-and-ash flow deposits (e.g., Freundt and others, 2000; Calder and others, 2002; Platz and others, 2007; Michol and others, 2008). Runout distance >50 km (31 mi) and mixing with other lithologies (Dalles Formation) east of Dufur likely indicates that flows (**Tpdd1**, **Tpdd2**) encountered water within the confines of the Pine Creek paleochannel and transitioned to a more water-saturated lahar-like slurry with distance downstream (e.g., Carrasco-Núñez, 1999). The total lack of incorporated CRBG clasts, which comprised the substrate over which flows traveled for most of its length, suggests that the flow may have been fluidized and non-erosive over a portion of its travel path. The eruption cycle ended with the emplacement of a non-welded pumice tuff (**Tppt**) that locally overlies breccia (**Tpdd1**) along the course of the Pine Creek paleochannel (**Figure 6-13**, **Figure 6-16**, **Figure 6-21**). Cobble conglomerate (**QTpg**), discontinuously preserved above breccia (**Tpdd1**) and pumice tuff (**Tppt**), marks a local hiatus in volcanism and return to fluvially-dominated stream environments along the paleo-Pine Creek drainage (**Figure 6-13**; Plate 2).

Pyroclastic rocks (**Tptf1**, **Tptf2**, **Tpdd1**) erupted from the Hood River graben between 3.83 and 3.68 Ma were accompanied in space and time by a series of lava flow eruptions that produced the 3.72 Ma intracanyon olivine basalt (**Tpbf**) and the 3.69 Ma trachydacite of Fivemile Creek (**Tpdv**), now cropping out along Fivemile Creek (**Figure 6-31**, **Figure 6-33**; Plate 1). Few lava flows of this age, with the exception of the 3.69 Ma trachydacite of Fivemile Creek (**Tpdv**), the andesite of Fret Creek (unit Tpaf of McClaughry and others, 2020a), and the younger 3.02 Ma dacite of Fifteenmile Creek (**Tpdf**), escaped the developing Hood River graben (**Figure 5-4**, **Figure 6-1**). Those lava flows that did exit the Hood River graben to the east were confined within channels incised into the older Dalles arc-adjacent plain, approximately paralleling modern-day canyon patterns and gradient.

The youngest Pliocene volcanic unit in the map area is the 3.02 Ma dacite of Fifteenmile Creek (**Tpdf**), a now topographically inverted intracanyon lava flow, which filled a shallow paleocanyon incised into late Pliocene pyroclastic rocks (**Tptf1**, **Tptf2**, **Tpdd1**) south of Fifteenmile Creek (**Figure 6-14**; Plate 1). This lava flow is mapped west to Cold Point, Lookout Mountain, and the eastern escarpment of the Hood River graben (McClaughry and others, 2020a; J.D. McClaughry unpublished geologic mapping, 2016). Several prominent N.15°E.- to N.25°E.-striking dikes in the eastern escarpment of the Hood River graben in the upper parts of Culvert Creek mark the vent area (McClaughry and others, 2020a).

Eruption of early Pliocene intermediate to silicic-composition tuff and breccia in the area between the Hood River graben and Dufur occurred over a relatively short time interval, temporally equivalent to a suite of silicic volcanic rocks emplaced at nearby Gordon and Graveyard Buttes between 3.8 and 3.6 Ma (~31 km [19 mi] southwest of Dufur; Westby, 2014). Westby (2014) considered early-phase silicic

volcanism in the Gordon and Graveyard Buttes areas to share geochemical and mineralogical traits consistent with petrogenesis in an intra plate or extensional setting, while late phase silicic rocks appear to be more arc related. Intermediate to silicic volcanism between Gordon Butte and the Hood River graben was contemporaneous with a more widespread pulse of high-magnesium mafic volcanism in the northern Oregon Cascade Range dated between 4.4 and 2.1 Ma (Conrey and others, 1996; McClaughry and others, 2012; McClaughry and others, 2013; McClaughry and others, 2020a). Extrusion of mafic lava flows during the late Pliocene was followed by a continuation of Yakima Fold Belt deformation of strata, inception of rifting along the axis of this part of the Cascade arc, and formation of the Hood River graben after 3.7 Ma (McClaughry and others, 2020a). Foundering of the Cascade volcanic arc into a half graben during the late Pliocene and early Pleistocene was also accompanied by regional uplift or upwarp of the Cascade Range and formation of the modern Columbia River Gorge after 3 Ma (Tolan and Beeson, 1984; Beeson and Tolan, 1990).

## 8.5 Early Pleistocene (~2.6 to 1.87 Ma)

Pliocene and older rocks are disconformably overlain locally by fluvial gravel (**QTpg**) and a series of latest Pliocene and early Pleistocene olivine-phyric basalt and basaltic andesite lava flows (**Qrbf**, **Qrbp**, **Qrbe**, **Qr5dr**) erupted from extant small volcanoes situated along the High Cascades crest and eastern escarpment of the Hood River graben (**Figure 5-2**, **Figure 5-4**, **Figure 5-5**, **Figure 5-14**, **Figure 5-15**, **Figure 6-1**, **Figure 6-5**, **Figure 6-8**, **Figure 6-10**; McClaughry and others, 2020a). Mafic to intermediate volcanism was predominant in the Hood River graben during Quaternary time, with basalt and basaltic andesite lava flows erupting from a north-south trending belt of vents situated above north-northwest trending fault strands along the graben's broad eastern escarpment (McClaughry and others, 2020a). Lava flows erupted high along the eastern escarpment of the Hood River graben flowed eastward away from source vents down an east-sloping landscape, confined to north-northeast-directed drainages carved into older late Miocene and Pliocene rocks (**Figure 5-4, Figure 5-5**). These drainages were of similar location and orientation to those had been followed by older Pliocene intracanyon lava flows, tuffs, and sediment-gravity flows (**Tpbf**, **Tpdv**, **Tptf1**, **Tpdd1**, **Tptf2**, **Tpdd2**, **Tppt**, **Tpdf**) (Plates 1 and 2).

The 2.57 Ma basaltic andesite of Flag Point (**Qrbf**) was erupted from an extant cinder cone-capped vent underlying the lookout at Flag Point (southwest of the map area, J.D. McClaughry unpublished geologic mapping). Lava flows erupted from Flag Point flowed north into the upper parts of Cedar Creek and northeast into Jordan Creek and Owl Hollow (J.D. McClaughry unpublished geologic mapping). The distal snout of intracanyon lava flows reached ~14 km (8.7 mi) northeast to the upper part of Larch Creek west of Friend (Plate 1). The 1.87 Ma basaltic andesite of Dog River (**Qr5dr**) erupted from a fault-controlled cinder cone-capped fissure at an altitude of 1,391 m (4,565 ft) along the Dog River-Mill Creek divide near Mill Creek Buttes (McClaughry and others, 2020a). Dog River lava flows (**Qr5dr**) descended northeast into South Fork Mill Creek, flowing at least 26 km (16 mi) downstream to Oak Flat, near The Dalles. Local accumulations of fluvial gravel are associated with the basaltic andesite of Dog River (**Qr5dr**) along South Fork Mill Creek. These gravels were deposited as river systems readjusted to emplacement of the canyon filling lava flow. Further canyon readjustments, post-emplacement of the basaltic andesite of Dog River (**Qr5dr**), are evidenced by a great number of landslides (**Qls**) originating along the length of the South Fork Mill Creek (J.D. McClaughry unpublished geologic mapping, 2016). An additional lobe of the basaltic andesite of Dog River (**Qr5dr**) was also directed west and northwest into the structural low of the Hood River graben (McClaughry and others, 2020a). This western lobe extended at least 6 km (3.7 mi) from the vent area to now down-faulted exposures, outcropping at an elevation of 716 m (2,350 ft) in the canyon

of the modern East Fork Hood River. Emplacement of Quaternary lava flows predates erosion that carved the modern canyons in the Dufur area.

## 8.6 Late Pleistocene to Holocene (~1 Ma to present)

Deeply incised Neogene geologic units exposed in the Dufur area are capped by a variably thick and discontinuous blanket of Pleistocene loess (**Qlo**) (**Figure 5-5**, **Figure 6-1**; **Figure 6-4a**; Plates 1, 2, and 3). Loess accumulated in this area as a result of episodic deposition of airborne silts by southwesterly winds during the Quaternary. Loess deposits in the Dufur area are assigned a Middle Pleistocene to Holocene age on the basis of stratigraphic position and may be as old as ~600 ka. Medley (2012) interprets loess deposits and Missoula Flood deposits exposed along U.S. Highway 197 between Dufur and The Dalles, to lie above a series of older paleosols that contain pumice correlated to the ~600 ka Dibekulewe tuff from Nevada (Cordero, 1997). Pluhar and others (2014) reported paleomagnetically reversed paleosols at the base of U.S. Highway 197 section, so loess in this area may in some places be older than 0.78 Ma.

Microrelief features, known as Mima mounds, are a prevalent geomorphic feature in the Dufur area, preserved mantling the landscape in areas between tilled loess-dominated agricultural fields or areas not plowed (**Figure 6-4**). Mounds excavated by the authors in the Dufur area are composed of a mixture of silt (loess), ash, and poorly sorted gravelly silt, with mound make-up determined by the substrate that they mantle. Mima mounds scattered across north-central Oregon formed during multiple cycles in the Pleistocene, occurring on a variety of landscapes, including plateau and ridge caps, as well as moderate to steep slopes, at differing elevations, on differing bedrock and soil substrates, and in areas of variable saturation (Nelson, 1977). Ideas on the formation of Mima mounds are numerous, and the causative forces, as such, remain controversial (see Appendix D in Johnson and Horwath Burnham, 2012). Mima mounds in the Pacific Northwest are ascribed a polygenetic and complex origin, due to both biological and physical causes including but probably not limited to: 1) bioturbation by animals (such as pocket gophers), plants, fungi, protoctists, microbes, etc. (Johnson and Horwath Burnham, 2012; Cox, 2012); 2) bioturbationally modified and shaped erosional remnants of a thicker soil mantle (Johnson and Johnson, 2012); 3) a relatively shallow soil mantle overlying an impermeable permafrost or bedrock layer (Nelson, 1977); 4) frost sorting and runoff flushing of stone gutters intervening between mounds (Johnson and Johnson, 2012); 5) intense frost action under former periglacial conditions (Nelson, 1977); 6) erosion, including snowmelt and surface runoff from mounds (Johnson and Johnson, 2012); 7) occasional eolian inputs (Johnson and Johnson, 2012); or 8) some complex combination thereof. Downslope elongation of many of the mounds and stone rings in north-central Oregon is likely the result of mass-wasting as slope increases (Nelson, 1977).

Steep slopes and valley bottoms have accumulated Late Pleistocene and Holocene surficial units including stream alluvium (**Qa, Qao**), fan deposits (**Qaf**), landslide deposits (**Qls**), and colluvium (**Qc**) (**Figure 5-5**, **Figure 6-3**; Plates 1, 2, and 3). These units reflect late Pleistocene and younger landscape adjustments as major drainages have continued to incise into bedrock units. In the Dufur area, streams and landforms are adjusting to late Quaternary geologic events including variations in climate, young faulting (after 3 Ma), changes in base level at the Columbia River, and land-use changes. These geomorphologic adjustments are further complicated by the presence of alternating hard and soft rock in the subsurface and nesting of Pliocene and Quaternary intracanyon lava flows within older bedrock units (Plates 1, 2, and 3).

# 9.0 GEOLOGIC RESOURCES

## 9.1 Aggregate Materials and Industrial Minerals

Aggregate, in the form of crushed rock and gravel, is the major mineral resource now being mined in the Dufur area. Available locations for aggregate and crushed rock resources in the area can be found in McClaughry and others (2020b) (https://www.oregongeology.org/milo/index.htm). Much of the Dufur area is underlain by volcanic rocks, but high-quality aggregate rock, preferred for construction purposes, is restricted to quarries sited within the CRBG. Aggregate-rock quarry sites within the Dufur area are sited mainly within the Sentinel Gap (**Twfs**) and Sand Hollow (**Twfh**) flows of the Frenchman Springs Member and to a lesser extent the Sentinel Bluffs and Winter Water members (**Tgsb**, **Tgww**) (Plates 1, 2, and 3). Lava flows in the lower part of the Grande Ronde Basalt (e.g., **Tgo**, **Tggc**) are typically the most desirable CRBG units mined for crushed rock across this part of the Columbia Plateau, but are not exposed in the map area. Many Grande Ronde Basalt units characteristically have hackly-jointed entablatures and smaller colonnades that break into smaller diameter fragments relative to the thicker and more massive sections of colonnade jointing in the Sentinel Bluffs (**Tgsb**) and Frenchman Springs (**Twfs**, **Twfh**, **Twfg**) members. The large-diameter basalt columns in some CRBG units may locally be suitable for decorative stone and for use as riprap for stabilization and erosion control purposes. Sand and gravel, suitable for use as aggregate, are limited in the area, being restricted to small pits hosted in the Dalles Formation (**Tmdl**) or unconsolidated alluvial deposits (**Qa**, **Qaf**). Younger Pliocene volcanic rocks exposed west of the map area are locally mined in small occurrences on private timber lands and on lands administered by the USFS for use as crushed rock and pit-run materials for forest road construction.

No industrial minerals are known to occur in the map area (McClaughry and others, 2020b).

### 9.1.1 Semiprecious gemstones

Several semiprecious gem material localities, containing deposits of siliceous sinter, were recognized during the course of geologic mapping in the Dufur area. The most notable localities of siliceous sinter in the area are from outcrops along U.S. Highway 197, south of Dufur. The northern locality (herein referred to as the Tygh Ridge locality) is located 0.4 km (0.25 mi) south of mile marker 19 on U.S. Highway 197 and consists of an ~4 m wide (13 ft) vertical neck of siliceous sinter that cross cuts a steeply northeast-dipping (~28° NE) section of thinly layered Sentinel Bluffs basalt (**Tgsb**) (**Figure 9-1a**). Near the top of the outcrop, siliceous material parallels bedding planes between Sentinel Bluffs (**Tgsb**) flow lobes (**Figure 9-1b**). Siliceous sinter at this locality is spatially associated with the Mays Creek Canyon fault located along the northern edge of the Dry Creek monocline (Plate 1).

Siliceous sinter at the Tygh Ridge locality consists of white (N9) to very pale orange (10 YR 8/2), pale yellowish orange (10 YR 8/6), and dark yellowish orange (10YR 6/6), brecciated and matted chalcedonic (amorphous silica) and opaline quartz (**Figure 9-1**). Siliceous masses in the deposit are locally characterized by spongy, botryoidal, nodule, and "snakeskin" textures (**Figure 9-1b,d**). Locally the silica masses completely enclose/envelope parts of the basalt host rock and may include organic fragments. The deposit is capped east of the highway by massive, moderate brown (5YR 3/4), brecciated and annealed jasper (**Figure 9-1c**).

The southern locality (herein referred to as Butler Canyon locality) is located 2.7 km (1.7 mi) south of the map area, near mile marker 29 on U.S. Highway 197, in Butler Canyon. The lower part of the Sentinel Bluffs Member (**Tgsb**) near its lower contact with the older Winter Water Member (**Tgww**) contains, bedding-parallel, 0.5- to 1-m- thick (1.6 to 3.3 ft), massive to finely banded veins of multi-colored white

(N9) to very pale orange (10 YR 8/2), light brown (5YR 5/6), pale yellowish orange (10 YR 8/6), dark yellowish orange (10YR 6/6), and light olive (10Y 5/4) veins of chalcedonic and opaline quartz (**Figure 9-2**). The Butler Canyon locality, in some places, contains varicolored banded jasper (picture jasper; **Figure 9-2c**). Other opaque varieties of chalcedony at both localities will take a subdued patina or semi-gloss polish and could be useful for a variety of lapidary uses (e.g., jewelry, decorative stone for rock collectors) (**Figure 9-2d**).

X-ray diffraction (XRD) results from siliceous sinter and clay samples obtained from both the Tygh Ridge and Butler Canyon localities indicate the presence of montmorillonite, vermiculite, quartz, tridymite, plagioclase, stilbite, and an abundance of amorphous limonitic material (Appendix). Inductive Coupled Mass Spectrometry (ICP-MS) and Inductive Coupled Atomic Emission Spectrometry (ICP-AES) analyses of siliceous sinter and clay samples show trace to nil values for silver (Ag <0.02 ppm), nil values for gold (Au < 0.02 ppm), and nil values for mercury (Hg < 0.02 ppm) with all three elements occurring at or below the lower analytical detection limits of the techniques (Appendix**, Table 12-4**). Two samples (82b DFWJ 14 and 171a DFWJ 14) have relatively anomalous iron enrichment (Fe = 15.3 and 23.8 weight percent) with corresponding higher values for arsenic (As = 2.2 and 4.4 ppm) (Appendix). An additional sample (82c-3 DFWJ 14) has higher amounts of the rare earth elements cerium (Ce = 41.9 ppm) and lanthanum (La = 19.2 ppm), and the alkali metal lithium (Li = 16.2 ppm) relative to other analyzed samples (Appendix).

Similar deposits, occurring within the CRBG, are reported from nearby areas including the Biggs Junction-Rufus area and Spanish Hollow Canyon, near Wasco, ~40 km (25 mi) northeast of Dufur (Lowry and others, 1946, DOGAMI department mining records; Madin and McClaughry, 2019). The Spanish Hollow locality is reported to contain a variety of intermixed, massive to locally banded chalcedony and opal, occurring in various shades of brown, reddish brown, and white; some samples contain numerous limonite inclusions. Samples submitted for analysis by DOGAMI in 1946 by a Mr. Ryland O. Scott, and reputedly collected from locations in Spanish Hollow, were determined to contain anomalously high values for both gold (1.8 to 21.2 oz Au/ton) and silver (1.0 to 12.9 oz Ag/ton) (DOGAMI mining records). Verification samples subsequently collected and assayed by DOGAMI geologists in 1946 (Lowry and others, 1946, DOGAMI department mining records) show high amounts of iron (Fe > 10 percent), but nil to trace amounts of gold (Au) and silver (Ag); one DOGAMI sample assayed at 0.02 oz Au/ton. Additional occurrences of semiprecious gem material localities, containing deposits of silicified sediment, sinter, and brecciated sinter, have been mined from the CRBG in the Biggs Junction-Rufus area (Madin and McClaughry, 2019). Virtually all of the Biggs Junction-Rufus mines extract material found along the contact between the Basalt of Sand Hollow (**Twfh**) and the overlying Basalt of Sentinel Gap (**Twfs**). The locally mined material has been known in the lapidary community as “Biggs jasper” and “wascoite”. Half a dozen occurrences are reported by McClaughry and others (2020b), and there is one active and two closed mine sites permitted by DOGAMI.

**Figure 9-1. Fossil hydrothermal features and semiprecious gemstones in the Dufur area: (a) An ~4-m-wide (13 ft) vertical neck of siliceous sinter vertically cross cuts a steeply northeast-dipping (~28°) section of thinly layered Sentinel Bluffs basalt (Tgsb) along U.S. Highway 197, south of Dufur (45.370542, -121.141916). Red-dashed line outlines the sinter deposit. White-dashed line is a flow bedding contact within the Sentinel Bluffs Member (Tgsb). Area marked 'B' shows the location of the photo in B. View is looking east. (b) Massive to matted beds of desiccated, sponge-textured chalcedony following bedding planes in the Sentinel Bluffs Member (Tgsb). Scale bar is 0.5 m (1.6 ft) tall. View is looking east. (c) The deposit along U.S. Highway 197 is capped by massive, moderate brown (5YR 3/4), brecciated and annealed jasper. Scale bar is 20 cm (7.9 in) tall. (d) Chalcedonic nodules with distinct snakeskin-type surface texture. Penny for scale bar is ~1.9 cm (0.7 in) across. Photo credits: J.D. McClaughry, 2014.**

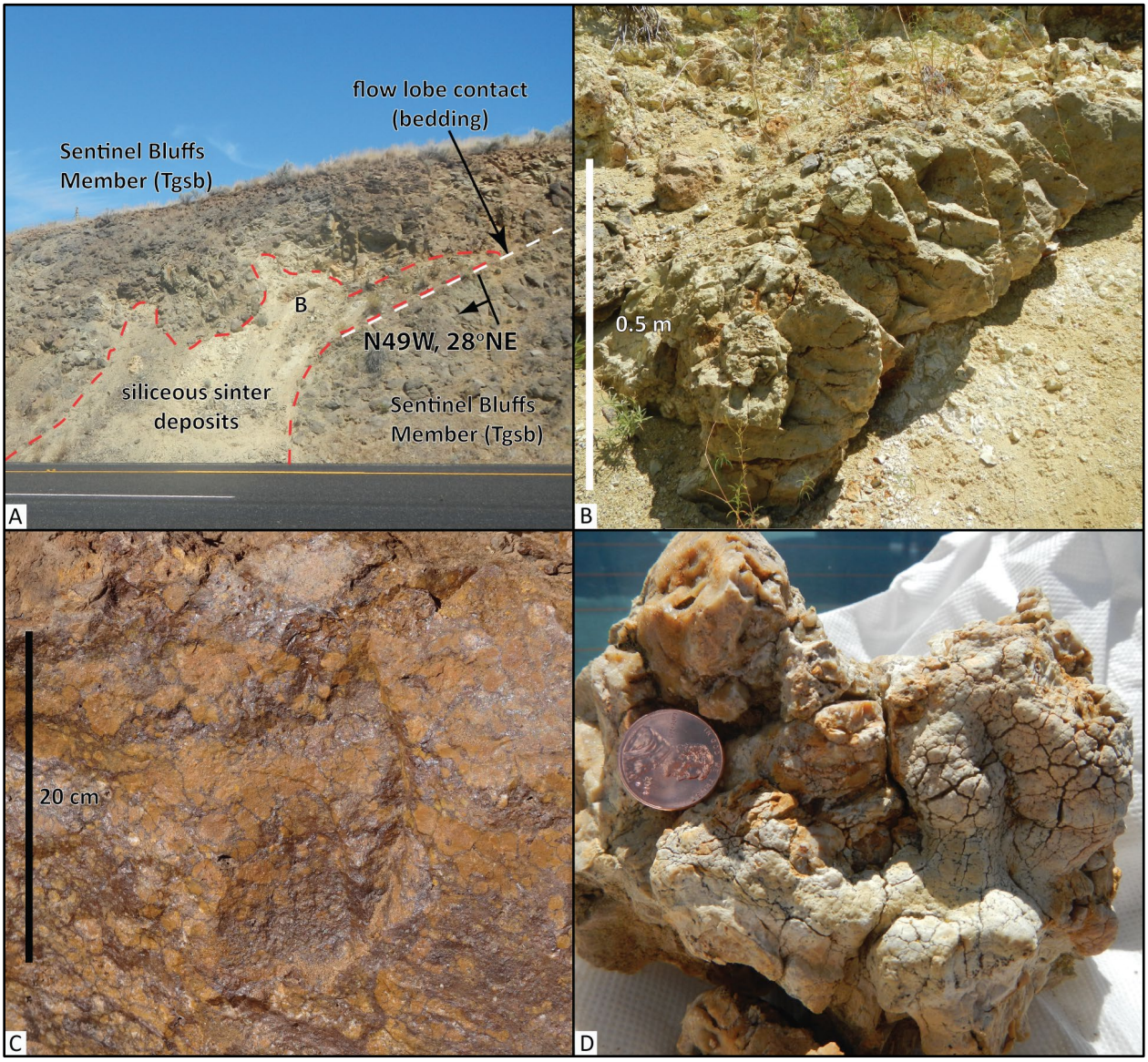

**Figure 9-2. Fossil hydrothermal features and semiprecious gemstones in the Dufur area. (a) Anastomosing, bedding-parallel, 0.5- to 1-m- thick (1.6 to 3.3 ft) veins of chalcedonic and opaline quartz invading the Sentinel Bluffs Member (Tgbs) along U.S. Highway 197 in Butler Canyon, just south of the map area (45.301228, -121.154032). View is looking west. (b) Massive bed of banded jasper overlain by a dark yellowish orange (10YR 6/6) horizon of friable clay. Pen for scale is 15 cm (5.9 in) tall. (c) Varicolored banded jaspers ("picture jaspers") are found in Butler Canyon. Scale bar is 2.5 cm (1 in) tall. (d) Multi-colored white (N9) to very pale orange (10 YR 8/2), light brown (5YR 5/6), pale yellowish orange (10 YR 8/6), dark yellowish orange (10YR 6/6), and light olive (10Y 5/4) opaque chalcedony with thin veins of opaline quartz in Butler Canyon. Quarter for scale is 2.5 cm (1 in) across. Photo credits: J.D. McClaughry, 2014.**

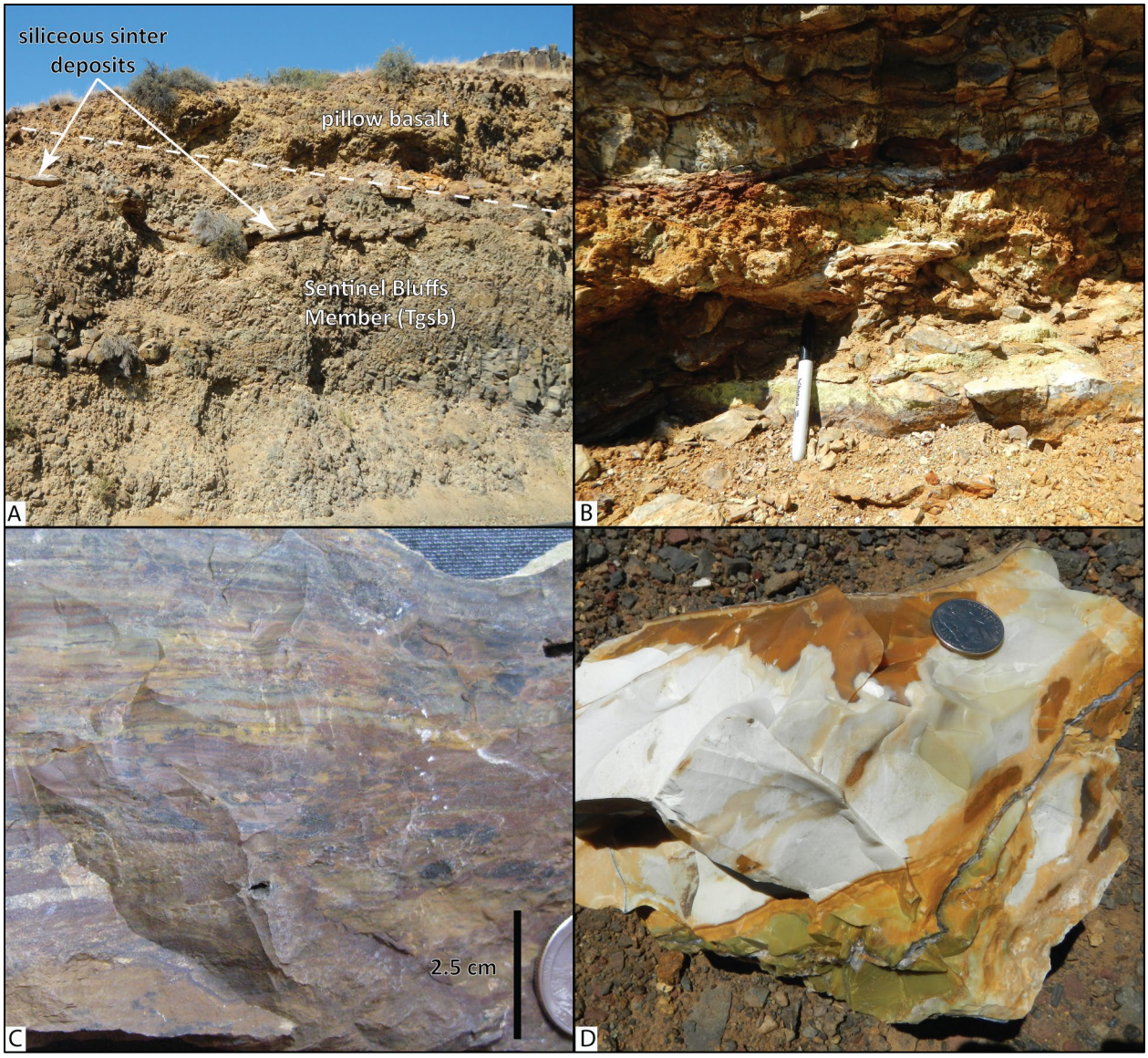

## 9.2 Energy Resources

Geothermal waters are not currently used near Dufur and to the knowledge of the authors no geothermal exploration has occurred in the map area. However, surface manifestations of past geothermal waters, such as deposits of siliceous sinter are locally present (**Figure 9-1**, **Figure 9-2**). The Dufur area does host a number of geologic characteristics (e.g., fault zone conduits, stratiform geologic units) that may be favorable for the occurrence of localized geothermal reservoirs at depth (Plates 1, 2, and 3, cross sections).

Several oil and gas exploration wells were drilled in the Dufur area in the early 1900s, in order to explore the reservoir potential of the late Miocene to early Pliocene Dalles Formation (**Figure 9-3**). Small pockets of gas were found within the formation, but large and potentially economic accumulations of petroleum or natural gas were not found (Buwalda, 1929). Five exploration wells were drilled starting in 1907 by the Dufur Oil Company along Fifteenmile Creek upstream of the confluence of Ramsey Creek, ~8 km (5 mi) west of the city of Dufur (**Figure 9-3**; Buwalda, 1929; Newton, 1965; Olmstead, 1989; Oregon Department of Geology and Mineral Industries, ~1955-1968). Articles of incorporation of the Dufur Oil Company were filed in the Wasco County clerk's office on April 19, 1907 with P.W. Knowles, C.P. Balch, L.M. Smith, and G.W. Johnston as the incorporators. The Dufur Oil Company wells reached a maximum depth of ±152 m (500 ft) but were abandoned; exploration discontinued in 1911 (Newton, 1965; Olmstead, 1989). The Beavis May Oil Company also examined the area starting in 1907, drilling two exploration wells located on Ramsey Creek, ~16 km (10 mi) west of the city of Dufur (**Figure 9-3**). The Beavis May well no. 1 bottomed at a depth of 521.2 m (1,710 ft). The Beavis May well no. 2, drilled in 1919, reached a depth >343 m (1,125 ft) (Buwalda, 1929; Newton, 1965; Olmstead, 1989; +Oregon Department of Geology and Mineral Industries, ~1955-1968).

Kastle Oil and Gas Company drilled the only other known oil and gas exploration well in the immediate area of Dufur in 1951 and 1952 (**Figure 9-3**). The precise location of the well is ambiguous, as the original notice of intention to drill a new well and well summary sheet locate the well in the headwaters of Dry Creek between Mosier and the Dalles (**Figure 9-3**; SE¼ of sec 20., T.2.N, R.12E.; Kastle Oil and Gas Company, 1951; Oregon Department of Geology and Mineral Industries, ~1955-1968). Subsequent publications (Newton, 1965; Olmstead, 1989) locate the well in upper Fifteenmile Creek (~18 km [11.2 mi] west of the city of Dufur), in a similar location to earlier wells drilled by the Dufur Oil Company (**Figure 9-3**). Total depth of the Kastle Oil and Gas Company well was ~67 m (220 ft) (Newton, 1965; Olmstead, 1989; Kastle Oil and Gas Company, 1951; Oregon Department of Geology and Mineral Industries, ~1955-1968).

**Figure 9-3. Partial view of the Oil and Gas Map of Eastern Oregon (Northern Half), produced but unpublished by DOGAMI between the years 1955 and 1968, shows the locations (red ovals) of exploration wells for the Dufur Oil Company, Beavis May Oil Company, and Kastle Oil and Gas Company in The Dalles and Dufur area. Public Land Survey (PLS) grid system shown on the map; each small square is 2.6 km$^2$ (1 mi$^2$). Logs describing the downhole geology are not known to exist.**

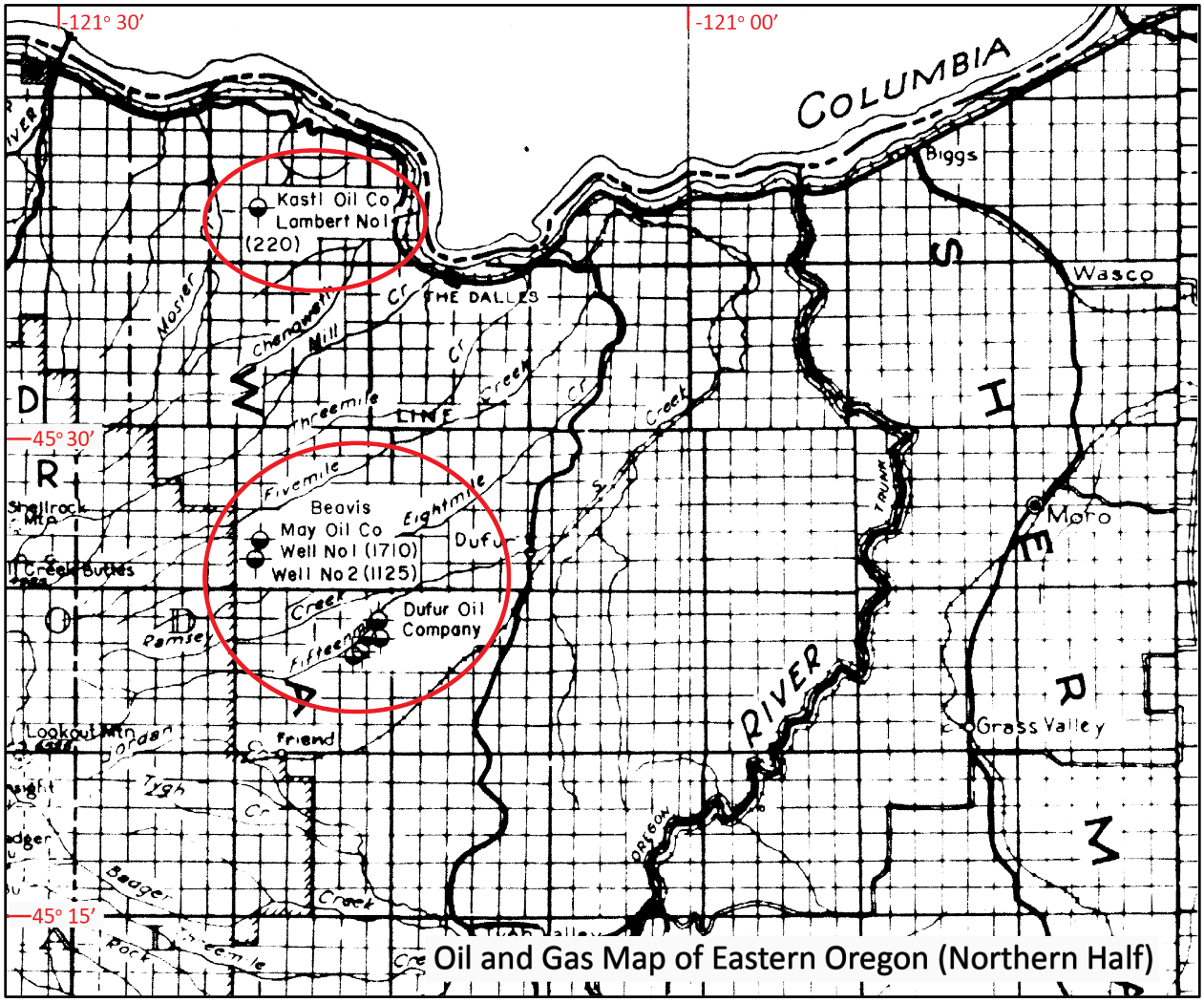


Available at: https://www.oregongeology.org/milo/archive/MineMaps/B1435-EastOreNorthHalfOilGas.pdf

## 9.3 Water Resources

A full discussion of the geologic controls on surface and groundwater resources in the Dufur area is beyond the scope of this report. The reader is directed to previous water resource-specific reports published by Piper (1932), Sceva (1966), Newcomb (1969), Grady (1983), Lite and Grondin (1988), Lindsey and others (2009), Burns and others (2012), and Lite (2013) for a more thorough discussion of groundwater resources and hydrogeology in the Middle Columbia Basin. Groundwater resources are strongly influenced by permeability differences between stratigraphic units and geologic structures, such as folds and faults. Several important hydrologic units have been identified in the area by the above cited workers. The lowermost parts of the groundwater flow systems in the map area lies within lava flows of the CRBG (Piper 1932; Newcomb, 1969). Overlying the CRBG are locally permeable epiclastic sedimentary and volcaniclastic rocks of the Dalles Formation, younger Pliocene and Pleistocene volcanics, and Quaternary surficial units.

### 9.3.1 CRBG aquifers

The extensive series of relatively stratiform units in the CRBG, many of which can be traced laterally from the Columbia Plateau west through the Columbia River Gorge, are a major host for groundwater in the Middle Columbia Basin (**Figure 5-6**). Most wells in the Dufur area rely on groundwater from aquifers hosted within the CRBG (Piper, 1932; Newcomb, 1969; Grady, 1983). Wells producing from these units typically intercept aquifers residing at multiple levels within the CRBG flow succession (Newcomb, 1963). However, interconnecting multiple aquifers in wells within the CRBG has elsewhere been shown to contribute to large water level declines in the aquifers (Lite and Grondin, 1988; Lindsey and others, 2009; Burns and others, 2012). Water-bearing horizons in the CRBG are generally associated with open framework interflow zones including vesicular flow-top breccia, flow-foot breccia, pillow lavas, and hyaloclastite complexes occurring near the base of a unit (**Figure 9-4**; Newcomb, 1969; Lite and Grondin, 1988; Tolan and others, 2009a; Lindsey and others, 2009). These horizons serve as horizontal to subhorizontal pathways for groundwater flow. Interiors to thick flow complexes typically have extremely low permeability and act as confining units unless secondary permeability exists due to fractures created by faults or folds, flow pinchouts or erosional windows, or where vertical conductivity occurs through cross-connected wells (**Figure 9-4**). Sedimentary interbeds can act as either a confining unit or a porous media serving as a pathway for lateral transport of groundwater. Permeability contrasts created by heterogeneities in flow successions creates a series of stacked confined aquifers in the CRBG aquifer system (**Figure 9-4**). Although some characteristics of CRBG flows are considered remarkably homogenous throughout their extent, hydrogeologic characteristics vary on local scales due to a difference in the environment of emplacement for each successive flow and the geologic setting of an area (Lite, 2013). Newcomb (1963) reported regional well yields from 300 gallons per minute (gpm) to 800 gpm from wells constructed in various formations of the CRBG in the nearby Mosier area (**Figure 1-1**). Grady (1983) reports yields of a few hundred to a few thousand gpm to wells.

Faults and folds in the Dufur area may act as flow boundaries within the CRBG aquifers (Plates 1, 2, and 3; e.g., Newcomb, 1969; Lite and Grondin, 1988; Burns and others, 2012; Lite, 2013). Faults in the Dufur area, like many described regionally within the Yakima Fold Belt, are roughly planar zones composed of coarsely shattered basalt that grades outward into areas of fine rock flour. Variations in the type and severity of deformation and extent of alteration along fault traces affects their ability to disrupt groundwater flow. Variability in the alteration process along the fault trace may leave open breccia zones that serve as ideal groundwater pathways, or alternatively may leave clay-altered or heavily cemented

(calcite) gouge that is likely to act as a low permeability zone. These low permeability fault zones inhibit lateral and vertical groundwater movement or create hydrologically isolated areas (Tolan and others, 2009a). Faults in the Dufur area, such as the Mays Canyon Creek fault are characterized by areas of siliceous sinter and clay-altered rock (**Figure 9-1**; Plate 1).

The narrow anticlinal ridges and broad synclinal valleys that compose this part of the Yakima Fold Belt are also known to influence the occurrence and movement of groundwater through CRBG aquifers, by affecting the hydraulic characteristics of interflow zones (Plates 1, 2, and 3; Newcomb, 1969; Lite and Grondin, 1988; Tolan and others, 2009a). The process of brittle folding in the Yakima Fold Belt has locally led to flexural slippage parallel to layering in the basalt in order to accommodate structural shortening. Flexural slippage typically occurs along interflow zones, with results ranging from minor shearing to complete alteration, reducing or destroying the permeability of these features (**Figure 9-4**; Newcomb, 1969; Tolan and others, 2009a).

**Figure 9-4. Schematic stratigraphic section of CRBG lava flows showing typical intraflow structures and vertical relationships of colonnade, entablature, and blocky columnar jointing, vesicular flow top, flow-top breccia, and pillow lava. Modified from Tolan and others (2009a). K values represent the typical hydraulic conductivity ranges in meters per second (m/s) and feet per day (ft/day).**

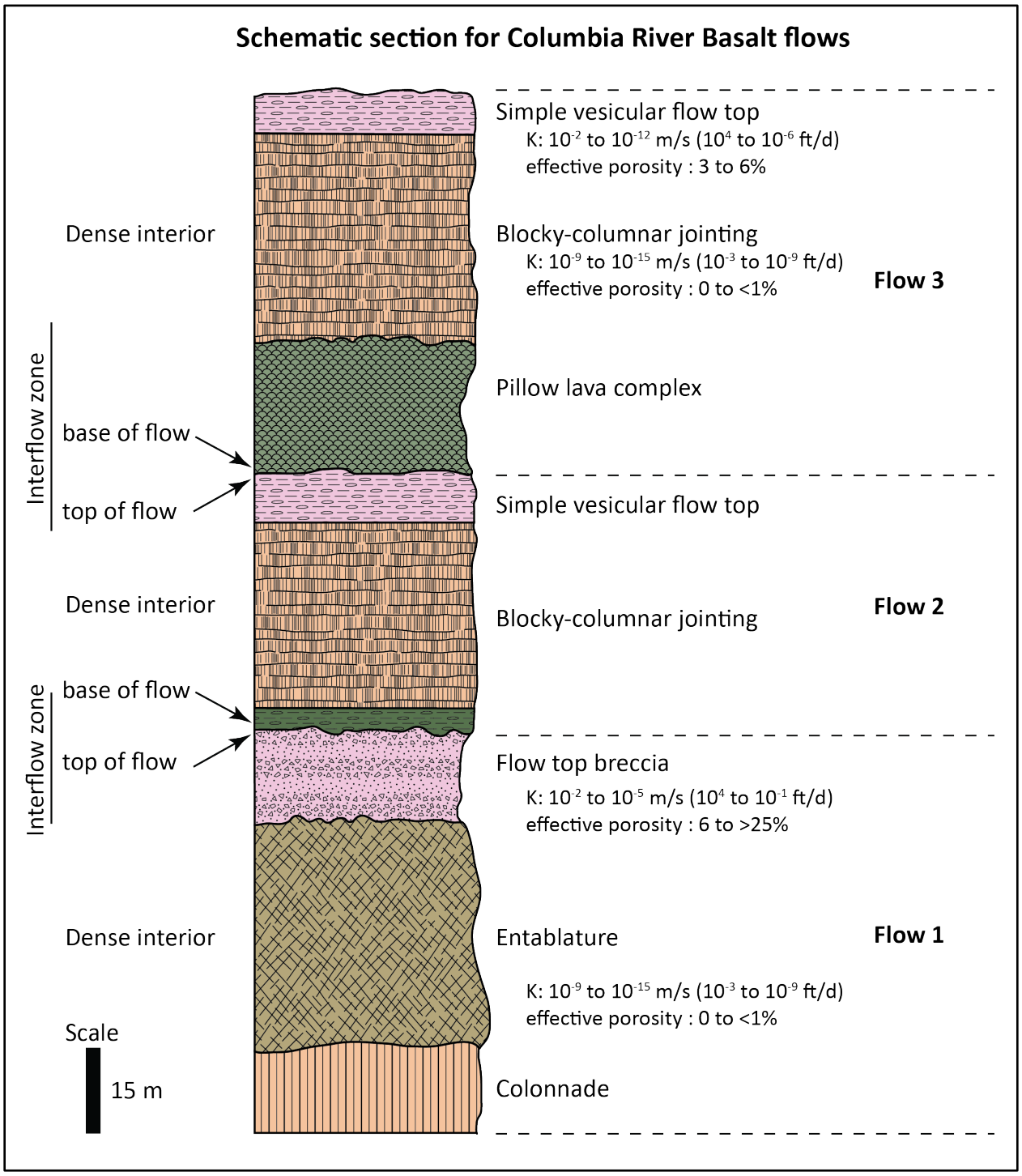

### 9.3.2 Dalles Formation aquifers

Permeability in the overlying Dalles Formation is generally very low due the common presence of lenticular to laterally discontinuous beds of poorly sorted, clay-matrix breccia and conglomerate, fine-grained tuff, tuffaceous clay, and tuffaceous sandstone (**Figure 6-37**; Piper, 1932; Lite and Grondin, 1988). More permeable beds or lenses of well-sorted cobble conglomerate and sandstone are present locally, especially in the lower part of the unit near the axes of regional synclines. However, these permeable beds are laterally discontinuous and share stark permeability differences between adjacent stratigraphic units, leading to a number of perched aquifers in the Dalles Formation (Piper, 1932). The catchment areas and recharge potential for permeable beds is also typically limited as many Dalles beds lie far above the nearby drainages and below the crests of narrow ridges (**Figure 6-35**, **Figure 6-36**; Plates 1, 2, and 3; Piper, 1932). Therefore, aquifers situated in more permeable layers within the formation may be suitable only for domestic use. Aquifers in the Dalles Formation may yield rates of 0.5 to 55 gpm, with larger production wells producing 150 to 250 gpm (Grady, 1983). Piper (1932) reported yields <20 gpm from the Dalles Formation in The Dalles and Dufur areas; where Dalles beds lie beneath principal surface streams, wells in the formation may yield as much as 100 gpm.

### 9.3.3 Pliocene and Pleistocene volcanic aquifers

Geographically restricted Pliocene and Pleistocene volcanics are not a significant source of groundwater in the map area. Physical properties of these units are similar to the older Dalles Formation. Wells completed in tuff beds or unconsolidated volcaniclastic beds are likely to yield only small quantities of water.

### 9.3.4 Alluvial deposits along local streams

Unconsolidated to partly consolidated alluvial sand and gravel preserved in terraces and floodplains (**Qa**, **Qao**) and on fans (**Qaf**) contains groundwater that typically saturates sediments just above the underlying bedrock platform and is usually in hydraulic connection with nearby streams (Plates 1, 2, and 3; Piper, 1932). The deposits are typically thin (<15 m [50 ft]), but are very permeable, except where they contain large amounts of silt (Piper, 1932). Alluvial wells developed in permeable sand and gravel intervals may intermittently yield 10 to 100 gpm, depending on annual precipitation (Piper, 1932). Relatively impermeable silt-rich sedimentary intervals do not contain much recoverable groundwater (Piper, 1932).

## 9.4 Geologic Hazards

### 9.4.1 Earthquakes and active faults

Numerous studies in the Pacific Northwest indicate the recent occurrence of large, regional earthquakes and the possibility of significant local events (e.g., Atwater, 1987; McCaffrey and Goldfinger, 1995; Atwater and Hemphill-Haley, 1997; Clague, 1997; McCaffrey and others, 2007; Frankel and Peterson, 2008). There has been little in the way of historic seismic activity in the Dufur area (Goter, 1994; Niewendorp and Neuhaus, 2003; https://earthquake.usgs.gov/earthquakes/search/). Historic (1896 to 2002) earthquake epicenters in the project area show events generally ranging in magnitude from M1.0 to 2.9 (Richter scale) with several larger events (M4.0 to M4.9) having occurred between Dufur and The Dalles in historic times (Beaulieu, 1977; Niewendorp and Neuhaus, 2003). Larger earthquake swarms are known nearby, beneath the volcanic edifice at Mount Hood (45 km [28 mi] west-southwest) and near Maupin (30 km [19 mi] south-southeast) (Niewendorp and Neuhaus, 2003; Braunmiller and others, 2014; https://earthquake.usgs.gov/earthquakes/search/). Communities in the Dufur area may be at risk from

four different types of earthquakes: 1) Cascadia subduction zone earthquakes; 2) crustal fault earthquakes; 3) those related to volcanic activity; and 4) deeper intraplate earthquakes occurring within the region (**Figure 9-5**; Madin and Wang, 2000). A map of maximum earthquake shaking (peak ground acceleration) produced by Madin and Mabey (1996) predicted a probabilistic ground shaking estimate for the Dufur area of 8 percent G (shaking felt by all, heavy objects move, slight damage) for the peak ground acceleration with a 10 percent chance of exceedance in 50 years. The 2018 USGS National Seismic Hazard Model for the conterminous United States estimated that the peak ground acceleration for the area with a 2 percent chance of exceedance in 50 years is 0.14 to 0.30 G (Rukstales and Petersen, 2019; https://www.sciencebase.gov/catalog/item/5d5597d0e4b01d82ce8e3ff1). The probabilistic ground shaking is dominated by local crustal sources.

**Figure 9-5. Schematic diagram showing tectonic setting of the Pacific Northwest and idealized locations of the four earthquake types described in the text. Modified from Madin and Wang (2000). Asterisks show the generalized locations of the types of earthquakes described in the text.**

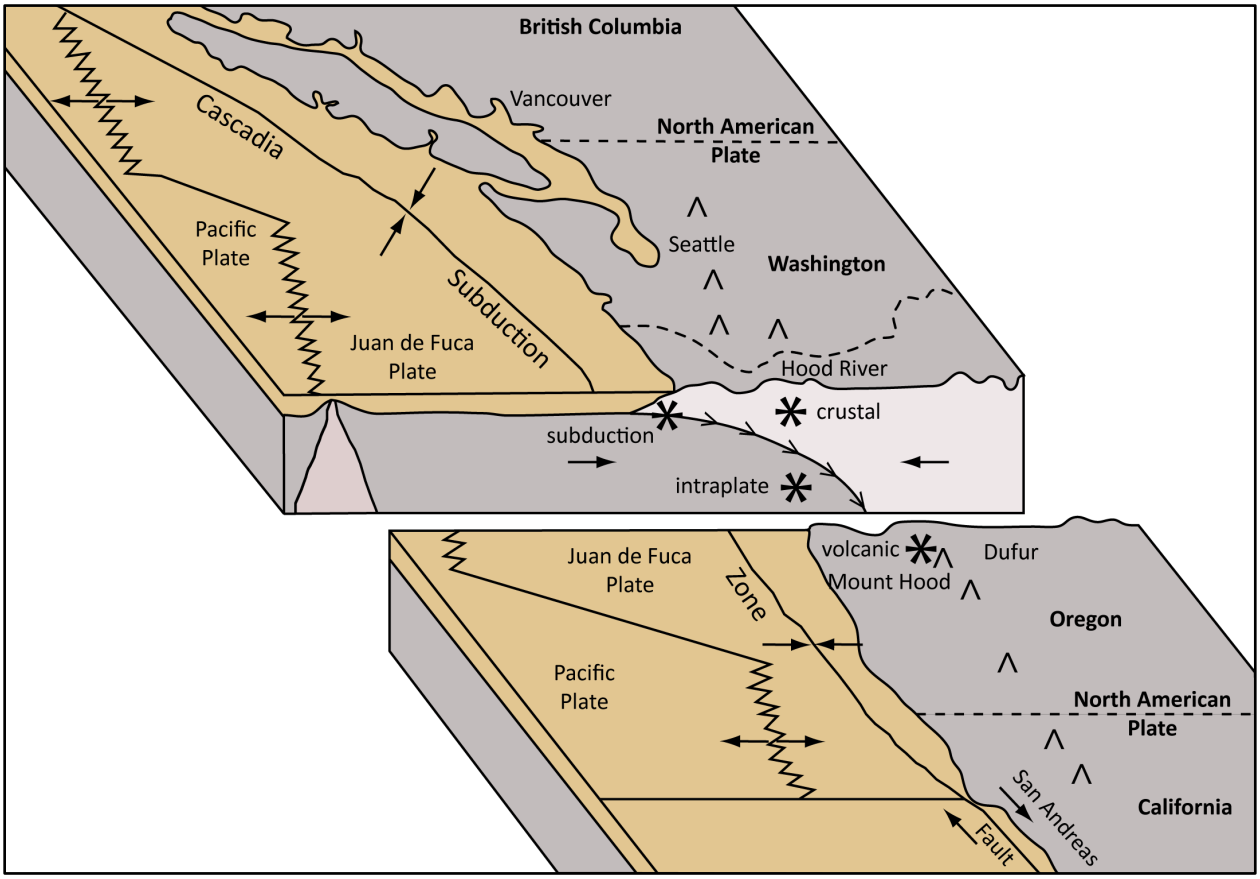


## 9.4.2 Subduction zone earthquakes

Subduction zone earthquakes occur where one crustal plate overrides an adjacent plate along a dipping interface, commonly known as a subduction zone. The Dufur area sits ~280 km (174 mi) east of the Cascadia subduction zone, which marks the plate boundary between the North American plate on the east and the underlying, smaller Juan de Fuca plate on the west (**Figure 5-1**; **Figure 9-3**). Beneath the Earth's surface, this zone extends eastward from the base of the continental slope, beneath western Oregon, and, as the lower plate continues to slide deeper into the Earth, it drives the processes that result in the

eruption of volcanoes in the Cascade Range. The Cascadia subduction zone is generally considered to be at high risk from large subduction zone earthquakes. Goldfinger and others (2003) and Nelson and others (2006) showed evidence of a number of great Cascadia subduction zone earthquakes, with the most recent occurring in 1700 A.D. (Satake and others, 1996). The Cascadia subduction zone is thought to produce earthquakes as a large as M9.0 every 400 to 500 years (Frankel and Peterson, 2008). More recent work by Goldfinger and others (2012) indicated more frequent intervals of ~240 years, with a 7 to 12 percent chance of a M9.0 Cascadia event in the next 50 years. Priest and others (2009) reported that at least 20 great subduction earthquakes have occurred on the Cascadia subduction zone during the last ~10,000 years. These events, with magnitudes in the range of M8.0 to M9.0 likely caused long duration, moderately strong shaking throughout much of the region, with intensity decreasing eastward from the epicenter. Site effects from such an event, including earthquake induced liquefaction, landsliding, and amplification of shaking by low-velocity surficial deposits could dramatically enhance damage in the area. Madin and Burns (2013) indicated that a M9.0 Cascadia event would result in light to very light damage in the Dufur area (see Plate 7 in Madin and Burns, 2013).

### 9.4.3 Crustal earthquakes

Crustal earthquakes result from shallow sources within the North American plate (**Figure 9-5**). Epicenters are located at relatively shallow depths of 10 to 20 km (6 to 12 mi) below land surface. East of the Cascades, the majority of earthquake shaking hazard comes from crustal earthquakes (Madin and Mabey, 1996). In the western part of the Columbia River Flood Basalt Province, focal mechanisms of small magnitude (<M3) earthquakes are associated with some northwest-striking wrench faults in the Yakima Fold Belt (**Figure 5-2**), providing direct evidence that some of these faults could remain active (Bela, 1982; USDOE, 1988; Yelin and Patton, 1991). The presence of other possibly Quaternary faults in north-central Oregon is indicated by new geologic mapping and compilations published by previous workers (Geomatrix Consultants, Inc., 1995; Madin and Mabey, 1996; Weldon and others, 2003; Lidke and others, 2003; Personius and others, 2003; McClaughry and others, 2012; McClaughry and others, 2020a). Direct and definitive evidence of youthful faulting at the surface, however, remains relatively sparse.

### 9.4.4 Volcanic earthquakes

Volcanic earthquakes in the area are usually small in magnitude and occur over infrequent intervals; earthquakes of this type of at least M4.5 or larger can occur around Mount Hood (**Figure 5-1**, **Figure 5-2**, **Figure 9-5**). During 2002 a swarm of earthquakes ranging from M3.2 to M4.5 occurred on the southeast flank of Mount Hood (Burns and others, 2011). These types of earthquake swarms are known to occur periodically within the vicinity of the volcano; they do not necessarily indicate impending eruptions. The USGS Cascades Volcano Observatory (CVO; https://www.usgs.gov/observatories/cascades-volcano-observatory) continuously monitors earthquakes in the Cascades through a regional seismograph network and will provide warning, as possible, if activity suggests potential for volcanic eruptions.

### 9.4.5 Intraplate earthquakes

The Dufur area may also experience site effects from deeper intraplate earthquakes, which result from movement within the underlying Juan De Fuca plate (**Figure 9-5**). These earthquakes could occur beneath much of the Pacific Northwest at depths of 40 to 60 km (25 to 37 mi). The large earthquakes that caused significant damage in the Puget Sound region in 1949 (Olympia), 1965 (Puget Sound), and 2001 (Nisqually) are considered to have been deep intraplate earthquakes (Haugerud and others, 1999).

### 9.4.6 Site effects

Ground shaking, soil liquefaction, landslides, surface ruptures, and seiches are all possible causes of damage during an earthquake in the Dufur area. The damaging effects of earthquakes can be enhanced by proximity to epicenters, amplification of shaking in soft soils, by liquefaction, or by induced landslides. Detailed relative hazard maps that incorporate all of these hazards into single risk categories have not been compiled for the Dufur area, but Madin and Burns (2013) have produced regional seismic hazard maps generated on the basis of statewide geologic data. Liquefaction hazards occur where the shaking of a water-saturated soil causes its material properties to change from a solid to a liquid. Soils that liquefy tend to be loose, granular soils that are saturated with water. Unsaturated soils will not liquefy but may settle. Areas underlain by artificial fill (**Qf**) and alluvium (**Qa**, **Qao**), such as Fifteenmile Creek (Plates 1, 2, and 3), have a moderate liquefaction susceptibility (see liquefaction susceptibility map in Madin and Burns, 2013). Where bedrock (volcanic rock or lithified sedimentary rock) is exposed at the surface, such as in uplands or in the bottoms of incised drainages, the liquefaction hazard is negligible (Madin and Burns, 2013).

## 9.5 Volcanic Hazards

The Dufur area lies ~45 km [28 mi] east of the axis of the intermittently active volcanic zone along Cascades volcanic arc and Quaternary Mount Hood volcano (**Figure 5-1**; **Figure 5-2**). Unlike other geologic hazards discussed in this report (e.g., earthquakes) which may occur over several seconds to minutes, a volcanic episode can last days to decades and may include multiple syn- and inter-eruptive events. Volcanic hazards for the Dufur area, identified by the USGS and by DOGAMI are restricted to fallout of tephra and lava flows.

### 9.5.1 Tephra fall

Tephra (volcanic ash) generated by larger eruptions at Mount Hood or other nearby Cascade volcanoes may fall on areas up to several hundred km downwind (**Figure 5-1**; **Figure 5-2**). Such events are inferred to pose little risk to communities in the vicinity of Mount Hood (Scott and others, 1997). On the basis of Mount Hood's past tephra production, it is estimated that nearby communities such as Dufur and the Dalles would likely receive a tephra thickness up to 1.5 cm (0.6 in) in any one event (Scott and others, 1997). The 30-year probability of accumulation of 1 cm (0.4 in) or more tephra in the Dufur area from eruptions in the Cascade Range is 1 in 30; the 30-year probability of accumulation of 10 cm (4 in) or more tephra in the Dufur area from eruptions in the Cascade Range is 1 in 150 (Scott and others, 1997). However, no such thickness of tephra in the map area is known from a Holocene eruption at Mount Hood. Hazards associated with tephra falls include tens of minutes or more of darkness, paint damage, clogging of engine filters with fine particles, short circuiting of electric transformers and power lines, and disruption of air traffic (e.g., Mount St. Helens eruptions, May 1980). Larger events may include the possibility of roof collapse of structures.

### 9.5.2 Lava flows

Several basaltic and basaltic andesite shield volcanoes have erupted west of the Dufur area over the past three million years, sending lava flows down northeast-directed stream channels. Remnants of the distal toes of several of these lava flows extend down the Threemile and Fivemile Creek drainages as far east as Mount Hood Flat (southwest corner of The Dalles South 7.5′ quadrangle, northwest corner of the Wolf Run 7.5′ quadrangle [Plate 1]) and Oak Flat (Brown Creek 7.5′ quadrangle, **Figure 1-2**). Corresponding

vents for these lava flows are located along the eastern escarpment of the Hood River graben, ~26 km (16 mi) southwest of Dufur (**Figure 5-2**; McClaughry and others, 2012; McClaughry and others, 2020a). Additional relatively youthful flows of note have erupted in the past 1 million years from Gordon Butte (near The Dalles) and entered the Deschutes River Canyon (Newcomb, 1969; O'Connor and others, 2003). Far-traveled lava flows may extend down paleochannels more than 20 to 30 km (12.4 to 18.6 mi) (e.g., basaltic andesite of Dog River [**Qr5dr**]; McClaughry and others, 2020a) from source volcanoes. Future eruptions in the Dufur area are expected to occur within and marginal to the broad structural zone associated with the Hood River graben on the west (McClaughry and others, 2012; McClaughry and others, 2020a). Hazards associated with lava flow events include tephra falls proximal to vents, lava flows in more distal areas (probably ≥20 km (12.4 mi) from the vent based on topography, and disruption of local stream drainages. Scott and others (1997) estimate the 30-year probability of such an eruption occurring in the area to be low at 1 in 100,000.

## 9.6 Landslide Hazards

The downslope movement of rock and soil, in the form of landslides, rock falls, and debris flows may present a geologic hazard to residents, infrastructure, and transportation corridors in the Dufur area. Three general types of landslide processes are present in the map area, including (1) typical and colluvial landslides, (2) rock fall, and (3) debris-flows.

### 9.6.1 Typical and colluvial landslides

Relatively few (*n* = 72) landslide deposits (**Qls**) were mapped in the Dufur area. Those landslide deposits (**Qls**) mapped cover 0.002 percent of the map area and are limited in size covering less than 12 hectares (30 acres) and more typically less than 0.8 hectares (2 acres). A majority of mapped landslide deposits are simple rotational or translational slides or shallow-seated earthflow-type features that occur along major drainages, originating on sparsely vegetated, moderately to steep slopes underlain by weakly consolidated rocks of the Dalles Formation (**Tmdl**) or from flow contacts within the CRBG (Plates 1, 2, and 3; Beaulieu, 1977). Many of these simple slides can be attributed to the combined influences of parallel topographic slope and bedding dip, undercutting by streams, heavy precipitation, groundwater conditions, and rock type (Beaulieu, 1977). The generally weakly consolidated nature of the Dalles Formation makes this unit especially prone to landslides on gently to steeply inclined slopes. Future landslides should be expected in this unit particularly in areas of changing land use where infrastructure development (e.g., drain fields, septic tanks, modified runoff, and/or irrigation) may alter local groundwater conditions (Beaulieu, 1977).

A few slopes in the study area are mantled by unstable colluvial wedges of soil and rock. These deposits, mapped as colluvium (**Qc**), typically form when weathered rock particles, ranging in size from clay to boulders, accumulate along a hillside contact (Plates 1, 2, and 3). When the mass of the accumulated material reaches a critical size, a triggering event such as heavy rainfall or seismogenic event may initiate the rapid down slope movement of this mass. Areas denuded by fire or other anthropogenic vegetative removal can especially be at risk from such events.

### 9.6.2 Rock fall

Rock fall and rockslide hazards may be present in the study area where very steep slopes are present (e.g., unit **Tmdw** exposed between Wolf Run and Eightmile Creek, Plate 2; **Figure 6-45**). Potential natural

triggering mechanisms for rock fall events may include freeze/thaw conditions, heavy rainfall, earthquakes, or extensive devegetation due to fire.

### 9.6.3 Debris-flows

Many small-sized alluvial and debris fans (**Qaf**) in the study area have been mapped along drainages in the Dufur area (**Figure 6-3**; Plate 2). Rapidly moving landslides in the form of debris flows may be expected on both alluvial and debris fans (**Qaf**) lying at the mouth of steep-sided, colluvium-filled canyons and upland drainages. The potential for inundation of fan areas by rapidly moving debris flows is increased during episodes of intense rainfall that occur after soils have been saturated by fall and early winter rainfall. Redirected drainage and poor construction practices are human activities that could initiate debris flows (Beaulieu, 1977). Debris flows have the potential to threaten life and may cause extensive damage to property and public lifelines including highways and railways.

## 9.7 Flooding Hazards

Flooding hazards in the study area typically result from a combination of steep topography, low bedrock infiltration rates, and the periodic occurrence of high-precipitation weather events or late fall and winter marine storms that place warm rain across significant accumulations of low-elevation snow. Other sources of flooding include flash floods associated with locally intense (summer) thunderstorms, channel migration, ice or debris jams, and much less frequently, artificial-dam or landslide-dam failures. A number of notable floods have occurred in the Pacific Northwest, as a result of high-precipitation or rain-on-snow-events during the years 1861/1862, 1894, 1948, 1964/1965, 1977, 1996, and 2005/2006 (Department of Land Conservation and Development, 2015). Five flood events have been declared major disasters in Wasco County since 1964 (1964, 1974, 1995, 1996, and 2007). The most significant flood events in this area have typically occurred in the larger drainages of Pine, Fifteenmile, Eightmile, and Fivemile creeks (Plates 1, 2, and 3).

Floods cause damage to buildings and infrastructure through inundation by water and by erosion and deposition of sediment and debris. Significant hazards related to channel migration are present in the area. Channel migration hazards can occur slowly, for example, by continuous erosion along a cutbank meander and deposition onto a point bar during high flows, or very rapidly during storm events through avulsion (the rapid abandonment of the current river channel for a new one) (Beaulieu, 1977; Easterbrook, 1993; Rapp and Abbe, 2003). Channel migration hazards in the drainages may be substantial within the narrow inner gorges of streams due to the large volume of loose sediment are added to the fluvial system from frequent upslope debris flows or loosely consolidated artificial fills (Plates 1, 2, and 3; **Figure 6-2b**). This loose sediment is easily eroded and transported through flood torrents, thereby amplifying the channel migration process downstream. Infrequent torrential floods accompanying periodic thunderstorms, should also be expected in the map area, where steep gradient canyons are incised into the CRBG. These canyons have narrow floodplains and are characterized by catastrophic streamflow, erosion, and deposition. Hazards along these channels include erosion of roads, fills, bridge pilings, and plugging of culverts.

Significant flood events, similar to that describe above, were triggered in the Middle Columbia Basin in 1974 and again in 1996, associated with heavy rainfall from severe storms across the Pacific Northwest. Flooding in January 1974 was generated by heavy precipitation at low elevations and inundated major parts of the Fifteenmile Creek and Eightmile Creek watersheds (Plates 1, 2, and 3). Floodwaters overtopped streambanks, extensively spread out along parts of adjacent floodplains, and locally eroded

steep cutbanks (see Figures 27, 28, 29, and 30 in Beaulieu, 1977; mapped as **Qa** on Plates 1, 2, and 3). Flooding in February 1996 occurred when warming and intense precipitation (5 to 6.4 cm [2 to 2.5 in]) initiated rapid snowmelt across the Middle Columbia Basin. Infiltration of intense rainfall was limited by several factors, including frozen soils, iced-over creeks, and hard-crusted snow. The resulting overland flows scoured soils and filled upland drainages where ice-jams, clogged culverts, and bridges had reduced stream capacity. The combination of these conditions led to widespread flooding, landslides, erosion, and debris flows downstream.

Relatively recent flash-flood-type events were triggered in the upper parts of the Fifteenmile Creek watershed on July 8 and 9, 1995 by intense thunderstorms focused above Tygh Ridge ("Twin Flash Floods of 1995", Clark, 2003; American Lifelines Alliance, 2005; FEMA [1995] DR-1061; http://www.fema.gov/disaster/1061). The resulting flash floods caused extensive damage downstream to local infrastructure, including roads, culverts, and bridges, and significantly changed large segments of stream bed that hosted important fish habitat. Infrastructure and stream-bed damages were accompanied by agricultural crop losses and soil erosion. Total damage for the two day "Twin Flash Floods" event was estimated to be ~$5.3 million (Clark, 2003; American Lifelines Alliance, 2005).

## 10.0 ACKNOWLEDGMENTS

Geologic mapping in the Dufur area was supported through the STATEMAP component of the National Cooperative Geologic Mapping Program under cooperative agreement numbers G15AC00180 (2015) and G20AC00202 (2020), and by the Oregon Water Resources Department (OWRD) through Interagency Agreements DOGAMI/OWRD IAA #12102013/OWRD 13 057 (2014) and DOGAMI IAA# DASPS-2542-16/OWRD IAA 16 047 (2016). Additional funds were provided by the State of Oregon through the Oregon Department of Geology and Mineral Industries. XRF geochemical analyses were prepared and analyzed by Dr. Scott Burroughs at the GeoAnalytical lab at Washington State University and by Dr. Stan Mertzman at Franklin and Marshall College. Isotopic ages were prepared and analyzed by Drs. Anthony Koppers and Daniel Miggins at the College of Oceanic and Atmospheric Sciences, Oregon State University, Corvallis, Oregon. The authors appreciate critical information shared by Michael Sawlan and Jonathan Hagstrum on the geology of Butler Canyon. Informative discussions and field trips with Ray Wells, Jim Anderson, Jim O'Connor, and Charlie Cannon added to our knowledge of CRBG and Dalles Formation stratigraphy in the Columbia River Gorge. Additional discussions with Mark Ferns, Tom Wiley, Mike Sawlan, Jon Le Marche, Ken Lite, Darrick Boschmann, and Frank Hladky are appreciated. Informative discussions with participants of a 2019 Geological Society of America field trip through the area significantly added to our knowledge and understanding of the Hood River graben and the Dufur area. The authors acknowledge many area landowners who provided local knowledge and graciously allowed access to private holdings. Larry McCollum, Water Quality Manager, granted access to lands administered by the City of The Dalles Municipal Watershed. We sincerely appreciate the gracious hospitality and support of Claire Sierra and Josiah Dean, Samantha and Jeff Irwin, and the staff at the Historic Balch Hotel in Dufur. Cartography for the map plates was provided by Jon J. Franczyk and John Bauer. Critical and insightful reviews by Jim O'Connor (USGS), Charlie Cannon (USGS), Mark Ferns (DOGAMI-retired), Bill Burns (DOGAMI), Bob Houston (DOGAMI), Nancy Calhoun (DOGAMI), Christina Appleby (DOGAMI), and John Bauer (DOGAMI-retired) greatly enriched the final manuscript, geodatabase, and geologic maps.

# 11.0 REFERENCES


Allen, J.E., 1966, The Cascade Range volcano-tectonic depression of Oregon, *in* Benson, G.T., ed., Transactions of the Lunar Geological Field Conference, Bend, Oregon, August 1965: Oregon Department of Geology and Mineral Industries Open-File Report O-66-01, p. 21-23. https://www.oregongeology.org/pubs/ofr/O-66-01.pdf, accessed March 12, 2021.

American Lifelines Alliance, 2005, Flood resistant local road systems: a report based on case studies: American Lifelines Alliance January 2005, 83 p. https://www.americanlifelinesalliance.com/pdf/ALA_Flood-Roads_January2005.pdf, accessed March 12, 2021.

Anderson, J.L., 1987, The structure and ages of deformation of a portion of the southwest Columbia Plateau, Washington and Oregon: Los Angeles, University of Southern California, Ph.D. dissertation, 272 p.

Anderson, J.L., and Tolan, T.L., 1986, Ages of wrench faulting in interridge basins, southwest Columbia Plateau, Washington and Oregon: Geological Society of America Abstracts with Programs, v. 18, p. 82.

Anderson, J.L., and Vogt, B.F., 1987, Intracanyon flows of the Columbia River Basalt Group in the southwestern part of the Columbia Plateau and adjacent Cascade Range, Oregon and Washington, *in* Schuster, J.E., ed., Selected papers on the geology of Washington: Washington Division of Geology and Earth Resources Bulletin 77, p. 249-267. https://www.dnr.wa.gov/publications/ger_b77_papers_on_wa_geology_pt3of3.pdf, accessed March 12, 2021.

Anderson, J.L., Tolan, T.L., and Wells., R.E., 2013, Strike-slip faults in the western Columbia River flood basalt province, Oregon and Washington, *in* Reidel, S.P., Camp, V., Ross, M.E., Wolff, J.A., Martin, B.E., Tolan, T.L., and Wells, R.E., eds., The Columbia River Flood Basalt Province: Geological Society of America Special Paper 497, p. 325-347. https://pubs.geoscienceworld.org/books/book/661/chapter/3807302/Strike-slip-faults-in-the-western-Columbia-River, accessed March 12, 2021.

Atwater, B.F., 1987, Evidence for great Holocene earthquakes along the outer coast of Washington State: Science, v. 236, p. 942–944. http://activetectonics.asu.edu/lipi/Lecture24_Tsunami/Atwater_Science1987.pdf, accessed March 12, 2021.

Atwater, B.F., and Hemphill-Haley, E., 1997, Recurrence intervals for great earthquakes of the past 3,500 years at northeastern Willapa Bay, Washington: U.S. Geological Survey Professional Paper 1576, 108 p. https://pubs.er.usgs.gov/publication/pp1576, accessed March 12, 2021.

Baksi, A.K., 2013, Timing and duration of volcanism in the Columbia River Basalt Group: A review of existing radiometric data and new constraints on the age of the Steens through Wanapum Basalt extrusion, *in* Reidel, S.P., Camp, V., Ross, M.E., Wolff, J.A., Martin, B.E., Tolan, T.L., and Wells, R.E., eds., The Columbia River Flood Basalt Province: Geological Society of America Special Paper 497, p 67-86. https://pubs.geoscienceworld.org/books/book/661/chapter/3807126/Timing-and-duration-of-volcanism-in-the-Columbia, accessed March 12, 2021.

Barry, T.L., Self, S., Kelley, S.P., Reidel, S., Hooper, P., and Widdowson, M., 2010, New $^{40}Ar/^{39}Ar$ dating of the Grande Ronde lavas, Columbia River Basalts, USA: implications for duration of flood basalt eruption episodes: Lithos, v. 118, p. 213–222. https://www.sciencedirect.com/science/article/abs/pii/S0024493710000897, accessed March 12, 2021.

Barry, T.L., Kelley, S.P., Reidel, S.P., Camp, V.E., Self, S., Jarboe, N.A., Duncan, R.A., and Renne, P.R., 2013, Eruption chronology of the Columbia River Basalt Group, *in* Reidel, S.P., Camp, V.E., Martin, M.E., Ross, M.E., Wolff, J.A., Martin, B.S., Tolan, T.L., and Wells, R.E., eds., Geological Society of America Special Paper 497, p. 45–66. https://pubs.geoscienceworld.org/books/book/661/chapter/3807104/Eruption-chronology-of-the-Columbia-River-Basalt, accessed March 12, 2021.

Beaulieu, J.D., 1977, Geologic hazards of parts of northern Hood River, Wasco, Sherman counties, Oregon: Oregon Department of Geology and Mineral Industries Bulletin 91, 95 p. 11 pl., scale 1:62,500. https://www.oregongeology.org/pubs/B/B-091.pdf, accessed March 12, 2021.

Beeson, M.H., and Tolan, T.L., 1990, The Columbia River Basalt Group in the Cascade Range: A middle Miocene reference datum for structural analysis: Journal of Geophysical Research, v. 95, p. 19,547-19,559. https://agupubs.onlinelibrary.wiley.com/doi/abs/10.1029/JB095iB12p19547, accessed March 12, 2021.

Beeson, M.H., Moran, M.R., Anderson, J.L., and Vogt, B.F., 1982, The relationship of the Columbia River Basalt Group to the geothermal potential of Mount Hood area, Oregon, *in* Priest, G. R., and Vogt, B. F., eds., Geology and geothermal resources of the Mount Hood area, Oregon: Oregon Department of Geology and Mineral Industries Special Paper 14, p. 43–46. https://www.oregongeology.org/pubs/sp/SP-14.pdf, accessed March 12, 2021.

Beeson, M.H., Fecht, K.R., Reidel, S.P., and Tolan, T.L., 1985, Regional correlations within the Frenchman Springs Member of the Columbia River Basalt Group: new insights into the middle Miocene tectonics of northwest Oregon: Oregon Geology, v. 47, no. 8, p. 87-96. https://www.oregongeology.org/pubs/OG/OGv47n08.pdf, accessed March 12, 2021.

Beeson, M.H., Tolan, T.L., and Anderson, J.L., 1989, The Columbia River Basalt Group in western Oregon: Geologic structures and other factors that controlled flow emplacement patterns, *in* Reidel, S. P., and Hooper, P. R., eds., Volcanism and tectonism in the Columbia River Flood-Basalt Province: Geological Society of America Special Paper 239, p. 223-246. https://pubs.geoscienceworld.org/books/book/375/chapter/3797037/The-Columbia-River-Basalt-Group-in-western-Oregon, accessed March 12, 2021.

Bela, J.L., 1982, Geologic and neotectonic evaluation of north-central Oregon: the Dalles 1° × 2° quadrangle: Oregon Department of Geology and Mineral Industries GMS 27, 2 pl., scale 1:250,000. https://www.oregongeology.org/pubs/gms/GMS-027.pdf, accessed March 12, 2021.

Bennett, S.E.K., Wells, R.E., Streig, A.R., Madin, I.P., and Stelten, M.E., 2019, Oblique slip history of active faults along the western margin of the Hood River graben, North-Central Oregon: Geological Society of America Abstracts with Programs., v. 51, no. 4. https://gsa.confex.com/gsa/2019CD/webprogram/Paper329235.html, accessed March 12, 2021.

Boyd, F.R., and Mertzman, S.A., 1987, Composition of structure of the Kaapvaal lithosphere, southern Africa, *in* Mysen, B.O., ed., Magmatic processes—physico-chemical principles: The Geochemical Society, Special Publication 1, p. 13–24. https://www.geochemsoc.org/files/8214/1258/3689/SP-1_013-024_Boyd.pdf, accessed March 12, 2021.

Braunmiller, J., Nabelek, J.L., and Trehu, A.M., 2014, A seasonally modulated earthquake swarm near Maupin, Oregon: Geophysical Journal International, v. 197, p. 1736-1743. https://ieeexplore.ieee.org/document/8144323, accessed March 12, 2021.

Bunker, R.C., Farooqui, S.M., and Thorns, R.E., 1982, K-Ar dates for volcanic rocks associated with Neogene sedimentary deposits in north-central and northeastern Oregon: Isochron/West, no. 33, p. 21-22.

Burchfiel, B.C., and Stewart, J.H., 1966, "Pull-apart" origin of the central segment of Death Valley, California: Geological Society of America Bulletin, v. 7, p. 439–442. https://pubs.geoscienceworld.org/gsa/gsabulletin/article-abstract/77/4/439/6063/PULL-APART-ORIGIN-OF-THE-CENTRAL-SEGMENT-OF-DEATH, accessed March 12, 2021.

Burns, E.R., Morgan, D.S., Lee, K.K., Haynes, J.V., and Conlon, T.D., 2012, Evaluation of long-term water-level declines in basalt aquifers near Mosier, Oregon: U.S. Geological Survey Scientific Investigations Report 2012-5002, 134 p., GIS files. https://pubs.usgs.gov/sir/2012/5002/, accessed March 12, 2021.

Burns, W.J., Hughes, K.L.B., Olson, K.V., McClaughry, J.D., Mickelson, K.A., Coe, D.E., English, J.T., Roberts, J.T., Lyles Smith, R.R., and Madin, I.P., 2011, Multi-hazard and risk study for the Mount Hood region, Multnomah, Clackamas, and Hood River counties, Oregon: Oregon Department of Geology and Mineral Industries Open-File Report O-11-16, 179 p., 7 pl., scale 1:72,000, spreadsheets. https://www.oregongeology.org/pubs/ofr/p-O-11-16.htm, accessed March 12, 2021.

Butler, R.F., 1992, Origins of natural remanent magnetism, *in* Paleomagnetism: Magnetic domains to geologic terranes: Boston, Blackwell Scientific Publications, p. 31-63.

Buwalda, J.P., 1929, A Neocene erosion surface in central Oregon: Washington, D.C., Carnegie Institution, Publications of the Carnegie Institution of Washington, no. 404, p. 1-10.

Buwalda, J.P., and Moore, B.N., 1929, Age of Dalles Beds and "Satsop" Formation and history of Columbia River gorge (abs.): Geological Society of America Bulletin, v. 40, p. 176-177.

Buwalda, J.P., and Moore, B.N., 1930, The Dalles and Hood River Formations and the Columbia River Gorge: Washington, D.C., Carnegie Institution, Publications of the Carnegie Institution of Washington, no. 404, p. 11-26. https://authors.library.caltech.edu/99607/1/Buwalda_1929p11.pdf, accessed March 12, 2021.

Cahoon, E.B., Streck, M.J., Koppers, A.A.P., and Miggins, D.P., 2020, Reshuffling the Columbia River Basalt chronology—Picture Gorge Basalt, the earliest- and longest-erupting formation: Geology, v. 48, p. 348-352. https://doi.org/10.1130/G47122.1, accessed March 12, 2021.

Calder, E.S., Luckett, R., Sparks, R.S.J., and Voight, B., 2002, Mechanisms of lava dome instability and generation of rockfalls and pyroclastic flows at Soufrière Hills Volcano, Montserrat, *in* Druitt, T.H., and Kokelaar, B.P., eds., The Eruption of Soufrière Hills Volcano, Montserrat, from 1995 to 1999: Geological Society London Memoir, 21, 173-190. https://mem.lyellcollection.org/content/21/1/173, accessed March 12, 2021.

Camp, V.E., 1981, Geologic studies of the Columbia Plateau: Part II, Upper Miocene basalt distribution reflecting source locations, tectonism, and drainage history of the Clearwater embayment, Idaho: Geological Society of America Bulletin, v. 92, no. 9, p. 669-678. https://pubs.geoscienceworld.org/gsa/gsabulletin/article-abstract/92/9/669/202710/Geologic-studies-of-the-Columbia-Plateau-Part-II?redirectedFrom=fulltext, accessed March 12, 2021.

Camp, V.E., and Ross, M.E., 2004, Mantle dynamics and genesis of mafic magmatism in the intermontane Pacific Northwest: Journal of Geophysical Research, v. 109. https://agupubs.onlinelibrary.wiley.com/doi/10.1029/2003JB002838, accessed March 12, 2021.

Camp, V.E., Ross, M.E., and Hanson, W.E., 2003, Genesis of flood basalts and Basin and Range volcanic rocks from Steens Mountain to the Malheur River Gorge, Oregon: The Geological Society of America Bulletin, v. 115, p. 105-128. https://pubs.geoscienceworld.org/gsa/gsabulletin/article-abstract/115/1/105/183895/Genesis-of-flood-basalts-and-Basin-and-Range?redirectedFrom=fulltext, accessed March 12, 2021.

Cande, S.C., and Kent, D.V., 1992, A new geomagnetic polarity time scale for the Late Cretaceous and Cenozoic: Journal of Geophysical Research, v. 97, p. 13,917-13,951. https://onlinelibrary.wiley.com/doi/10.1029/92JB01202/abstract, accessed March 12, 2021.

Cannon, C.M., and O'Connor, J.E., 2019, New constraints on the timing of Neogene filling and incision of the Dalles Basin, Oregon and Washington: Geological Society of America Abstracts with Programs, v. 51, no. 4. https://gsa.confex.com/gsa/2017AM/webprogram/Paper303186.html, accessed March 12, 2021.

Carrasco-Núñez, G., 1999, Holocene block-and-ash flows from summit dome activity of Citlaltépetl volcano, Eastern Mexico: Journal of Volcanology and Geothermal Research, v. 88, p. 47-66. https://www.sciencedirect.com/science/article/abs/pii/S0377027398001103, accessed March 12, 2021.

Clague, J.J., 1997, Evidence for large earthquakes at the Cascadia subduction zone: Reviews in Geophysics, v. 35, p. 439–460. https://onlinelibrary.wiley.com/doi/10.1029/97RG00222/epdf, accessed March 12, 2021.

Clark, J.S., 2003, Fifteenmile Watershed Assessment: Wasco County Soil and Water Conservation District, p. 65. https://wascoswcd.org/linked/15mile_ws_assessment.pdf, accessed March 12, 2021.

Cohen, K.M., Finney, S.C., Gibbard, P.L. and Fan, J.-X., 2013 (updated 2015), The ICS International Chronostratigraphic Chart: Episodes 36, p. 199-204. http://www.stratigraphy.org/index.php/ics-chart-timescale, accessed March 12, 2021.

Condon, T., 1874, Preliminary report of the State Geologist to the Legislative Assembly, 8th regular session: Salem, Oregon, 22 p.

Conrey, R.M., Sherrod, D.R., Uto, K., and Uchiumi, S., 1996, Potassium-argon ages from Mount Hood area of Cascade Range, northern Oregon: Isochron/West, no. 63, p. 10-20.

Conrey, R.M., Sherrod, D.R., Hooper, P.R., and Swanson, D.A., 1997, Diverse primitive magmas in the Cascade Arc, northern Oregon and southern Washington: The Canadian Mineralogist, v. 35, p. 367-396. https://pubs.geoscienceworld.org/canmin/article-abstract/35/2/367/12854/Diverse-primitive-magmas-in-the-Cascade-Arc?redirectedFrom=fulltext, accessed March 12, 2021.

Conrey, R.M., Taylor, E.M., Donnelly-Nolan, J.M., and Sherrod, D.R., 2002, North-central Oregon Cascades: Exploring petrologic and tectonic intimacy in a propagating intra-arc rift, *in* Moore, G. W., ed., Field guide to geologic processes in Cascadia: Oregon Department of Geology and Mineral Industries Special Paper 36, p. 47-90. https://www.oregongeology.org/pubs/sp/p-SP.htm, accessed March 12, 2021.

Conrey, R.M., Sherrod, D.R., and McClaughry, J.D., 2019, Reconnaissance summary of High Cascades graben structures in central and northern Oregon: Geological Society of America Abstracts with Programs. v. 51, no. 4. https://gsa.confex.com/gsa/2019CD/webprogram/Paper329797.html, accessed March 12, 2021.

Cope, E.D., 1880, Corrections of the geological maps of Oregon: American Naturalist, v. 14, p. 457-458.

Cordero, D.I., 1997, Early to Middle Pleistocene catastrophic flood deposits, The Dalles, Oregon: Portland, Portland State University, M.S. thesis, 162 p.

Cox, G.W., 2012, Alpine and montane Mima mounds of the western United States, *in* Horwath Burnham, J.L., and Johnson, D.L., eds., Mima mounds: the case for polygenesis and bioturbation: Geological Society of America Special Paper 490, p. 63-70. https://pubs.geoscienceworld.org/books/book/652/chapter/3806617/Alpine-and-montane-Mima-mounds-of-the-western, accessed March 12, 2021.

Cox, K.G., Bell, J.D., and Pankhurst, R.J., 1979, The interpretation of igneous rocks: London, George Allen and Unwin, 450 p.

Crowell, J.C., 1974, Origin of late Cenozoic basins in southern California, *in* Dickinson, W.R., ed., Tectonics and sedimentation: Society of Economic Paleontologists and Mineralogists (SEPM) Special Publication 22, p. 190-204. https://pubs.geoscienceworld.org/aapgbull/article-abstract/57/4/774/555406/Origin-of-Late-Cenozoic-Basins-in-Southern?redirectedFrom=fulltext, accessed March 12, 2021.

Dicken, S.N., 1965, Oregon geography: The people, the place, and the time, 4th ed: Ann Arbor, Mich., Edwards Brothers, 147 p.

Duda, C.J.M., McClaughry, J.D., Houston, R.A., and Niewendorp, C.A., 2018, Lidar and Structure from Motion-enhanced geologic mapping, examples from Oregon, *in* Thorleifson, L. H., ed., 2018, Geologic Mapping Forum 2018 Abstracts: Minnesota Geological Survey Open File Report OFR-18-1, 107 p. https://conservancy.umn.edu/handle/11299/194852, accessed March 12, 2021.

Duda, C.J.M., McClaughry, J.D., and Madin, I.P., 2019, Building the modern geologic map in Oregon: a multi-faceted field- and technology-based approach: Geological Society of America Abstracts with Programs. v. 51, no. 4. https://gsa.confex.com/gsa/2019CD/meetingapp.cgi/Paper/329552, accessed March 12, 2021.

Due, J.F., and French, G., 1979, Rails to the Mid-Columbia wheatlands: The Columbia Southern and Great Southern railroads and the development of Sherman and Wasco counties, Oregon: Washington, D.C, University Press of America, Inc., 297 p, ISBN: 08191079809780819107985.

Duncan, R.A., and Keller, R.A., 2004, Radiometric ages for basement rocks from the Emperor Seamounts, ODP Leg 197: Geochemistry, Geophysics, Geosystems, v. 5, no. 8. https://agupubs.onlinelibrary.wiley.com/doi/full/10.1029/2004GC000704, accessed March 12, 2021.

Easterbrook, D.J., 1993, Surface processes and landforms: New York, Macmillan, 520 p.

Farooqui, S.M., Bunker, R.C., Thoms, R.E., and Clayton, D.C.; Bela, J.L., map comp., 1981a, Post-Columbia River Basalt Group stratigraphy and map compilation of the Columbia Plateau, Oregon: Oregon Department of Geology and Mineral Industries Open-File Report O-81-10, 79 p, 6 pl., scale 1:250,000. https://www.oregongeology.org/pubs/ofr/O-81-10.pdf, accessed March 12, 2021.

Farooqui, S.M., Beaulieu, J.D., Bunker, R.C., Stensland, D.E., and Thomas, R.E., 1981b, Dalles Group: Neogene formations overlying the Columbia River Basalt Group in north-central Oregon: Oregon Geology, v. 43, no. 10, p. 131–140. https://www.oregongeology.org/pubs/OG/OGv43n10.pdf, accessed March 12, 2021.

Farooqui, S.M., Beaulieu, J.D., Bunker, R.C., Stensland, D.E., and Thoms, R.E., 1981b, Post-Columbia River Basalt Group stratigraphy and map compilation of the Columbia Plateau, Oregon: Oregon Department of Geology, v. 43, no. 10, p. 131-140. https://www.oregongeology.org/pubs/ofr/O-81-10.pdf, accessed March 12, 2021.

Federal Emergency Management Administration (FEMA), 1995, Oregon Flash Flooding (DR-1061-OR). https://www.fema.gov/disaster/1061, accessed March 12, 2021.

Ferns, M.L., and McClaughry, J.D., 2013, Stratigraphy and volcanic evolution of the middle Miocene La Grande–Owyhee eruptive axis in eastern Oregon, *in* Reidel, S.P., Camp, V., Ross, M.E., Wolff, J.A., Martin, B.E., Tolan, T.L., and Wells, R.E., eds., The Columbia River Flood Basalt Province: Geological Society of America Special Paper 497, p. 401-427. https://pubs.geoscienceworld.org/books/book/661/chapter/3807352/Stratigraphy-and-volcanic-evolution-of-the-middle, accessed March 12, 2021.

Frankel, A.D., and Peterson, M.D., 2008, Cascadia subduction zone, Appendix L in the Uniform California Earthquake Rupture Forecast, version 2 (UCERF2): U.S. Geological Survey Open File Report 2007-1437L and California Geological Survey Special Report 203L, 7 p. https://pubs.usgs.gov/of/2007/1437/, accessed March 12, 2021.

Freundt, A., Wilson, C.J.N., and Carey, S.N., 2000, Ignimbrites and block-and-ash flow deposits, *in* Sigurdsson, H., Houghton, B., McNutt, S.R., Rymer, H., and Stix, J., eds., Encyclopedia of Volcanoes: San Diego, Calif., Academic Press, p. 581-599.

Gannett, M.W., 1982, A geochemical study of the Rhododendron and the Dalles Formations in the area of Mount Hood, Oregon: Portland, Oregon, Portland State University, M.S. thesis, 70 p. https://pdxscholar.library.pdx.edu/open_access_etds/3166/, accessed March 12, 2021.

Geological Society of America Rock-Color Chart Committee, 1991, Rock color chart, 7th printing: Boulder, Colo.

Geomatrix Consultants, Inc., 1995, Seismic design mapping, State of Oregon: technical report to Oregon Department of Transportation, Salem, Oregon, under contract 11688, Jan. 1995, unpaginated, 5 pl., scale 1:1,250,000.

Gillespie, M.R., and Styles, M.T., 1999, BGS rock classification scheme, v. 1, Classification of igneous rocks: British Geological Survey Research Report (2nd ed.) RR99-06, 52 p. https://nora.nerc.ac.uk/id/eprint/3223/1/RR99006.pdf, accessed March 12, 2021.

Goldfinger, C., Nelson, C.H., Johnson, J.E., and the Shipboard Scientific Party, 2003, Deep-water turbidites as Holocene earthquake proxies: the Cascadia subduction zone and Northern San Andreas Fault systems: Annuals of Geophysics, v. 46, no. 5, p. 1169-1194. https://www.annalsofgeophysics.eu/index.php/annals/article/view/3452, accessed March 12, 2021.

Goldfinger, C., Nelson, C.H., Morey, A.E., Johnson, J.E., Patton, J.R., Karabanov, E., Gutiérrez-Pastor, J., Eriksson, A.T., Gràcia, E., Dunhill, G., Enkin, R.J., Dallimore, A., and Vallier, T., 2012, Turbidite event history—methods and implications for Holocene paleoseismicity of the Cascadia subduction zone: U.S. Geological Survey Professional Paper 1661-F, 170 p. https://pubs.usgs.gov/pp/pp1661f/, accessed March 12, 2021.

Goter, S.K., 1994, Earthquakes in Washington and Oregon: 1872–1993: U.S. Geological Survey Open-File Report 94-226-A, 1 p., 1 plate, scale 1:1,000,000. https://pubs.er.usgs.gov/publication/ofr94226A, accessed March 12, 2021.

Gradstein, F.M., and others, 2004, A geologic time scale 2004, Cambridge University Press, 589 p.

Grady, S.J., 1983, Ground-water resources in the Hood Basin, Oregon: U.S. Geological Survey Water-Resources Investigations Report 81-1108, 68 p., 2 pl., scale 1:62,500. https://pubs.er.usgs.gov/publication/wri811108, accessed March 12, 2021.

Gray, L.B., Sherrod, D.R., and Conrey, R.M., 1996, Potassium-argon ages from the northern Oregon Cascade Range: Isochron/West, no. 63, p. 21-28.

Green, G.L., 1982, Soil survey of Wasco County, Oregon, northern part: Natural Resources Conservation Service Soil Conservation Survey 673, 83 p. https://soildatamart.nrcs.usda.gov/Manuscripts/OR673/0/or673_text.pdf, accessed March 12, 2021.

Hagstrum, J.T., Sawlan, M.G., Wells, R.E., Evarts, R.C., and Niem, A.R., 2010, New paleomagnetic and geochemical reference sections in Miocene Grande Ronde Basalt flows on the Columbia Plateau are fundamental to stratigraphic, structural, and tectonic studies in the Portland Metro area and Coast Ranges of Oregon and Washington: American Geophysical Union Fall Meeting 2010, abstract #GP11A-0745. https://ui.adsabs.harvard.edu/abs/2010AGUFMGP11A0745H/abstract, accessed March 12, 2021.

Hallsworth, C.R., and Knox, R.W.O'B., 1999, BGS rock classification scheme, v. 3, Classification of sediments and sedimentary rocks: British Geological Survey Research Report 99-03, 44 p. https://nora.nerc.ac.uk/3227/1/RR99003.pdf, accessed March 12, 2021.

Hildreth, W., 2007, Quaternary magmatism in the Cascades—Geologic perspectives: U.S. Geological Survey Professional Paper 1744, 125 p. https://pubs.usgs.gov/pp/pp1744/, accessed March 12, 2021.

Haugerud, R.A., Ballantyne, D., Weaver, C.S., Meagher, K., and Barnett, E.A., 1999, Lifelines and earthquake hazards in the greater Seattle area: U.S. Geological Survey, Open-file Report, 10 p. https://geomaps.wr.usgs.gov/pacnw/lifeline/index.html, accessed March 12, 2021.

Hooper, P.R., 2000, Chemical discrimination of Columbia River Basalt flows: Geochemistry, Geophysics, and Geosystems, v. 1, no. 1, p. 1-14. https://onlinelibrary.wiley.com/doi/10.1029/2000GC000040/pdf, accessed March 12, 2021.

Hooper, P.R., Steele, W.K., Conrey, R.M., Smith, G.A., Anderson, J.L., Bailey, D.G., Beeson, M.H., Tolan, T.L., and Urbanczyk, K.M., 1993, The Prineville basalt, north-central Oregon: Oregon Geology, v. 5, p. 3-12. https://www.oregongeology.org/pubs/OG/OGv55n01.pdf, accessed March 12, 2021.

Hull, D.A., principal investigator, and Riccio, J.F., ed., 1979, Geothermal resource assessment of Mount Hood: Oregon Department of Geology and Mineral Industries Open-File Report O-79-8, part 1, 273 p. Compressed file available from https://www.oregongeology.org/pubs/ofr/p-OFR.htm, accessed March 12, 2021.

Johnson, A.K., 2011, Dextral shear and north-directed crustal shortening defines the transition between extensional and contractional provinces in north-central Oregon: Corvallis, Oregon State University, M.S. thesis, 77 p., 3 pl., scale 1:24,000. http://ir.library.oregonstate.edu/xmlui/handle/1957/20928, accessed March 12, 2021.

Johnson, D.L., and Horwath Burnham, J.L., 2012, Introduction: Overview of concepts, definitions, and principles of soil mound studies, *in* Horwath Burnham, J.L. and Johnson, D.L., eds., Mima mounds: The case for polygenesis and bioturbation: Geological Society of America Special Paper 490, p. 1-19. https://pubs.geoscienceworld.org/books/book/652/chapter/3806551/Introduction-Overview-of-concepts-definitions-and, accessed March 12, 2021.

Johnson, D.L., and Johnson, D.N., 2012, The polygenetic origin of prairie mounds in northeastern California, *in* Horwath Burnham, J.L. and Johnson, D.L., eds., Mima mounds: The case for polygenesis and bioturbation: Geological Society of America Special Paper 490, p. 135-159. https://pubs.geoscienceworld.org/books/book/652/chapter/3806693/The-polygenetic-origin-of-prairie-mounds-in, accessed March 12, 2021.

Johnson, D.M., Hooper, P.R., and Conrey, R.M., 1999, XRF analysis of rocks and minerals for major and trace elements on a single low dilution Li-tetraborate fused bead: Advances in X-ray Analysis, v. 41, p. 843-867. httpd://cahnrs.wsu.edu/soe/facilities/geolab/technotes/xrf_method/, accessed March 12, 2021.

Kasbohm, J., and Schoene, B., 2018, Rapid eruption of the Columbia River flood basalt and correlation with mid-Miocene climate optimum; Science Advances, v. 4, no. 9. https://advances.sciencemag.org/content/4/9/eaat8223, accessed March 12, 2021.

Kastle Oil and Gas Company, 1951, Notice of intention to drill new well, Oct. 10, 1951; well summary sheet 1951-1952. Available at https://www.oregongeology.org/mlrr/logs/og/Lambert1/noi.pdf and https://www.oregongeology.org/mlrr/logs/og/Lambert1/wellsummarysheet.pdf, accessed March 12, 2021.

Keith, T.E.C., Donnelly-Nolan, J.M., Markman, J.L., and Beeson, M.H., 1985, K-Ar ages of rocks in the Mount Hood area, Oregon: Isochron/West, no. 42, p. 12-16.

Korosec, M.A., 1987, Geologic map of the Hood River quadrangle, Washington and Oregon: Washington Division of Geology and Earth Resources Open File Report 87-6, 41 p., 1 pl., scale 1:100,000. httpd://ngmdb.usgs.gov/Prodesc/proddesc_30784.htm, accessed March 12, 2021.

Kuehn, S.C., 1995, The Olympic-Wallowa lineament, Hite fault system, and CRBG stratigraphy in northeast Umatilla County, Oregon: Pullman, Washington State University, M.S. thesis, 170 p.

Le Bas, M.J., and Streckeisen, A.L., 1991, The IUGS systematics of igneous rocks: London, Journal of the Geological Society, v. 148, p. 825-833.

Le Bas, M. J., Le Maitre, R. W., Streckeisen, A., and Zanettin, B., 1986, A chemical classification of volcanic rocks based on the total alkali-silica diagram: Journal of Petrology, v. 27, part 3, p. 745–750.

Le Maitre, R.W., Bateman, P., Dudek, A., Keller, J., Lemeyre, J., Le Bas, M. J., Sabine, P. A., Schmid, R., Sorenson, H., Streckeisen, A., Wooley, A. R., and Zanettin, B., 1989, A classification of igneous rocks and glossary of terms: Oxford, Blackwell, 193 p.

Le Maitre, R.W. (ed.), and others, 2004, Igneous rocks: A classification and glossary of terms: Cambridge University Press, Recommendations of the International Union of Geological Sciences, Subcommission on the Systematics of Igneous Rocks, 236 p.

Lidke, D.J., Johnson, S.Y., McCrory, P.A., Personius, S.F., Nelson, A.R., Dart, R.L., Bradley, L., Haller, K.M., and Machette, M.N., 2003, Map and data for Quaternary faults and folds in Washington State: U.S. Geological Survey Open-File Report 03-428, 579 p., 1 pl., scale 1:750,000. https://pubs.usgs.gov/of/2003/428/, accessed March 12, 2021.

Lindsey, K., Morgan, D., Vlassopoulos, D., Tolan, T.L., and Burns, E., 2009, Hydrogeology of the CRBG in the Columbia Plateau: Road log and field trip stop descriptions, *in* O'Connor, J.E., Dorsey, R.J., and Madin, I.P., eds., Volcanoes to vineyards: Geologic field trips through the dynamic landscape of the Pacific Northwest: Geological Society of America Field Guide 15, p. 673-696. https://pubs.geoscienceworld.org/books/book/885/chapter/3931795/Hydrogeology-of-the-Columbia-River-Basalt-Group-in, accessed March 12, 2021.

Lite, K.E., 2013, The influence of depositional environment and landscape evolution on groundwater flow in Columbia River Basalt – examples from Mosier, Oregon, *in* Reidel, S.P., Camp, V.E., Martin, M.E., Ross, M.E., Wolff, J.A., Martin, B.S., Tolan, T.L., and Wells, R.E., eds., Geological Society of America Special Paper 497, p. 429-440. https://pubs.geoscienceworld.org/books/book/661/chapter/3807362/The-influence-of-depositional-environment-and, accessed March 12, 2021.

Lite, K.E., and Grondin, G.H., 1988, Hydrogeology of the basalt aquifers near Mosier, Oregon: A ground water resource assessment: Oregon Water Resources Department Ground Water Report 33, 119 p., 5 pl., scale 1:24,000. https://www.oregon.gov/owrd/pages/gw/gw_pubs.aspx, accessed March 12, 2021.

Lite, K.E., Jr., and Gannett, M.W., 2002, Geologic framework of the regional ground-water flow system in the upper Deschutes Basin, Oregon: U.S. Geological Survey Water Resources Investigation Report 02-4015, 44 p. 1 pl., scale 1:100,000. https://pubs.er.usgs.gov/publication/wri024015, accessed March 12, 2021.

Lowry, W.D., Mason, R.S., and Libbey, F.W., 1946, Occurrence of gold near Wasco, Sherman County: Oregon Department of Geology and Mineral Industries department mining records, 8 p. https://www.oregongeology.org/milo/archive/MiningDistricts/ShermanCounty/UnclassifiedDistrict/GoldOccurrenceNearWasco/VanGilderGoldReport.pdf, 8 p. accessed March 12, 2021.

Luttrell, G.W., Hubert, M.L., and Murdock, C.R., 1991, Lexicon of new formal geologic names of the United States1981-1985: U.S. Geological Survey Bulletin 1565, 376 p. http://pubs.er.usgs.gov/publication/b1565, accessed March 12, 2021.

Lux, D.R., 1982, K-Ar and $^{40}Ar/^{39}Ar$ ages of mid-Tertiary volcanic rocks from the West Cascades Range, Oregon: Isochron/West, no. 33, p. 27-32.

Mackenzie, W.S., Donaldson, C.H., and Guilford, C., 1997, Atlas of igneous rocks and their textures: Addison Wesley Longman Ltd., 7th ed., 148 p.

Mackin, J.H., 1961, A stratigraphic section in the Yakima Basalt and Ellensburg Formation in south-central Washington: Washington Division of Mines and Geology Report of Investigations, 19, 45 p.

Madin, I.P., and Burns, W.J., 2013, Ground motion, ground deformation, tsunami inundation, coseismic subsidence, and damage potential maps for the 2012 Oregon resilience plan for Cascadia subduction zone earthquakes: Oregon Department of Geology and Mineral Industries Open-File Report O-13-06, 39 p., 38 pl., various scales. https://www.oregongeology.org/pubs/ofr/p-O-13-06.htm, accessed March 12, 2021.

Madin, I.P., and Ma, L., 2012, The Blue Ridge Fault, a newly discovered Holocene fault near Mt. Hood, Oregon: Technical session abstract, SSA 2012 Annual Meeting, San Diego, Calif., April 17-19, 2012: Seismological Society of America Seismological Research Letters, v. 83, no. 2, p. 374.

Madin, I.P., and Mabey, M.A., 1996, Earthquake hazard maps for Oregon: Oregon Department of Geology and Mineral Industries Geological Map Series GMS-100, 1 pl., various scales. https://www.oregongeology.org/pubs/gms/p-GMS.htm, accessed March 12, 2021.

Madin, I.P., and McClaughry, J.D., 2019, Geologic map of the Biggs Junction and Rufus 7.5′ quadrangles, Wasco and Sherman counties, Oregon: Oregon Department of Geology and Mineral Industries Geological Map Series GMS 124, 105 p., 1 pl., scale 1:24,000, Esri™ format geodatabase; shapefiles, metadata; spreadsheet (4 sheets). https://www.oregongeology.org/pubs/gms/p-GMS-124.htm, accessed March 12, 2021.

Madin, I.P., and Wang, Z., 2000, Relative earthquake hazard maps for selected areas in western Oregon: Oregon Department of Geology and Mineral Industries Interpretive Map Series IMS-7, scale 1:24,000. https://www.oregongeology.org/pubs/ims/p-ims.htm, accessed March 12, 2021.

Madin, I.P., Streig, A.R., Burns, W.J., and Ma, L., 2017, The Mount Hood Fault Zone—Late Quaternary and Holocene fault features newly mapped with high resolution lidar imagery: U.S. Geological Survey Scientific Investigations Report 2017-5022-G, p. 99-109. http://doi.org/10.3133/sir20175022G, accessed March 12, 2021.

Mahood, G.A., and Benson, T.R., 2017, Using $^{40}Ar^{39}Ar$ ages of intercalated silicic tuffs to date flood basalts: Precise ages for Steens Basalt Member of the Columbia River Basalt Group: Earth and Planetary Science Letters, v. 459, p. 340-351. https://www.sciencedirect.com/science/article/abs/pii/S0012821X16306720?via%3Dihub, accessed March 12, 2021.

Martin, B.S., Tolan, T.L., and Reidel, S.P., 2013, Revisions to the stratigraphy and distribution of the Frenchman Springs Member, Wanapum Basalt, *in* Reidel, S.P., Camp, V.E., Martin, M.E., Ross, M.E., Wolff, J.A., Martin, B.S., Tolan, T.L., and Wells, R.E., eds., Geological Society of America Special Paper 497, p. 155-180. https://pubs.geoscienceworld.org/books/book/661/chapter/3807169/Revisions-to-the-stratigraphy-and-distribution-of, accessed March 12, 2021.

McCaffrey, R., and Goldfinger, C., 1995, Forearc deformation and great subduction earthquakes: Implications for Cascadia offshore earthquake potential, Science, v. 267, p. 856-859. https://pubmed.ncbi.nlm.nih.gov/17813913/, accessed March 12, 2021.

McCaffrey, R., Qamar, A. I., King, R. W., Wells, R., Khazaradze, G., Williams, C. A., Stevens, C. W., Vollick, J. J., and Zwick, P. C., 2007, Fault locking, block rotation and crustal deformation in the Pacific Northwest: Geophysical Journal International, v. 169, no. 3, p. 1315-1340. https://pubs.er.usgs.gov/publication/70029869, accessed March 12, 2021.

McClaughry, J.D., Ferns, M.L., and Gordon, C.L., 2009, Field trip guide to the Neogene stratigraphy of the Lower Crooked Basin and the ancestral Crooked River, Crook County, Oregon: Oregon Geology, v. 69, no. 1, p. 45-60. https://www.oregongeology.org/sub/quarpub/OrGeo.htm, accessed March 12, 2021.

McClaughry, J.D., Wiley, T.J., Ferns, M.L., and Madin, I.P., 2010, Digital geologic map of the southern Willamette Valley, Benton, Lane, Linn, Marion, and Polk counties, Oregon: Oregon Department of Geology and Mineral Industries Open-File Report O-2010-03, 116 p., 1 pl., scale 1:63,360, Esri ArcGIS geodatabase, GIS files, spreadsheets. https://www.oregongeology.org/pubs/ofr/p-O-10-03.htm, accessed March 12, 2021.

McClaughry, J.D., Wiley, T.J., Conrey, R.C., Jones, C.B., and Lite, K.E., 2012, Digital geologic map of the Hood River Valley, Hood River and Wasco counties, Oregon: Oregon Department of Geology and Mineral Industries Open-File Report O-12-03, 142 p., 1 pl., scale 1:36,000, Esri ArcGIS™ geodatabase, GIS files, spreadsheets. https://www.oregongeology.org/pubs/ofr/p-O-12-03.htm, accessed March 12, 2021.

McClaughry, J.D., Wiley, T.J., Conrey, R.C., Jones, C.B., and Lite, K.E., 2013, The Hood River graben: a late Pliocene and Quaternary intra-arc half graben in the northern Oregon Cascade Range: Geological Society of America Abstracts with Programs v. 45, no. 6, p. 14. https://gsa.confex.com/gsa/2013CD/webprogram/Paper219572.html, accessed March 12, 2021.

McClaughry, J.D., Scott, W.E., Duda, C.J.M., and Conrey, R.M., 2020a, Geologic map of the Dog River and northern part of the Badger Lake 7.5′ quadrangles, Hood River County, Oregon: Oregon Department of Geology and Mineral Industries Geological Map Series GMS-126, 145 p., 1 pl., scale 1:24,000, Esri™ format geodatabases; shapefiles, metadata; spreadsheet (5 sheets). https://www.oregongeology.org/pubs/gms/p-GMS-127.htm, accessed March 12, 2021.

McClaughry, J.D., Niewendorp, C.A., Franczyk, J.J., Duda, C.J.M., and Madin, I.P., 2020b, Mineral Information Layer for Oregon, release 3 [MILO-3]: Oregon Department of Geology and Mineral Industries Digital Data Series MILO-3, Esri™ geodatabase. https://www.oregongeology.org/milo/index.htm, accessed March 12, 2021.

McDonald, E.V., Sweeney, M.R., and Busacca, A.J., 2012, Glacial outburst floods and loess sedimentation documented by Oxygen Isotope Stage 4 on the Columbia Plateau, Washington State: Quaternary Science Reviews, v. 45, p. 18-30. https://www.sciencedirect.com/science/article/abs/pii/S0277379112001412, accessed March 12, 2021.

McPhee, D.K., Langenheim, V.E., Wells, R.E., and Blakely, R.J., 2014, Tectonic evolution of the Tualatin basin, northwest Oregon, as revealed by inversion of gravity data: Geosphere, v. 10, no. 2, p. 264-275. https://pubs.geoscienceworld.org/gsa/geosphere/article/10/2/264/132124/Tectonic-evolution-of-the-Tualatin-basin-northwest, accessed March 12, 2021.

Medley, E., 2012, Ancient cataclysmic floods in the Pacific Northwest: Ancestors to the Missoula Floods: Portland, Portland State University, M.S. thesis, 174 p. http://pdxscholar.library.pdx.edu/open_access_etds/581/, accessed March 12, 2021.

Mertzman, S.A., 2000, K-Ar results from the southern Oregon–northern California Cascade Range: Oregon Geology, v. 62, p. 99-122. https://www.oregongeology.org/pubs/og/p-OG.htm, accessed March 12, 2021.

Michol, K.A., Russell, J.K., and Andrews, G.D.M., 2008, Welded block-and-ash flow deposits from Mount Meager, British Columbia, Canada: Journal of Volcanology and Geothermal Research, v. 169, p. 121-144. https://www.sciencedirect.com/science/article/abs/pii/S0377027307002624, accessed March 12, 2021.

Miyashiro, A., 1974, Volcanic rock series in island arcs and active continental margins: American Journal of Science, v. 274, p. 321-355. https://www.ajsonline.org/content/274/4/321.abstract, accessed March 12, 2021.

Moore, N.E., Grunder, A.L., and Bohrson, W.A., 2018, The three-stage petrochemical evolution of the Steens Basalt (southeast Oregon, USA) compared to large igneous provinces and layered mafic intrusions: Geosphere, v. 14, p. 2505-2532. https://pubs.geoscienceworld.org/gsa/geosphere/article/14/6/2505/548601/The-three-stage-petrochemical-evolution-of-the, accessed March 12, 2021.

Nelson, A.R., Kelsey, H.M., and Witter, R.C., 2006, Great earthquakes of variable magnitude at the Cascadia subduction zone: Quaternary Research v. 65, p. 354-365. https://pubs.er.usgs.gov/publication/70030439, accessed March 12, 2021.

Nelson, C.A., 1977, The origin and characteristics of soil mounds and patterned ground in north central Oregon: Corvallis, Oregon State University, M.S. thesis, 51 p. https://ir.library.oregonstate.edu/downloads/k930bx66x, accessed March 12, 2021.

Niewendorp, C.A., and Neuhaus, M. E., 2003, Map of selected earthquakes for Oregon, 1841 through 2002: Oregon Department of Geology and Mineral Industries Open-File Report O-03-02, 1 pl. https://www.oregongeology.org/pubs/ofr/p-O-03-02.htm, accessed March 12, 2021.

Newcomb, R.C., 1963, Ground water in the Orchard Syncline, Wasco County, Oregon: The Ore Bin, v. 25, no. 10, p. 133-138. https://www.oregongeology.org/pubs/og/p-OG.htm, accessed March 12, 2021.

Newcomb, R.C., 1966, Lithology and eastward extension of The Dalles Formation, Oregon and Washington: U.S. Geological Survey Professional Paper 550-D, p. 059-063. https://pubs.er.usgs.gov/publication/pp550D, accessed March 12, 2021.

Newcomb, R.C., 1969, Effect of tectonic structure on the occurrence of groundwater in the basalt of the Columbia River Group of The Dalles area, Oregon and Washington: U.S. Geological Survey Professional Paper 383-C, 33 p., 1 pl., scale 1:62,500. https://pubs.er.usgs.gov/publication/pp383C, accessed March 12, 2021.

Newton, V.C., Jr., 1965, Oil and gas exploration in Oregon, 41 p., 1 pl., scale 1:977,777. https://www.oregongeology.org/pubs/mp/MP-06.pdf, accessed March 12, 2021.

NOAA National Centers for Environmental Information, 2020, Data tools: 1981-2010 Normals: https://www.ncdc.noaa.gov/cdo-web/datatools/normals, accessed March 12, 2021.

O'Connor, J.E., Curran, J.H., Beebees, R.A., Grant, G.E., and A.M., Warna-Wojcick, 2003, Quaternary geology and geomorphology of the Lower Deschutes River Canyon, Oregon, *in* Grant, G.E., and O'Connor, J.E., eds., Deschutes River geomorphology, hydrology, and sediment transport: American Geophysical Union Water Science and Application Series 7, 22 p. https://www.fs.fed.us/pnw/pubs/journals/pnw_2003_oconnor002.pdf, accessed March 12, 2021.

Ogg, J.G., Ogg, G., and Gradstein, F.M., 2008, Concise geologic time scale. Cambridge, University Press, 177 .

Olmstead, D.L., 1989, Hydrocarbon exploration and occurrences in Oregon, 78 p. https://www.oregongeology.org/pubs/ogi/OGI-15.pdf, accessed March 12, 2021.

Oregon Department of Geology and Mineral Industries, undated, circa 1955-1968, Oil and gas map of Oregon, northern half of eastern Oregon: Oregon Historical Mining Information, scale 1:380,000. Available at https://www.oregongeology.org/milo/archive/MineMaps/B1435-EastOreNorthHalfOilGas.pdf, accessed March 12, 2021.

Peccerillo, A., and Taylor, S.R., 1976, Geochemistry of Eocene calc-alkaline volcanic rocks from the Kastamonu area, northern Turkey: Contributions to Mineralogy and Petrology, v. 58, p. 63-81.

Peck, D.L., Griggs, A.B., Schlicker, H.G., Well, F.G., and Dole, H.M., 1964, Geology of the central and northern parts of the Western Cascade Range in Oregon: U.S. Geological Survey Professional Paper 449, 56 p., 1 pl., scale 1:250,000. https://pubs.er.usgs.gov/publication/pp449, accessed March 12, 2021.

Personius, S.F., Dart, R.L., Bradley, L.-A., and Haller, K.M., 2003, Map and data for Quaternary faults and folds in Oregon: U.S. Geological Survey Open-File Report 03-095, 16 p., 1 pl., scale 1:750,000. https://pubs.usgs.gov/of/2003/ofr-03-095/, accessed March 12, 2021.

Phillips, W.M., Korosec, M.A., Schasse, H.W., Anderson, J.L., and Hagen, R.A., 1986, K-Ar ages of volcanic rocks in southwest Washington: Isochron/West, v. 47, p. 18-24.

Piper, A.M., 1932, Geology and ground-water resources of The Dalles region, Oregon: U.S. Geological Survey Water-Supply Paper 659-B, p. 107–189, 2 pl., scale 1:62,500. https://pubs.er.usgs.gov/publication/wsp659B, accessed March 12, 2021.

Platz, T., Cronin, S.J., Cashman, K.V., Stewart, R.B., and Smith, I.E.M., 2007, Transitions from effusive to explosive phases in andesite eruptions—a case-study from the AD 1655 eruption of Mt. Taranaki, New Zealand: Journal of Volcanology and Geothermal Research, 161, 15–34. https://www.sciencedirect.com/science/article/abs/pii/S0377027306003908, accessed March 12, 2021.

Pluhar, C.J., Burns, S.F., Carpenter, B., Yazzie, K., and Melton, D., 2014, Paleomagnetism of Early and Middle Pleistocene cataclysmic flood deposits in the Pacific Northwest: American Geophysical Union, Fall Meeting 2014, abstract id. GP21A-3653. https://ui.adsabs.harvard.edu/abs/2014AGUFMGP21A3653P/abstract, accessed March 12, 2021.

Powell, J.E., 1982, Geology of the Columbia Hills, Klickitat County, Washington: Moscow, University of Idaho, M.S. thesis, 56 p., 4 pl.

Powell, L.V., 1978, The structure, stratigraphy, and correlation of Grande Ronde Basalt on Tygh Ridge, Wasco County, Oregon: Moscow, University of Idaho, M.S. thesis, 57 p.

Priest, G.R., 1990, Volcanic and tectonic evolution of the Cascade volcanic arc, central Oregon: Journal of Geophysical Research, v. 95, no. B12, p. 19,583–19,599. https://agupubs.onlinelibrary.wiley.com/doi/abs/10.1029/JB095iB12p19583, accessed March 12, 2021.

Priest, G.R., Woller, N.M., Black, G.L., and Evans, S.H., 1983, Overview of the geology of the central Oregon Cascade Range, *in* Priest, G. R., and Vogt, B. F., eds., Geology and geothermal resources of the central Oregon Cascade Range: Oregon Department of Geology and Mineral Industries Special Paper 15, 123 p., 3 pl., 1:24,000, 1:62,500. https://www.oregongeology.org/pubs/sp/p-SP.htm, accessed March 12, 2021.

Priest, G.R., Goldfinger, C., Wang, K., Witter, R.C., Zhang, Y., and Baptista, A.M., 2009, Tsunami hazard assessment of the northern Oregon coast: A multideterministic approach tested at Cannon Beach, Clatsop County, Oregon: Oregon Department of Geology and Mineral Industries Special Paper 41, 87 p., GIS files, time histories, animations. https://www.oregongeology.org/pubs/sp/p-SP.htm, accessed March 12, 2021.

Rapp, C.F., and Abbe, T.B., 2003, A framework for delineating channel migration zones: Olympia, Washington State Department of Ecology Publication 03-06-027, 65 p. https://www.whatcomcounty.us/DocumentCenter/View/15491/3---DOE-WSDOT---Framework-for-Delineating-Channel-Migration-Zones-2003?bidId=, accessed March 12, 2021.

Reidel, S.P., and Campbell, N.P., 1989, Structure of the Yakima Fold Belt, Central Washington, *in* Joseph, N.L. and others, eds., Geologic guidebook for Washington and adjacent areas: Washington Division of Geology and Earth Resources Information Circular 86, p. 275-303. https://www.dnr.wa.gov/Publications/ger_ic86_geol_guide_wa_area.pdf, accessed March 12, 2021.

Reidel, S.P., and Tolan, T.L., 2013, Grande Ronde Basalt, Columbia River Basalt Group, *in* Reidel, S.P., Camp, V.E., Martin, M.E., Ross, M.E., Wolff, J.A., Martin, B.S., Tolan, T.L., and Wells, R.E., eds., Geological Society of America Special Paper 497, p. 117-154. https://pubs.geoscienceworld.org/books/book/661/chapter/3807152/The-Grande-Ronde-Basalt-Columbia-River-Basalt, accessed March 12, 2021.

Reidel, S.P., Tolan, T.L., Hooper, P.R., Beeson, M.H., Fecht, K.R., Bentley, R.D., and Anderson, J.L., 1989, The Grande Ronde Basalt, CRBG; Stratigraphic descriptions and correlations in Washington, Oregon, and Idaho, *in* Reidel, S. P., and Hooper, P. R., eds., Volcanism and tectonism in the Columbia River Flood-Basalt Province: Geological Society of America Special Paper 239, p. 21-53. https://pubs.geoscienceworld.org/books/book/375/chapter/3796997/The-Grande-Ronde-Basalt-Columbia-River-Basalt, accessed March 12, 2021.

Reidel, S.P., Johnson, V.G., and Spane, F.A., 2002, Natural gas storage in basalt aquifers of the Columbia Basin, Pacific Northwest USA: a guide to site characterization: Richland, Wash., Pacific Northwest National Laboratory, 277 p. https://www.pnnl.gov/main/publications/external/technical_reports/PNNL-13962.pdf, accessed March 12, 2021.

Reidel, S.P., Camp, V.E., Tolan, T,L., and Martin, B.S., 2013, The Columbia River flood basalt province: Stratigraphy, aerial extent, volume, and physical volcanology, *in* Reidel, S.P., Camp, V.E., Martin, M.E., Ross, M.E., Wolff, J.A., Martin, B.S., Tolan, T.L., and Wells, R.E., eds., Geological Society of America Special Paper 497, p. 1-43. https://pubs.geoscienceworld.org/books/book/661/chapter/3807083/The-Columbia-River-flood-basalt-province, accessed March 12, 2021.

Robertson, S., 1999, BGS rock classification scheme, v. 1, Classification of igneous rocks: British Geological Survey Research Report 99-06, 24 p. https://www.bgs.ac.uk/download/bgs-rock-classification-scheme-igneous/, accessed March 12, 2021.

Ross, M.E., 1978, Stratigraphy, structure, and petrology of Columbia River Basalt in a portion of the Grande Ronde River–Blue Mountains area of Oregon and Washington: Moscow, University of Idaho, Ph.D. dissertation, 407 p.

Rukstales, K.S., and Petersen, M.D., 2019, Data release for 2018 update of the U.S. National Seismic Hazard Model: U.S. Geological Survey data release. https://doi.org/10.5066/P9WT5OVB, accessed March 12, 2021.

Satake, K., Shimazaki, K., Tsuji, Y., and Ueda, K., 1996, Time and size of a giant earthquake in Cascadia inferred from Japanese tsunami records of January 1700: Nature, v. 379, p. 246-249. https://www.nature.com/nature/journal/v379/n6562/abs/379246a0.html, accessed March 12, 2021.

Sceva, J.E., 1966, A reconnaissance of the ground-water resources of the Hood River Valley and the Cascade Locks area, Hood River County, Oregon: State of Oregon Groundwater Resources Report 10, 45 p, 1 pl. https://www.oregon.gov/owrd/pages/gw/gw_pubs.aspx, accessed March 12, 2021.

Scott, W.E., and Gardner, C.A., 2017, Field-trip guide to Mount Hood, Oregon, highlighting eruptive history and hazards: U.S. Geological Survey Scientific Investigations Report 2017-5022-G, 115 p. https://doi.org/10.3133/sir20175022G, accessed March 12, 2021.

Scott, W.E., Pierson, T.C., Schilling, S.P., Costa, J.E., Gardner, C.A., Vallance, J.W., and Major, J.J., 1997, Volcano hazards in the Mount Hood region, Oregon: U.S. Geological Survey Open-File Report 97-89, 14 p. https://vulcan.wr.usgs.gov/Volcanoes/Hood/Hazards/OFR97-89/OFR97-89.pdf, accessed March 12, 2021.

Seims, B.A., Bush, J.G., and Crosby, J.W., 1974, $TiO_2$ and geophysical logging criteria for Yakima Basalt correlation, Columbia Plateau: Geological Society of America Bulletin, v. 85, 1061-1068. https://pubs.geoscienceworld.org/gsa/gsabulletin/article-abstract/85/7/1061/201633/TiO2-and-Geophysical-Logging-Criteria-for-Yakima, accessed March 12, 2021.

Shannon and Wilson, 1973, Geologic studies of Columbia River basalt structures and age of deformation; the Dalles Umatilla region, Washington and Oregon; Boardman Nuclear Project: Portland General Electric Company.

Sherrod, D.R., 2019, Cascade Mountain Range in Oregon (essay): The Oregon Encyclopedia. https://oregonencyclopedia.org/articles/cascade_mountain_range/#.XuAE3UVKhaR, accessed March 12, 2021.

Sherrod, D.R., and Pickthorn, L.G., 1989, Some notes on the Neogene structural evolution of the Cascade Range in Oregon, *in* Muffler, L. J. P., Weaver, C. S., and Blackwell, D. D., eds., Geology, geophysics, and tectonic setting of the Cascade Range: U.S. Geological Survey Open-File Report 89-178, p. 351-368. https://pubs.usgs.gov/of/1989/0178/report.pdf, accessed March 12, 2021.

Sherrod, D.R., and Scott, W.E., 1995, Preliminary geologic map of the Mount Hood 30- by 60-minute quadrangle, Northern Cascade Range, Oregon: U.S. Geological Survey Open-File Report 95-219, 36 p., scale 1:100,000. https://pubs.usgs.gov/of/1995/of95-219/, accessed March 12, 2021.

Sherrod, D.R., and Smith, J.G., 2000, Geologic map of upper Eocene to Holocene volcanic and related rocks of the Cascade Range, Oregon: U.S. Geological Survey Map I-2569, 17 p., 2 pl., scale 1:500,000. https://pubs.usgs.gov/imap/i-2569/, accessed March 12, 2021.

Smith, G.A., 1986, Stratigraphy, sedimentology, and petrology of Neogene rocks in the Deschutes Basin, central Oregon: a record of continental margin volcanism: Corvallis, Oregon, Oregon State University, Ph.D. dissertation, 467 p, 3 pl., scale 1:24,000. http://ir.library.oregonstate.edu/xmlui/handle/1957/17932, accessed March 12, 2021.

Smith, G.A. and Taylor, E.M., 1983, The central Oregon High Cascade graben: What? Where? When?: Geothermal Resources Council Transactions, v. 7, p. 275-279.

Smith, G.A., Snee, L.W., and Taylor, E.M., 1987, Stratigraphic, sedimentologic, and petrologic record of late Miocene subsidence of the central Oregon High Cascades: Geology, v. 15, p. 389-392. https://geology.gsapubs.org/content/15/5/389.abstract, accessed March 12, 2021.

Smith, R.A., and Roe, W.P., compilers, 2015, Oregon Geologic Data Compilation [OGDC], release 6 (statewide): Oregon Department of Geology and Mineral Industries Digital Data Series OGDC-6, Esri™ geodatabase. https://www.oregongeology.org/pubs/dds/p-OGDC-6.htm, accessed March 12, 2021.

Swanson, D.A., Anderson, J.L., Bentley, R.D., Byerly, G.R., Camo, V.E., Gardner, J.N., and Wright, T.L., 1979a, Reconnaissance geologic map of the Columbia River Basalt Group in parts of eastern Washington and northern Idaho: U.S. Geological Survey Open-File Report 79-1363, 44 p., 12 pl., scale 1:250,000. https://pubs.er.usgs.gov/publication/ofr791363, accessed March 12, 2021.

Swanson, D.A., Wright, T.L., Hooper, P.R., and Bentley, R.D., 1979b, Revisions in stratigraphic nomenclature of the Columbia River Basalt Group: U.S. Geological Survey Bulletin 1457-G, 59 p., 1 pl. https://pubs.er.usgs.gov/publication/b1457G, accessed March 12, 2021.

Swanson, D.A., Anderson, J.A., Camp, V.E., Hooper, P.R., Taubeneck, W.H., and Wright, T.L., 1981, Reconnaissance geologic map of the Columbia River Basalt Group, Northern Oregon and Western Idaho: U.S. Geological Survey Open-File Report 81-797, 35 p., 6 pl., scale 1:250,000. https://pubs.er.usgs.gov/publication/ofr81797, accessed March 12, 2021.

Taylor, E.M., 1981, Central High Cascade roadside geology—Bend, Sisters, McKenzie Pass, and Santiam Pass, Oregon, *in* Johnston, D.A., and Donnelly-Nolan, J., eds., Guides to some volcanic terranes in Washington, Idaho, Oregon, and northern California: U.S Geological Survey Circular 838, p. 55-83. https://pubs.er.usgs.gov/publication/cir838, accessed March 12, 2021.

Tolan, T.L., 1982, The stratigraphic relationships of the Columbia River Basalt Group in the lower Columbia River Gorge of Oregon and Washington: Portland, Portland State University, M.S. thesis, 169 p. https://doi.org/10.15760/etd.3232, accessed March 12, 2021.

Tolan, T.L., and Beeson, M.H., 1984, Intracanyon flows of the CRBG in the lower Columbia River Gorge and their relationship to the Troutdale Formation: Geological Society of America Bulletin, v. 95, no. 4, p. 463-477. https://pubs.geoscienceworld.org/gsa/gsabulletin/articleabstract/95/4/463/202924/Intracanyon-flows-of-the-Columbia-River-Basalt?redirectedFrom=fulltext, accessed March 12, 2021.

Tolan, T.L., and Reidel, S.P., compilers, 1989, Structure map of a portion the Columbia-River Flood-Basalt Province, *in* Reidel, S. P., and Hooper, P. R., eds., Volcanism and tectonism in the Columbia River Flood-Basalt Province: Geological Society of America Special Paper 239, scale 1:576,000, 1 pl. https://pubs.geoscienceworld.org/books/book/375/chapter/4697946/Map, accessed March 12, 2021.

Tolan, T.L., Beeson, M.H., and Lindsey, K.A., 2002, The effects of volcanism and tectonism on the evolution of the Columbia River System: a field guide to selected localities in the southwestern Columbia Plateau and Columbia River Gorge of Washington and Oregon State: Northwest Geological Society Field Trips in Pacific Northwest Geology, September 28-29, 2002, 74 p.

Tolan, T.L., Reidel, S.P., Beeson, M.H., Anderson, J.L., Fecht, K.R., and Swanson, D.A., 1989, Revisions to the estimates of the areal extent and volume of the CRBG, *in* Reidel, S. P., and Hooper, P. R., eds., Volcanism and tectonism in the Columbia River Flood-Basalt Province: Geological Society of America Special Paper 239, p. 1-20. https://pubs.geoscienceworld.org/books/book/375/chapter/3796993/Revisions-to-the-estimates-of-the-areal-extent-and, accessed March 12, 2021.

Tolan, T.L., Martin, B.S., Reidel, S.P., Anderson, J.L., Lindsey, K.A., and Burt, W., 2009a, An introduction to the stratigraphy, structural geology, and hydrogeology of the Columbia River flood-basalt province: A primer for the GSA CRBG field trips, *in* O'Connor, J. E., Dorsey, R. J., and Madin, I. P., eds., Volcanoes to vineyards: geologic field trips through the dynamic landscape of the Pacific Northwest: Geological Society of America Field Guide 15, p. 599-643. https://pubs.geoscienceworld.org/books/book/885/chapter/3931355/An-introduction-to-the-stratigraphy-structural, accessed March 12, 2021.

Tolan, T.L., Martin, B.S., Reidel, S.P., Kauffman, J.D., Garwood, D.L., and Anderson, J.L., 2009b, Stratigraphy and tectonics of the central and eastern portions of the Columbia River Flood-Basalt Province: An overview of our current state of knowledge, *in* O'Connor, J. E., Dorsey, R. J., and Madin, I. P., eds., Volcanoes to Vineyards: geologic field trips through the dynamic landscape of the Pacific Northwest: Geological Society of America Field Guide 15, p. 645-672. https://pubs.geoscienceworld.org/books/book/885/chapter/3931564/Stratigraphy-and-tectonics-of-the-central-and, accessed March 12, 2021.

Uppuluri, V.R., 1974, Prineville chemical type: a new basalt type in the Columbia River group: Geological Society of America Bulletin, v. 85, p. 1315-1318. http://gsabulletin.gsapubs.org/content/85/8/1315.abstract, accessed March 12, 2021.

USDOE (U.S. Department of Energy), 1988, Site characterization plan, Reference Repository Location, Hanford Site, Washington—consultation draft: Washington, D.C., Office of Civilian Radioactive Waste Management, DOE/RW-0164, v. 1 and 2, 1245 p.

U.S. Geological Survey National Cooperative Geologic Mapping Program, 2020, GeMS (Geologic Map Schema)—A standard format for the digital publication of geologic maps: U.S. Geological Survey Techniques and Methods, book 11, chap. B10, 74 p. https://doi.org//10.3133/tm11B10, accessed March 12, 2021.

Vallance, J.W., 1999, Postglacial lahars and potential hazards in the White Salmon River system on the southwest flank of Mount Adams, Washington: U.S. Geological Survey Bulletin 2161, 49 p. https://pubs.er.usgs.gov/publication/b2161, accessed March 12, 2021.

Venkatakrishnan, R., Bond, J.G., and Kauffman, J.D., 1980, Geological linears of the northern part of the Cascade Range, Oregon: Oregon Department of Geology and Mineral Industries, Special Paper 12, 25 p., 5 pl., scale 1:250,000. https://www.oregongeology.org/pubs/sp/SP-12.pdf, accessed March 12, 2021.

Verplanck, E.P., and Duncan, R.A., 1987, Temporal variations in plate convergence and eruption rates in the Western Cascades Oregon: Tectonics, v. 6, p. 197-209. https://agupubs.onlinelibrary.wiley.com/doi/abs/10.1029/TC006i002p00197, accessed March 12, 2021.

Vogt, B.F., 1981, The stratigraphy and structure of the Columbia River Basalt Group in the Bull Run Watershed, Oregon: Portland, Portland State University, M.S. thesis, 151 p. https://pdxscholar.library.pdx.edu/open_access_etds/3267/, accessed March 12, 2021.

Waters, A.C., 1968, Reconnaissance geologic map of the Dufur quadrangle, Hood River, Sherman, and Wasco counties, Oregon: U.S. Geological Survey Miscellaneous Geologic Investigations Map I-556, scale 1:125,000. https://pubs.er.usgs.gov/publication/i556, accessed March 12, 2021.

Watters, T.R., 1989, Periodically spaced anticlines of the Columbia Plateau, *in* Reidel, S.P., and Hooper, P.R., eds., Volcanism and tectonism in the Columbia River flood-basalt province: Geological Society of America Special Paper 239, p. 283-292. https://pubs.geoscienceworld.org/books/book/375/chapter/3797045/Periodically-spaced-anticlines-of-the-Columbia, accessed March 12, 2021.

Weldon, R.J., II, Fletcher, D.K., Weldon, E.M., Scharer, K.M. and McCrory, P.A., 2003, An update of Quaternary faults of central and eastern Oregon: U.S. Geological Survey Open-File Report 2002-301,

Wells, R.E., Simpson, R.W., Bentley, R.D., Beeson, M.H., Mangan, M.T., and Wright, T.L., 1989, Correlation of Miocene flows of the CRBG from the central Columbia River Plateau to the coast of Oregon and Washington, *in* Reidel, S. P., and Hooper, P. R., eds., Volcanism and tectonism in the Columbia River Flood-Basalt Province: Geological Society of America Special Paper 239, p. 113-129. https://pubs.geoscienceworld.org/books/book/375/chapter/3797019/Correlation-of-Miocene-flows-of-the-Columbia-River, accessed March 12, 2021.

Wells, R.E., Niem, A.R., Evarts, R.C., and Hagstrum, J.T., 2009, The Columbia River Basalt Group—From the Gorge to the sea, *in* O'Connor, J.E., Dorsey, R.J., and Madin, I.P., eds., Volcanoes to vineyards: geologic field trips through the dynamic landscape of the Pacific Northwest: Geological Society of America Field Guide 15, p. 737-774. https://pubs.geoscienceworld.org/books/book/885/chapter/3932152/The-Columbia-River-Basalt-Group-From-the-gorge-to, accessed March 12, 2021.

Wentworth, C.K., 1922, A scale of grade and class terms of clastic sediments: Journal of Geology, v. 30, p. 377-392.

Westby, E.G., 2014, The geology and petrology of enigmatic rhyolites at Graveyard and Gordon Buttes, Mount Hood quadrangle, Oregon: Portland, Portland State University, M.S. thesis, 138 p. http://pdxscholar.library.pdx.edu/open_access_etds/2063/, accessed March 12, 2021.

Williams, D.L., Hull, D.A., Ackerman, H.D., and Beeson, M.H., 1982, The Mount Hood region: Volcanic history, structure, and geothermal potential: Journal of Geophysical Research, v. 87, p. 2767-2781.

Wise, W.S., 1969, Geology and petrology of the Mt. Hood area: a study of High Cascade volcanism: Geological Society of America Bulletin, v. 80, no. 6, p. 969-1006. https://pubs.geoscienceworld.org/gsa/gsabulletin/article-abstract/80/6/969/6609/Geology-and-Petrology-of-the-Mt-Hood-Area-A-Study?redirectedFrom=fulltext, accessed March 12, 2021.

Wright, T.L., Maurice, J.G., and Swanson, D.A., 1973, Chemical variation related to the stratigraphy of the Columbia River Basalt: Geological Society of America Bulletin, v. 84, p. 371-386. https://pubs.geoscienceworld.org/gsa/gsabulletin/article-abstract/84/2/371/201255/Chemical-Variation-Related-to-the-Stratigraphy-of?redirectedFrom=fulltext, accessed March 12, 2021.

Wu, J.E., McClay, K., Whitehorse, P., and Dooley, T., 2009, 4D analogue modeling of transtensional pull-apart basins: Marine and Petroleum Geology, v. 26, p. 1608-1623. https://www.sciencedirect.com/science/article/abs/pii/S0264817208001177, accessed March 12, 2021.

Yelin, T.S., and Patton, H.J., 1991, Seismotectonics of the Portland, Oregon region: Seismological Society of America Bulletin, v. 81, p. 109-130. https://pubs.geoscienceworld.org/ssa/bssa/article-abstract/81/1/109/119420/Seismotectonics-of-the-Portland-Oregon-region?redirectedFrom=fulltext, accessed March 12, 2021.

Zakšek, K., Oštir, K., and Kokalj, Ž., 2011, Sky-View Factor as a relief visualization technique: Remote Sensing, v. 3, p. 398-415. http://iaps.zrc-sazu.si/en, accessed March 12, 2021.

# 12.0 APPENDIX

This Appendix contains a summary of the geodatabases along with a description of analytical and field methods and the list of attribute fields for spreadsheets (see page viii of this report). The Appendix is divided into two sections:

- Section 12.1 describes the digital databases included with this publication.
- Section 12.2 contains a summary of analytical and field methods. Accompanying tables explain the fields listed in spreadsheets.

## 12.1 Geographic Information Systems (GIS) database

***Geodatabase specifications***

Digital geologic data created for the Dufur area are stored in three Esri™ format geodatabases. The geodatabase structure of each follows that outlined by the U.S. Geological Survey (USGS) Geologic Map Schema (GeMS), version 2.7 (U.S. Geological Survey National Cooperative Geologic Mapping Program, 2020). The following information describes the overall database structure, the feature classes, and supplemental tables (**Figure 12-1**, **Figure 12-2**, **Table 12-1**, **Table 12-2**).

The data are stored in a file geodatabase feature dataset (GeologicMap). Accessory file geodatabase tables (DataSources, DescriptionOfMapUnits, GeoMaterialDict, and Glossary) were created by using ArcGIS version 10.7 (SP 1). The GeologicMap feature dataset contains all the spatially oriented data (feature classes) (**Figure 12-1**). The file geodatabase tables are used to hold additional geologic attributes (**Figure 12-2**). Each feature class within the GeologicMap feature dataset in the geodatabase contains detailed metadata (**Figure 12-1**). Please see the embedded metadata for detailed information such as process descriptions, accuracy specifications, and entity attribute descriptions. Additional information and complete descriptions of the "GeMS" — Geologic Map Schema can be found at https://doi.org//10.3133/tm11B10.

All spatial data are stored in the Oregon Statewide Lambert Conformal Conic projection. The datum is NAD83 HARN. The linear unit is international feet. See detailed projection parameters below:

Projection: Lambert_Conformal_Conic
False_Easting: 1312335.958005
False_Northing: 0.0
Central_Meridian: -120.5
Standard_Parallel_1: 43.0
Standard_Parallel_2: 45.5
Latitude_Of_Origin: 41.75
Linear Unit: Foot (0.3048)

Geographic Coordinate System: GCS_North_American_1983_HARN
Angular Unit: Degree (0.0174532925199433)
Prime Meridian: Greenwich (0.0)
Datum: D_North_American_1983_HARN
Spheroid: GRS_1980
Semimajor Axis: 6378137.0
Semiminor Axis: 6356752.314140356
Inverse Flattening: 298.257222101

**Figure 12-1. Dufur area feature datasets and data tables contained in geodatabases WRF2021_GeMS_v10.7.gdb, DWPS2021_GeMS_v10.7.gdb, and DESBSR2021_GeMS_v10.7.gdb.**

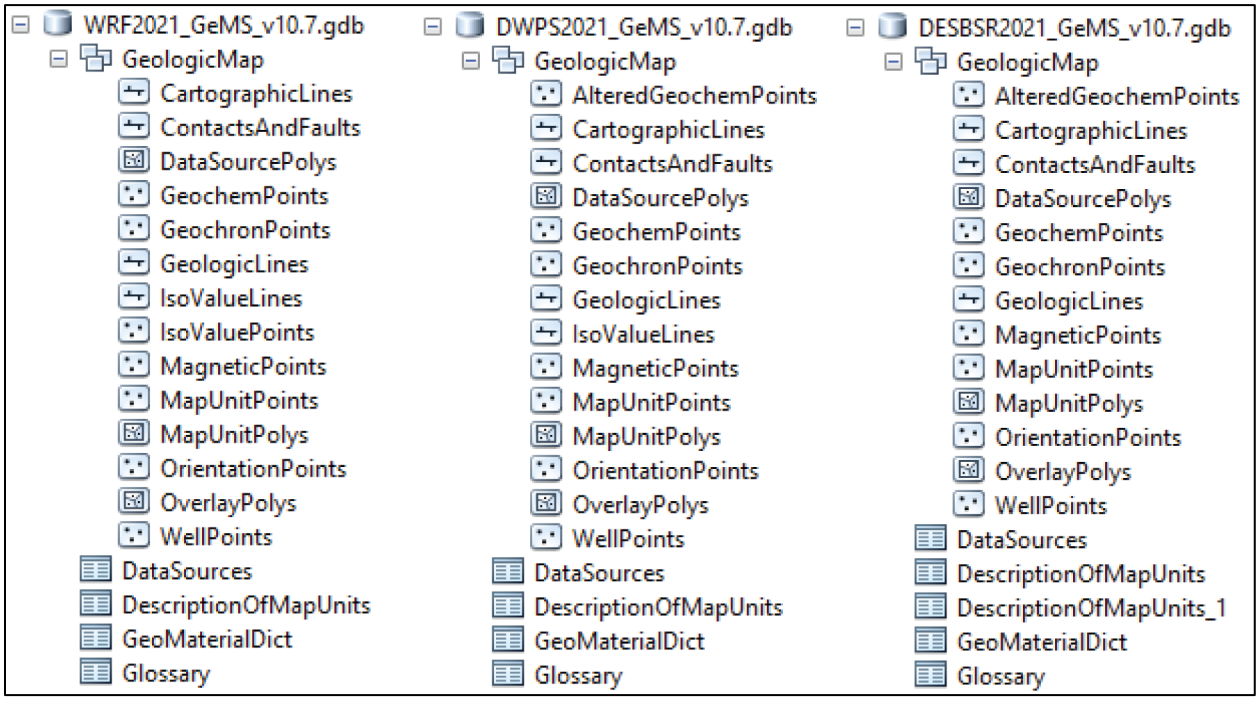


**Figure 12-2. Dufur area geodatabase data tables.**

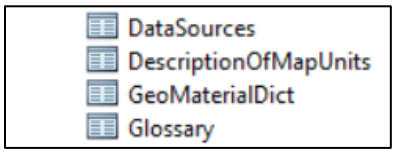

**Table 12-1. Feature class descriptions.**

| Name | Description |
|---|---|
| AlteredGeochemPoints | This feature class represents point locations where alteration-zone samples have been analyzed by Inductive Coupled Mass Spectrometry (ICP-MS) and Inductive Coupled Atomic Emission Spectrometry (ICP-AES) methods. Includes data collected by the authors during this study or compiled from previous studies. These data are also contained in the alteredgeochempoints spreadsheet. |
| CartographicLines | Vector lines that have no real-world physical existence and do not participate in map-unit topology. The feature class includes cross section lines used for cartography. |
| ContactsAndFaults | The vector lines in this feature class contain geologic content including contacts and fault locations used to create the map unit polygon boundaries. The existence and location confidence values for the contacts and faults are provided in the feature class attribute table. |
| DataSourcePolys | This feature class contains polygons that delineate data sources for all parts of the geologic map. These sources may be a previously published map, new mapping, or mapping with a certain technique. For a map with one data source, for example all new mapping, this feature class contains one polygon that encompasses the map area. |
| GeochemPoints | This feature class represents point locations where whole-rock samples have been analyzed by X-ray fluorescence (XRF) techniques. Includes data collected by the authors during this study or compiled from previous studies. These data are also contained in the geochemistry spreadsheet. |
| GeochronPoints | This feature class represents point locations where isotopic ages have been obtained for rock samples in the map area. Data collected by the authors or compiled during the course of this study. These data are also contained in the geochronology spreadsheet. |
| GeologicLines | These vector lines represent known fold axis locations in the quadrangle. The existence and location confidence for the fold axes are provided in the feature class attribute table. |
| IsoValueLines | These vector lines represent 10-ft structure contours on the upper surface of the Basalt of Sentinel Gap (Twfs). Contours were generated from elevation points contained within the feature class IsoStructurePoints, using ArcToolbox/Spatial Analyst Tools/Interpolation/Spline with Barriers. |
| MagneticPoints | This feature class represents point locations where measurements of natural remanent magnetization have been obtained for strongly magnetized lava flows. Includes data collected by the authors during the course of this study. These data are also contained in the magnetic polarity spreadsheet. |
| MapUnitPoints | This feature class represents points used to generate the MapUnitPolys feature class from the ContactsAndFaults feature class. |
| MapUnitPolys | This polygon feature class represents the geologic map units as defined by the authors. |
| OrientationPoints | This feature class represents point locations in the quadrangle where structural measurements were made or were compiled from previous studies. These data are also contained in the bedding (strike and dip) spreadsheet described in more detail below. |
| OverlayPolys | This feature class holds the reference map outline for each map plate. |
| WellPoints | This feature class represents point locations of water wells in the quadrangle. Includes data obtained by the authors from the Oregon Department of Water Resources (OWRD). These data are also contained in the Wells Points spreadsheet. |

**Table 12-2. Geodatabase tables.**

| Name | Description |
|---|---|
| DataSources | Data table that contains information about data sources used to compile the geology of the area. |
| DescriptionOfMapUnits | Data table that captures the content of the Description of Map Units (DMU), or equivalent List of Map Units and associated pamphlet text, included in a geologic map. |
| GeoMaterialDict | Data table providing definitions and hierarchy for GeoMaterial names prescribed by the GeMS database schema. |
| Glossary | Data table that contains information about the definitions of terms used in the geodatabase. |

## *Geologic maps*

This report is accompanied by three map plates displaying the surficial and bedrock geology for the Dufur area at a scale of 1:24,000 and geologic cross sections (see Plates 1, 2, and 3 facsimiles below). The map plates were generated from detailed geologic data (scale of 1:8,000 or better) contained in the accompanying Esri™ format geodatabases.

**Plate 1. Reproduction of the geologic map of the Wolf Run and northern part of the Friend 7.5' quadrangles, Wasco County, Oregon (Plate 1). Plate dimensions are 46 by 50 inches, scale 1;24,000. See digital folder for map plate.**

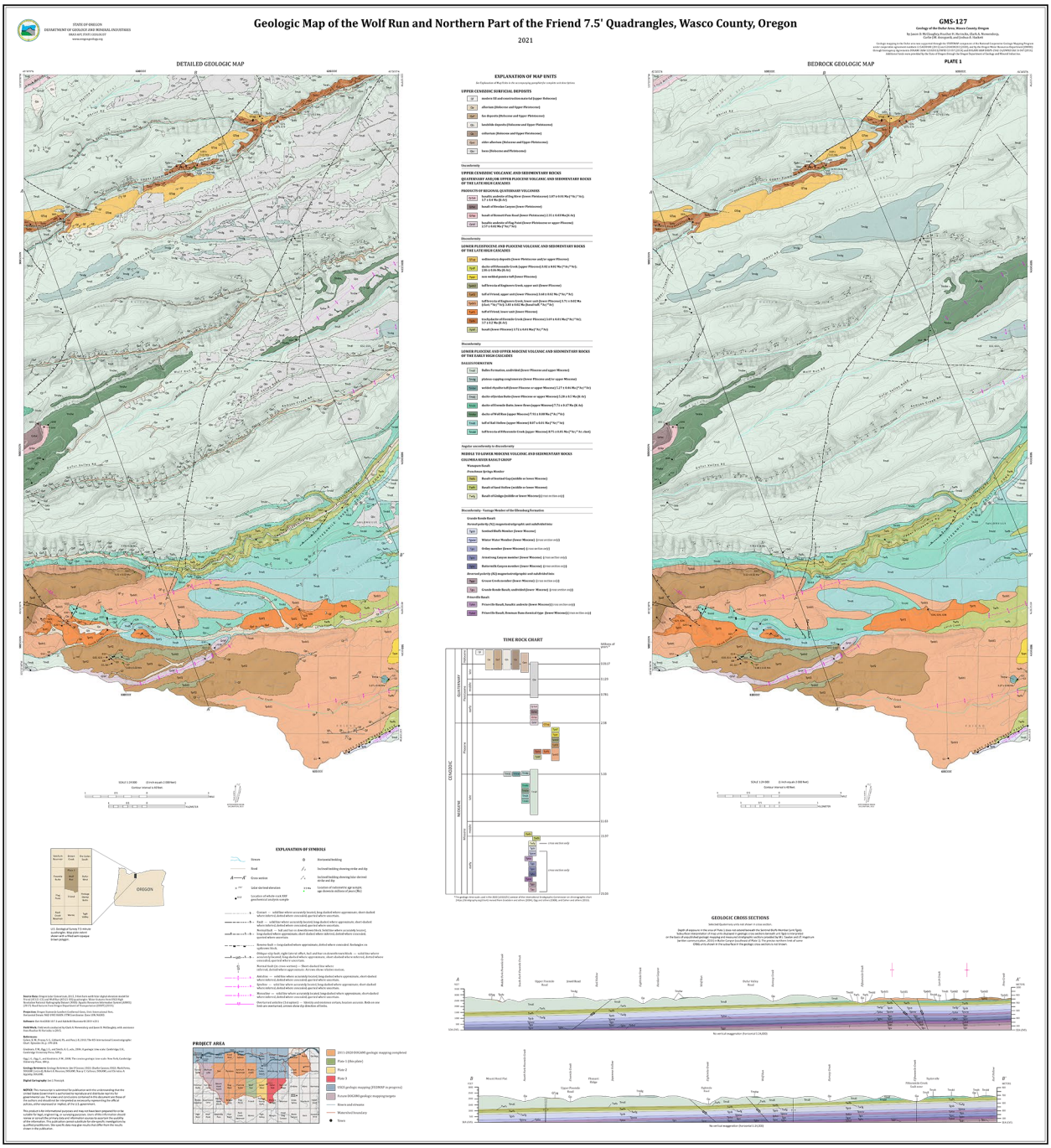

**Plate 2. Reproduction of the geologic map of the Dufur West and northern part of the Postage Stamp Butte 7.5’ quadrangles, Wasco County, Oregon (Plate 2). Plate dimensions are 44 by 56 inches, scale 1;24,000. See digital folder for map plate.**

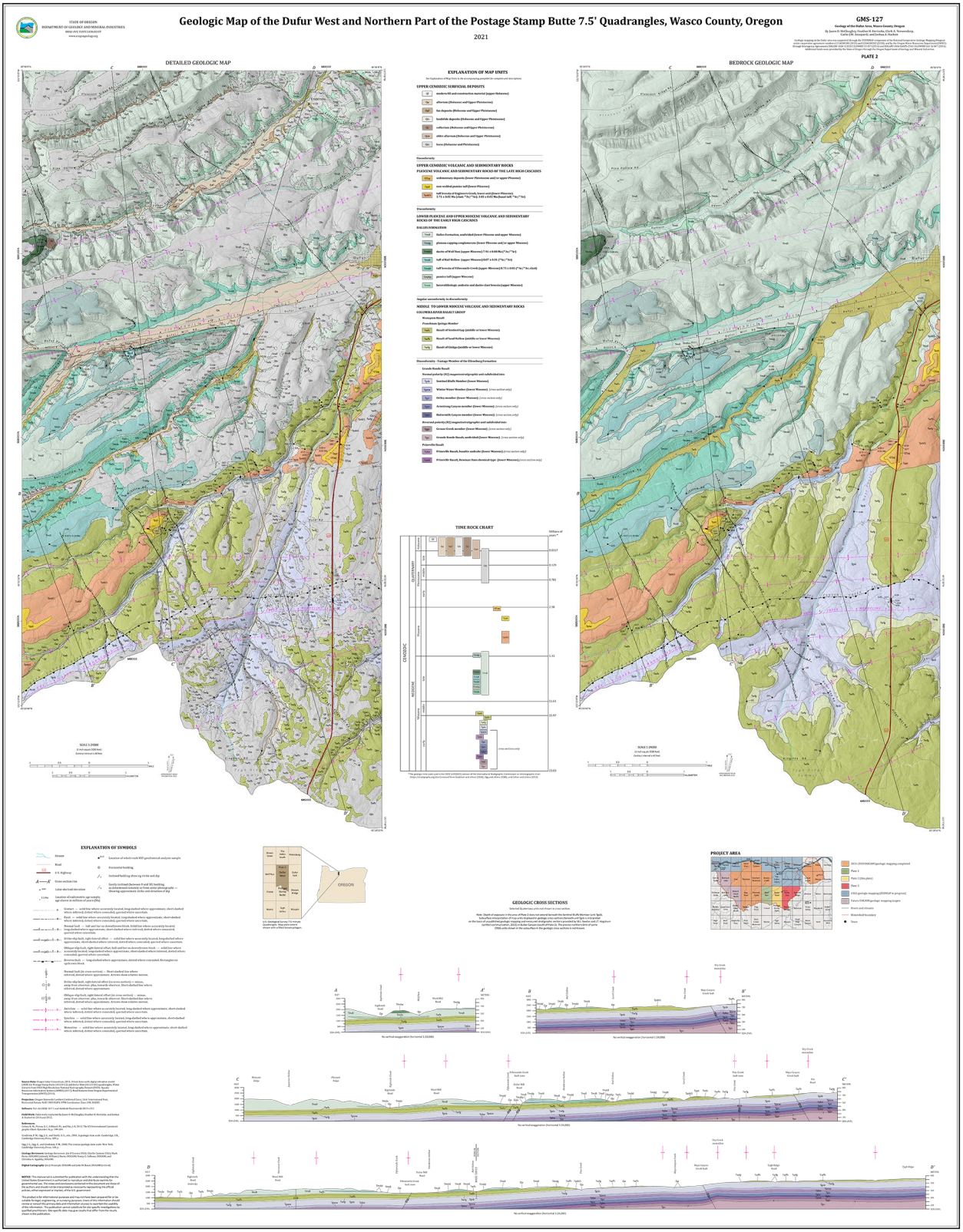

**Plate 3. Reproduction of the geologic map of the Dufur East and parts of the Sherars Bridge and Summit Ridge 7.5' quadrangles, Wasco County, Oregon (Plate 3). Plate dimensions are 62 by 50 inches, scale 1;24,000. See digital folder for map plate.**

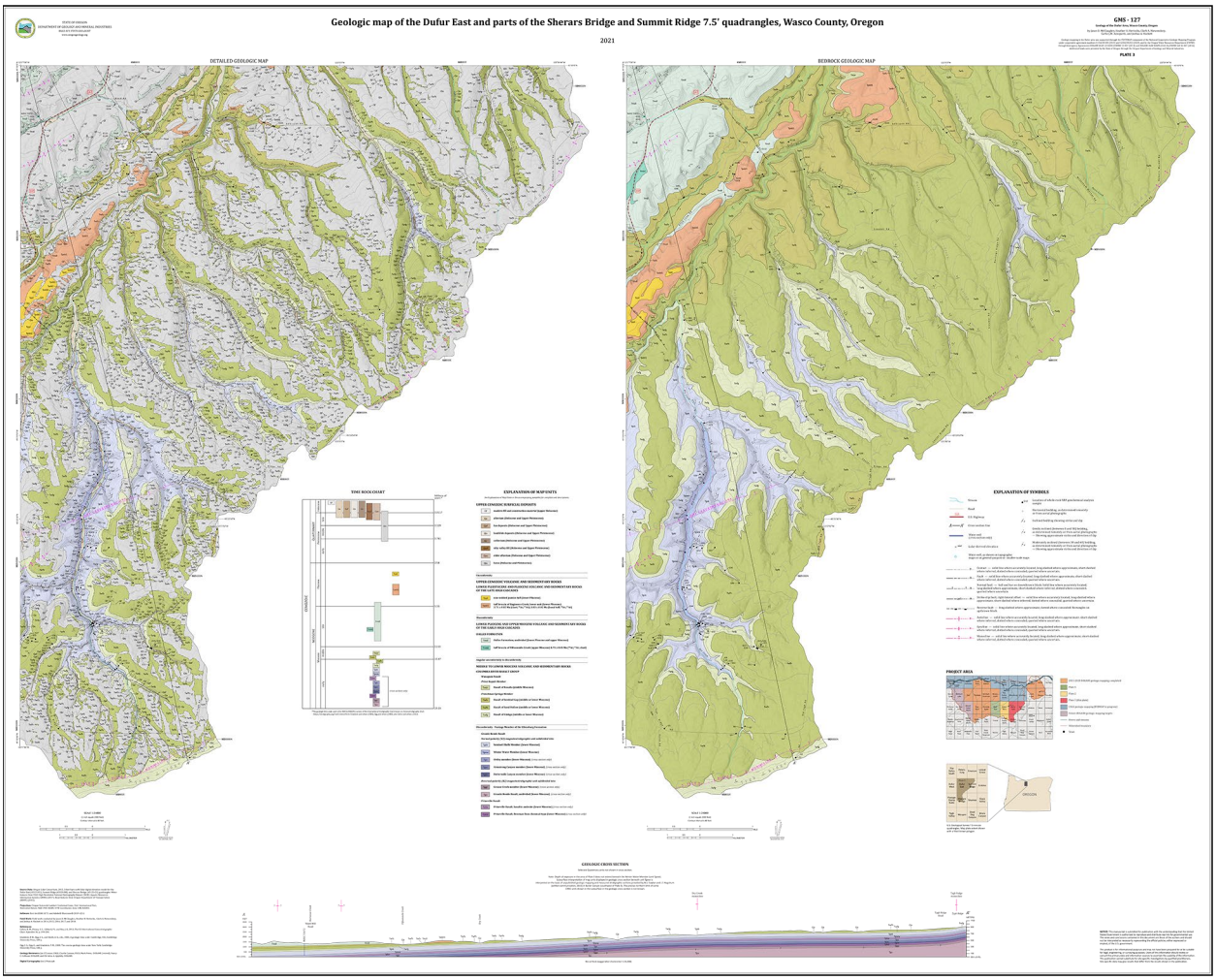

## 12.2 Methods

***Geochemical analytical methods***

Geologic mapping in the Dufur area was supported by 437 X-ray fluorescence (XRF) geochemical analyses of whole-rock samples. Whole-rock geochemical samples were prepared and analyzed by XRF at the Washington State University GeoAnalytical Lab, Pullman, Washington, and at the Franklin and Marshall X-ray laboratory, Lancaster Pennsylvania. Analytical procedures for the Washington State University GeoAnalytical Lab are described by Johnson and others (1999) and are available online at https://environment.wsu.edu/facilities/geoanalytical-lab/technical-notes/; analytical procedures for the Franklin and Marshall X-ray laboratory are described by Boyd and Mertzman (1987) and Mertzman (2000), and are available online at https://www.fandm.edu/earth-environment/laboratory-facilities/xrf-and-xrd-lab. Samples denoted by lab abbreviation WSU were analyzed at Washington State University; samples denoted by lab abbreviation FM were analyzed at Franklin and Marshall College. Descriptive rock unit names for igneous rocks are based on normalized major element analyses plotted on the total alkalis ($Na_2O + K_2O$) versus silica ($SiO_2$) diagram (TAS) of Le Bas and others (1986), Le Bas and Streckeisen (1991), and Le Maitre and others (1989, 2004). New and compiled XRF-geochemical analyses are included in each of the geodatabases:

- WRF2021_GeMS_v10.7.gdb,
- DWPS2021_GeMS_v10.7.gdb,
- DESBSR2021_GeMS_v10.7.gdb,

in separate shapefiles:

- WRF2021_GeochemPoints.shp,
- DWPS2021_GeochemPoints.shp,
- DESBSR2021_GeochemPoints.shp,

and in Microsoft Excel workbooks**:**

- WRF2021_DATA.xlsx (sheet WRF2021_GeochemPoints),
- DWPS2021_DATA.xlsx (sheet DWPS2021_GeochemPoints),
- DESBSR2021_DATA.xlsx (sheet DESBSR2021_GeochemPoints).

**Table 12-3** describes the fields listed in the databases. The locations of all geochemical samples are given in five coordinate systems: UTM Zone 10 (datum = NAD 27, NAD 83, units =meters), Geographic (datum = NAD 27, NAD 83, units = decimal degrees), and Oregon Lambert (datum = NAD 83, HARN, units = international feet). Notes for spreadsheet: -9 equals no data for numerical fields for analytical data; nd equals no data in text fields; na equals information not applicable for text fields; samples shown with an "R" (e.g., 121 DRBLJ 19R) are a repeat analysis of a single sample.

**Table 12-3. Geochemical database spreadsheet columns.**

| Field | Description |
|---|---|
| Type | The geochemical method used by laboratory that analyzed the sample – e.g., XRF, ICP-MS |
| FieldSampleID | Unique alpha-numeric id applied to the sample – e.g., 21 DWFJ 14. |
| AlternateSampleID | Unique alpha-numeric id applied to the sample – e.g., 21 DWFJ 14. |
| Symbol | References a symbol in the GeMS style file – e.g., 31.21. |
| Label | A unique number assigned to the sample for cartographic purposes – e.g., G1. |
| LocationConfidenceMeters | Radius in meters of positional uncertainty envelope for the observation locale. Null values not permitted. Recommended value is -9 if value is not otherwise available. |
| PlotAtScale | Cartographic map scale or larger that the observation or analysis should be plotted at. Value is scale denominator. |
| Quadrangle | The USGS 7.5' quadrangle in which the sample is located – e.g., Dufur West. |
| Elevation | Elevation of data location in feet – e.g., 22. |
| MapUnit | Map unit from which the analyzed sample was collected – e.g., Tpdv. |
| MaterialAnalyzed | Type of material analyzed – e.g., whole rock. |
| TASLithology | Rock name assigned based on the total alkalis ($Na_2O + K_2O$) versus silica ($SiO_2$) diagram (TAS) of Le Bas and others (1986), Le Bas and Streckeisen (1991), and Le Maitre and others (1989) – e.g., basalt. |
| MajorElements | $SiO_2$, $Al_2O_3$, $TiO_2$, FeOTotal, MnO, CaO, MgO, $K_2O$, $Na_2O$, $P_2O_5$. In wt. percent. |
| TraceElements | Ni, Cr, Sc, V, Ba, Rb, Sr, Zr, Y, Nb, Ga, Cu, Zn, Pb, La, Ce, Th, Nd, U, Cs, Co, Hf, Sm, Eu, Yb, Lu. In ppm. |
| TotalInitial | Original analytical total as reported by the lab. |
| LossOnIgnition | Value for loss on ignition as reported by the laboratory. |
| FE2O3 | Iron (III) oxide or ferric oxide reported in original analysis. |
| FeO | Iron (II) oxide or ferrous oxide reported in original analysis. |
| UTMNorthingNAD27 | Meters north in NAD 27 UTM projection, zone 10. |
| UTMEastingNAD27 | Meters east in NAD 27 UTM projection, zone 10. |
| LatitudeNAD27 | Latitude in NAD 27 geographic coordinates. |
| LongitudeNAD27 | Longitude in NAD 27 geographic coordinates. |
| UTMNorthingNAD83 | Meters north in NAD 83 UTM projection, zone 10. |
| UTMEastingNAD83 | Meters east in NAD 83 UTM projection, zone 10. |
| LatitudeNAD83 | Latitude in NAD 83 geographic coordinates. |
| LongitudeNAD83 | Longitude in NAD 83 geographic coordinates. |
| Northing83HARN | Feet north in Oregon Lambert NAD 83, HARN, international feet. |
| Easting83HARN | Feet east in Oregon Lambert NAD 83, HARN, international feet. |
| LocationSourceID | Unique data source from which the data were obtained – e.g., McClJD2020. |
| AnalysisSourceID | Foreign key to DataSources. Identifies source of analytical data for this sample. Null values not permitted – e.g., WSU. |
| Notes | Special information about certain samples – e.g., alteration. |
| GeochemPoints_ID | e.g., GCM01 |

***Alteration zone geochemical analytical methods***

The distribution of alteration zones in Dufur area is defined on the basis of field mapping during the current study and unpublished mineral resource reports archived by DOGAMI. Eleven samples obtained from hot-spring alteration zones in the Dufur area were analyzed at ALS Chemex (ALS) in Reno, Nevada by Inductive Coupled Mass Spectrometry (ICP-MS) and Inductive Coupled Atomic Emission Spectrometry (ICP-AES) methods using their ME-MS41 analytical package. Samples were prepared using an aqua regia digestion where samples are treated with a 3:1 mixture of hydrochloric and nitric acids. Nitric acid destroys organic matter and oxidizes sulphide material. It reacts with concentrated hydrochloric acid to generate aqua regia: $3HCl + HNO_3 = 2H_2O + NOCL + CL_2$. Aqua regia is an effective solvent for most base metal sulphates, sulphides, oxides, and carbonates, but only provides a partial digestion for most rock forming elements of a refractory nature. Therefore, results reported in tables DWPS2021_AltChemistry and DESBSR 2021_AltChemistry represent only the leachable portion of any particular analyte. A stronger dissolution technique would recover analytes from more resistive minerals but is not deemed necessary here as the objective was a "first pass" screening of alteration zones. A table of detection limits for the ME-MS41 analytical package at ALS is shown in **Table 12-4**. The detection limits stated by ALS has an uncertainty of ± 100 percent. Therefore, a detection limit of 1 part per million (ppm) implies an uncertainty of 1 ppm ± 1 ppm. Please note that gold (Au) determinations by the ICP-MS and ICP-AES method are semi-quantitative due to the small sample weight used (0.5 g). Six additional samples were analyzed by XRD at the Department of Geosciences, Franklin and Marshall College, Lancaster, Pennsylvania under the direction of S. A. Mertzman. Detailed analytical procedures for the Franklin and Marshall X-ray laboratory are described by Boyd and Mertzman (1987) and Mertzman (2000), and are available online at https://www.fandm.edu/earth-environment/laboratory-facilities/xrf-and-xrd-lab. Alteration zone geochemical analyses are included in the geodatabases:

- DWPS2021_GeMS_v10.7.gdb,
- DESBSR2021_GeMS_v10.7.gdb,

in separate shapefiles:

- DWPS2021_AltChemistry.shp,
- DESBSR2021_AltChemistry.shp,

and in Microsoft Excel workbooks:

- DWPS2021_DATA.xlsx (sheet DWPS2021_AltChemistry),
- DESBSR2021_DATA.xlsx (DESBSR2021_AltChemistry).

**Table 12-5** describes the fields listed in the databases. Elements in ppm except those denoted as weight percent (%); nd = no data. The locations of all alteration zone geochemical samples are given in five coordinate systems: UTM Zone 10 (datum = NAD 27, NAD 83, units =meters), Geographic (datum = NAD 27, NAD 83, units = decimal degrees), and Oregon Lambert (datum = NAD 83, HARN, units = international feet). Notes for spreadsheet: -9 equals no data for numerical fields for analytical data; nd equals no data in text fields; na equals information not applicable for text fields.

**Table 12-4. List of the 41 elements analyzed by ALS Chemex and their detection limits.**

| Analyte | Range | Analyte | Range | Analyte | Range | Analyte | Range |
|---|---|---|---|---|---|---|---|
| Ag | 0.01-100 | Cs | 0.05-500 | Mo | 0.05-10,000 | Sr | 0.2-10,000 |
| Al% | 0.01%-25% | Cu | 0.2-10,000 | Na% | 0.01%-10% | Ta | 0.01-500 |
| As | 0.1-10,000 | Fe% | 0.01%-50% | Nb | 0.05-500 | Te | 0.01-500 |
| Au | 0.2-25 | Ga | 0.05-10,000 | Ni | 0.2-10,000 | Th | 0.2-10,000 |
| B | 10-10,000 | Ge | 0.05-10,000 | P | 10-10,000 | Ti% | 0.005%-10% |
| Ba | 10-10,000 | Hf | 0.02-500 | Pb | 0.2-10,000 | Tl | 0.02-10,000 |
| Be | 0.05-1,000 | Hg | 0.01-10,000 | Rb | 0.1-10,000 | U | 0.05-10,000 |
| Bi | 0.01-10,000 | In | 0.005-500 | Re | 0.001-50 | V | 1-10,000 |
| Ca% | 0.01-25% | K% | 0.01%-10% | S% | 0.01%-10% | W | 0.05-10,000 |
| Cd | 0.01-1,000 | La | 0.2-10,000 | Sb | 0.05-10,000 | Y | 0.05-500 |
| Ce | 0.02-500 | Li | 0.1-10,000 | Sc | 0.1-10,000 | Zn | 2-10,000 |
| Co | 0.1-10,000 | Mg | 0.01%-25% | Se | 0.2-1,000 | Zr | 0.5-500 |
| Cr | 0.1-10,000 | Mn | 5-50,000 | Sn | 0.2-500 | | |

Note: Data reported from an aqua regia leach should be considered as only representing the leachable portion of the particular analyte. ME-MS41 gold determinations by this method are semi-quantitative due to the small sample weight used (0.5 g). Elements reported in parts per million (ppm), except those denoted as weight percent (%).

**Table 12-5. Alteration zone geochemical database spreadsheet columns.**

| Field | Description |
|---|---|
| Type | The geochemical method used by laboratory that analyzed the sample – e.g., XRD, ICP-MS |
| FieldSampleID | Unique alpha-numeric id identifying the sample – e.g., 82b DFWJ 14. |
| AlternateSampleID | Unique alpha-numeric id identifying the sample – e.g., DWPS-5. |
| Symbol | References a symbol in the GeMS style file – e.g., 31.21. |
| Label | A unique number assigned to the sample for cartographic purposes – e.g., AG1. |
| LocationConfidenceMeters | Radius in meters of positional uncertainty envelope for the observation locale. Null values not permitted. Recommended value is -9 if value is not otherwise available. |
| PlotAtScale | Cartographic map scale or larger that the observation or analysis should be plotted at. Value is scale denominator. |
| Quadrangle | The USGS 7.5' quadrangle in which the sample is located – e.g., Dufur West. |
| Elevation | Elevation of data location in feet – e.g., 22. |
| MapUnit | Map unit from which the analyzed sample was collected – e.g., Tgsb. |
| MaterialAnalyzed | Type of material analyzed – e.g., chalcedonic quartz. |
| ElementsAnalyzed | Ag, Al (%), As, Au, B, Ba, Be, Bi, Ca (%), Cd, Ce, Co, Cr, Cs, Cu, Fe (%), Ga, Ge, Hf, Hg, In, K (%), La, Li, Mg, Mn, Mo, Na%, Nb, Ni, P, Pb, Rb, Re, S (%), Sb, Sc, Se, Sn, Sr, Ta, Te, Th, Ti (%), Tl, U, V, W, Y, Zn, Zr |
| UTMNorthingNAD27 | Meters north in NAD 27 UTM projection, zone 10. |
| UTMEastingNAD27 | Meters east in NAD 27 UTM projection, zone 10. |
| LatitudeNAD27 | Latitude in NAD 27 geographic coordinates. |
| LongitudeNAD27 | Longitude in NAD 27 geographic coordinates. |
| UTMNorthingNAD83 | Meters north in NAD 83 UTM projection, zone 10. |
| UTMEastingNAD83 | Meters east in NAD 83 UTM projection, zone 10. |
| LatitudeNAD83 | Latitude in NAD 83 geographic coordinates. |
| LongitudeNAD83 | Longitude in NAD 83 geographic coordinates. |
| Northing83HARN | Feet north in Oregon Lambert NAD 83, HARN, international feet. |
| Easting83HARN | Feet east in Oregon Lambert NAD 83, HARN, international feet. |
| LocationSourceID | Unique data source from which the data were obtained – e.g., McClJD2020. |
| AnalysisSourceID | Foreign key to DataSources. Identifies source of analytical data for this sample. Null values not permitted – e.g., WSU. |
| Notes | Special information about certain samples – e.g., alteration. |
| AlteredGeochemPoints_ID | e.g., AGC1 |

***Geochronology analytical methods***

Fourteen radiometric ages are summarized in this report and geologic maps, including 12 new $^{40}Ar/^{39}Ar$ ages. Sample preparation and $^{40}Ar/^{39}Ar$ analysis was done by Dr. Dan Miggins at the College of Oceanic and Atmospheric Sciences, Oregon State University, Corvallis (OSU). The methodology for $^{40}Ar/^{39}Ar$ geochronology at OSU is summarized at https://geochronology.coas.oregonstate.edu/ and in Duncan and Keller (2004). Original data sheets for new $^{40}Ar/^{39}Ar$ isotopic ages are located in the folder Appendix/, Spreadsheets/NEW_40Ar39Ar_ANALYTICALDATA. Our map also includes 2 K-Ar ages, originally published by Anderson (1987) and Gray and others (1996). Geochronological data are included in the geodatabases:

- WRF2021_GeMS_v10.7.gdb,
- DWPS2021_GeMS_v10.7.gdb,

in separate shapefiles

- WRF2021_GeochronPoints.shp,
- DWPS2021_GeochronPoints.shp,

and in Microsoft Excel workbooks:

- WRF2021_DATA.xlsx (sheet WRF2021_GeochronPoints),
- DWPS2021_DATA.xlsx (sheet DWPS2021_GeochronPoint).

**Table 12-6** describes the fields listed in the databases. The location of each radiometric age is given in five coordinate systems: UTM Zone 10 (datum = NAD 27, NAD 83, units = meters), Geographic (datum = NAD 27, NAD 83, units = decimal degrees), and Oregon Lambert (datum = NAD 83, HARN, units = international feet). Notes for spreadsheet: -9 equals no data for numerical fields for analytical data; nd equals no data in text fields; na equals information not applicable for text fields.

**Table 12-6. Geochronology database spreadsheet columns.**

| Field | Description |
|---|---|
| Type | The geochronological method – e.g., $^{40}Ar^{39}Ar$, K-Ar, radiocarbon, mineral - whole-rock Rb-Sr isochron, etc.) used to estimate the age. |
| FieldSampleID | Unique alpha-numeric id applied to the sample – e.g., 383 DFWJ 14. |
| AlternateSampleID | Unique alpha-numeric id applied to the sample – e.g., 383 DFWJ 14. |
| MapUnit | Map unit from which the analyzed sample was collected. |
| Symbol | References a symbol in the GeMS style file. |
| Label | Radiometric age of sample with error – e.g., 3.83 ± 0.02 Ma |
| LocationConfidenceMeters | Radius in meters of positional uncertainty envelope for the observation locale. Null values not permitted. Recommended value is -9 if value is not otherwise available. |
| PlotAtScale | Cartographic map scale or larger that the observation or analysis should be plotted at. Value is scale denominator. |
| MaterialAnalyzed | Type of material analyzed – e.g., amphiboles, plagioclase. |
| NumericAge | Interpreted (preferred) age calculated from geochronological analysis, not necessarily the date calculated from a single set of measurements. |
| AgePlusError | Plus error in age determination in thousands of years. |
| AgeMinusError | Minus error in age determination in thousands of years. |
| AgeUnits | Values = years, Ma, ka, radiocarbon ka, calibrated ka, etc. |
| UTMNorthingNAD27 | Meters north in NAD 27 UTM projection, zone 10. |
| UTMEastingNAD27 | Meters east in NAD 27 UTM projection, zone 10. |
| LatitudeNAD27 | Latitude in NAD 27 geographic coordinates. |
| LongitudeNAD27 | Longitude in NAD 27 geographic coordinates. |
| UTMNorthingNAD83 | Meters north in NAD 83 UTM projection, zone 10. |
| UTMEastingNAD83 | Meters east in NAD 83 UTM projection, zone 10. |
| LatitudeNAD83 | Latitude in NAD 83 geographic coordinates. |
| LongitudeNAD83 | Longitude in NAD 83 geographic coordinates. |
| Northing83HARN | Feet north in Oregon Lambert NAD 83, HARN, international feet. |
| Easting83HARN | Feet east in Oregon Lambert NAD 83, HARN, international feet. |
| StationID | Foreign key to Stations point feature class. |
| LocationSourceID | Unique data source from which the data were obtained; e.g., McClJD2020. |
| AnalysisSourceID | Foreign key to DataSources. Identifies source of analytical data for this sample. Null values not permitted – e.g., OSU. |
| Notes | Special information about certain samples – e.g., alteration. |
| GeochronPoints_ID | e.g., GCR1 |

***Natural remanent magnetization (magnetic polarity) methods***

Field measurements of natural remanent magnetization (the magnetic field of a sample measured when induced magnetic fields are absent or zeroed out by probe; Butler, 1992) were determined from strongly magnetized lava flows exposed in the Dufur area during the course of this study in order to distinguish between flow units with normal and reversed magnetic polarity. Magnetic polarity also serves as a check on the permissible age of isotopically-dated samples, when compared to the paleomagnetic time scale of Cande and Kent (1992) (**Figure 5-13**). This method of constraining isotopic ages by magnetic polarity determinations is most effective when the analytical error is less than 0.20 m.y. Larger errors reported for isotopic ages may overlap so many polarity subchrons that no constraint is provided by knowing a samples magnetic polarity. Magnetic polarity values reported were determined using a MEDA, Inc. μMag handheld digital fluxgate magnetometer. The measured point data are included in the geodatabases:

- WRF2021_GeMS_v10.7.gdb,
- DWPS2021_GeMS_v10.7.gdb,
- DESBSR2021_GeMS_v10.7.gdb,

in separate shapefiles:

- WRF2021_MagneticPoints.shp,
- DWPS2021_MagneticPoints.shp,
- DESBSR2021_MagneticPoints.shp,

and in Microsoft Excel workbooks:

- WRF2021_DATA.xlsx (sheet WRF2021_MagneticPoints),
- DWPS2021_DATA.xlsx (sheet DWPS2021_MagneticPoints),
- DESBSR2021_DATA.xlsx (sheet DESBSR2021_MagneticPoints).

**Table 12-7** describes the fields listed in the databases. The locations of magnetics data are given in five coordinate systems: UTM Zone 10 (datum = NAD 27, NAD 83, units = meters), Geographic (datum = NAD 27, NAD 83, units = decimal degrees), and Oregon Lambert (datum = NAD 83, HARN, units = international feet). Notes for spreadsheet: -9 equals no data for numerical fields for analytical data; nd equals no data in text fields; na equals information not applicable for text fields.

The natural remanent magnetization (magnetic polarity) of strongly magnetized lava flows was determined using the following method:

1. A north-pointing arrow and near horizontal line were drawn on and around (to the extent possible) an approximately fist-sized equidimensional sample that was then removed from the outcrop (**Figure 12-3a).**
2. The magnetometer was placed on the most level ground available in a relatively magnetically clean area. The probe was then placed in a fixed position in the horizontal plane and rotated to null the local magnetic field (μMag reads zero). This procedure was done incrementally beginning with minimum range sensitivity (2000 mG [milliGauss]), increasing the sensitivity (20 mG) and re-rotating the probe until maximum sensitivity was reached. Magnetic polarity was then checked with the north end of a locked compass needle. Total field value will decrease when the compass needle is moved horizontally toward and remains parallel to the probe.
3. The polarity of a sample was determined by placing the oriented sample in a path parallel to the probe. The north-verging line drawn to represent the approximate magnetic pole of the sample was held horizontally (approximately) with the north end facing toward the probe at a distance of at least 10 times further than the measurement distance. A reading was then determined with the sample absent from the probe. The sample was then moved to a point

(typically within 1 to 2 cm) toward the probe in order to cause a change of at least several times greater than the minimum resolution of the magnetometer (**Figure 12-3b**). A decrease in the total field value indicated normal-polarity (N); an increase in total field value indicated reversed-polarity (R).

4. The sample was then rotated backward (top away from the probe) about a horizontal axis approximately 45° to see if field strength increased as the sample's inclined magnetic field was rotated into parallel with the probe.
5. The polarity of two to ten representative samples from different portions of an outcrop or from different outcrops was determined to verify the repeatability of results. Erratic results, due to re-magnetization resulting from lighting strikes, obscure post-emplacement alteration, or aberrant declination and inclination are reported as indeterminate (I).

**Figure 12-3. Procedure for determining natural remanent magnetism of lava flows. (a) Ideal sample is selected and oriented in outcrop. North arrow is drawn on upper surface; horizontal lines are drawn around the exposed edges of the sample. Fist-sized sample is then removed. (b) Magnetometer probe is placed in a fixed position in the horizontal plane and rotated to null the local magnetic field. Sample polarity is determined by moving the oriented sample into the path of the probe.**

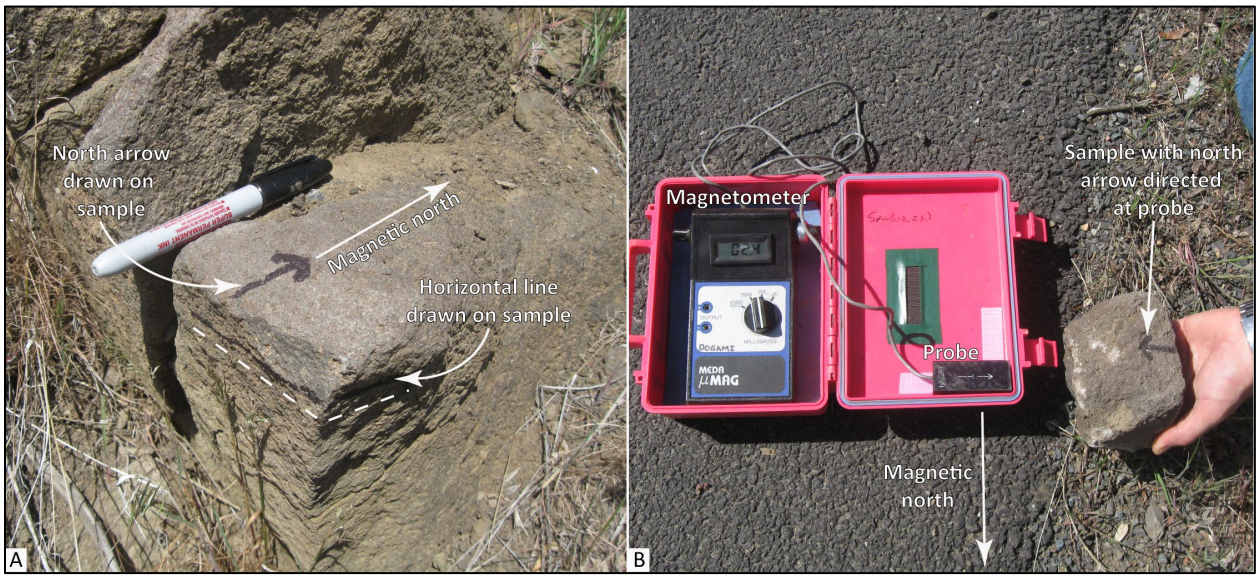

**Table 12-7. Magnetic polarity database spreadsheet columns.**

| Field | Description |
|---|---|
| Type | The method of measurement – e.g., Digital Portable Fluxgate |
| FieldSampleID | Unique alpha-numeric id applied to the sample – e.g., 18 DFWJ 14. |
| NaturalRemanentMagnetization | Natural remanent magnetization of sample as determined from a portable fluxgate magnetometer. Normal, reversed, indeterminate. |
| MapUnit | Map unit from which the analyzed sample was collected. |
| Symbol | References a symbol in the GeMS style file. |
| Label | <Null> |
| LocationConfidenceMeters | Radius in meters of positional uncertainty envelope for the observation locale. Null values not permitted. Recommended value is -9 if value is not otherwise available. |
| PlotAtScale | Cartographic map scale or larger that the observation or analysis should be plotted at. Value is scale denominator. |
| Quadrangle | The USGS 7.5' quadrangle in which the sample is located – e.g., Dufur West. |
| Elevation | Elevation of sample location in feet – e.g., 1928. |
| UTMNorthingNAD27 | Meters north in NAD 27 UTM projection, zone 10. |
| UTMEastingNAD27 | Meters east in NAD 27 UTM projection, zone 10. |
| LatitudeNAD27 | Latitude in NAD 27 geographic coordinates. |
| LongitudeNAD27 | Longitude in NAD 27 geographic coordinates. |
| UTMNorthingNAD83 | Meters north in NAD 83 UTM projection, zone 10. |
| UTMEastingNAD83 | Meters east in NAD 83 UTM projection, zone 10. |
| LatitudeNAD83 | Latitude in NAD 83 geographic coordinates. |
| LongitudeNAD83 | Longitude in NAD 83 geographic coordinates. |
| Northing83HARN | Feet north in Oregon Lambert NAD 83, HARN, international feet. |
| Easting83HARN | Feet east in Oregon Lambert NAD 83, HARN, international feet. |
| LocationSourceID | Unique data source from which the data were obtained; e.g., McClJD2020. |
| AnalysisSourceID | Foreign key to DataSources. Identifies source of analytical data for this sample. Null values not permitted – e.g., OSU. |
| Notes | Special information about certain samples – e.g., alteration. |
| MagneticPoints_ID | e.g., MGP001 |

***Orientation Points***

Orientation measurements of inclined bedding were taken in the Dufur area during the course of this study by traditional compass and clinometer methods. Additional structural measurements were determined from interpretation of lidar imagery. DOGAMI has developed a routine and model in Esri ArcGIS™ Model Builder to calculate three-point solutions for lidar-derived bedding (Duda and others, 2018, 2019). The modeling process incorporates the use of 1) a 1-m lidar-derived DEM (digital elevation model); 2) the registration of three non-collinear points picked along the trace of a geological plane or contact discernable from a 1-m lidar DEM; 3) updating these points with their lidar-derived elevation values; and 4) creating a TIN (triangular irregular network) facet of the three points. The aspect of the TIN facet is equivalent to the dip direction, and the slope corresponds to the dip (0 to 90 degrees). The strike is then determined from the dip direction, subtracting or adding 90 degrees on the basis of the right-hand rule (described in below).

The factors influencing the certainty of lidar-derived bedding are the subjectivity of the digitizer and the clarity of the feature presumed to be indicative of bedding. To improve the clarity of lidar visualization, lidar-derived bedding was compiled using both a hillshade and slopeshade image, each at 50 percent transparency, draped over a Sky-View Factor (SVF) image. Sky-View Factor images are enhanced 1-m lidar DEMs, processed using the Sky-View Factor computation tool. The Sky-View Factor computation tool is part of the Relief Visualization Toolbox (RVT), open-source processing software produced by the Institute of Anthropological and Spatial Studies (http://iaps.zrc-sazu.si/en) at the Research Centre of the Slovenian Academy of Sciences and Arts (ZRCSAZU), to help visualize raster elevation model datasets. Sky-View visualizes hillshade models using diffuse illumination, overcoming the common problem of direct illumination, which can obscure linear objects that lie parallel to the direction of the light source and saturation of shadow areas. This brings improvements in detection of linear structures because the method exposes edges and holes (Zakšek and others, 2011). DOGAMI's visualization routine, combining a lidar-derived hillshade, slopeshade, and SVF imagery, helps illuminate shadows and amplifies the edges/ridges related to bedding features. Where possible, aerial photography, combined with a contextual knowledge of the geology of the area, was used to verify bedding features interpreted from lidar.

Orientation points are reported in both quadrant format (e.g., N. 30° W., 15° NE.) and azimuthal format using the right-hand rule (e.g., 330°, 15° NE., American convention). Field-measured bedding is coded by its appropriate Federal Geographic Data Committee (FGDC) reference number for geologic map symbolization. The measured point data are included in the geodatabases:

- WRF2021_GeMS_v10.7.gdb,
- DWPS2021_GeMS_v10.7.gdb,
- DESBSR2021_GeMS_v10.7.gdb,

in separate shapefiles:

- WRF2021_OrientationPoints.shp,
- DWPS2021_OrientationPoints.shp,
- DESBSR2021_OrientationPoints.shp,

and in Microsoft Excel workbooks:

- WRF2021_DATA.xlsx (sheet WRF2021_OrientationPoints),
- DWPS2021_DATA.xlsx (sheet DWPS2021_OrientationPoints),
- DESBSR2021_DATA.xlsx (sheet DESBSR2021_OrientationPoints).

**Table 12-8** describes the fields listed in the databases. The locations of these point data are given in five coordinate systems: UTM Zone 10 (datum = NAD 27, NAD 83, units = meters), Geographic (datum = NAD 27, NAD 83, units = decimal degrees), and Oregon Lambert (datum = NAD 83, HARN, units = international feet). Strike and dip symbols can be properly drawn by the Esri ArcMap™ product by opening the layer properties, categorizing by type, choosing the appropriate symbol, and rotating the symbol based on the "Strike_Azi" field. (The Advanced button allows you to select the rotation field.) The rotation style should be set to geographic in order to maintain the right-hand rule property. Azimuths are given in true north; an additional clockwise correction of about 1.6 degrees is needed to plot strikes and dips properly on the Oregon Lambert conformal conic projection in this area. Notes for spreadsheet: nd, no data.

**Table 12-8. Orientation points database spreadsheet columns.**

| Field | Description |
|---|---|
| Type | Type of geologic structure from which feature was determined – e.g., Inclined bedding. |
| Azimuth | Strike or trend, measured in degrees clockwise from geographic North. Values limited to range 0-360. Use right-hand rule (dip is to right of azimuth direction). Horizontal planar features may have any azimuth – e.g., 20. |
| Inclination | Dip or plunge, measured in degrees down from horizontal. Values limited to range -90 to 90. Types defined as horizontal (e.g., horizontal bedding) have Inclination = 0. Null values not Data type=float – e.g., 45. |
| StrikeQuadrant | Strike direction of the inclined plane, stated in a north-directed quadrant format – e.g., N35E. |
| DipQuadrant | Amount of dip, degrees from horizontal, with direction – e.g., 45SE. |
| Symbol | References a symbol in the GeMS style file – e.g., 6.40. |
| Label | Amount of dip, degrees from horizontal – e.g., 45. |
| LocationConfidenceMeters | Radius in meters of positional uncertainty envelope for the observation locale. Null values not permitted. Recommended value is -9 if value is not otherwise available. |
| IdentityConfidence | Specifies confidence that observed structure is of the type specified; e.g., 'certain', 'questionable', 'unspecified'. |
| OrientationConfidenceDegrees | Estimated circular error, in degrees – e.g., 20. |
| PlotAtScale | Cartographic map scale or larger that the observation or analysis should be plotted at. Value is scale denominator. |
| Quadrangle | The USGS 7.5' quadrangle in which the sample is located – e.g., Dufur West. |
| Elevation | Elevation of data location in feet – e.g., 22. |
| MapUnit | Map unit from which the analyzed sample was collected. |
| UTMNorthingNAD27 | Meters north in NAD 27 UTM projection, zone 10. |
| UTMEastingNAD27 | Meters east in NAD 27 UTM projection, zone 10. |
| LatitudeNAD27 | Latitude in NAD 27 geographic coordinates. |
| LongitudeNAD27 | Longitude in NAD 27 geographic coordinates. |
| UTMNorthingNAD83 | Meters north in NAD 83 UTM projection, zone 10. |
| UTMEastingNAD83 | Meters east in NAD 83 UTM projection, zone 10. |
| LatitudeNAD83 | Latitude in NAD 83 geographic coordinates. |
| LongitudeNAD83 | Longitude in NAD 83 geographic coordinates. |
| Northing83HARN | Feet north in Oregon Lambert NAD 83, HARN, international feet. |
| Easting83HARN | Feet east in Oregon Lambert NAD 83, HARN, international feet. |
| LocationSourceID | Unique data source from which the data were obtained – e.g., McClJD2020. |
| OrientationSourceID | Unique data source from which the data were obtained – e.g., McClJD2020. |
| Notes | Special information about the point – e.g., lidar derived. |
| OrientationPoints_ID | Primary key – e.g., ORP001. |
| PTTYPE | e.g., Bedding |
| RuleID1 | Rule ID used for cartographic representation – e.g., 6.40. |

### *Well Points*

The well points database is derived from written drillers' logs provided by Oregon Department of Water Resources (OWRD). Well logs vary greatly in completeness and accuracy, therefore locally limiting the utility of subsurface interpretations based upon these data. Water well logs, compiled and used for interpretation during the course of this study were not field located. The approximate locations were estimated using tax lot maps, street addresses (coordinates obtained from Google Earth™), and aerial photographs to plot locations on the map. The accuracy of the locations ranges widely, from errors of one-half mile possible for wells located only by section and plotted at the section centroid to a few tens of feet for wells located by address or tax lot number on a city lot with bearing and distance from a corner. At each mapped location the number of the well log is indicated. This number can be combined with the first four letters of the county name (e.g., WASC 5473), to retrieve an image of the well log from the OWRD web site. The point data are included in the geodatabases:

- WRF2021_GeMS_v10.7.gdb,
- DWPS2021_GeMS_v10.7.gdb,
- DESBSR2021_GeMS_v10.7.gdb,

in separate shapefiles:

- WRF2021_WellPoints.shp,
- DWPS2021_WellPoints.shp,
- DESBSR2021_WellPoints.shp,

and in Microsoft Excel workbooks:

- WRF2021_DATA.xlsx (sheet WRF2021_WellPoints),
- DWPS2021_DATA.xlsx (sheet DWPS2021_WellPoints),
- DESBSR2021_DATA.xlsx (DESBSR2021_WellPoints).

**Table 12-9** and **Table 12-10** explain the fields in the databases. The locations of water well point data are given in six coordinate systems: UTM Zone 10 (datum = WGS 84, NAD 27, NAD 83, units = meters), Geographic (datum = NAD 27, NAD 83, units = decimal degrees), and Oregon Lambert (datum = NAD 83, HARN, units = international feet).

Well intervals listed in the well log database sometimes alternate between consolidated and unconsolidated lithologies and may be listed as alternating between bedrock and surficial geologic units. This may occur where bedrock units are soft, where paleosols or weak zones lie within bedrock, or where cemented or partly cemented zones alternate with unconsolidated zones in surficial deposits.

**Table 12-9. Well log database lithologic abbreviations.**

*Lithologic abbreviations (alphabetical by group)*

| **UNCONSOLIDATED SURFICIAL UNITS** | |
|---|---|
| **Abbreviation** | **Description** |
| a | ash |
| bd | boulders |
| c | clay |
| ch | clay, hard (often logged as claystone but probably not bedrock) |
| g | gravel |
| gc | cemented gravel |
| gs | gravel and sand (also sandy gravel) |
| m | mud |
| s | sand |
| sg | sand and gravel (also gravelly sand) |
| st | silt |
| *Rock, sedimentary* | |
| bc | breccia |
| cg | conglomerate |
| cs | claystone |
| sh | shale |
| ss | sandstone |
| *Rock, igneous* | |
| an | andesite |
| b | basalt |
| ba | basaltic andesite |
| cd | cinders |
| da | dacite |
| pu | pumice |
| gr | granite |
| l | lava |
| r | rhyolite |
| sc | scoria |
| t | tuff |
| v | volcanic, undivided |
| vb | volcanic breccia |
| *Other* | |
| af | artificial fill |
| cl | coal (lignite) |
| dg | decomposed granite |
| o | other (drillers unit listed in notes column of spreadsheet) |
| rk | rock |
| sl | soil |
| u | unknown (typically used where a well has been deepened) |

**Table 12-10. Well log database spreadsheet columns.**

| Field | *Description and Example |
|---|---|
| Type | Type of well located; e.g., well used for domestic-water supply, well used for irrigation-water supply, drill hole for hydrocarbon exploration or exploitation- Showing name and number. |
| Symbol | References a symbol in the GeMS style file – e.g., 26.1.25. |
| Label | A unique label identifying the well, if applicable – e.g., Federal 1-10. |
| IdentityConfidence | Specifies confidence that observed structure is of the type specified; e.g., 'certain', 'questionable', 'unspecified'. |
| LocationConfidenceMeters | Radius in meters of positional uncertainty envelope for the observation locale. Null values not permitted. Recommended value is -9 if value is not otherwise available. |
| PlotAtScale | Cartographic map scale or larger that the observation or analysis should be plotted at. Value is scale denominator. |
| TownshipRangeSection | Two digits for township, two digits for range, and two for section; negative if township is south of Willamette baseline. Exception for township and range if they contain a decimal – e.g., −2132.503. |
| County | Wasco County – e.g., WASC. |
| Grid | Well log number for wells. Wells in Wasco County preceded by acronym WASC – e.g., WASC53799. |
| WellElevation | Wellhead elevation in feet as given by Google Earth™ at corresponding WGS 84 location. e.g., 1978. |
| LocatedBy | Google Earth™ elevation for cursor location at a given address – e.g., Google.<br>Google Earth™ elevation at house in vicinity of given address – e.g., House.<br>Pad identifying approximate well location, visible in air photo – e.g., Pad.<br>Approximate tax lot centroid or other best guess for well location using a combination of tax lot maps and aerial photographs – e.g., Tax lot.<br>Owner name – e.g., Owner.<br>Address of well listed on Oregon Water Resources Department (OWRD) Startcard.<br>Wells located by Oregon Water Resources Department (OWRD) using handheld GPS – e.g., OWRD.<br>GPS coordinates of wellhead included with well log – e.g., GPS.<br>Approximate quarter-quarter-quarter section centroid – e.g., QQQ.<br>Approximate quarter-quarter-section centroid – e.g., QQ.<br>Approximate quarter-section centroid – e.g., Q.<br>Approximate fit to sketch map included with well log – e.g., map. |
| Lithology | Best interpretation of driller's log using abbreviations above – e.g., g. |
| Base | Record base of driller's interval or, if lithology abbreviation would not change, similar intervals, in feet below wellhead – e.g., 17. |
| Top | Calculated top of driller's interval or similar intervals, in feet below wellhead – e.g., 14. |
| TopElevation | Calculated elevation at top of driller's interval, or similar intervals, in feet above sea level – e.g., 86. |
| BaseElevation | Calculated elevation at base of driller's interval, or similar intervals, in feet above sea level – e.g., 83. |
| BedrockLithology | Lists bedrock lithologies, when encountered, abbreviations listed above – e.g., b. |
| BedrockElevation | Calculated elevation at which bedrock or soil over bedrock was first encountered, in feet above sea level – e.g., 1924. |
| Tax lot | Tax lot number. Where it is determined that a tax lot number is used more than once in the section then the appropriate subdivision of the section is indicated in the notes field – e.g., 800. |
| Color | Color of interval as reported by the well driller – e.g., green. |
| MapUnit | Geologic unit interpreted in subsurface based on drillers log and designated by map unit label used in accompanying geodatabase. Intervals labeled "suna" (surface unit not applicable) are those where the lithology as interpreted by the original drillers' log do not correspond; also denotes intervals in the subsurface where a precise unit label cannot be applied – e.g., Tb. |
| Quadrangle | The USGS 7.5' quadrangle in which the sample is located – e.g., Dufur West. |
| UTMNorthingWGS84 | Meters north in WGS84 UTM projection, zone 10. |
| UTMEastingWGS84 | Meters east in WGS84 UTM projection, zone 10. |
| UTMNorthingNAD27 | Meters north in NAD 27 UTM projection, zone 10. |
| UTMEastingNAD27 | Meters east in NAD 27 UTM projection, zone 10. |
| LatitudeNAD27 | Latitude in NAD 27 geographic coordinates. |
| LongitudeNAD27 | Longitude in NAD 27 geographic coordinates. |
| UTMNorthingNAD83 | Meters north in NAD 83 UTM projection, zone 10. |
| UTMEastingNAD83 | Meters east in NAD 83 UTM projection, zone 10. |

| | |
|---|---|
| LatitudeNAD83 | Latitude in NAD 83 geographic coordinates. |
| LongitudeNAD83 | Longitude in NAD 83 geographic coordinates. |
| Northing83HARN | Feet north in Oregon Lambert NAD 83, HARN, international feet. |
| Easting83HARN | Feet east in Oregon Lambert NAD 83, HARN, international feet. |
| LocationSourceID | Unique data source from which the data were obtained – e.g., OWRD2020. |
| WellSourceID | Unique data source from which the data were obtained – e.g., OWRD2020. |
| Notes | Notes about the stratigraphic interval as originally described by the well driller or observer. |
| WellPoints_ID | Primary key – e.g., WLP593 |
| PTTYPE | e.g., Water Well, Oil and Gas. |

*Well location given in six coordinate systems calculated by reprojecting original WGS 84 UTM, zone 10 locations.